Experimental Study On Seismic Performance Of Reinforced Concrete Coupling Beams And Rectangular Squat Walls With Innovative Reinforcement Configurations

by

POORYA HAJYALIKHANI

Presented to the Faculty of the Graduate School of

The University of Texas at Arlington in Partial Fulfillment

of the Requirements

for the Degree of

DOCTOR OF PHILOSOPHY

THE UNIVERSITY OF TEXAS AT ARLINGTON

December 2015

Acknowledgements

I would like to acknowledge Professor Shih-Ho (Simon) Chao for his invaluable guidance and support throughout this study. His encouragement during hard times and help in both technical and non-technical issues are deeply appreciated and will never be forgotten.

I would like to thank to my family, Rahman Hajialikhani, Farzaneh Ziadlou, and Pooyan Hajyalikhani for their limitless patience, help, and support during all the phases of his study and to all my friends in University of Texas at Arlington for their inspiration, encouragement, and support.

I would like to extend a special thanks to Xuejian Liu, Sanputt Simasathien, Israel Galicia, He Shi, Mohammadreza Zarrinpour, Chatchai Jiansinlapadamrong, Youngjae Choi, Venkateshbab Kaka, Guillermo Palacios, and Regina Wawerud for their help at various phase of this study; the technicians of the Structural Engineering Laboratory, Oleh Kinash, for his help and support.

November 24, 2015

Abstract

Experimental Study on Seismic Performance of Reinforced Concrete Coupling Beams and Squat Walls with Innovative Reinforcement Configurations

Poorya Hajyalikhani, PhD

The University of Texas at Arlington, 2015

Supervising Professor: Shih-Ho Chao

Reinforced concrete core walls, coupled by diagonally reinforced coupling beams (DCBs), are a very efficient seismic force resisting system for medium- to high-rise buildings. The diagonal reinforcing bars in DCBs are most effective when the beam has a span-to-depth ratio, l_n/h, less than 2. Modern construction, due to architectural requirements, typically requires span-to-depth ratios between 2.4 to 4, which leads to a very shallow angle of inclination of the diagonal reinforcement (generally between 10 to 20 degrees). The lower angles of inclination, combined with the detailing requirements specified in ACI 318, results in reinforcement congestion as well as design and construction difficulties. These issues with DCBs can be considerably minimized by utilizing an innovative and simplistic reinforcing scheme as investigated in this study. This reinforcement scheme consists of two separate cages similar to those used for typical beams in RC special moment frames. The proposed coupling beam has high elastic stiffness and acts like a conventional coupling beam under small displacements. Upon large displacements, cracks begin developing at the mid-span and mid-height of the beams where the narrow gap is located, gradually propagating towards the beam's ends. The cracks eventually separate the coupling beam into two slender beams where each has nearly twice the aspect ratio of the original coupling beam. This essentially

transforms the shear-dominated behavior into a flexure-dominated behavior, as conventional slender beams. Because damage initiates from the center of the beam; then spreads towards the ends, the beam's ends maintain their integrity even under very large displacements, thereby eliminating the sliding shear failure at the beam-to-wall interface. Preliminary testing results on half-scale coupling beam specimens with span-to-depth ratio of 2.4 showed that coupling beams with the proposed reinforcement scheme were able to sustain high shear stresses and large rotations before strength degradation occurred.

Subsequently, six rectangular squat wall specimens with height-to-length ratio 0.5 and 1, which were designed based the second innovative design concept using discrete confining cages to reinforce the web of the walls, were tested under lateral displacement reversals. Each wall consisted of several separate cages similar to those used for typical beams in RC special moment frames. The response of squat wall specimens showed very high shear strength and stiffness, while maintain adequate ductility due to well confinement of the wall.

Table of Contents

List of Illustrations

List of Tables

Chapter 1

Introduction

1.1 First Phase: Background Of The Coupling Beam

Reinforced concrete structural walls are commonly used as the primary seismic force resisting system in buildings, as shown in Figure 1.1. The majority of the lateral loads on multistory buildings, originating from wind or seismic disturbances, are resisted by structural walls, due to their stiffness and strength. Based on the architect's design, these walls have numerous openings for entities such as elevators, windows, and doors, which divide a single wall into more slender walls, connected by short beams. These beams are known as coupling beams. The use of the coupled wall system leads to a more efficient and economical structure system than single walls because properly designed coupled wall systems possess significantly higher strength, stiffness, and energy dissipation capacity.

Figure 1-1 Reinforced concrete structural walls system (Dawn et al., 2010)

In a traditional structural wall system, as shown in Figure 1.2, the total overturning moment due to lateral loading, M, is resisted by the walls flexural capacity at the base of the cantilever walls. In a coupled wall structure, as shown in Figure 1.2, the external lateral load generates axial load, shear force, and moment in the walls, and moment in the coupling beam due to high shear stresses. Shear force in coupling beams creates a coupling action that resists a portion of the total overturning moment induced by ground motion, thus reducing the moments that must be resisted by the individual walls resulting in a more efficient structural system and high lateral stiffness and strength is provided by the coupling effect.

Therefore in coupled wall structures the overturning moment, M, is resisted by two mechanisms; 1) the flexural capacity of individual structural walls (M1 and M2), and 2) the coupling action (TL) due the axial forces that is generated by shear forces of the coupling beams.

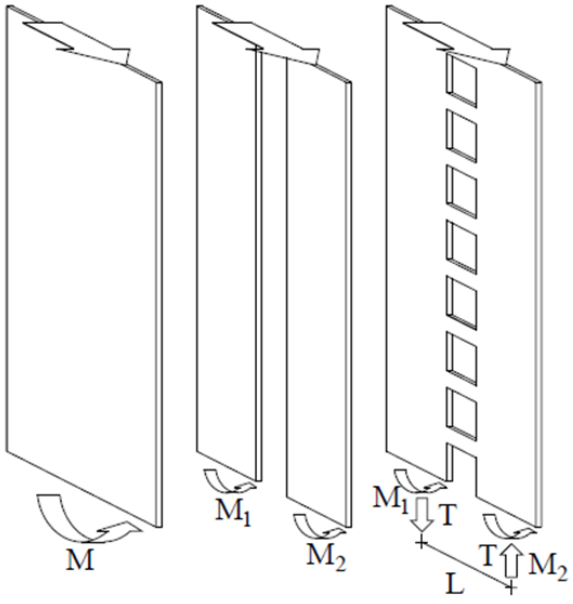

Figure 1-2 Coupling of shear wall (Lequesne et al., 2011)

The sum of the shear force developed in the coupling beams in the upper level is equivalent to the axial force in the wall, therefore, the strength and stiffness of these coupling beams may significantly affect the behavior of the coupled wall system. Consequently, to get maximum axial forces in resisting the overturning moment, M, the coupling beams must possess adequate shear resistance. If the coupling beams cannot resist shear forces, the coupled walls will no longer work as an integrated system due to losing the coupling action, therefore, the stiffness of the system is reduced which will substantially increase the structural drift. The importance of this shear property can be seen in the aftermath of the 1964 Alaska earthquake.

As a result, for the desired behavior of the coupled wall system to be attained, the coupling beam is required to sustain high shear forces while undergoing large displacement. Also, the coupling beams must yield before the wall piers, behave in a ductile manner, and exhibit significant energy dissipating characteristics.

In 1964, the earthquake in Alaska caused significant damage throughout the Anchorage Alaska area. Conventionally detailed coupling beams in the perimeter walls of the Mount McKinley Hotel were severely damaged during this earthquake, shown in Figure 1.3. This event and subsequent experimental research after the earthquake showed that coupling beams with conventional reinforcement consisting of longitudinal bars and stirrups are vulnerable when subjected large load reversals (Paulay, 1971).

Figure 1-3 Diagram showing failure of conventional coupling beam during Alaska Earthquake (United States Geological Survey (1964))

On the other hand, prior studies have shown that conventional longitudinally reinforced concrete coupling beams that are flexure-dominant, exhibited satisfactory seismic performance under a shear stress below $3\sqrt{f_c'}$. Beyond this stress level, the sliding shear at the beam-to-wall interface started affecting the response and eventually led to failure (Aktan et al., 1981; Aristizabal-Ochoa, 1982). Also, recent experiments showed that slender conventional longitudinally reinforced coupling beams can reach approximately 4% rotation at a peak stress of $3.4\sqrt{f_c'}$ prior to strength degradation (Naish et al., 2009). As for the required ductility demands of a typical beam, prior

nonlinear time-history analyses (Harries et al., 2006) indicated that coupling beams would need average rotation capacities of approximately 3% and 6% for design basis earthquake (DBE) (10% probability of exceedance in 50 years) and maximum considered earthquake (MCE) (2% probability of exceedance in 50 years) level ground motions, respectively, to maintain the integrity of the coupled wall systems.

Based on the shear resistance and adverse failure mechanisms of conventional coupling beams, Paulay and Binney (1974) recommended a new detailing consisting of two intersecting diagonal reinforcement groups combined with closely spaced transverse reinforcement. In this reinforcement detail, the diagonal bars need to be well confined by transverse reinforcement and carefully anchored in the walls. In a design using this type of coupling beam, the whole shear transfer mechanism is resisted by heavily reinforced diagonal cages. Experimental studies (Paulay et al., 1974, Shiu et al., 1978, and Tassios et al., 1996, and Galano et al., 2000) have shown that diagonal reinforcement prevents the development of sliding-shear failure, and significantly improves deformation and energy dissipation capacity compared to conventional detailing (longitudinal and vertical rebars) for coupling beams subjected to reverse cyclic loading. Furthermore, for coupling beams with a span-to-depth ratio less than or equal to 2.0, diagonal reinforcement over the full beam span has proven to be the most efficient solution. However, modern architectural specifications typically require span-to-depth ratios between 2.4 to 4, which leads to a very shallow angle of inclination for the diagonal reinforcement (generally between 10 to 20 degrees). The lower angles of inclination, combined with the detailing requirements specified in ACI 318 (2014), can cause several major issues, as show in Figure 1.4, for both design and construction (Naish et al., 2009, Harries et al., 2006, Moehle et al., 2011):

1. A small angle of inclination significantly decreases the efficiency of diagonal reinforcement in resisting shear forces; thus, more reinforcing bars are needed, which ultimately increases the difficulty of construction. There is significant difficulty in placing the diagonal reinforcement with this small angle of inclination because the diagonal bars can be easily obstructed by transverse reinforcement.

2. The minimum width requirement for diagonal elements necessitates interlock of the two diagonal elements. This in turn demands increased clear distance between reinforcement in order for one diagonal element to pass through the other. The minimum dimensions and required reinforcement clearances can make the coupling beam very wide, which controls the wall width.

3. It can be very challenging and time-consuming to thread the diagonal reinforcement through the congested vertical and horizontal bars in the wall's boundary elements (Figure 1.4).

4. ACI 318-14, Section 18.10.7.4, limits the gross concrete section shear stress to $10\sqrt{f_c'}$ (or factored shear stress $8.5\sqrt{f_c'}$). However, structural analysis according to current codes often results in a coupling beam shear demand close to $14\sqrt{f_c'}$ or higher. In order to satisfy ACI stress limits, designers often increase the concrete strength. But this approach leads to even more steel because ACI 318-14 Eq. (18.10.7.4) requires that the entirety of the shear force be resisted by reinforcing steel. The consequence is that bundled bars are usually needed, resulting in an even shallower angle of inclination, requiring additional reinforcing steel. This eventually results in severe congestion and construction difficulties.

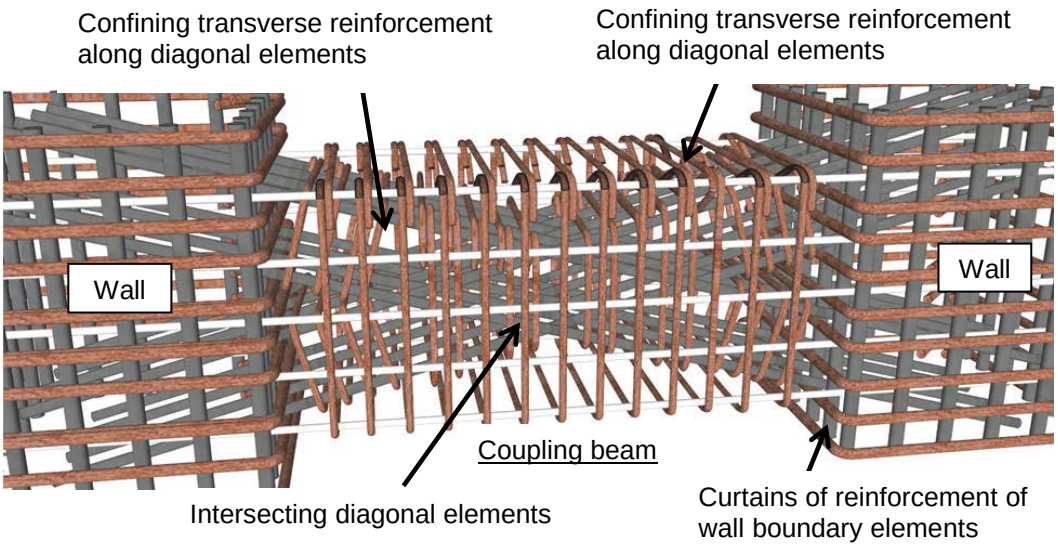

Figure 1-4 Diagonally reinforced coupling beam details with aspect ratios greater than 2.0, according to ACI 318-14 (Lequesne et al., 2010)

5. According to Naish et al. (2009), coupling beam with cross section dimensions of 24" x 30" reinforced with two bundles of 8#11 diagonal bars is common for residential construction. Also, for a coupling beam with aspect ratio 2.4, angle of the diagonal bars is about 15.7º. As is shown in Figure 1.5, it is almost impossible to place the diagonal bars at the right angle with all the required hoops for both option of confinement.

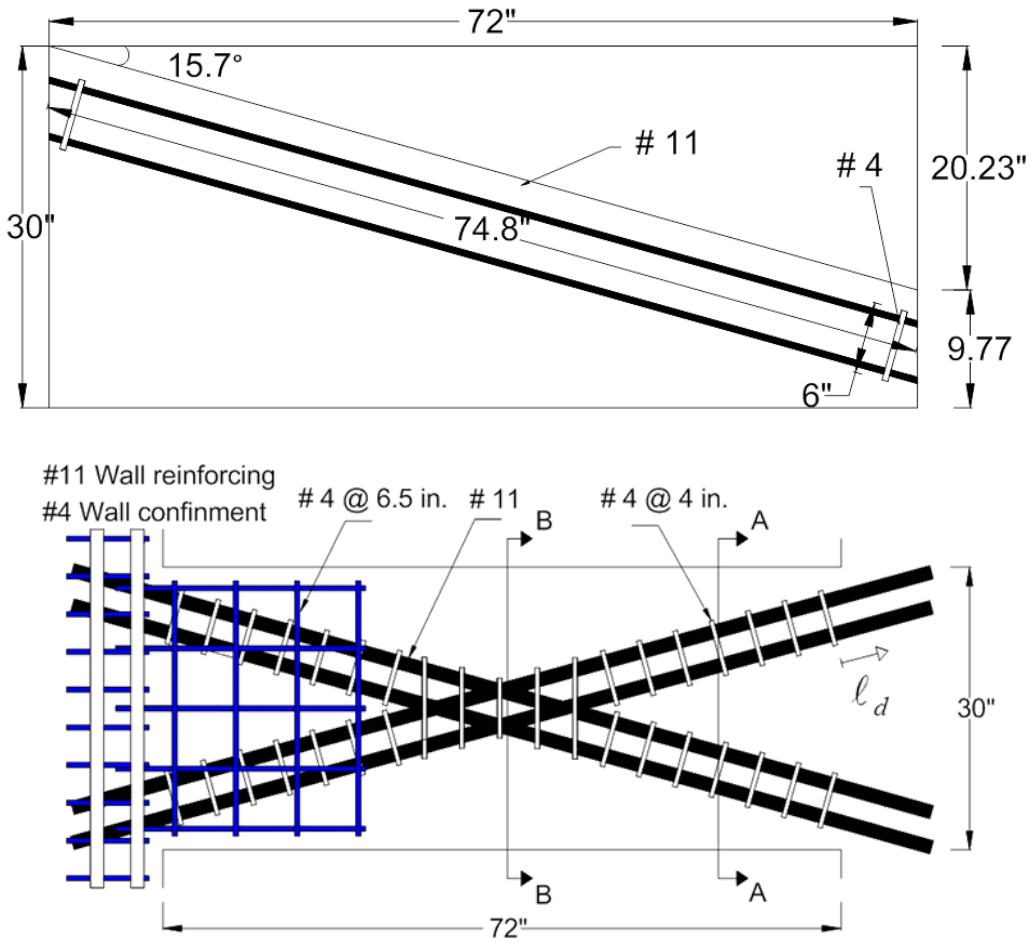

a) Confinement of individual diagonals

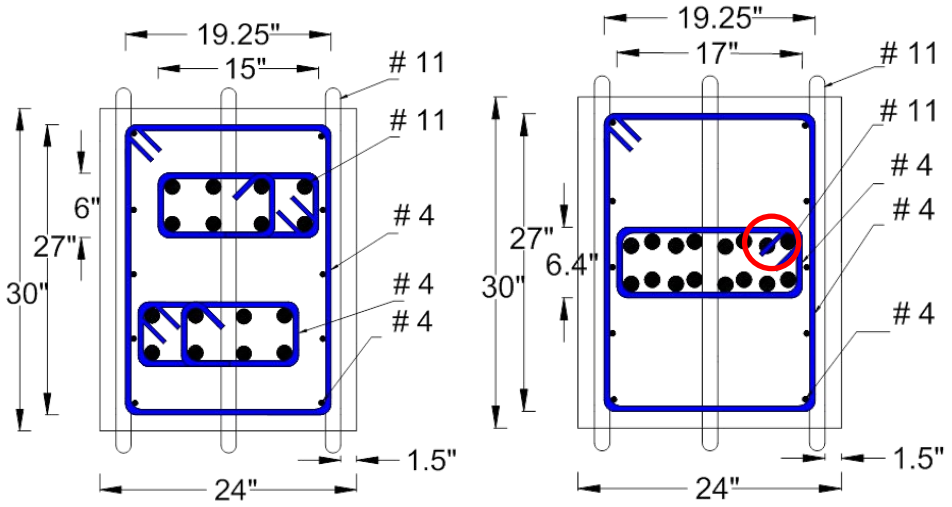

Section A-A Section B-B

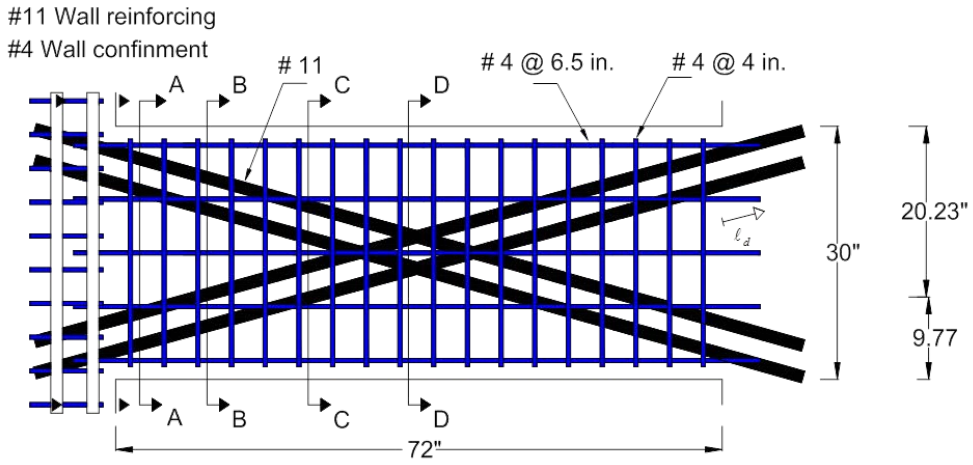

b) Full confinement of diagonally reinforced concrete beam section

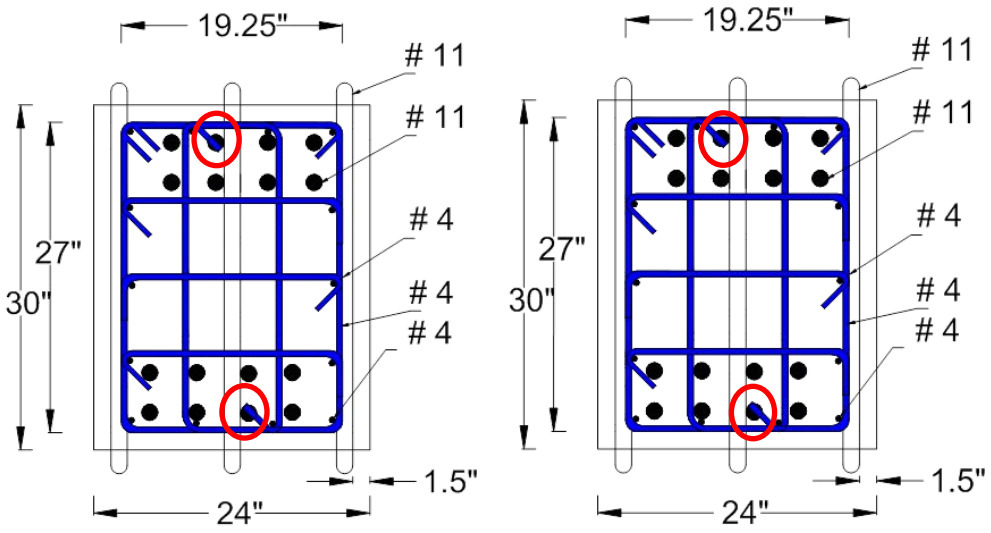

Section A-A

Section B-B

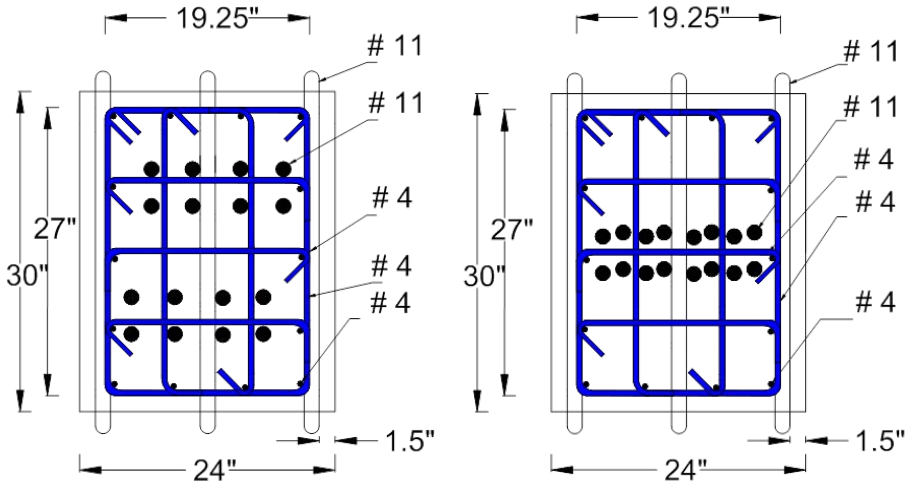

Section C-C

Section D-D

Figure 1-5 Full scale coupling beam confinement details (aspect ratio 2.4, according to ACI 318-14)

Further, according to the Hooper et al. (2014), in the recent construction due to the mechanical or electrical requirement, several utility pipes should pass through the coupling beam which can effect on the strength, stiffness and ductility of the diagonally reinforced coupling beam.

Other alternative reinforcement schemes have been investigated (Tegos et al., 1988; Tassios et al., 1996; Galano et al., 2000), such as a rhombic reinforcement layout, diagonal reinforcement located only at the beam-wall interface, or the addition of dowels at the ends of the coupling beams. However, it was experimentally demonstrated that coupling beams with these alternative reinforcement details did not exhibit satisfactory seismic behavior, and/or they posed construction difficulties.

Another coupling beams design alternatives have been designed by Harries et al. (1998). Their specimens consisted of steel shape encased coupling beams. The results indicated the steel and hybrid steel-concrete coupling beam perform adequately and exhibit the most favorable response to reversed cyclic loading. However, steel elements require a long embedment into the adjoining structural walls to ensure a full development of flexural and shear capacities, which is created severe interference problems with the wall boundary reinforcement.

Recently, precast high-performance fiber-reinforced concrete (HPFRC) coupling beams with span-to-depth ratios ranging between 1 and 3.3 were proposed as alternative (Canbolat et al., 2004, Lequesne et al., 2010, Sekit et al., 2012). Test results have shown that the HPFRC coupling beams with aspect ratios of 1.75, 2.75 and 3.3 exhibit large drift and shear capacity, while reinforcement detailing was simplified by reducing the diagonal and confinement reinforcement.

1.2 Second Phase: Background Of The Rectangular Squat Wall

Reinforced concrete walls are often used as the primary component of seismic force resisting system in building located in earthquake region because of their high strength and stiffness. These walls with a height-to-length ratio smaller than two are widely used in squat buildings such as parking structures, in high-rise structures, when the walls extend only a few stories above the foundation level and nuclear structure, as shown in Figure 1.6, (Paulay et al., 1981; Whyte et al., 2013). These walls are known as squat wall.

Figure 1-6 Shear wall in a nuclear reactor, Olkiluoto, Finland

(http://www.envirospace.com)

Squat walls can be found in different configuration in the building plan. Symmetrical sections are rectangular and barbell shape and asymmetrical wall sections are flanged shape such as T and L, as shown in Figure 1.7. Rectangular cross section is

commonly used in the building because they are relatively easy to design and construct and the bar-bell and flanged walls could create an architectural impediment and increase the forming cost. The behavior of properly designed walls with height-to-length less than 1.0 is dominated by shear while the behavior of the walls with height-to-length 1.0 to 2.0, usually is dominated by an interaction between shear and flexure. According to the ACI building code (ACI committee 318, 2014), the reinforcement requirement for squat walls, include the flexural reinforcement with close hoops at the boundary and distributed vertical and horizontal reinforcement in the web of the wall.

Experimental studies showed the peak shear strengths for rectangular squat walls could not reach to the upper limit of the ACI 318-14 ($10\sqrt{f_c'}$), and ASCE 43-05 ($20\sqrt{f_c'}$). On the other hand, prior studies on the behavior of the squat walls have shown limited wall deformation capacity, in some cases as low as 0.3% (Barda et al., 1977; Paulay et al., 1982; Hidalgo et al., 2002). Also, recent experiments showed that the squat wall with aspect ratio less than two compliant with ACI code requirements could reach approximately 1% rotation before strength degradation (Athanasopoulou et al., 2013). Therefore, there is room for improvement the performance of the squat wall in term of the shear strength and ductility capacity.

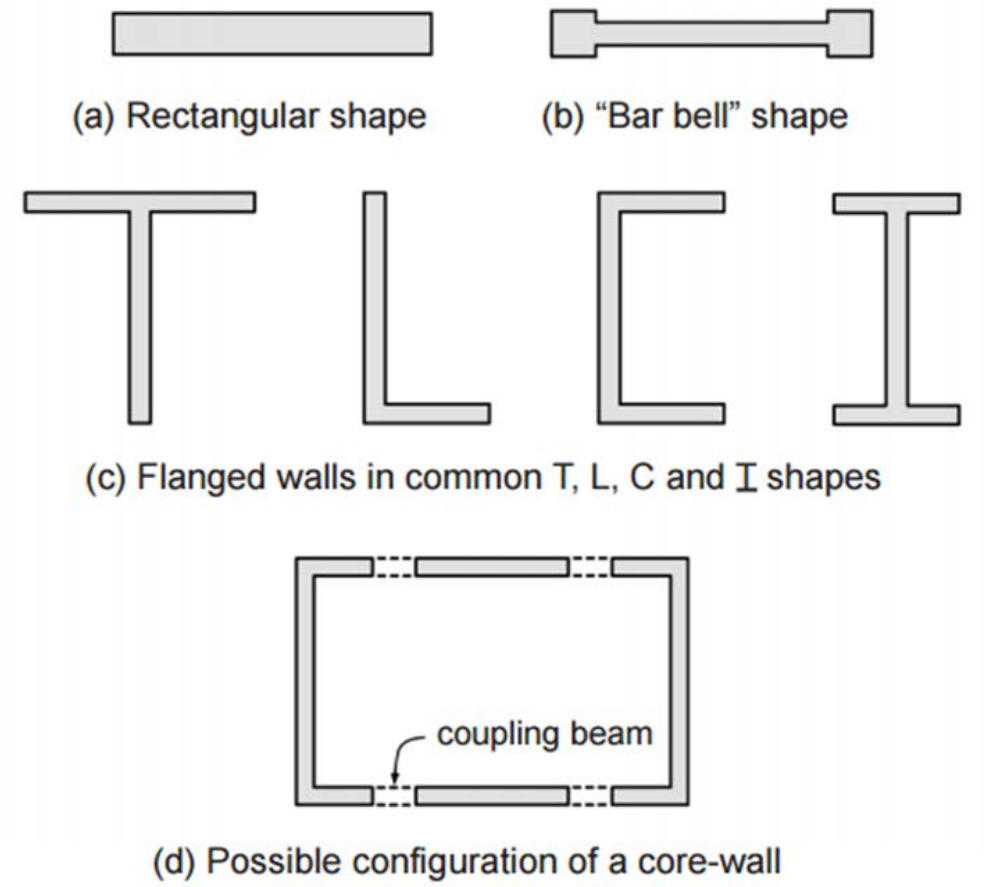

Figure 1-7 Various wall cross sections (National Institute of Standard and Technology (2012))

1.3 Research Objectives

The main objective of the first phase of this research was to evaluate the proposed innovative coupling beam, double beam coupling beam (DBCB), to simplify current reinforcement requirements in RC coupling beams while enhancing shear strength and deformation capacity when subjected to strong earthquake loads. DBCB consists of two separate cages similar to those used for typical beams in reinforced concrete special moment frames. The simple reinforcement detailing can be seen in Figure 1.8. To accomplish this research, eight coupling beams with span-to-depth ratios of 2.2, 2.4, and 3.3 were tested under large displacement reversals to evaluate their seismic performance. The results from this research indicated that the new detailing approach considerably simplifies construction while reducing costs and provides equal, if not improved seismic behavior as compared to the diagonal arrangement.

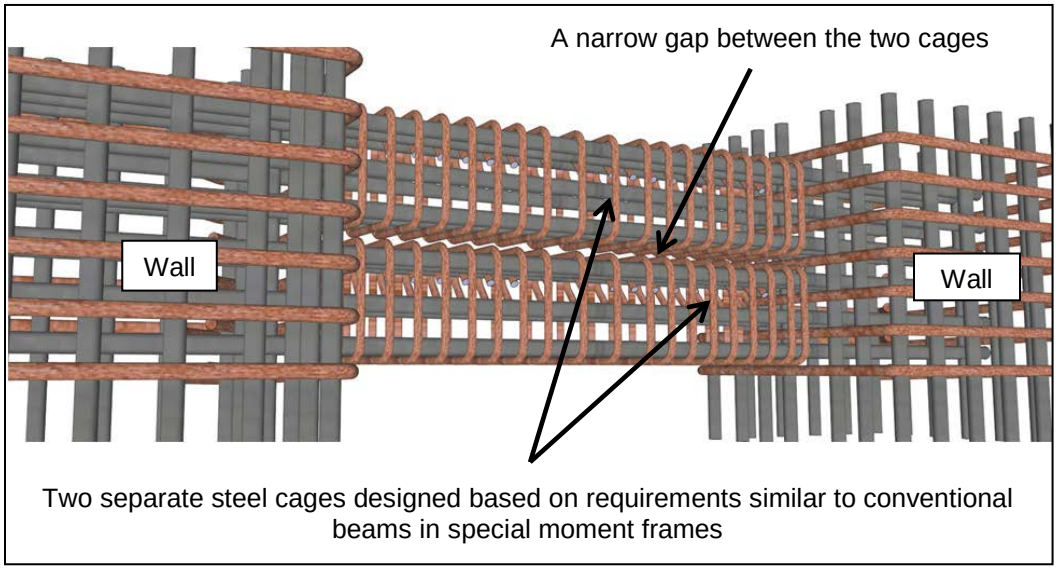

Figure 1-8 Double Beam coupling beam details

The main objective of the second phase of this research was to evaluate the new arrangement for rectangular squat wall to improve the shear strength while enhancing deformation capacity when subjected to lateral loads. To accomplish this research, six scaled rectangular squat walls with height-to-length ratio 0.5 and 1 were tested under displacement reversal to evaluate the seismic performance of these structures. The results from this research indicated that the new detailing approach improved seismic behavior as compared to the conventional wall.

The following were considered important in this study:

1. Coupling beam span-to-depth ratio (2.2, 2.4, 3.3)
2. Squat wall height-to-length ratio (0.5, 1)
3. Innovative reinforcement detailing

1.4 Organization of the Dissertation

This dissertation is organized into five chapters. Details of each chapter are described as follows.

Chapter 1 – Introduction: This chapter contains general idea of coupling beams and squat wall, as well as the motivation and objectives of the research.

Chapter 2 – Literature Review: This chapter reviews previous researches of coupling beam and squat wall.

Chapter 3 – Experimental Program: Large-scale experimental program is described in this chapter including design and fabrication of specimen, mix proportions for the concrete, test setup, load protocol and types of instrumentation used.

Chapter 4 – Analysis of Experimental Results: The behavior of coupling beams and squat wall during and after the test is explained.

Chapter 5 – Summary and Conclusions: This chapter presents a summary of the overall research study, main conclusions of the research.

Chapter 2

Literature Review

2.1 First Phase: Coupling Beam

2.1.1 Reinforced Concrete Coupling Beam

For desirable behavior of the coupled walls, coupling beams must possess large deformation capacity without significant loss in strength and stiffness under load reversal. The deformed shape of a coupling beam under the earthquake loading is shown in Figure 2.1.

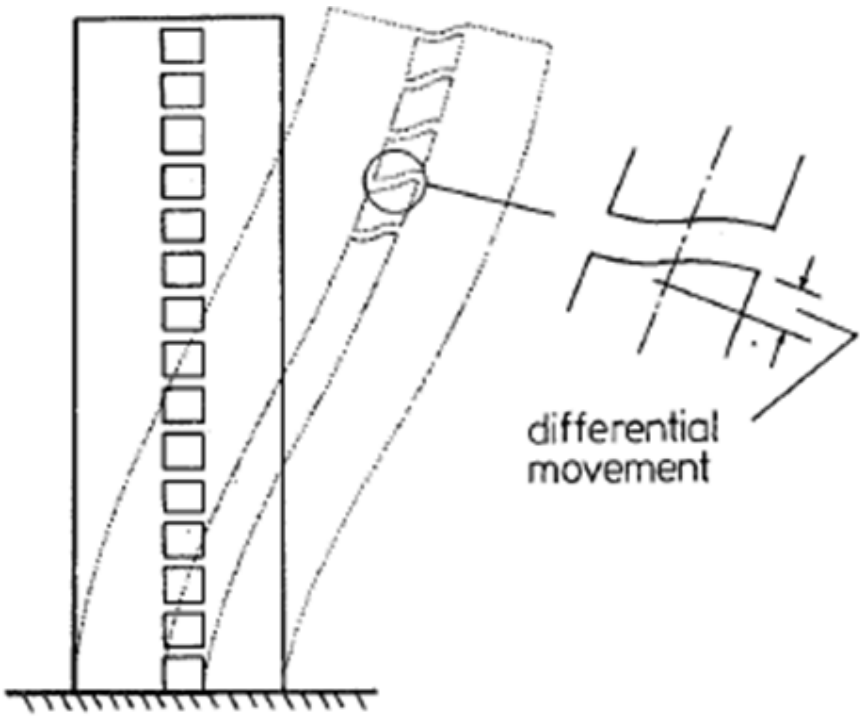

Figure 2-1 Deformation of a coupling beam (Subedi, 1991)

Prior to the 1964 Alaska earthquake, coupling beams have been designed and detailed similar to the regular deep beams, therefore they consist of longitudinal flexural bars with vertical close stirrups and distributed horizontal bars, as shown in Figure 2.2.

Also, a span-to-depth ratio of less than 4 is typically used for coupling beams (Aktan and Bertero, 1981). In this design, shear strength of the coupling beam provide by the traditional "concrete" mechanism consist of shear resistance of concrete compression zone, dowel action of the longitudinal reinforcement, and aggregate interlock along the crack interface and arch action in beams with small span-to-depth ratio (Paulay et al., 1971). The shear force which was not resisted by these mechanisms was accounted for by using transverse reinforcement to bridge the diagonal cracks.

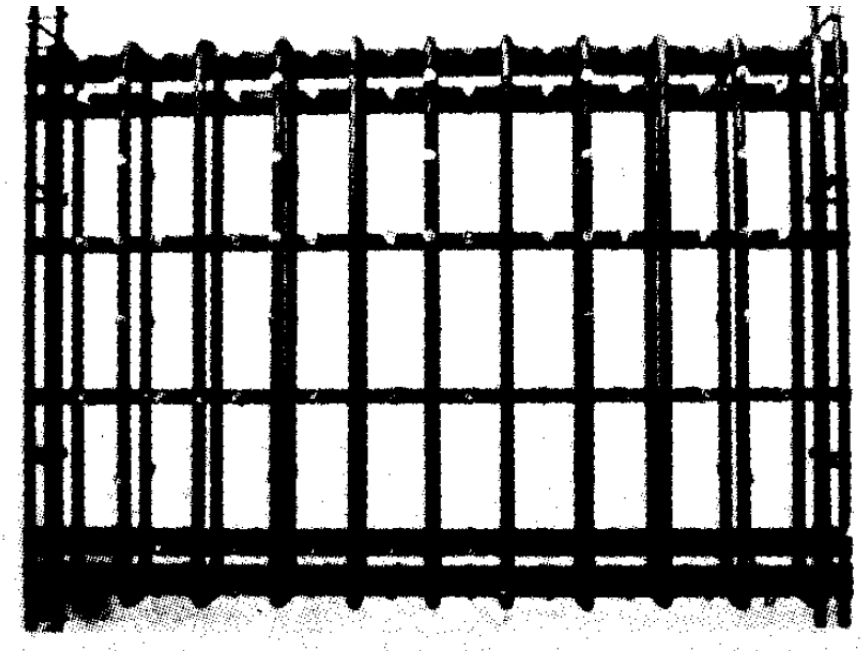

Figure 2-2 Conventional coupling beam (Paulay et al., 1974)

Conventional coupling beams will inevitably fail in diagonal tension. This was experienced in the 1964 Alaska Earthquake (Figure 2.3). This event indicated a conventional coupling beam does not have adequate shear capacity. As a result, there is a need for reformation which would allow these beams to sustain large shear reversals without a substantial degradation of strength and stiffness. Thus, after the earthquake extensive research was conducted to understand the seismic behavior and the reasons

of the failure of the conventional coupling beam under monotonic and reversal cyclic loading.

Figure 2-3 Diagonal tension failure of conventional coupling beam during Alaska Earthquake (NISEE)

Paulay (1971) performed the first detailed experimental study on reinforcement concrete coupling beams. In this study, nine RC coupling beam specimens in two different span-to-depth (1.29, 102) ratios were tested under monotonic loading. The result shown, RC coupling beam tend to fail in a diagonal tension mode (Figure 2.4) due to the lack of the stirrups in around the longitudinal bars. This failure mode can be eliminated by using the stirrups with a capacity equal to or greater than the entire shear demand.

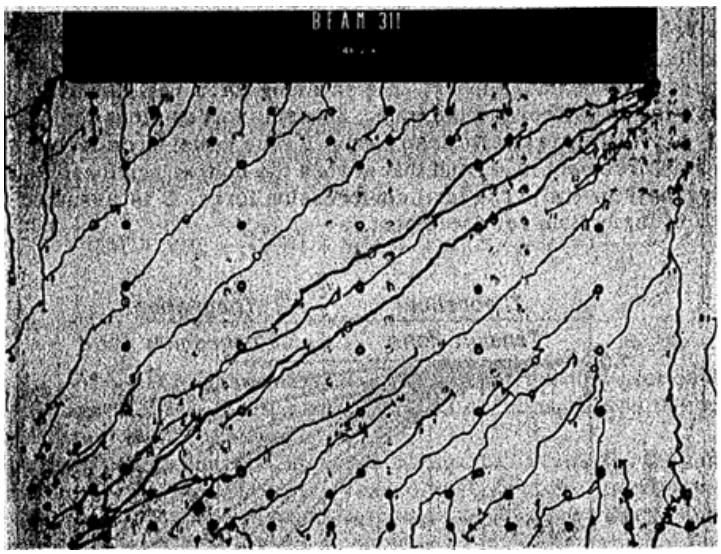

Figure 2-4 Crack pattern for beam with shear reinforcement ratio less than 1.65% (Paulay, 1971)

On other hand, Paulay and Binney (1974) investigated the behavior of conventional reinforcement coupling beams with span-to-depth ratio 1.3 under cyclic loading. They were designed such that the entirety of the shear resisting mechanism was provided by the stirrups without concrete contribution. The test result demonstrated that the failure of the RC coupling beam is sliding shear failure at the beam-wall interface although the diagonal tension failure was prevented in coupling beam, as demonstrated in Figure 2.5. This failure happens because after the few cycles the flexural crack at the boundary becomes wide and will interconnect, thus, the sudden sliding shear failure occurs at the boundary. The test results by Paulay and Binney (1974) was confirmed by later investigation (Paulay et al., 1978; Shiu et al., 1978; Tassios et al., 1996; Galano et al., 2000).

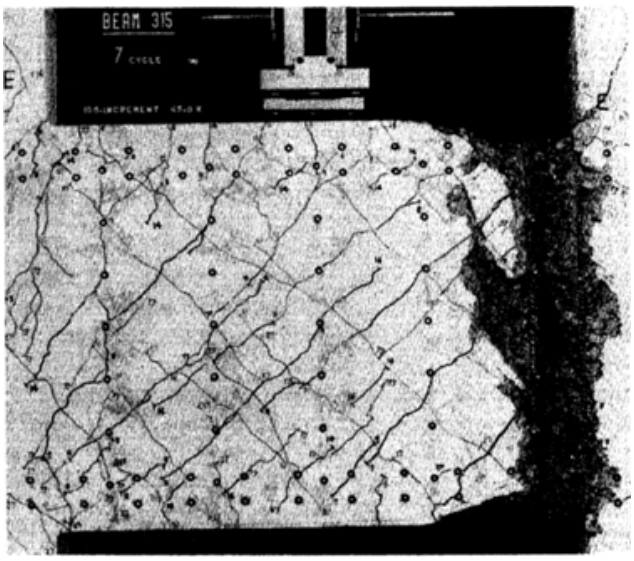

Figure 2-5 Sliding shear failure of conventionally reinforced coupling beams (Paulay et al., 1974)

Also, Shiu et al. (1978) reported that the sliding shear failure happens when the shear stress range is 3.5 to $6\sqrt{f_c'}$. Therefore, providing additional longitudinal bars at the intermediate depth of the coupling beam can improve the hysteresis response and delay the sudden sliding shear failure. However, if the shear stress is more than $6\sqrt{f_c'}$, the additional longitudinal bars are not effective (Scribner and Wight 1978; Shiu et al. 1978).

Based on the inadequate ductility and failure mechanisms of conventional coupling beams, a new detailing consisting of diagonal reinforcement cages, enable whole shear force to be transferred by diagonal bars was suggested by Paulay and Binney (1974). Their testing program was the first to show the effectiveness of diagonal reinforcement for large-scale coupling beam specimens subjected to reversed cyclic displacement. In this scheme, reinforcement was placed diagonally to enable the beam to

act as a cross bracing with equal diagonal tension and compression capacity and transfer all the shear force. Horizontal and vertical reinforcement was distributed for cracking control. To verify this reinforcement scheme, Paulay and Binney (1974) tested three diagonal reinforcement coupling beam specimens with span to ratios of 1.3 and 1 under reversed cyclic loading. Test results showed that diagonal reinforcement detailing can prevent diagonal tension and sliding shear failure and significantly improved the ductility and energy dissipation capacity compared to conventional detail for coupling beam subjected to reversing cyclic loading, as shown in Figure 2.6.

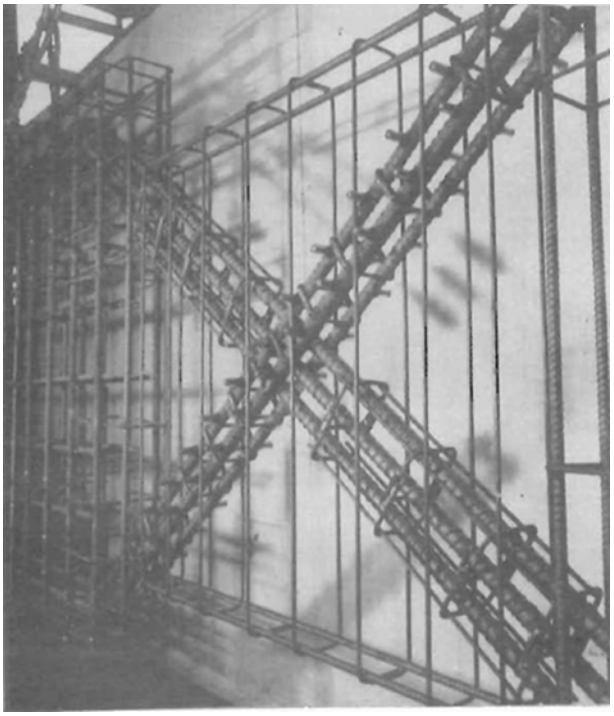

Figure 2-6 The reinforcing cages for diagonally reinforced coupling beams (Paulay et al., 1974)

All three specimens failed due to buckling of the compression bars, association with concrete crushing at the corner of the beams. Therefore, it was recommended that closely spaced stirrups be provided around the diagonal bars, similar that used in RC

column, to delay bar at large displacement reversals. In addition, the diagonal bars must be adequately anchored in the walls to prevent potential bar slippage problems. The suggested design procedure for diagonal reinforcement coupling beam is demonstrated in Figure 2.7.

$$T_u = C_u = A_s f_y \qquad \text{[Equation 2-1]}$$

$$V_u = 2T_u \sin\alpha \qquad \text{[Equation 2-2]}$$

$$A_s = \frac{V_u}{2 f_y \sin\alpha} \qquad \text{[Equation 2-3]}$$

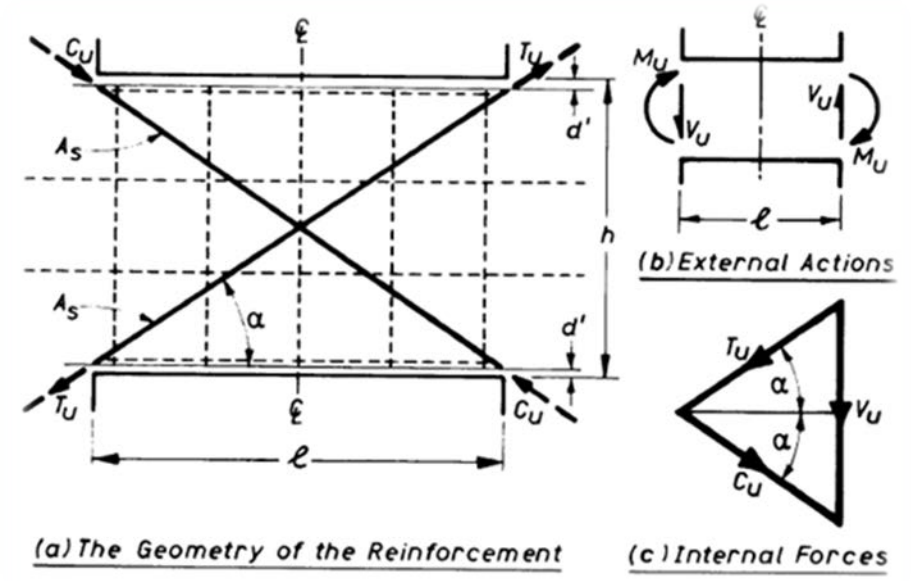

Figure 2-7 Principal Dimensions used in the design of coupling beam (Paulay et al., 1976)

Also, Paulay et al. (1976) tested two one-quarter scale diagonally reinforced coupling beam with span-to-depth ratios of 1.25. The experimental result was confirmed that the new detail proposed with Paulay and Binney (1974) show the ductile behavior for coupling beam and the failure was due to buckling of the compression bars.

Shiu et al. (1978) tested eight coupling beam specimens with three different reinforcement detailing and span-to-depth ratios of either 1.4 or 2.8 to evaluate strengths, ductility, and energy dissipation capacities of coupling beams subjected to cyclic loading. The reinforcement layouts are shown in Figure 2.8. In the first set, performance of three beams with conventional reinforcement was investigated. Based on previous research (Paulay, 1971), stirrups were designed to carry the entire shear force in the conventionally reinforced specimens. According to the test result, the coupling beam with conventional arrangements did not show adequate performance and failed by sliding shear failure, so, the stirrups could not eliminate this failure because vertical cracks propagated across the entire depth at the end of the beam. The second set consisted of three beams with diagonal bars in the hinging regions and it is called rhombic reinforcement. The diagonal bars are designed to carry the entire shear force. The rhombic reinforcement could prevent the sliding shear failure in coupling beam but the beam did not show desirable improvement in performance due to crushing and spalling the concrete within the region of diagonal reinforcement. The third set was included two coupling beams with full-length diagonal reinforcement and span-to-depth ratios of 2.5 and 5. In the full-length diagonal reinforcement coupling beams, a single bar in one direction and two bars in the opposite direction were used and stirrups were designed to contain concrete in the core during reversals and to prevent buckling of the diagonal bars. The test results confirmed that the full-length diagonal reinforcement significantly improved ductility, and energy-dissipation capacity of the coupling beam with small aspect ratio. The full-length diagonal bars failed due to buckling and subsequent fracture of the diagonal bars. The diagonal reinforcement improves the ductility of the coupling beams but it has construction difficulty.

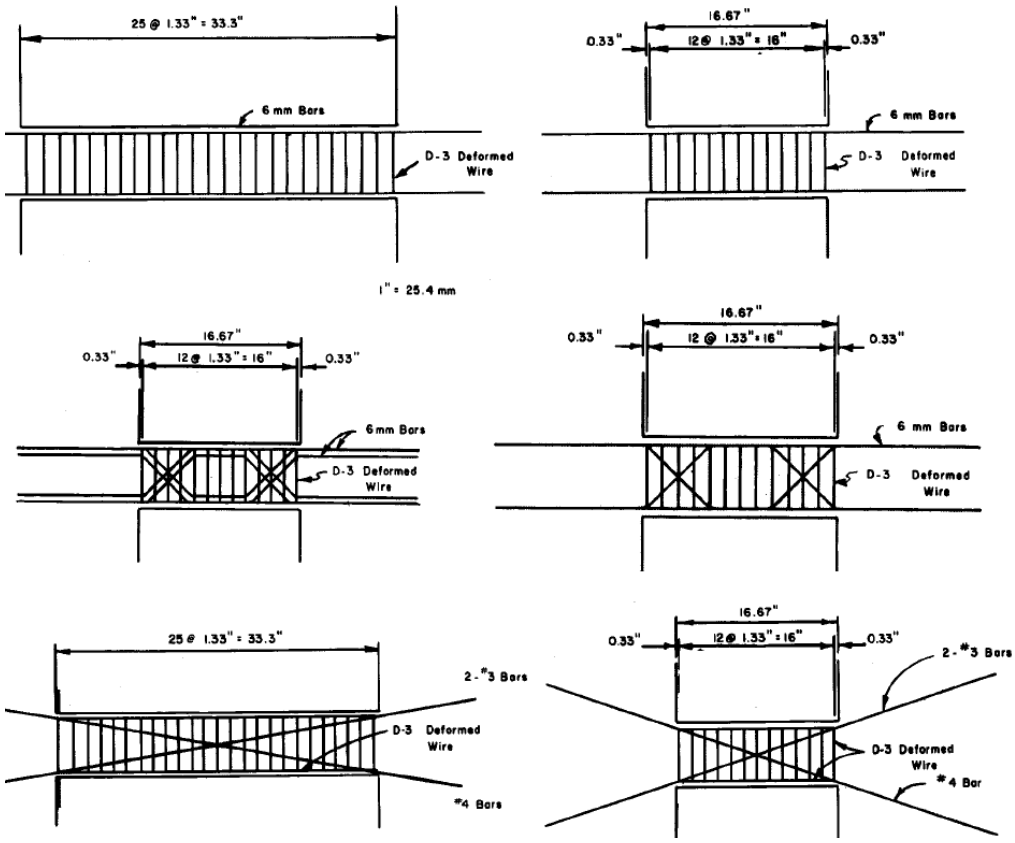

Figure 2-8 The reinforcement details for coupling beams (Shiu et al., 1978)

Tegos and Penelis (1988) proposed a new detailing, such as form a rhombic truss, for coupling beam. They tested eighteen specimens with new detailing, three specimens with diagonal reinforcement, and three specimens with conventional arrangement. All the specimens had the span-to-depth ratios between 2 to 5, as shown in Figure 2.9. It was concluded that the failure occurred due to buckling of the bars under compression and the rhombic arrangements performed satisfactorily in a manner similar to diagonally reinforced coupling beam.

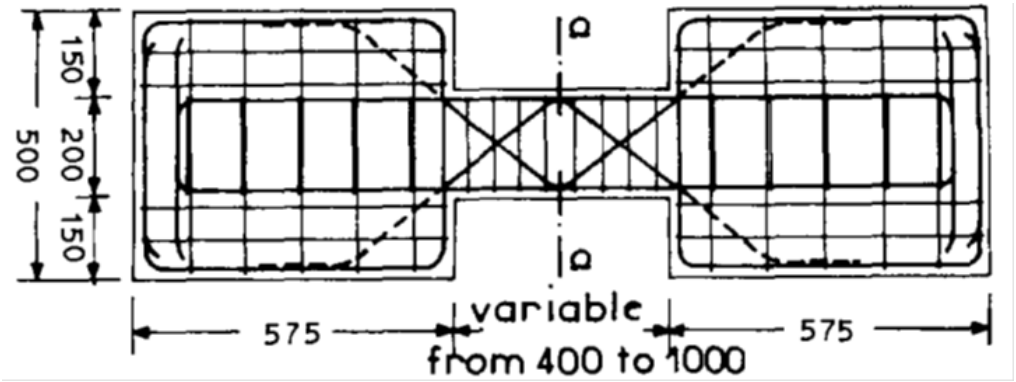

Figure 2-9 Rhombic arrangements for coupling beam (Tegos et al., 1988)

Tassios et al. (1996) tested ten half-scale specimens consisting of three different alternative reinforcement layouts and Conventional and diagonally reinforced coupling beam to evaluate the possibility of alternative configuration and compare the behavior of them with conventional and diagonally reinforced coupling beam. These specimens had span-to-depth ratios 1.0 and 1.7 as shown in Figure 2.10. The first trial was the rhombic layout, which used additional bent-up bars intersecting at the mid-height of the beam, aimed to improve the sliding resistance without significantly increase the flexural capacity at the beam ends. The second and third trial contained long and short dowels across the ends of the beams, which were expected to prevent sliding shear failure at the beam-wall boundaries. According to the result, conventional reinforcement detailing did not show adequate performance for short coupling beams subjected to high shear stresses and failed in diagonal tension along the main diagonal and shear-compression failure at the end of the beam. The specimen with rhombic layout lids to improve the overall behavior of the coupling beam compare to the conventional coupling beam details; but it failed by bond-splitting due to inadequate anchorage of the bars. The specimen with dowels could help to prevent the sliding at the beam ends. However, this arrangement could not prevent shear-compression failure in the beam, therefore, exhibited inadequate energy

dissipation. The diagonally reinforced specimen failed due to buckling of the diagonal bars close to end of the beam. Hysteresis loops indicated that the diagonally reinforced specimen showed the best performance in terms of shear resistance and energy dissipation compare to other alternatives detailing. In conclusion, for coupling beams with a span-to-depth ratio less than 2.0, diagonally reinforced over the full beam showed best performance in terms of shear resistance and energy dissipation and still found the best solution.

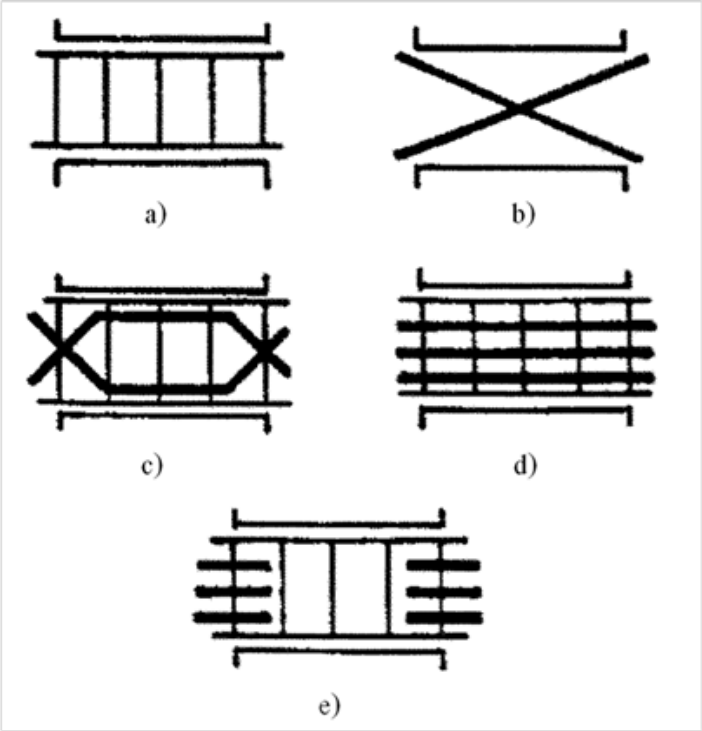

Figure 2-10 a) Conventional reinforcement, b) Diagonal reinforcement, c) Bent-up reinforcement, d) Conventional reinforcement with long dowels, and e) Conventional reinforcement with short dowels

(Tassios et al., 1996)

Galano and Vignoli (2000) have tested fifteen short coupling beams with shear-span-to-depth ratios of 1.5 and four different reinforcement layouts under monotonic and cyclic loading. They consisted of the conventional layout, diagonal (with and without confinement), and inclined bars in a rhombic layout, as demonstrated in Figure 2.11. Test results showed that the beams with diagonal or rhombic reinforcement layouts behaved better than beams with longitudinal arrangement of the steel bars. When the test results of diagonal and rhombic detailing were compared, it is concluded that the rhombic layout had better energy dissipation capacity and highest rotational ductility value and exhibited less strength and stiffness degradation but this claim contradicts the finding by Tassios et al. (1996).

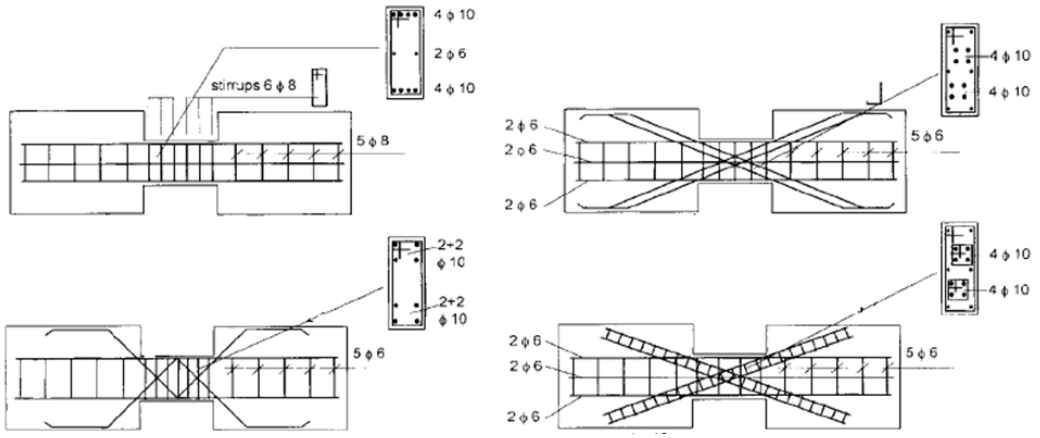

Figure 2-11 The reinforcement layout of the coupling beams (Galano et al., 2000)

Typical aspect ratios of the coupling beam based on the opening are around 2.4 for residential buildings and 3.33 for office buildings. Most of the coupling beam tests before 2000 were with span-to-depth ratios less than 2 and it was found the diagonal reinforced coupling beam can improve the ductility and stiffness of the beam compare to the conventional details. Due to the lack of the results to evaluate the efficiency of the

diagonal coupling beam with span-to-depth ratio more than 2, which case to shallow angle of the diagonal bars, several studies were performed after 2000.

Adebar et al. (2001) performed the full scale coupling beam with span-to-depth ratios 2.75. The test result showed good ductility and stable hysteresis behavior of the diagonal reinforced coupling beam and the specimen failed due to bucking of the diagonal bars and crushing of the concrete core.

Recently Naish et al. (2009) proposed a new detailing for slender coupling beams, span-to-depth ratios raging 2 to 4, to improve the constructability and design while maintaining adequate strength and ductility to compare the new detailing with the diagonal reinforcement and conventional coupling beam. In this arrangement, permits confinement of the entire section, rather than only the diagonal reinforcement to simplify design and construction of the beam (Figure 2.12). Eight half-scale coupling beams with span-to-depth ratio of 2.4 and the rest had a ratio 3.3 were tested under reversed cyclic loading in order to evaluate the performance of coupling beams with new details (ACI 318-08) and old details (ACI 318-05). Five of them had a span-to-depth ratio of 2.4 and the rest had a ratio 3.3. In all specimens two groups of diagonal bars were provided as truss members, therefore, the first group act as the tension member and the second group performs as the compression member and two different transverse reinforcement arrangements, Full section confinement and stirrups along the diagonal bars were used for these specimens. Test results show that "the new detailing approach provides equal, if not improved behavior as compared to the alternative detailing approach, that simple modeling approaches reasonably capture measured force versus deformation behavior, and that including a slab had only a modest impact on strength, stiffness, ductility, and observed damage" (Naish et al., 2009).

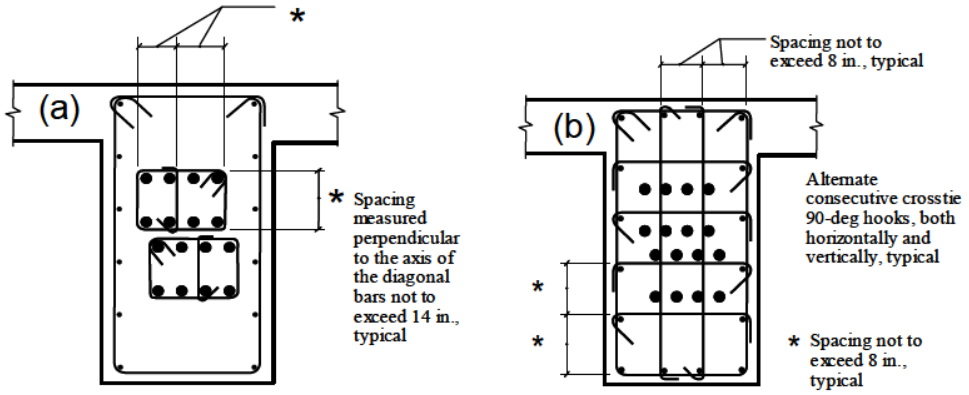

Figure 2.12 a) Confinement of individual diagonals; and b) Full Section Confinement (Naish et al., 2009)

On the other hand, Harries et al. (2004) reported that a practical design of diagonally reinforced concrete coupling beams according to ACI Provisions is difficult to achieve, especially for those have span to depth ratio more than 2. They designed several diagonal reinforcement coupling beams with different span to depth ratio, shear stress and concrete strength to evaluate their constructability (Figure 2.13). All the specimens had the span-to-depth ratios ranging from 1 to 4 and the shear stress was assumed between $6\sqrt{f_c'}$ and $14\sqrt{f_c'}$, according to the elastic analysis by Harries et al. (2004). The results showed that bundled bars should be provided for diagonal reinforced coupling beam with span-to-depth ratio more than 2 and shear stress equal or more than $10\sqrt{f_c'}$ which leads to increasing the height of the hoops around the diagonal bars due to required spacing between bundles. Consequently, the diagonal bars have a lower angle of inclination, and therefore require extra reinforcing steel which ultimately increases the difficulty of construction. On the other hand, bundled bars result an increased width of the hoops around the diagonal bars due to clear distance between reinforcement in order for one diagonal element to pass through the other, increasing the width of the beam, which

controls the wall width. Additionally, bundled bars and the development of them will result in more congestion in pier wall and it is very challenging and time-consuming to accommodate them through the congested vertical and horizontal bars in the wall's boundary with the right angle which may cause to eliminate the vertical and horizontal bars in pier wall. Finally, they claimed that it is simply not possible to design a practically constructible diagonally reinforced coupling beam having shear strength of $10\sqrt{f_c'}$, according to ACI 318-05, therefore, shear stress equal or less than $6\sqrt{f_c'}$ was recommended for practical upper limit of shear stress to design the diagonally reinforced coupling beams.

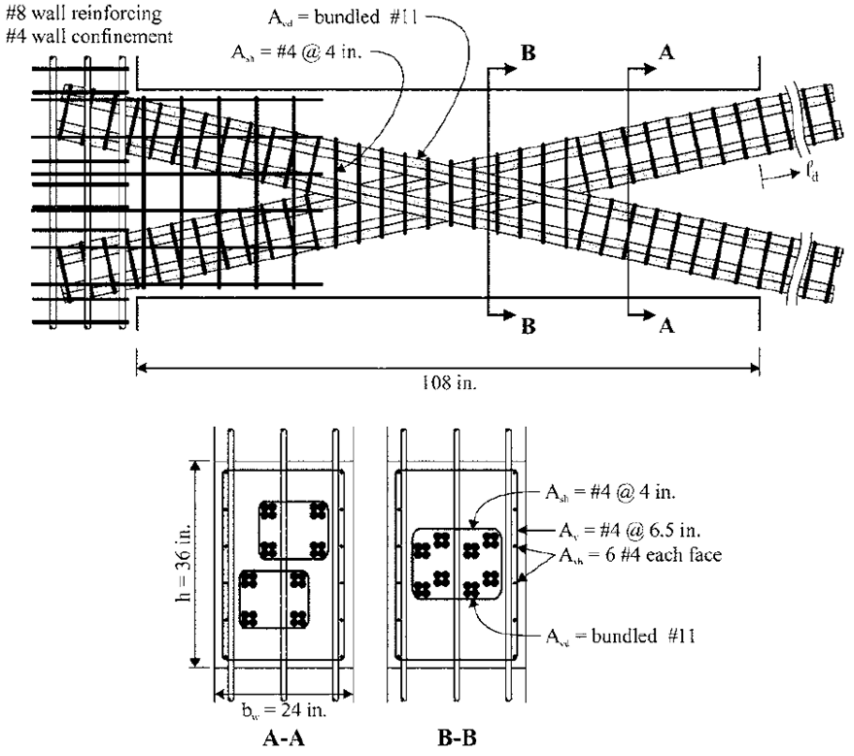

Figure 2-13 Example of the diagonal coupling beam with span-to-depth ratio 3 (Harries et al., 2004)

2.1.2 Composite Coupling Beams

Steel or steel-concrete composite beams could be an alternative to diagonally reinforced coupling beam due to difficulties associated with designing and constructing diagonally reinforced concrete coupling beams, as shown in Figure 2.15.

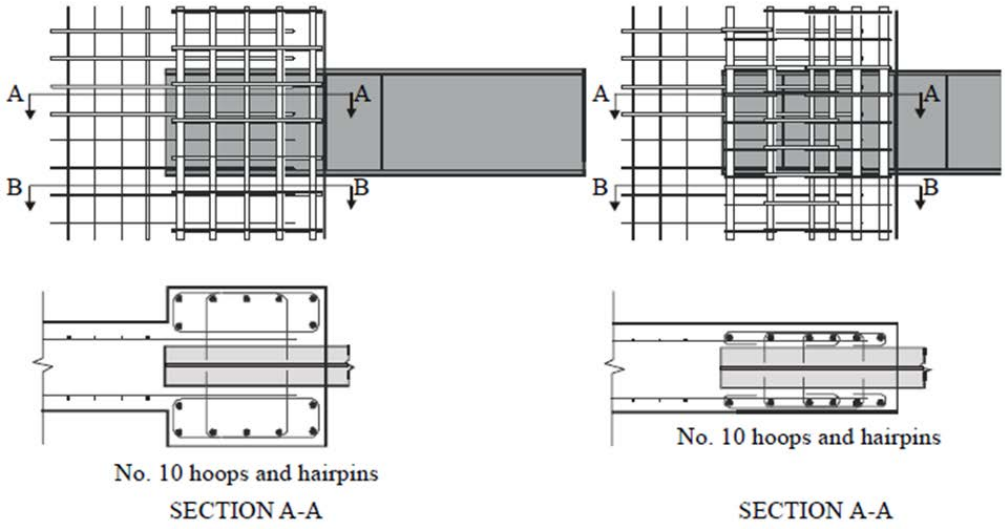

Figure 2-15 Composite coupling beams layout (Harries et al., 1998)

Several studies evaluated the performance of steel or steel-concrete composite coupling beams by Paparoni (1972), Shahrooz (1992), Shahrooz et al. (1993), Harries et al. (1993), Gong et al. (1998), Harries et al. (2000), and Park et al. (2005). Test results indicated that these alternatives have shown excellent hysteresis response, ductility, and good energy dissipation under cyclic loading; when the steel coupling beam is properly embedded in concrete shear walls and fully anchored to the adjoining structural walls. In addition, based on the research performed by various researchers (Shahrooz et al., 1998, Gong et al., 2001a, Gong et al., 2001b, and Lam et al., 2005), using the wide flange section or steel plate in the concrete could be desirable alternative compare to the plain steel for diagonally reinforced concrete coupling beam due to provide the lateral

stability to prevent undesirable web-buckling and flange instability at higher deformation levels. However, these steel and steel-concrete coupling beams had construction difficulties because they require the long embedment length in to the concrete shear walls at the boundary. The embedment length interferes with the stirrups and longitudinal reinforcement in the wall boundary; therefore, eliminating some of them which led to redesign the structure shear wall.

2.1.3 HPFRC Coupling Beams

Another alternative is proposed by Canbolat et al. (2005) to use the high-performance fiber-reinforced cementitious composites (HPFRC) in the design of short coupling beam with span-to-depth ratio equal to 1.0 to simplify the reinforcement requirements in diagonally reinforced coupling beam. An alternative design consisting of four precast HPFRC coupling beams with different reinforcement configurations was experimentally investigated. The first specimen was made of conventional concrete with diagonal reinforcement based on the ACI Building Code (ACI 318-02, 2002) requirements; the second specimen had precast HPFRC coupling beams without diagonal bars. Also, third specimen included precast diagonally reinforced HPFRC coupling beams without confinements and the fourth specimen had precast diagonally reinforced HPFRC coupling beams without confinements that the diagonal bars were bent at the beam ends to ease placement it in to the walls, as shown in Figure 2.16. The test results showed that HPFRC provided abundant confinement to the diagonal reinforcement, eliminating the need for transverse reinforcement to prevent buckling, thus simplifying the beam construction process and increasing the shear resistance and energy dissipation.

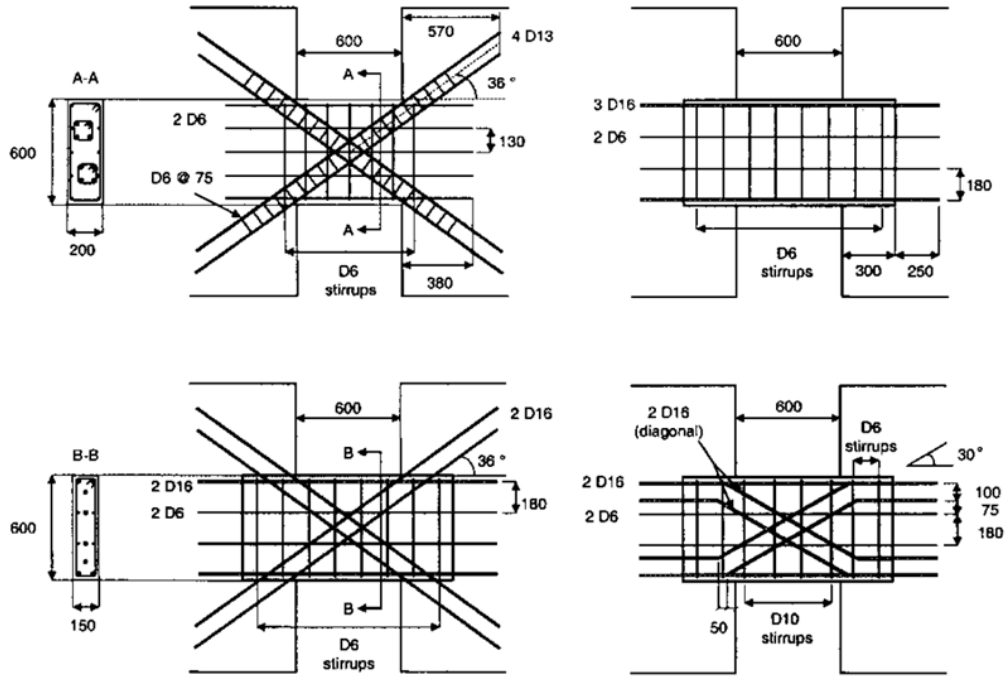

Figure 2-16 HPFRC coupling beams schemes (Canbolat et al., 2005)

Lequesne et al. (2010) reported on an experimental program that consists of three precast coupling beam specimens with span-to-depth ratio equal to 1.75 to investigate the performance of the fiber-reinforced concrete (HPFRC) for coupling beam. In these specimens, the diagonal reinforcement was bent before entering the wall that make easier details to put the coupling beam reinforcement through the reinforcement in the walls. No confinement reinforcement was used around the diagonal bars in all three specimens. To enhance the sliding shear resistance and move possible flexural damage from the cold joint between the precast beam and cast-in-place walls, two U-shaped reinforcing bars extending six inches into the coupling beam and straight dowel bars was used at these specimens. The details of three specimens are demonstrated in Figure 2.17. Test results confirmed the use of HPFRC allowed elimination of transverse reinforcement requirements for diagonal bars and ensure stable hysteresis behavior of

coupling beams subjected to large displacement reversals. From a construction viewpoint, the success of these connection details, which do not interfere with wall reinforcement, makes precast HPFRC a more attractive option for coupling beams than structural steel member.

Furthermore, Setkit et al. (2012) tested six high-performance fiber reinforced concrete (HPFRC) coupling beams with span-to-depth ratio 2.75 and 3.3 under large displacement reversals. The aim was 70% reducing or totally eliminating diagonal bars and substantially reduces confinement reinforcement. The results showed excellent damage tolerance, and strength and stiffness retention capacity for slender HPFRC coupling beams. Moreover, tests results showed that diagonal reinforcement can be completely eliminated without a detrimental effect on seismic behavior.

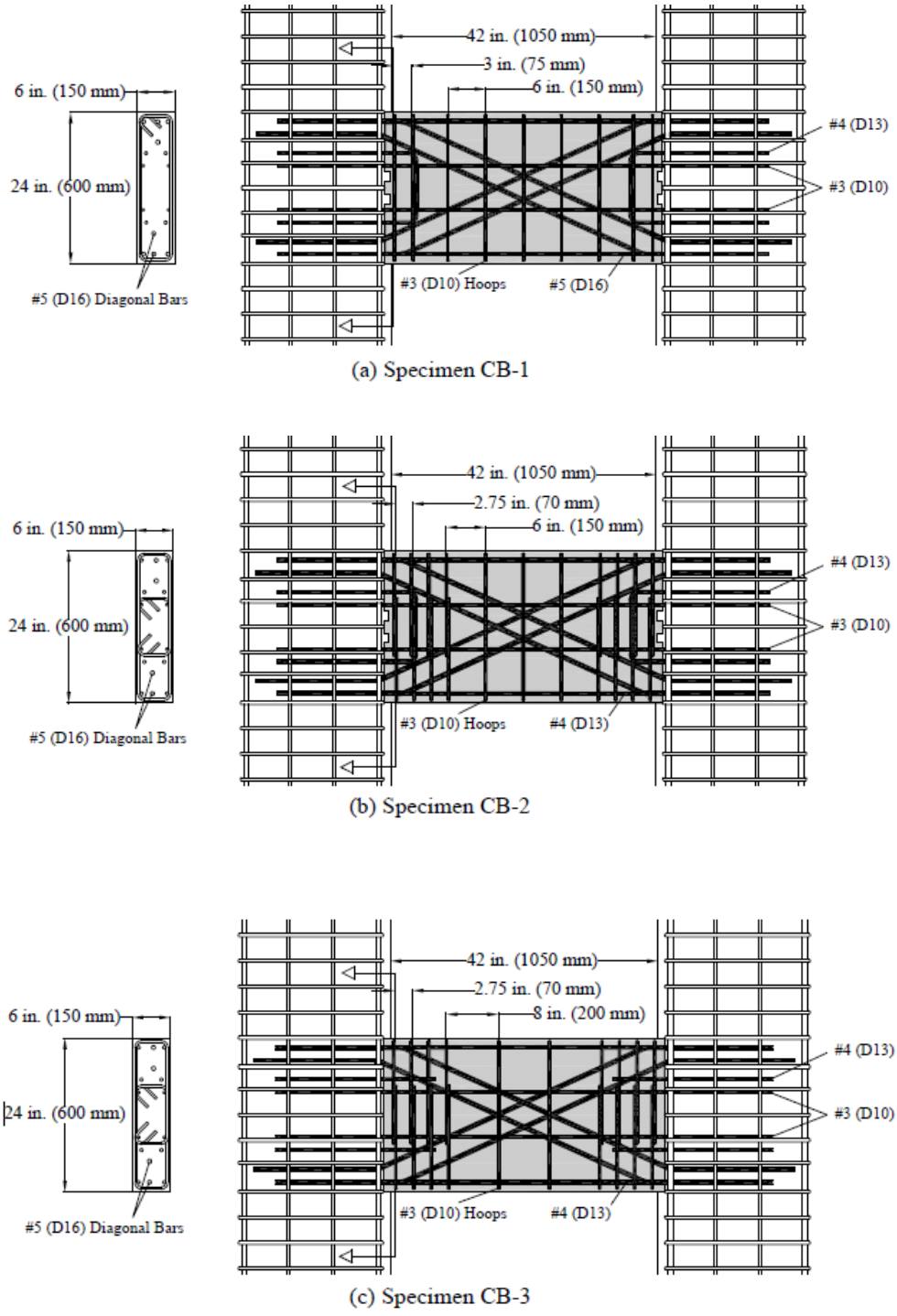

Figure 2.17 Reinforcement layouts for HPFRC coupling beams (Lequesne et al., 2010)

2.1.4 Provisions For Design Of Coupling Beams In ACI 318-14

Requirements for the design of coupling beams in ACI 318-14 (ACI 2014) are provided in Chapter 18 (18.10.7). Coupling beams with clear span-to-depth ratios greater than four, $(\ell_n/h) \geq 4$, designed as flexural member. When the span-to-depth ratio of coupling beams is less than four and greater than two, $2 \leq (\ell_n/h) \prec 4$, it is allowable to use either the conventional or diagonal reinforcement for coupling beams (Sect. 21.9.7.3). When span-to-depth ratio is less than 2, $(\ell_n/h) \prec 2$, and the shear force, V_u, is more than $4\sqrt{f_c'}A_{cw}$, sliding shear failure may govern. Therefore, the use of two intersecting groups of diagonal bars, symmetrically placed about the beam mid-span, is required. Two different transverse reinforcement details are provided in the ACI 318-14. In the first detail, the individual diagonals are confined in accordance with ACI code Section 18.10.7.4, as illustrated in Figure 2.17 (a). This detail has been in the 2005 and earlier editions of the ACI code. In an alternative detailing, which was introduced in the 2008 code, the entire cross-section of the coupling beam is by transverse reinforcement (Section 18.10.7.4), as shown in figure 2.17 (b). This new option improves the constructability of the coupling beam, especially for coupling beams with relatively narrow webs.

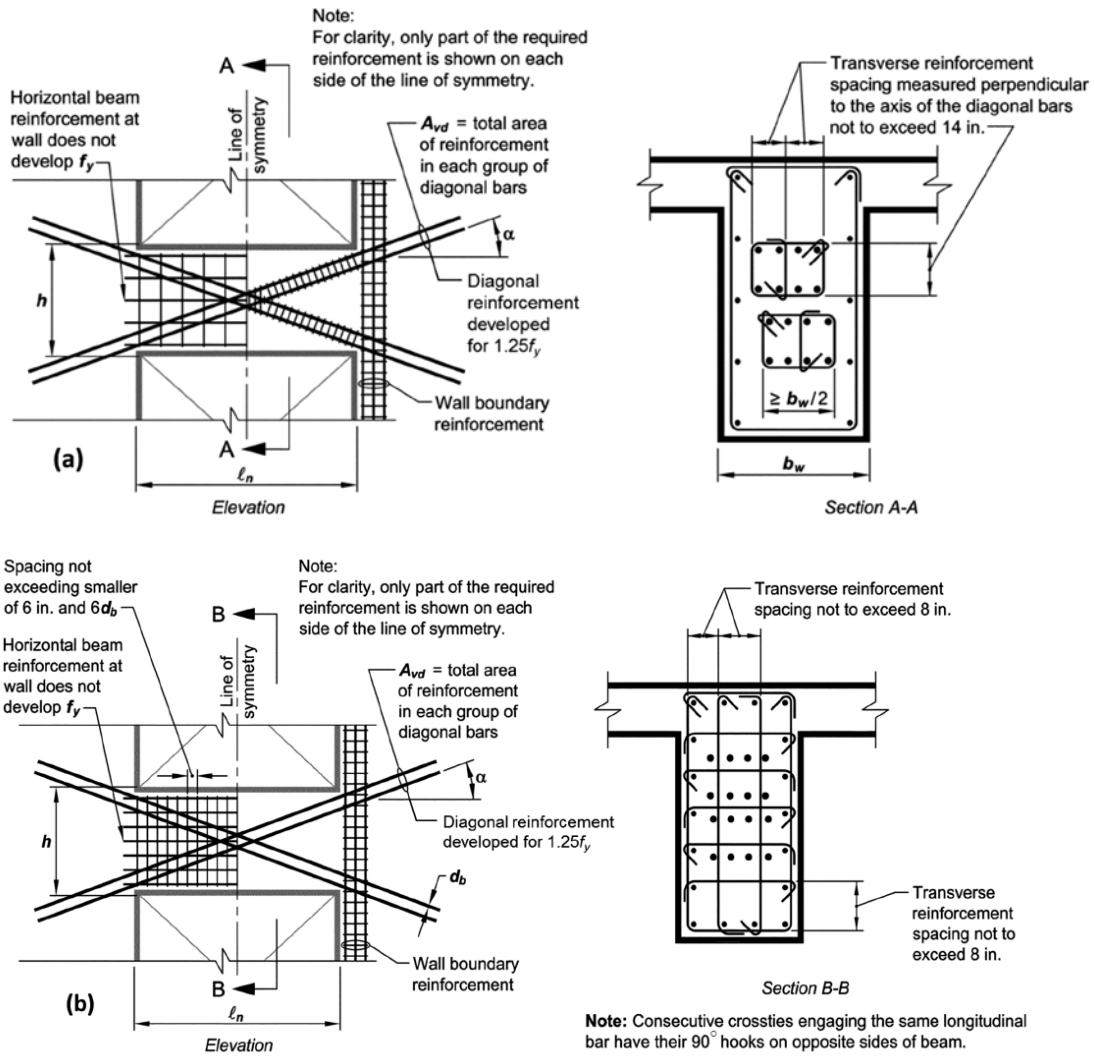

Figure 2-18 Coupling beams details with diagonally reinforcement (ACI 318-14)

2.2 Second Phase: Reinforced Concrete Rectangular Squat Wall

Reinforced concrete walls with a ratio of height-to-length ratio smaller than two are widely used in in squat buildings such as parking structures and in high-rise structures, when the walls extend only a few stories above the foundation level, and nuclear structure to resist the lateral load, as shown in Figure 2.18 (Paulay et al., 1981, Whyte et al., 2013). The behavior of properly design squat walls with height-to-length less than 1.0 is dominated by shear while the behavior of the squat walls with height-to-length 1.0 to 2.0, usually is dominated by an interaction between shear and flexure.

Figure 2-18 Shear wall in a nuclear reactor, Olkiluoto, Finland

(http://www.envirospace.com)

Three principal shear failure modes are observed in squat wall subjected to the lateral loading, namely, diagonal tension failure, diagonal compression failure, and sliding shear failure (Paulay et al., 1992). Diagonal tension failure is generally observed when

horizontal shear reinforcement is inadequate. In this failure usually the inclined cracks developed from corner to corner of the specimen as shown in Figure 2.19 (a). Also, diagonal tension failure can occur along a steeper failure plane, as shown in Figure 2.19 (b) when horizontal and vertical shear reinforcement is not sufficient.

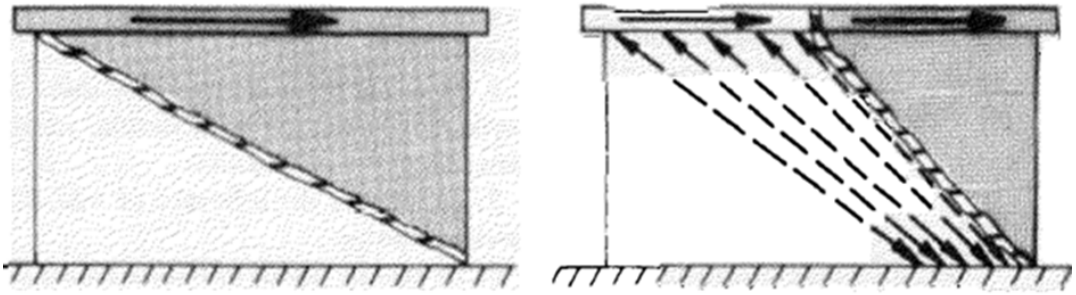

Figure 2-19 Diagonal tension failures (Paulay et al., 1992)

Squat walls with high shear stress and sufficient horizontal reinforcement, may crush under diagonal compression. This failure in barbells and flanges wall with the high flexural strength is more common, due to high flexural strength, than wall with rectangular cross section. In this case moderate axial load can help to keep the crack widths small. Therefore, the maximum shear stress in the section of the wall is limited to ensure that diagonal compression failure will not occur.

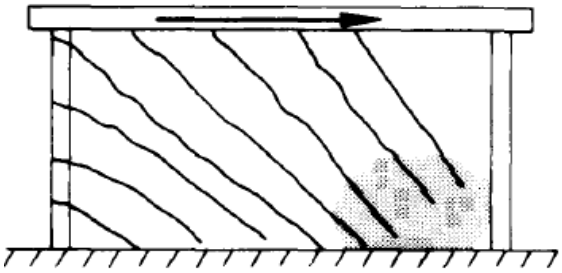

Figure 2-20 Diagonal compression failures (Paulay et al., 1992)

Even though diagonal tension and compression failure can be avoided, heavily reinforced walls subjected to cyclic load may be failed due to sliding shear failure Figure 2.21. The sliding shear failures are observed after significant yielding has occurred in the flexural reinforcement then sliding displacement can occur at the base of the wall or along flexural cracks that interconnected and form a continues. Paulay et al. (1982) reported that the increase the shear stress and low axial compression force can increase the sliding shear deformation. Also, Corley et al. (1981) stated sliding shear failure is predicted when the nominal shear stress is between $3\sqrt{f_c'}$ to $7\sqrt{f_c'}$ (psi).

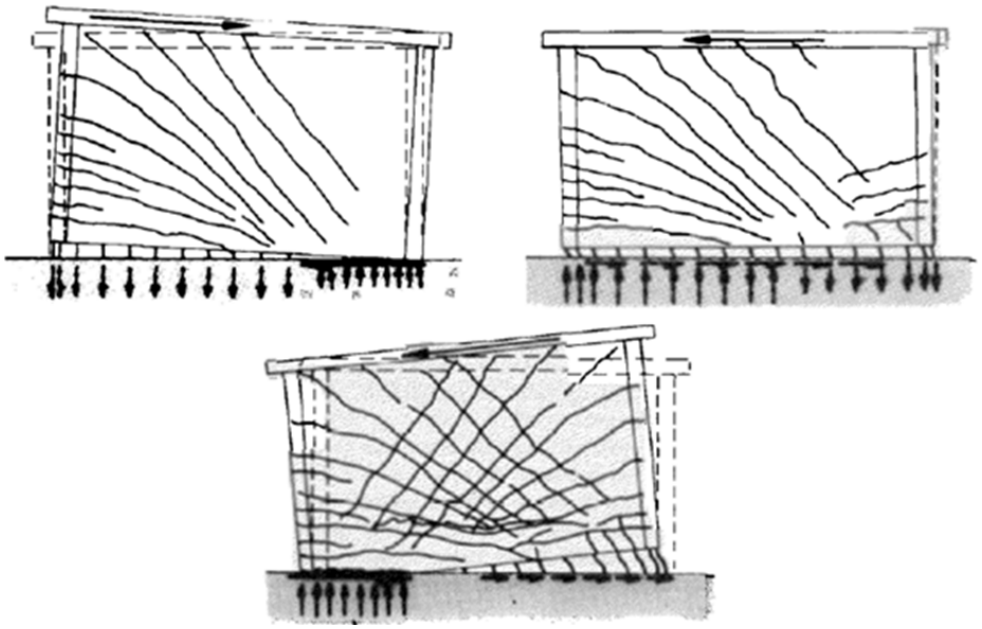

Figure 2-21 Sliding shear failures (Paulay et al., 1992)

Cardenas et al. (1980) tested seven rectangular cross section walls with moment-to-shear ratio 1.08. One of the walls was loaded cyclically, whereas the rest were loaded monotonically. The amount of vertical and horizontal reinforcement was investigated in this study. The test result showed that the shear strength of the wall is

depended to both vertical and horizontal reinforcement. Also, very limited drift, 0.5%, was reported at the failure of the specimen that subjected to the load reversal. In addition, Cardenas was proposed the $10\sqrt{f_c'}$ (psi) for the upper limit of the shear stress of the squat wall.

Synge (1980) and Paulay et al. (1982) reported on the result of two rectangular reinforced concrete walls with moment-to-shear ratio 0.6. One of the wall with rectangular cross section and one of the flanged wall included diagonal web reinforcement to evaluate the effect of the diagonal reinforcement in sliding shear resisting, as shown in Figure 2.22.

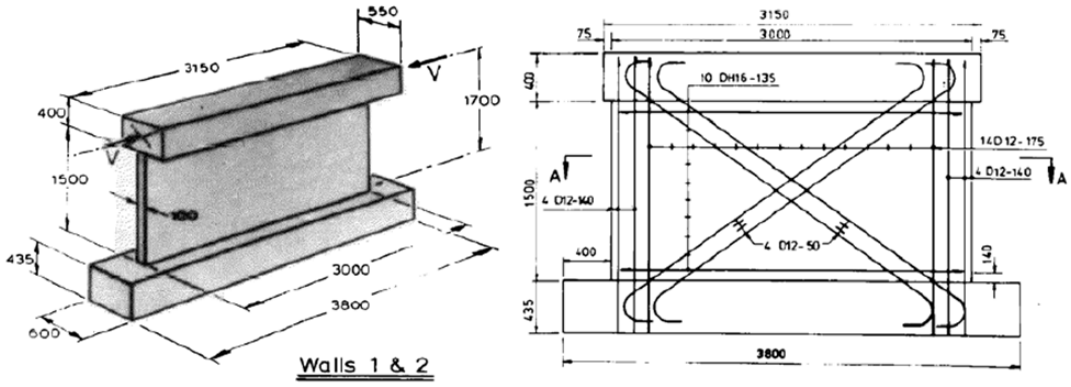

Figure 2-22 Squat wall specimen layouts (Paulay et al., 1982)

To prevent the early buckling of the longitudinal reinforcement, transverse reinforcement in the wall boundary was provided. The rectangular wall with and without diagonal reinforcement in the web attains its peak strength during the second cycle to a drift of 0.6% and 0.8%; its strength and stiffness degrade rapidly with repeated cycling (Figure 2.23(a),(b)). The peak shear strength for the specimens was in the range of 6.2 $\sqrt{f_c'}$ to $6.8\sqrt{f_c'}$ (psi). The results showed the better performance in term of energy

dissipation capacity and control the sliding shear was observed in the wall where diagonal reinforcement was used.

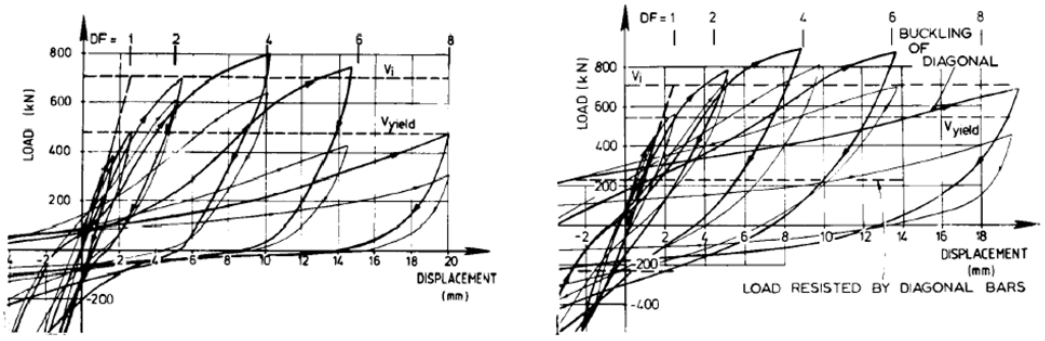

Figure 2-23 Hysteresis response of rectangular wall (Paulay et al., 1982)

a) Rectangular wall without diagonal reinforcement,

b) Rectangular wall with diagonal reinforcement

Thirteen rectangular reinforced concrete walls with transverse reinforcements in the wall boundary region and with moment-to-shear ratios 1.1 to 2.12 were tested by Lefas et al. (1990). The reinforcement details are shown in Figure 2.24. Seven walls were tested under the combined action of a constant axial and a horizontal load monotonically and the other specimens were loaded monotonically to investigate the effect of the axial load, aspect ratio, and horizontal reinforcement on the wall behavior. The result shown that wall with moment-to-shear ratio 1.1 sustains high shear stresses from $8\sqrt{f_c'}$ to 12.5 $\sqrt{f_c'}$ (psi). Also, the range of the peak shear stress for wall with moment-to-shear ratio 2 was from $4.5\sqrt{f_c'}$ to $7.7\sqrt{f_c'}$ (psi). Drift at failure ranged from 1% to 1.6%. It is concluded that the axial load increases the shear strength in the wall. Also, author reported that the horizontal reinforcement ratio has the small effect on the shear strength of the wall.

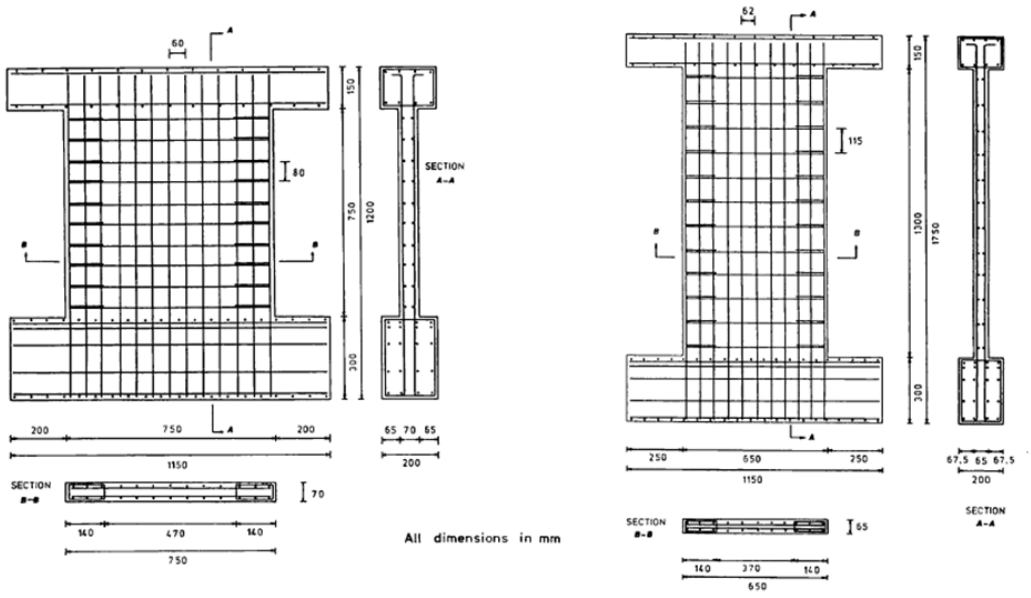

Figure 2-24 rectangular wall specimen details (Lefas et al., 1990)

Maier et al. (1985) tested three walls with rectangular cross section under monotonic load and with moment-to-shear ratios 1.02. Drift at failure was approximately 1%. It was concluded that the increasing the amount of the horizontal reinforcement ratio had a small effect on the shear strength capacity of the wall, while could improve the deformation capacity of the specimen.

Pilette et al. (1987) tested two walls with rectangular cross-sections under the cyclic loading without axial load. The moment-to-shear ratio of each wall was 0.58. Both wall failed by sliding shear. The maximum shear stress for the first and second specimen observed $4.2\sqrt{f_c'}$ and $6.3\sqrt{f_c'}$ (psi) respectably. Drift at failure for first and second specimen was 1.2% and 1.6%.

Two walls with rectangular cross-sections with moment-to-shear ratios ranged between 0.82 and 1.09 were tested using cyclic loading by Doostdar et al. (1994). The researcher reported the wall failed by sliding shear. Also, the specimens were tested

under low shear stresses (2.6 $\sqrt{f_c'}$ and 3.4$\sqrt{f_c'}$ (psi)) and exhibited approximately 1.45% and 1.6% drift capacity.

Salonikios et al. (1999; 2000) tested eleven walls with rectangular cross section with moment-to-shear ratio of either 1.1 or 1.6 under cyclic loading. Four walls had cross inclined bars. In this study effect of the axial load and diagonal bars in the wall was investigated. In all of the specimens close hoops (1.7" center to center) was provided at the boundary. Peak shear stress was recorded during the test was between 2.4$\sqrt{f_c'}$ and 5.6$\sqrt{f_c'}$ (psi). Also, drift was between 0.9% and 1.9% for the moment-to-shear ratio 1.1 and 1.6 respectably. Hysteresis loop for LSW1, LSW2, and LSW3 is shown in Figure 2.25. All three specimens had vertical and horizontal reinforcement ratio more than 0.25%. LSW1 and LSW2 were tested without compression axial load. LSW3 is the same as the LSW2 but it was tested with compression axial load to evaluate the influence of the axil load on the behavior of the squat wall especially span-to-depth ratio less than 1. It is concluded that the compression axial load can improve the Drift capacity and shear stress of the wall (approximately 0.35%) with aspect ratio less than 1. The author reported that compression axial load could reduce the sliding deformation in LSW3 and it prevented the diagonal cracks open fast, therefore, the crack pattern is widespread in this specimen.

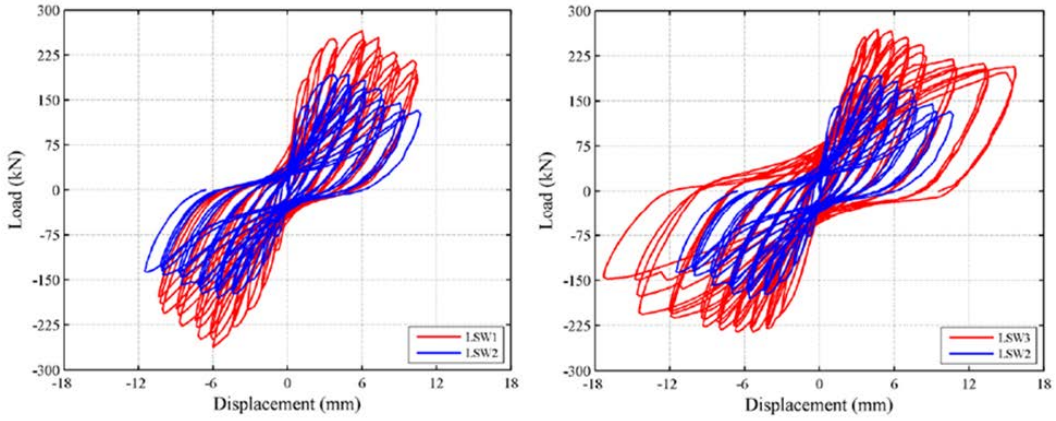

Figure 2-25 Hysteresis responses of Specimen SWL1, SWL2, SWL3 (Salonikios et al., 1999; 2000)

Four rectangular walls with moment-to-shear ratio 1.1 were tested by Lopes (2001) to investigate the amount and detailing of the horizontal and confinement reinforcement. Three specimen failed in diagonal tension and one specimen failed by web crushing. Maximum shear stress observed during the test was between $7\sqrt{f_c'}$ and $9.5\sqrt{f_c'}$ (psi). Also, drift capacity for all of the specimens was approximately 1% at the peak shear strength.

Hidalgo et al. (2002) reported on the tests of twenty-six walls with rectangular cross-section under cyclic loading without compression axial load. All walls moment-to-shear ratio ranged between 0.7 and 2. Due to the lateral load was applied at the mid-height of the wall, the moment-to-shear ratios of the walls were between 0.35 and 1. The test setup used in this study is shown in Figure 2.26. It was concluded that the distributed web reinforcement did not have effect on the maximum shear strength. Also, deformation capacity of walls decreases by decreasing the aspect ratio of the wall. Drift at maximum shear strength varies between 0.2% and 1.3%.

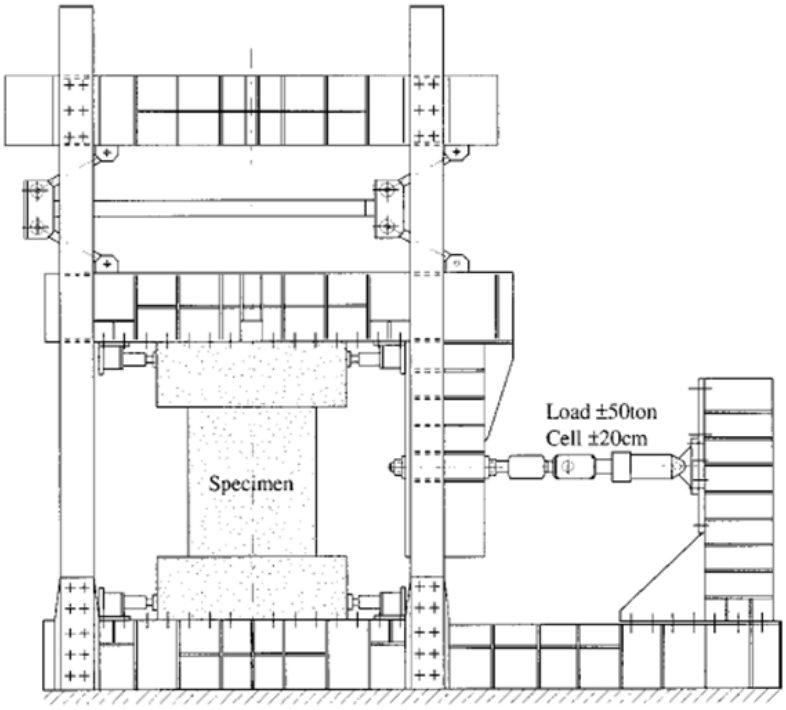

Figure 2-26 Test set up (Hidalgo et al., 2002)

Greifenhagen et al. (2005) tested four rectangular walls with moment-to-shear ratios of 0.69 under the loading reversal. The author reported that all of the walls failed by sliding shear. The result showed, the maximum shear stresses ranging were between 3.4 $\sqrt{f_c'}$ and $6.5\sqrt{f_c'}$ (psi). Also, drift at peak shear strength was varies between 0.2% and 1.3%.

Gulec et al. (2010) reviewed and cataloged the results of tests of 352 reinforced concrete squat walls. All of the specimens had the aspect ratio less than 2. Figure 2.27 showed the peak shear strength versus moment-to-shear ratio plot for all of the walls in this study.

The conclusions of this study for rectangular walls were:

1. The peak shear strength for walls with boundary elements is generally much higher than maximum shear strength of the rectangular walls.
2. The peak shear strength for rectangular walls is generally smaller than 10 $\sqrt{f_c'}$ (psi), which is upper limit of the shear strength in ACI 318-14.
3. Wood's (1990) equation provides the best estimates of peak shear strength for rectangular squat walls.
4. The shear strength upper limit in ASCE 43-05 (20 $\sqrt{f_c'}$ (psi)) was not reached by rectangular squat walls.

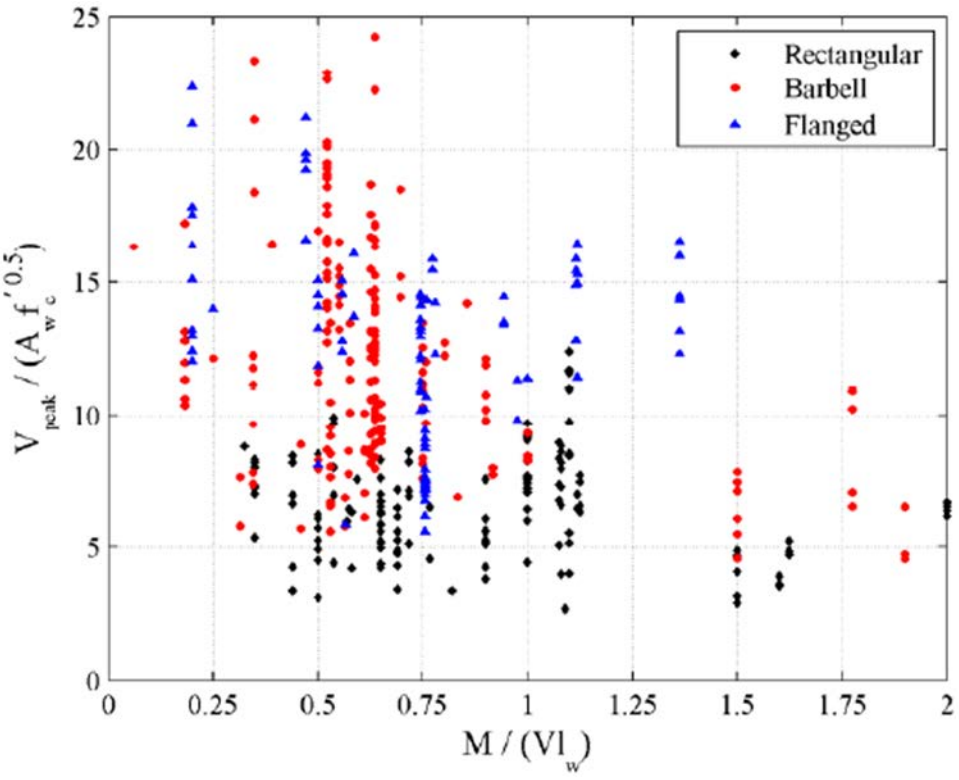

Figure 2-27 Peak shear strength versus moment-to-shear ratio (Gulec et al., 2010)

Four reinforced concrete walls under cyclic loading were tested by Athanasopoulou et al. (2012). All walls had the shear moment-to-shear ratios of either 1.2 or 1.5. Dimensions of test specimen are demonstrated in Figure 2.28. It was observed that RC wall with aspect ratio 1.2 under moderate shear stress exhibited a stable hysteresis behavior with the drift capacities of approximately 2%, whereas the shear stress in these wall increases approximately 0.35%, drift capacity decrease almost 50%. Therefore, it was concluded increasing the shear stress demand led to a decrease in drift capacity.

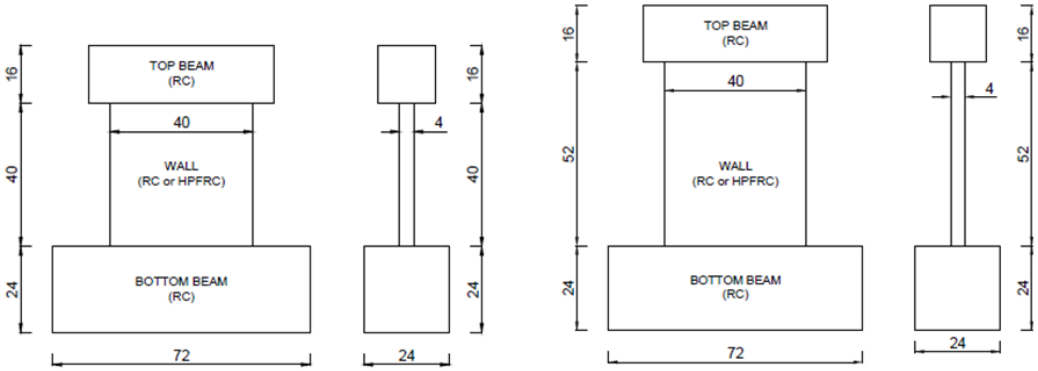

Figure 2.28 Dimensions of test specimen (Athanasopoulou et al., 2012)

Two walls with moment-to-shear ratio 0.5 were tested under the different ground motion level loading sequence by Whyte et al. (2013). The walls had 0.67% horizontal and vertical reinforcement ratios and a sliding shear failure reported for both walls. In First wall local buckling of the vertical wall reinforcement and opening of the hooks is observed. Also in second wall local buckling of the vertical wall reinforcement is reported but the hooks did not open. The maximum shear stress for the first and second wall was $5.41\sqrt{f_c^{'}}$ and $5.29\sqrt{f_c^{'}}$ (psi) respectively, which was corresponding approximately 0.6% drift in positive direction, as shown in Figure 2.29.

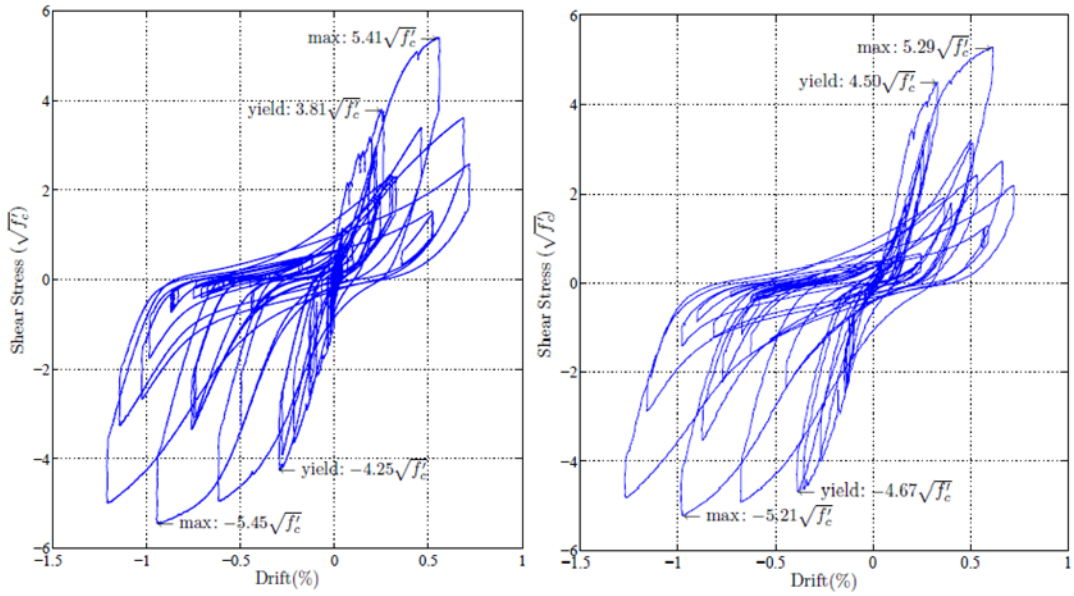

Figure 2-29 Hysteresis responses of Wall 1 and Wall 2 (Whyte et al., 2013)

Sakashita et al. (2014) tested five rectangular walls under cyclic reversed loading combined with axial load. All walls moment-to-shear ratio ranged between 1.1 and 1.7. Main parameters in the tests were the wall cross section, the effect of transverse reinforcement ration at the boundary, and aspect ratio of the wall. In the rectangular section walls the maximum drift was 1.4% while the shear stress was $5\sqrt{f_c'}$ (psi). By increasing the shear stress and changing the detailing of the end region the drift was decreased to 0.7%. It was concluded that the end region of the wall should be well confined to sustain large drift capacity.

Twelve rectangular walls were tested by Bismarck et al. (2015). All walls Moment-to-shear ratio ranged between 0.33 and 0.94. Main parameters in the tests were aspect ratio, vertical and horizontal reinforcement ratio, and the presence of boundary elements. Specimen SW1 to SW10 had the same boundary arrangement. The difference between these specimens was aspect ratio and vertical and horizontal reinforcement

ratio. Boundary elements were constructed at the end of the Specimen SW11 and Sw12 using crosstie and stirrups. The result showed, the shear resistance of walls without boundary elements degrades rapidly with repeated cycling at lateral displacements beyond the peak shear strength. The maximum peak shear stress is observed for Specimen SW5 ($11.5\sqrt{f_c'}$) and SW8 ($11\sqrt{f_c'}$) which had the lowest aspect ratio (0.33) and highest web reinforcement ratio ($\rho_l = \rho_t = 1.5\%$) respectively (Figure 2.30).

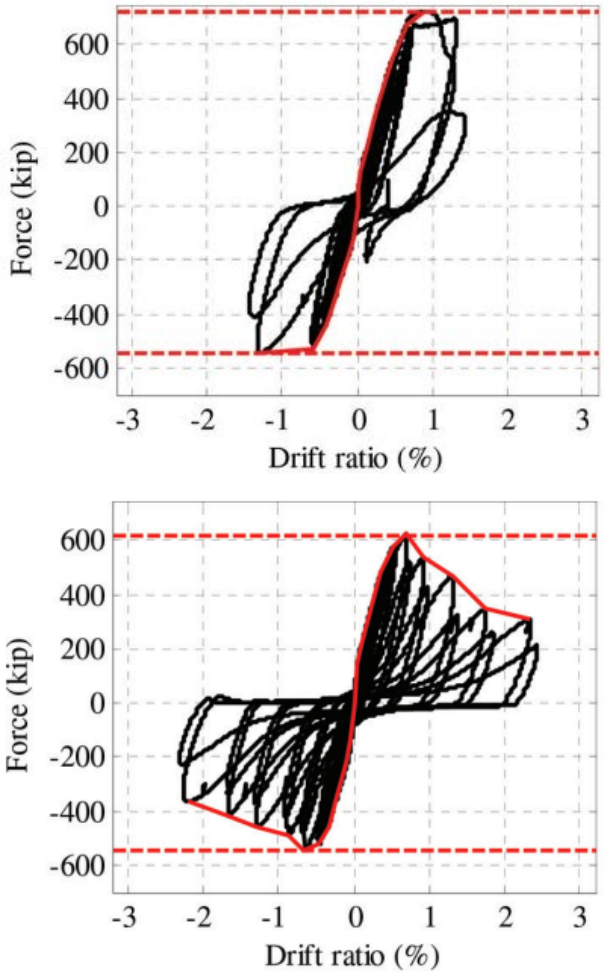

Figure 2-30 Hysteresis responses of Wall 5 and Wall 8 (Bismarck et al., 2015)

2.2.1 Seismic Design For Squat Walls In ACI 318-14

Design usually begins by considering shear strength requirements. Section 18.10.4.1 (ACI 318-14) defines the nominal shear strength for individual wall segments as:

$$V_n = A_{cw}(\alpha_c \lambda \sqrt{f_c^{'}} + \rho_t f_y) \leq 10\sqrt{f_c^{'}} A_{cw} \qquad \text{[Equation 4]}$$

Where α_c is 3.0 for $h_w/l_w \leq 1.5$, is 2.0 for $h_w/l_w \geq 2$, and varies linearly between these limits; and $\lambda = 0.75$ for all lightweight concrete, 0.85 for sand-lightweight concrete, and 1.0 for normal weight concrete, $f_c^{'}$ is the compressive strength of the concrete (psi unit), ρ_t is the horizontal web reinforcement, and f_y is the yield strength of the horizontal reinforcement (psi unit), A_{cw} is the gross area of concrete bounded by web thickness and length of section in the direction of the shear force. To prevent diagonal compression failure, the nominal peak shear stress is limited to $10\sqrt{f_c^{'}}$. The design strength of members per ACI 318-14 is calculated by multiplying the calculated nominal strength by a strength reduction factor. The strength reduction factor for squat wall is $\varphi = 0.6$. According to ACI 318-14, the minimum horizontal and vertical web reinforcement ratio is limited to 0.0025 and maximum allowed spacing between the reinforcement is 18 in. Also, for squat wall the vertical web reinforcement ratio (ρ_l) shall not be less than horizontal web reinforcement ratio (ρ_t).

Chapter 3

Experimental Program

3.1 Introduction

As mentioned in chapter 1 and 2, the diagonal reinforced coupling beam has construction difficulty and also, rectangular squat wall has limited deformation capacity and shear stress. Therefore, the main objective of this research was to develop a new arrangement for coupling beam with aspect ratio between 2 to 4 and a low-rise wall with aspect ratio less or equal to one to simplify reinforcement detailing and enhance seismic behavior.

The experimental work of this research contained two phases. The first phase consisted of two parts. In the first part three half scale coupling beams with truss reinforcement arrangements are tested under displacement reversal to evaluate the performance of the coupling beam with this arrangement. In the second experimental part five full and half scale coupling beams with new detailing, double beam coupling beam (DBCB), consisting of two separate cages was performed under cyclic loading to evaluate the feasibility of using two flexural beams in the coupling beam. The aspect ratio (ℓ / h) 2.2, 2.4, 3.3, where ℓ and h are the length and height of the coupling beam, was selected based on the two common tall building configurations, residential and office building. The following factors were considered in the first and second experimental phase:

- Coupling beam span-to-depth ratio (2.2, 2.4, 3.3)
- Reinforcement detailing (Truss and DBCB)
- Full scale and half scale

In the second phase the lessons learned from coupling beam with DBCB detailing were performed in the design of Six approximately 1/3-scale of rectangular squat wall.

The aspect ratio (ℓ / h) 1, 0.5 where ℓ and h are the length and height of the squat wall, was selected based on the common wall in mid-rise and nuclear industrial building. The main objective of this phase was to investigate the seismic behavior of squat wall with new details, with emphases on their displacement capacity, shear behavior and damage tolerance. The following parameters were considered in the third experimental phase:

- Rectangular Squat wall with height-to-length ratio 1 and 0.5
- Reinforcement detailing
- Shear stress

In the following sections, a detailed description of the experimental, including the specimen geometry, design, the materials used, test set up, and instrumentation is presented.

3.2 Phase1: General Description of Coupling Beam Specimen

Eight full and half scale coupling beams with different configuration were tested under the large displacement reversals to better evaluate the influence of the new arrangement and compare the results with recent research on the diagonally reinforced coupling beam arrangement by Naish et al. (2009). Each specimen consisted of a coupling beam, big and loading rigid reinforced concrete blocks representing structural walls. The dimension of the test specimens are shown in Figure 3.1.

Naish et al. (2009) designed and tested eight half-scale diagonally reinforced coupling beams with two different confinements which are the current ACI 318-14 practice. According to them, the cross section dimension of the full scale coupling beam with aspect ratio of approximately 2.4 and 3.3 is 24"x30" and 24"x36". Therefore, in this study, the length and height of the half-scale coupling beam with aspect ratio 2.4 picked up 36", and 15" respectively. However, instead of using a beam width of 12" as in the diagonally reinforced coupling beam specimens tested by Naish et al. (2009), the width of

the coupling beam was reduced to 5" and 6" because this width is sufficient to accommodate the bars and to bring the nominal gross section shear stress level up to 10 $\sqrt{f_c'}$. The length, height, and width of the coupling beam with aspect ratio 3.3 were 49.5", 15", and 6". Also, the full scale coupling beam with aspect ratio 2.2 had the length, height, and width equal to 60", 49.5", and 10.75". The main features of the test specimen are provided in table 3.1.

Table 3-1 Description of the Test Specimen

specimen	Dimension (inch)	Aspect Ratio	Reinforcement Arrangement	Gap Width (inch	Shear Stress (psi)	Concrete Material
CB-1	36x15x5	2.4 (Half Scale)	Truss	-	$10\sqrt{f_c'}$	Regular concrete
CB-2	36x15x6	2.4 (Half Scale)	Truss	-	$10\sqrt{f_c'}$	Regular concrete
CB-3	36x15x7	2.4 (Half Scale)	Truss	-	$10\sqrt{f_c'}$	Regular concrete
CB-4	36x15x6	2.4 (Half Scale)	DBCB	1"	$10\sqrt{f_c'}$	Regular concrete
CB-5	36x15x6	2.4 (Half Scale)	DBCB	1"	$10\sqrt{f_c'}$	Regular concrete
CB-6	36x15x6	2.4 (Half Scale)	DBCB	0.25"	$13\sqrt{f_c'}$	Regular concrete
CB-7	49.5x15x6	3.3 (Half Scale)	DBCB	1"	$10\sqrt{f_c'}$	Regular concrete
CB-8	60x27.5x10.75	2.2 (Full Scale)	DBCB	1.5"	$10\sqrt{f_c'}$	Regular concrete

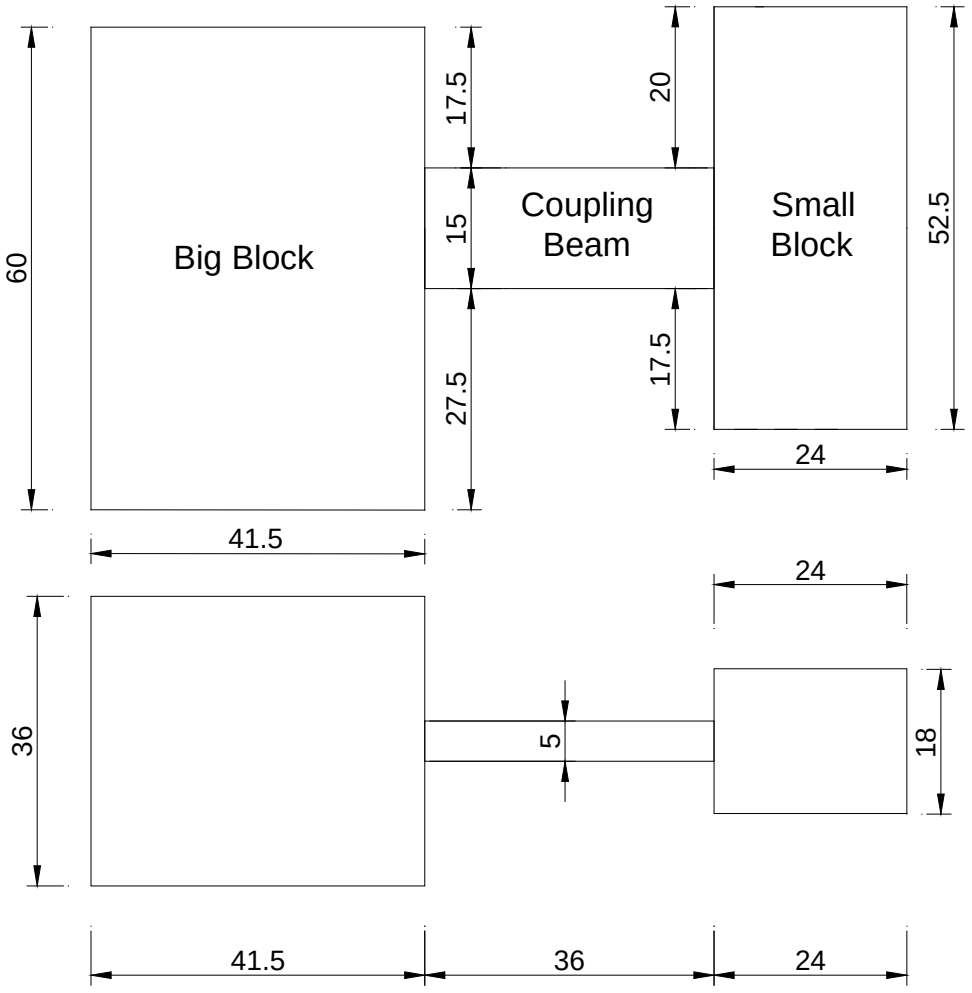

a) Specimen CB-1 (all dimensions in inches)

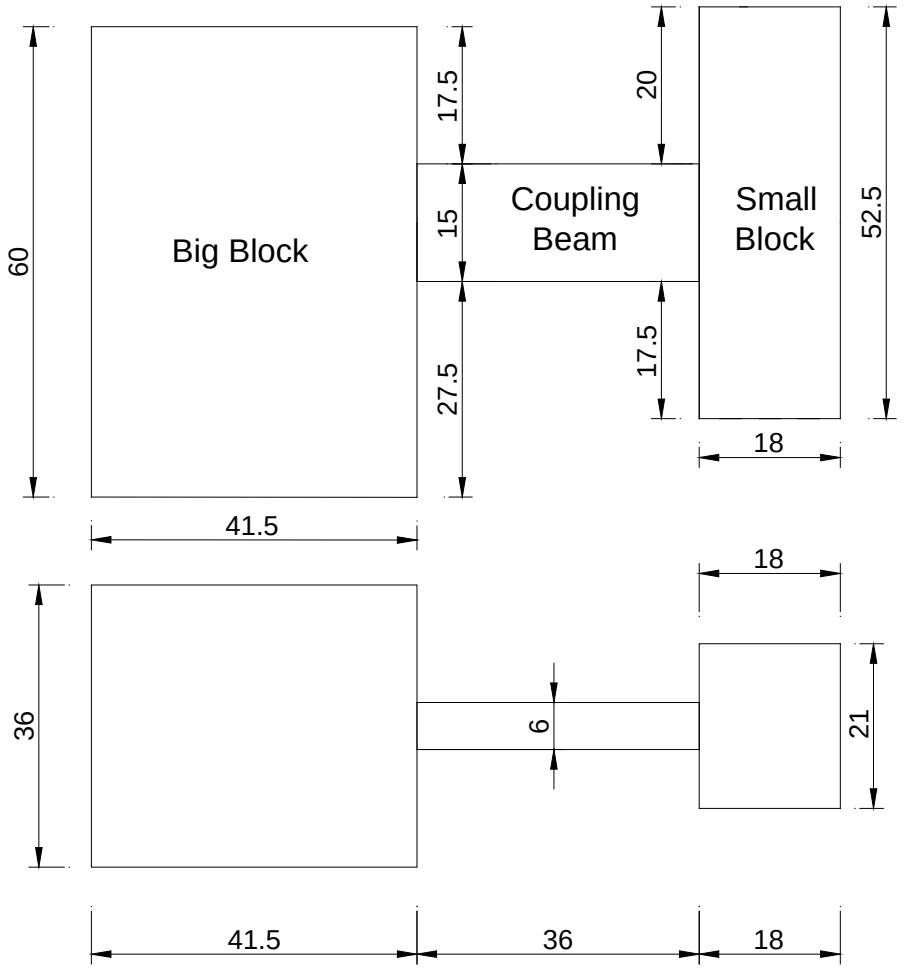

b) Specimen CB-2, CB-3, CB-5 and CB-6 (all dimensions in inches)

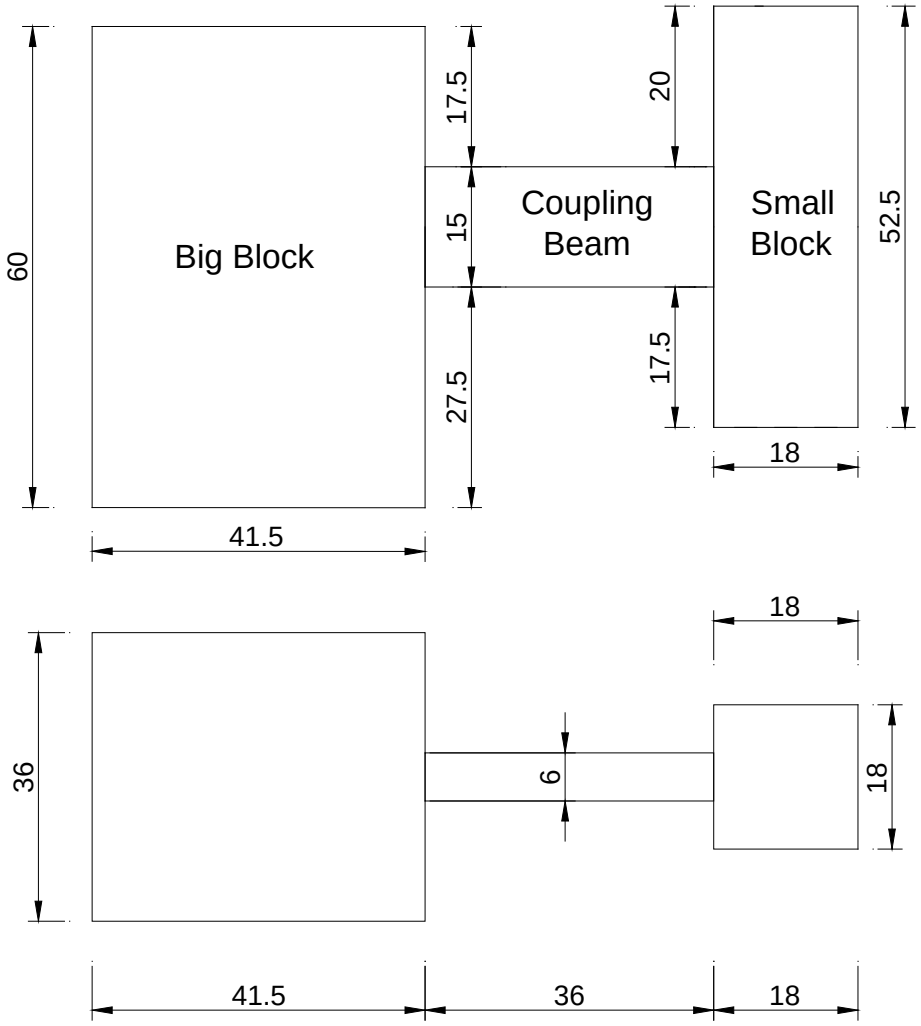

c) Specimen CB-4 (all dimensions in inches)

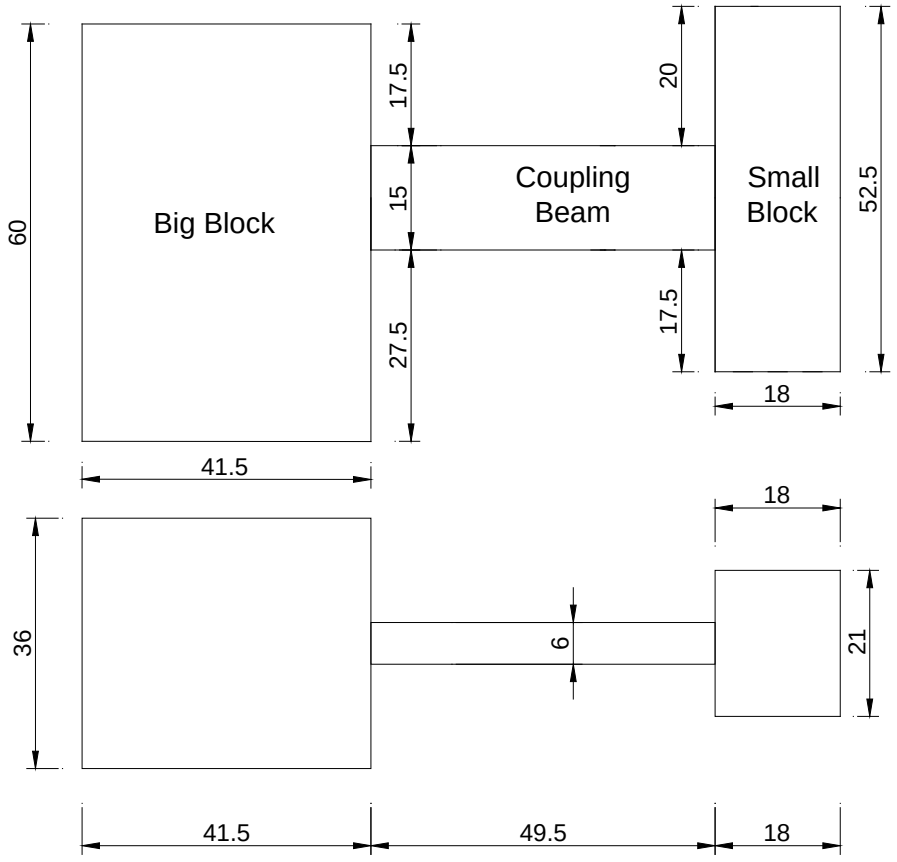

d) Specimen CB-7 (all dimensions in inches)

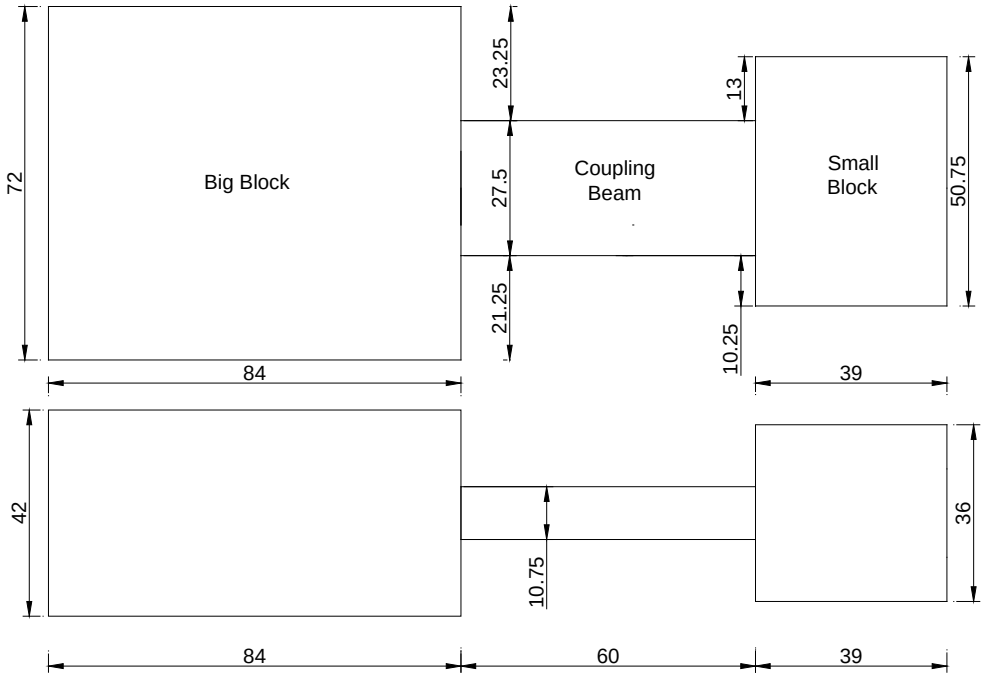

e) Specimen CB-4 (all dimensions in inches)

Figure 3-1 Dimension of the test specimens

3.2.1 Design of the Coupling Beam with Truss Detailing

First three coupling beam specimens had the truss arrangement. This reinforcement was provided to reduce shear deterioration. Design of these diagonal reinforcements was based on the assumption that they would behave as diagonal truss members under the cyclic loading, thus carry the entire shear force. The main function of these bars was to provide the efficient resistance to the opening of the diagonal shear cracks than that offered by vertical ties, and also, prevent the sliding shear in the coupling beam.

According to ACI 318-14 coupling beam with span-to-depth ratio between 2 and 4, can design as a diagonally reinforced or as a beam in special moment frame. For diagonally reinforced coupling beam, ACI 318-14 requires the diagonal reinforcement to be design to resist the entire shear demand. Therefore, in this study for design purpose, shear resistance was assumed to be provided by the diagonal reinforcement which had the angle 45º in truss arrangement. The design process of the coupling beam started with selection of the diagonal bars. The diagonal reinforcement design based on the Section 18.10.7.4 ACI 318-14, where A_{vd} is the area of the steel in each group of diagonal bars, f_y is the yield stress of the steel and α is the angle between the diagonal reinforcement and the longitudinal axis of the beam which was 45º. In other words, the diagonal reinforcement was designed to resist of the target shear demand. The design shear force demand, V_n, of $10\sqrt{f_c'}A_{cw}$ (psi), where A_{cw} is the cross sectional area of the coupling beam and f_c' is the specified compressive strength of the concrete, was selected for all specimens because it is upper limit for shear capacity permitted by ACI Building Code (318-14) for coupling beams.

$$V_n = 2A_{vd} f_y \sin\alpha \le 10\sqrt{f_c'}A_{cw} \qquad \text{[Equation 3-1]}$$

Both sides of the diagonal bar were bent, and made them parallel to other longitudinal reinforcement. This bent diagonal detail makes it easier to thread the coupling beam reinforcement through the adjacent walls, and facilitates the beam construction. In addition, the bent of the diagonal bars provides enough development length for each part of the truss.

Besides the diagonal bars, transverse reinforcements were designed to provide confinement for the beam and to prevent the buckling of main reinforcement. Also, close transverse reinforcements were designed, similar to special beam detailing in flexural members of special moment frame, in the region where the diagonal bars were bent to resist the outward force component developed by these diagonal bars. The amount of special transverse was calculated as the required for flexural members of special moment frame confinement in Section 18.6.4, ACI 318-14.

The behavior of these coupling beam specimens were expected to be governed by flexural yielding at both ends. Therefore, appropriate amount of longitudinal reinforcement control the capacity of the coupling beam. On the other hand, flexural capacity of the coupling beam correlated with the target shear demands. Based on the shear force demand ($10\sqrt{f_c'}A_{cw}$), moment demand, M_u, was calculated as $M_u = V_u l_n / 2$, where l_n is the length of the coupling beam.

All of the longitudinal reinforcements for each specimen were fully developed into the big and loading block that represents the wall boundary. Development length for all of specimens was considered shorter than ACI 318-14 requirement, as is shown in table 3.2, to evaluate the new assumption for the development length. For the ACI equation, compressive strength of the concrete, $f_c^{'}$, is assumed 6000 psi and $\frac{C_b + K_{tr}}{d_b}$ assumed

1.5 based on the current practice construction that commentary of the ACI 318-14 mentioned.

For the first three specimens, No.3 U-shaped bars at the end of the beam were used to help longitudinal bars regarding to prevent sliding shear and move the plastic rotation away from beam-wall interface.

Table 3-2 Development Length for Longitudinal Bars

	Development Length Equation	#6	#7	#8
Development Length for Coupling Beam Specimens	-	18"	18"	31"
ACI318-14	$\left(\frac{3}{40}\frac{f_y}{\lambda\sqrt{f_c'}}\frac{\Psi_t\Psi_e\Psi_s}{\left(\frac{C_b+K_{tr}}{d_b}\right)}\right)d_b$ $\left(\frac{C_b+K_{tr}}{d_b}\right)=1.5$, $f_c'=6000$ (psi)	30"	34"	39"
ACI318-14(18.8.5)	$\frac{1.25\times 3.25\times\left(f_y d_b\right)}{65\sqrt{f_c'}}$, $f_c'=6000$ (psi)	37"	43"	49"

The big and loading block representing the walls were designed to resist the forces associated with a coupling beam shear target of 100 kips for half scale and 250 kips for full scale specimen. The maximum shear force in this study approximately was 90 and 170 kips for half and full scale respectively. The design was conservative to ensure that the blocks did not damage during the test. The reinforcement detailing for big and small block are demonstrated in Figure 3.2 and 3.3 respectively.

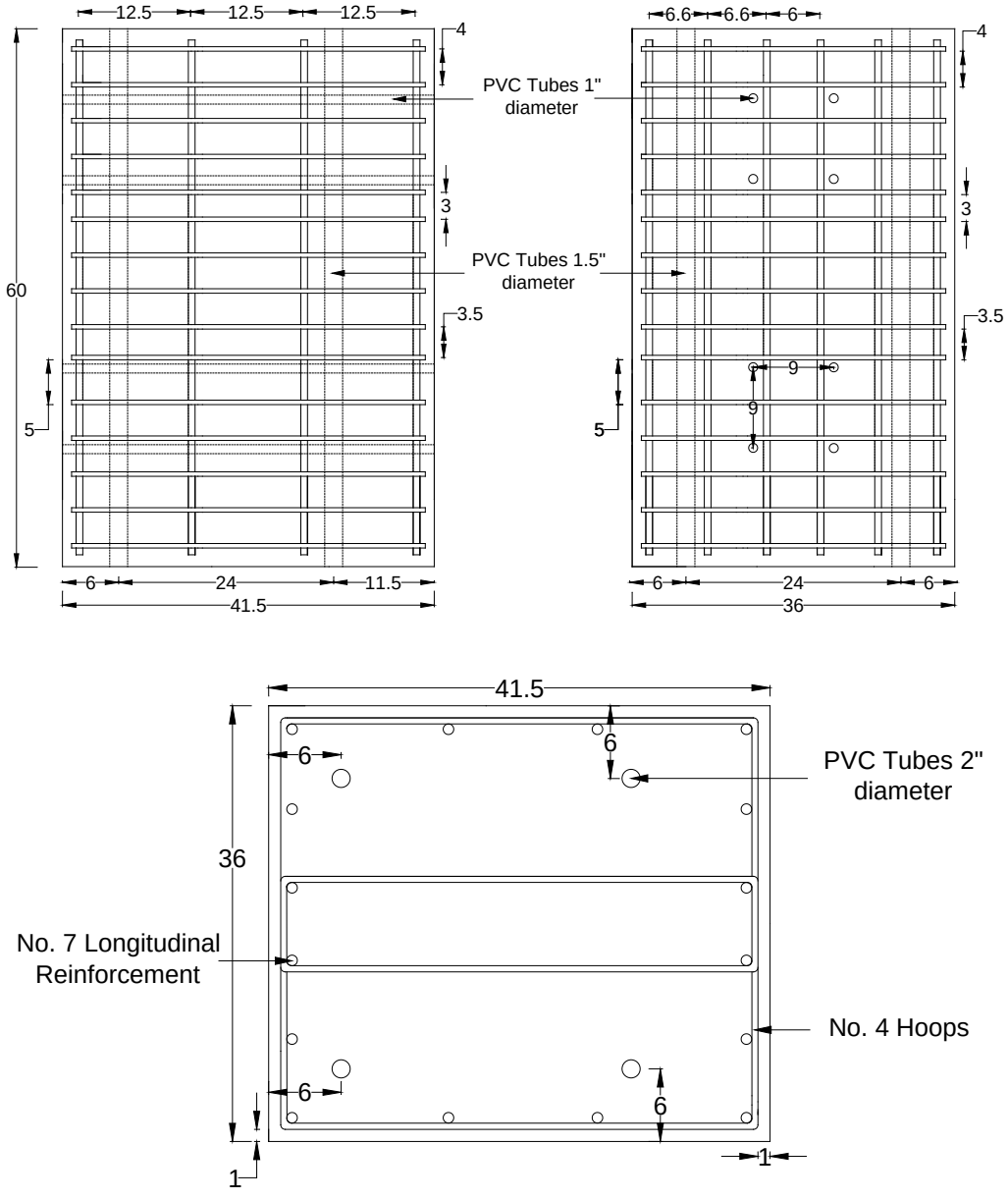

Figure 3-2 Big block reinforcement detailing for CB-4 (all dimensions in inches)

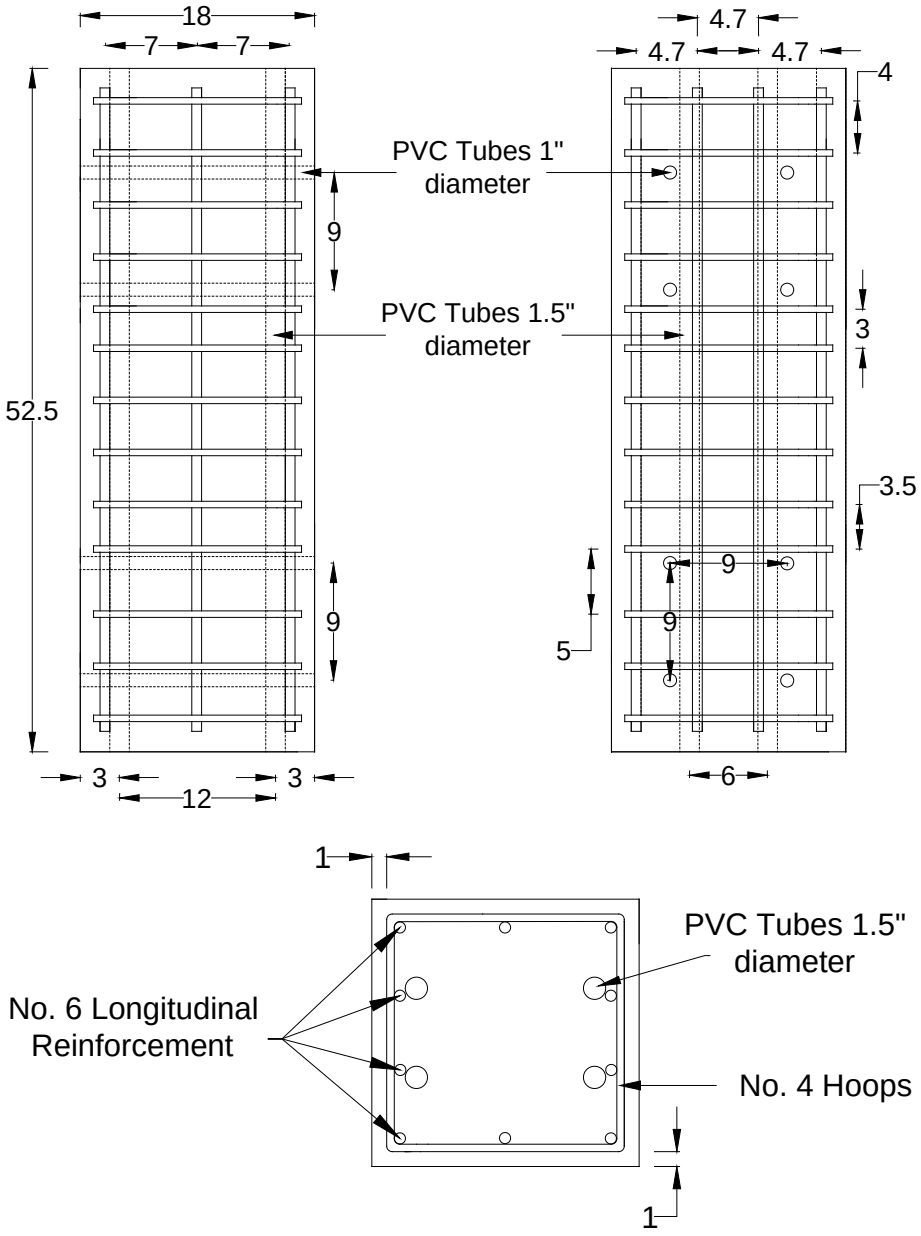

Figure 3-3 Small block reinforcement detailing for CB-4 (all dimensions in inches)

In the design of the coupling beam four types of reinforcement bars were used, longitudinal reinforcement, diagonal reinforcement, hoops, and U-shaped reinforcement. In the following, a summary of the design details for the three specimens is provided.

3.2.1.1 Specimen CB-1 (Truss with $\ell/h = 2.4$)

The first specimen with span-to-depth ratio of 2.4 and truss arrangement was constructed with regular concrete and design according to the design provision of the coupling beam in ACI 318-14. The cyclic load was applied via an actuator that was placed on the top of the loading block. The coupling beam was designed to resist a shear stress approximately $10\sqrt{f'_c}$ (psi). Compressive strength of the concrete, f'_c, was 5000 psi. The dimensions of the coupling beam were 36" length, 15" height and 5" width. This length and height dimensions represent the half scale coupling beam with aspect ratio of 2.4. The coupling beam's main longitudinal reinforcement consisted of two layers of three No.6 Grade 60 bars. These bars were continued through the wall boundary approximately 18". The truss arrangement consisted of three groups of the diagonal reinforcement in each side of the beam. Each group of the diagonal bars consisted of two No. 5 designed based on the shear stress $10\sqrt{f'_c}$ (psi) and placed between the main longitudinal reinforcement. Therefore, it was assumed half of the diagonal bars acted as the tension member and the rest as the compression member. The angle of the diagonal bars was approximately 45º with respect to the beam longitudinal axis. No. 5 U-shaped bars were embedded in end of the beam to help longitudinal bars regarding to prevent sliding shear and move the plastic rotation away from beam-wall interface. Transverse reinforcement designed to carry the shear demand and confine the concrete core. No. 3 hoops spaced at 3.5" were selected based on the requirement of the Chapter 18 of ACI building code (ACI 318-14) for flexural member of special moment frames. Hoops space

was designed 1.5" conservatively at both end of the beam where flexural yielding normally occurs, and also, end of the each group of diagonal bars to resist the outward force component developed by these diagonal bars. Figure 3.4(a) shows the reinforcement details for first coupling beam.

3.2.1.2 Specimen CB-2 (Truss with $\ell/h = 2.4$)

Test results of the first specimen were not successful due to the test set up and construction issue therefore, second specimen with regular concrete and with specified compressive strength, f_c' , of 5300 psi was constructed using same reinforcement detailing as that of the fist specimen. Test set up was edited, thus, specimen was braced laterally to prevent out-of-plane movements and twisting. The coupling was designed to sustain under the shear stress approximately $10\sqrt{f_c'}$ (psi). The shear stress in the first specimen result was high, thus, the width of the coupling beam was increased to 6" to reduce the shear stress in the beam and make more room to embed all of the bars easier. The same longitudinal, diagonal and U-shaped bars were used in this specimen. Due to the first test strain gauge result the hoops in the middle of the diagonal bars eliminated to reduce the amount of the hoops and improve the constructability of the coupling beam. The reinforcement layout for second specimen is shown in Figure 3.4(b).

3.2.1.3 Specimen CB-3 (Truss with $\ell/h = 2.4$)

The results of Specimen CB-1 and CB-2 motivated a change for the design of Specimen CB-3 and test setup. The third specimen was constructed with regular concrete with compressive strength 7000 psi. In this specimen, the location of the actuator was changed and the cyclic load was applied via an actuator, with the line of action of the actuator's force passing through the mid-span of the coupling beam. In this specimen link was not use on the top and bottom of the coupling beam. The response of previous specimen confirmed that three groups of diagonal reinforcement in the coupling

beam could not prevent the sliding shear failure, thus, the diagonal bars need to place at both end of the beam without any space between them and blocks. Therefore, four groups of diagonal reinforcement were designed with the close hoops in the beam to provide the satisfactory shear resistance and confinement for the coupling beam. The first and last group consisted of two No.4 diagonal reinforcements at each side of the beam. Also, two No.3 diagonal reinforcements were used at the second and third group of the diagonal reinforcements at both sides of the beam. The diagonal bars from top and bottom was bent 45º.

The main longitudinal reinforcement consisted of two layers of No.7 bars instead of three No.6 bars placed at the end of the beam near the top and bottom of the specimen to make more room for the diagonal bars. Also, due to high shear stress in previous specimen, longitudinal bars did not continue from one side to the other side of the coupling beam and just placed at both end of the specimen, thus, the contribution of the longitudinal bars in the shear stress was almost eliminated. The hoops space was 2" to satisfying the ACI building code (ACI 318-14) requirements for flexural members of special moment frames and provided satisfactory confinement to the coupling beam. Figure 3.4(c) shows the reinforcement details for first coupling beam.

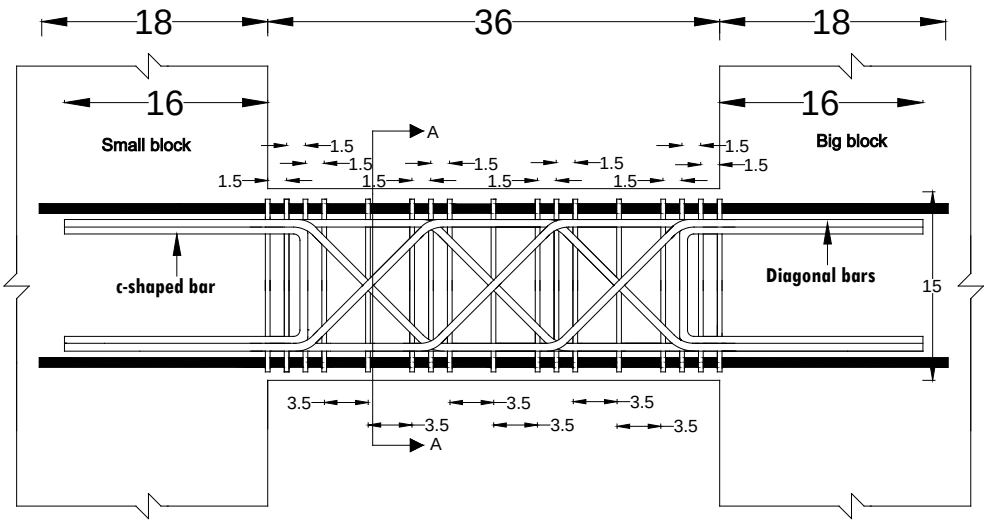

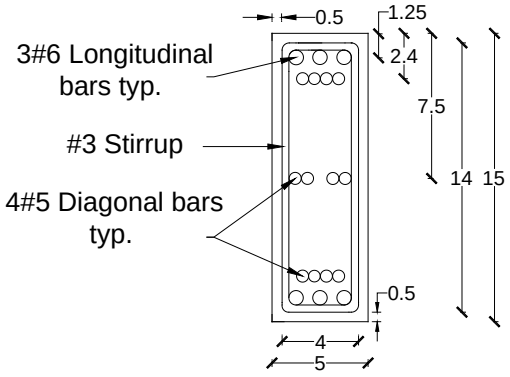

Section A-A

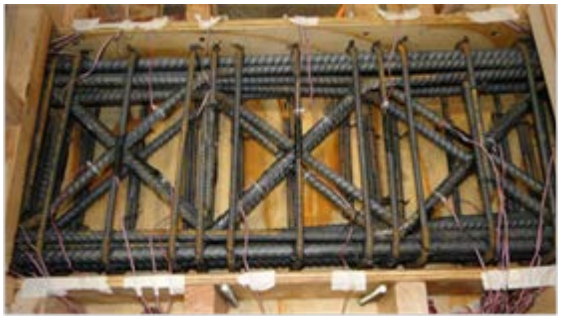

a) Specimen CB-1 (all dimensions in inches)

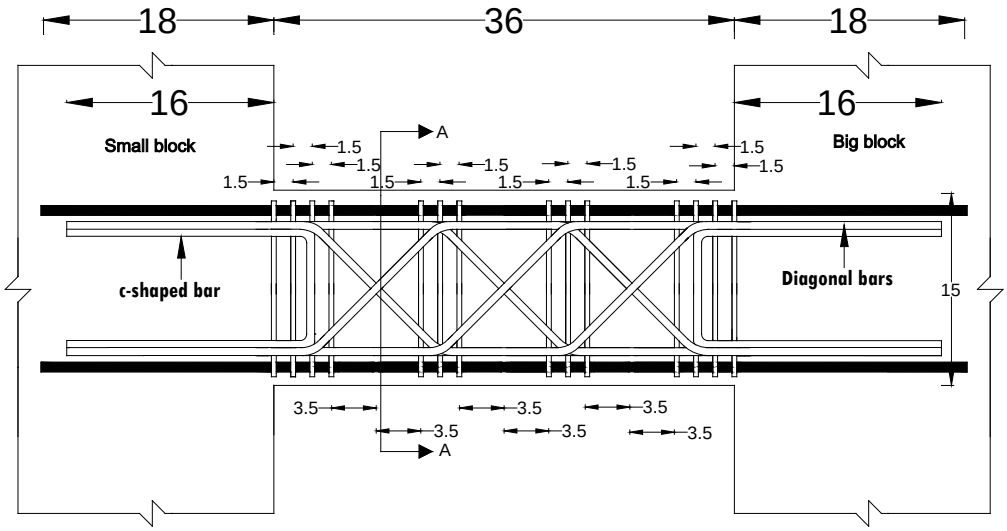

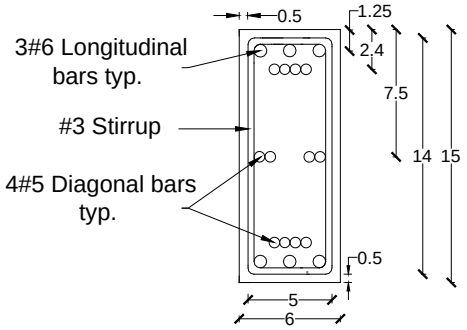

Section A-A

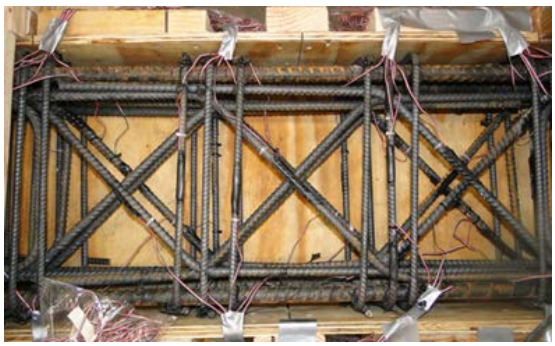

b) Specimen CB-2 (all dimensions in inches)

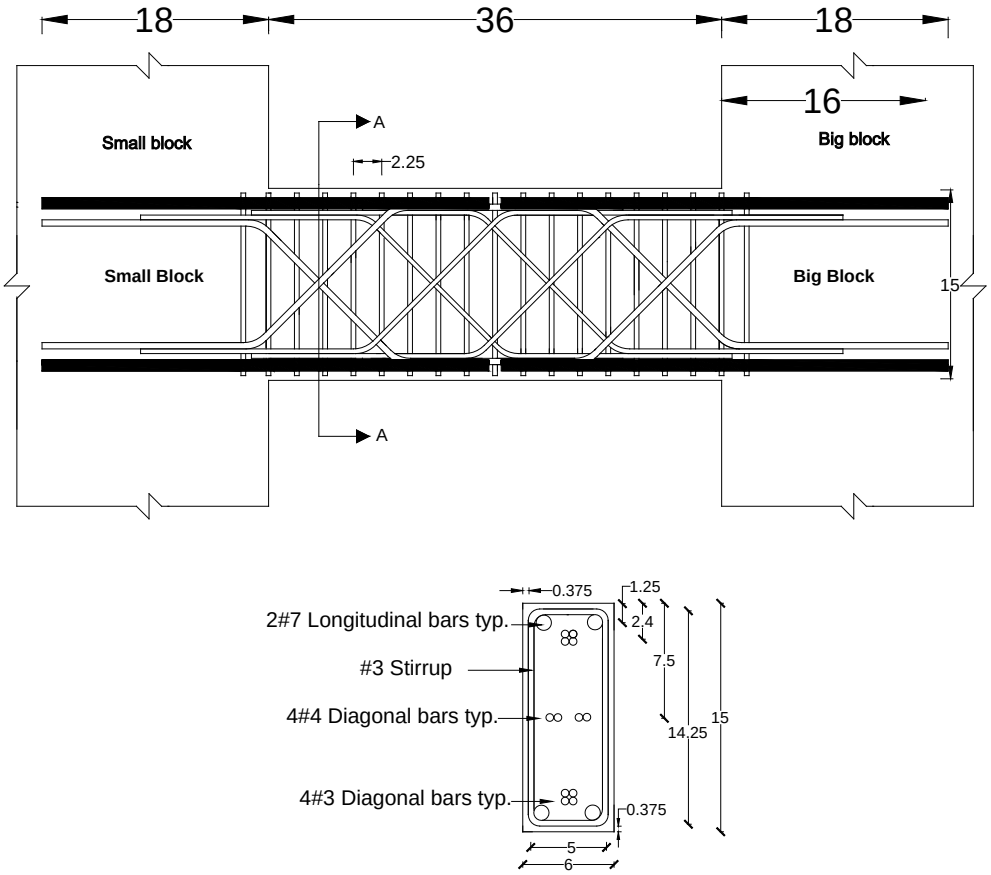

Section A-A

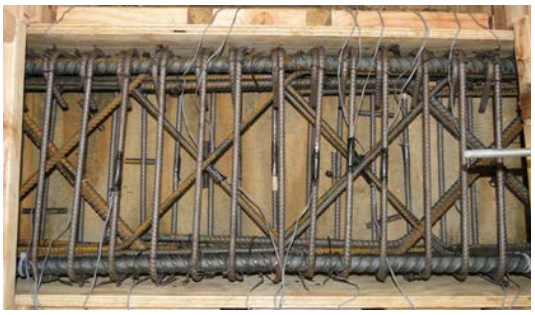

Specimen CB-3 (all dimensions in inches)

Figure 3-4 Reinforcement layouts for test coupling beam 1, 2, and 3

3.2.2 Design of the Double-Beam Coupling Beam

The results of previous specimen showed that the shear behavior governed in short coupling beam. Use of truss arrangement in the previous coupling beam did not result in the anticipated improvement in performance. Since shear failure is brittle in conventional coupling beams, the performance of the coupling beam could be enhanced if flexural behavior governs. One way to get the flexural behavior is increasing the aspect ratio. In order to increase the aspect ratio, if coupling beam could be cut into two beams at mid-height, the aspect ratio of each beam would be doubled. As a result, the behavior should be dominated by flexure.

Therefore, Double-Beam Coupling Beam (DBCB) reinforcement scheme consists of two separate cages and the gap between the cages was proposed in this study. The dimension of the half scale DBCB coupling beams was 36" length, 15" height and 6" width. These coupling beams were designed similar to those used for typical beams in reinforced concrete special moment frames. The behavior of the DBCB coupling beam specimens was expected to be dominated by flexural yielding at both ends. Therefore, the capacity of the coupling beam could be controlled by selecting the appropriate longitudinal reinforcement. For most of the specimen longitudinal reinforcement were designed base on the moment demand, $M_u = V_u l_n / 2$, where V_u is the shear force demand ($10\sqrt{f_c'}A_{cw}$), and l_n is the length of the coupling beam. All the longitudinal reinforcement was fully developed in to the big and loading block. The development length for each bar is demonstrated in table 3.2. The transverse reinforcement in the DBCB specimens was designed according to the confinement and shear requirements specified for flexural members of special moment frames in Section 18.6.4 in ACI 318-14. The 0.25", 1", 1.5" gaps (clear distance between transverse reinforcement) were chosen

for the study beams based on nonlinear finite element analyses using VecTor2. This gap is one of the critical factors that influence the behavior of DBCBs under large displacement reversals. A large gap could lead to reduced stiffness of the beams at small story drift levels; on the other hand, if the gap is too small the beam would not completely separate into two slender beams, thus leads to shear failure in the coupling beam with small drift capacity. Also, due to the current tall building construction, concrete compressive strength for all tests approximately was in the range of 6000 to 8000 psi; expect the full scale coupling beam.

Three types of reinforcement bars were used in the design of DBCB coupling beam, longitudinal reinforcement, and hoops. Detailing for DBCB coupling beam specimen is explained below.

3.2.2.1 Specimen CB-4 (DBCB with $\ell/h = 2.4$)

To evaluate the influence of using two separate cages with 1" gap in the coupling beam, the fourth specimen was constructed with regular concrete. Concrete specified compressive strength was 6700 psi. The specimen was intended to sustain shear stress demand of approximately $10\sqrt{f'_c}$ (psi). The longitudinal reinforcement for each cage was designed based on the half of the total moment demand. The main longitudinal reinforcement consisted of one layer of No.6 placed near the top, bottom, and middle of the each cage.

Transverse reinforcement was designed for entire length of the beam to carry the shear force demand ($10\sqrt{f'_c}A_{cw}$). Moreover, additional transverse reinforcement was provided overall the lengths as specified in Section 18.6.4 ACI 318-14. The purpose of this requirement is to confine the region where flexural yielding and spalling of the concrete shell very likely to occur. The length of this region is equal to twice of the depth

for each beam and measured from the face of the blocks toward mid-span which is 15" for each end of this specimen. Therefore, No. 4 hoops were selected and spaced at 1.7" and 2.5" for inside and outside of this region respectively. Figure 3.5(a) shows the reinforcement details of the first coupling beam.

3.2.2.2 Specimen CB-5 (DBCB with $\ell/h = 2.4$)

With success of the specimen fourth test with the unsymmetrical loading protocol, the behavior of the coupling beam with symmetrical loading protocol was investigated. Specimen five with the same reinforcement detailing was constructed with regular concrete, as shown in figure 3.5(a). The specific concrete compressive strength was 5900 (psi).

3.2.2.3 Specimen CB-6 (DBCB with $\ell/h = 2.4$)

Specimen six was constructed with specific compressive strength of 6000 psi to evaluate the influence of the gap and shear stress on the behavior of the coupling beam. The height of the gap was selected 0.25". In addition, this specimen was designed to carry a shear stress of approximately $13\sqrt{f_c'}$ (psi). To satisfy the shear stress target, 2 layers of No.7 bars placed at the top and bottom of the cage and a layer of No.6 placed at middle of the cage.

Hoops were expected to approximately carry the shear stress target. Special hoops based on the hoop's requirement in the flexural members in special moment frame, consisted of No.4 stirrups spaced at 1.7" in both end of the beam to provide adequate confinement. In the mid-span (outside of the plastic hinge) the stirrups spaced at 2.5". The reinforcement details for this coupling beam are demonstrated in Figure 3.5(b).

3.2.2.4 Specimen CB-7 (DBCB with $\ell/h = 3.3$)

Test result for the first three specimens with double-beam arrangement confirmed the effectiveness of using the two cages with the 1" gap to improve the constructability while provided the adequate strength, stiffness, and ductility. The coupling beam with aspect ratio 3.3 designed to investigate the potential of using new configuration for such slender coupling beams which is usually used for office building. The specific compressive strength for this specimen was 6000 psi. The maximum shear demand of approximately $10\sqrt{f_c'}$ (psi) was aimed for this specimen. Large amount of the longitudinal reinforcement was required to develop the shear stress as in the fifth specimen. Three layers of the No.7 bars were designed for the longitudinal reinforcement in each cage. The same transverse reinforcement as that used in both end of the coupling beam with aspect ratio 2.4 and 1" gap were used. A No.4 stirrup was designed and spaced 4" for mid-span. The reinforcement details for specimen six is shown in Figure 3.5(c).

3.2.2.5 Specimen CB-8 (DBCB with $\ell/h = 2.2$)

With the successful test of the half scale coupling beams with aspect ratio 2.4 and 3.3, the possibility of decrease the aspect ratio was explored. In additional, in the recent construction needs several utility pipe embedded in to the coupling beam due to the electrical and mechanical requirement, therefore, in this specimen utilize the gap by using the pipe was investigated.

An aspect ratio 2.2 was chosen and concrete compressive strength of 4000 (psi) was specified. The pipe with 2.5" diameter was selected based on the gap height and placed at the mid-span of the gap. The dimension of the coupling beams was 60" length, 27.5" height and 10.75" width. Also, the gap height 1.5" was selected. This coupling

beam was designed based on the maximum shear stress of approximately $10\sqrt{f_c'}$ (psi). Main flexural reinforcement for each cage consisted of No.8 bars at the top and bottom layer and No.6 in middle layer.

Due to the shear strength of the coupling beam relied on stirrups; No. 5 stirrups spaced at 3.75" were selected to carry the maximum shear demand. To satisfy the requirement of Chapter 18 (ACI 318-14), flexural member in special moment frame, additional confinement were designed and placed at 3" spacing at both end of each beam. The reinforcement configuration for specimen eight is illustrated in Figure 3.5(d).

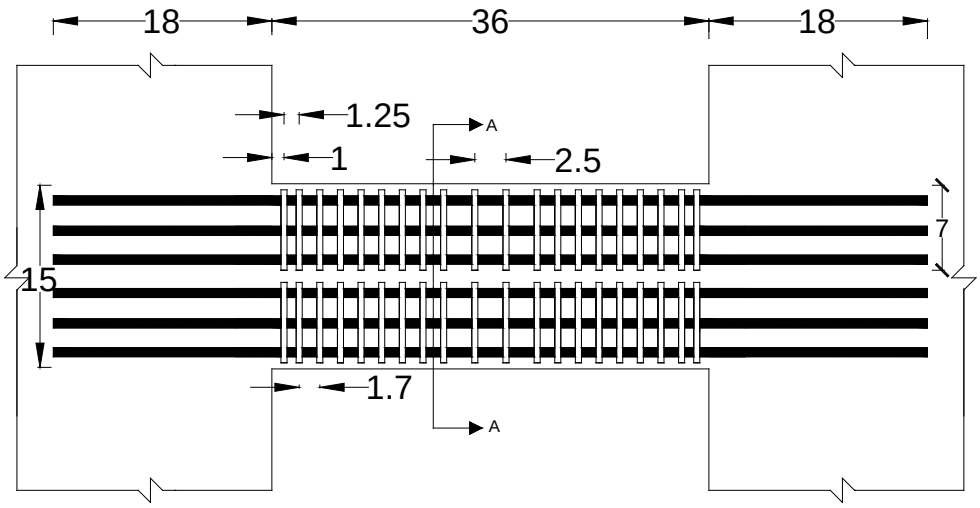

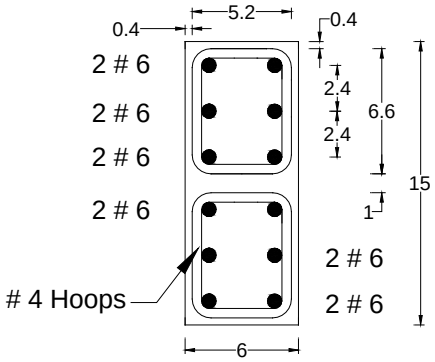

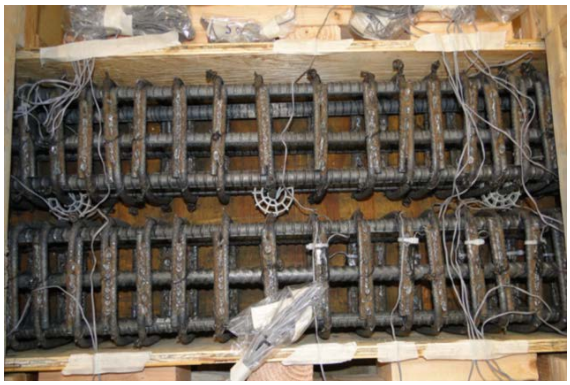

a) Specimen CB-4 and CB-5 (all dimensions in inches)

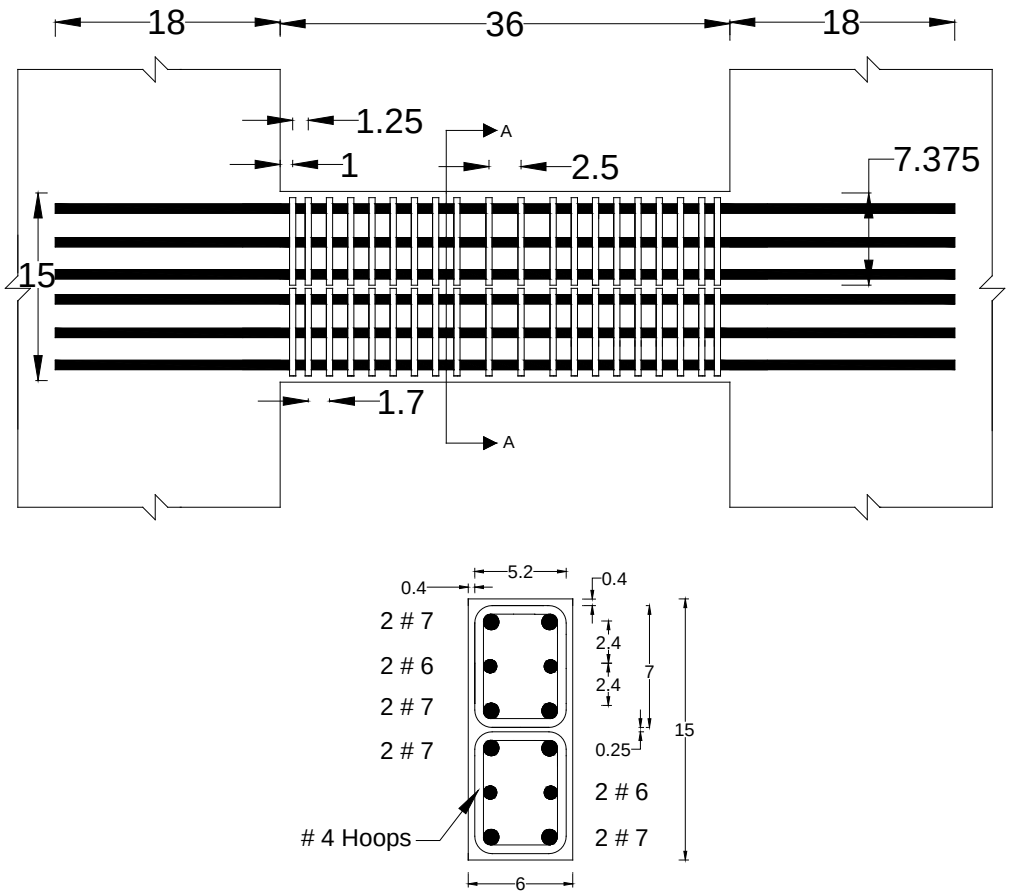

Section A-A

b) Specimen CB-6 (all dimensions in inches)

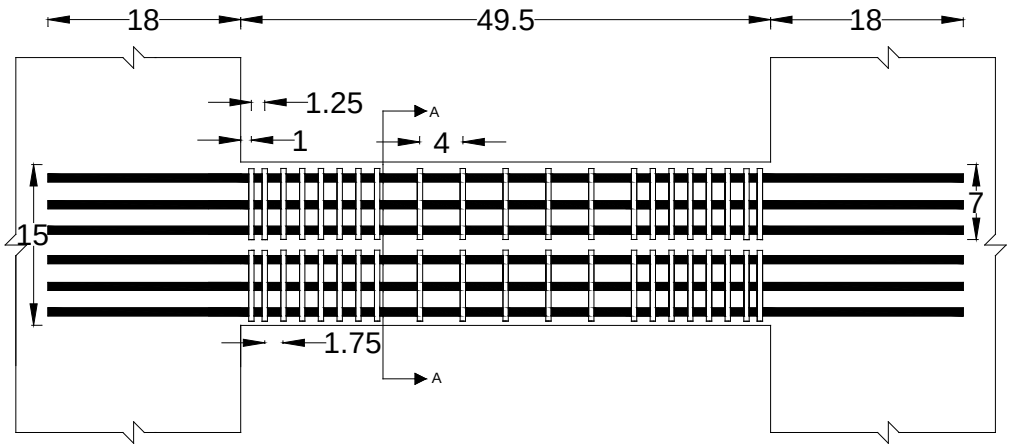

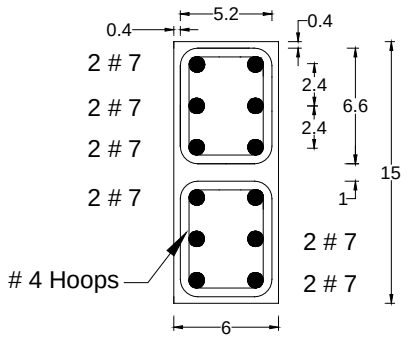

Section A-A

c) Specimen CB-7 (all dimensions in inches)

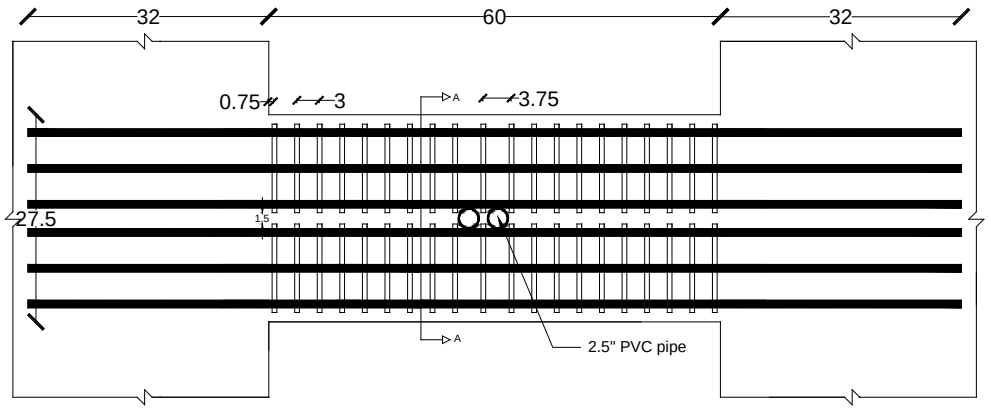

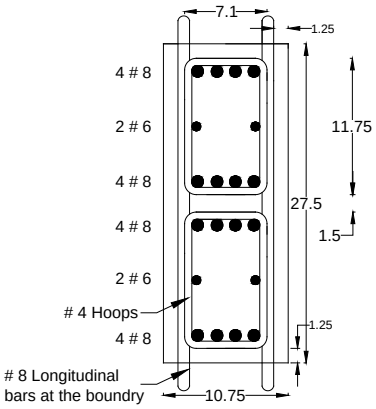

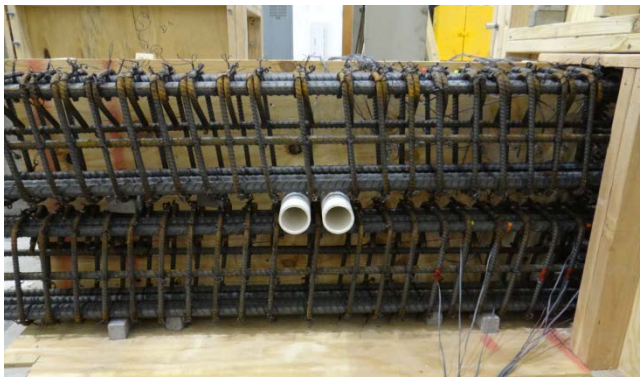

Section A-A

d) Specimen CB-8 (all dimensions in inches)

Figure 3-5 reinforcement layouts for test coupling beam 4, 5, 6, 7, and 8

3.3 Phase2: General Description of Squat Wall Specimen

Based on pervious experimental investigations, discussed in Section 2.2, maximum shear stress for rectangular squat walls which design based on ACI 318-14, is generally smaller than $10\sqrt{f_c'}$ (psi), which is upper limit of the shear strength in ACI 318-14. The shear strength upper limit in ASCE 43-05 ($20\sqrt{f_c'}$ (psi)) was not reached by any rectangular squat walls as well. Also, deformation capacity for rectangular squat walls is small. Therefore, the purpose of this research was to proposed new concept for rectangular squat walls which results showed great potential to improve the peak shear strength while maintaining adequate ductility of the squat walls. This new concept is to use discrete reinforcing cages to reinforce the rectangular squat wall, with concrete in each cage fully confined by hoops. These cages can be easily pre-fabricated and installed quickly on-site.

Six large-scales rectangular squat walls with different details was constructed with regular concrete and tested under the large displacement reversals to investigate the behaviors of the new details for the squat wall, with emphasis on their ductility, shear strength and damage tolerance. Each specimen consisted of a squat wall, footing and loading rigid reinforced concrete blocks. The dimension of the test specimens are shown in Figure 3.6. The load was applied through a hydraulic actuator connected to top of the loading block. In order to investigate the influence of the new arrangement on the squat wall, aspect ratio of 1 and 0.5 was selected to represent the wall in mid-rise and nuclear industrial building. In all of the specimens, the wall had the rectangular cross section, 40" long and 4" thick. In the first group of specimens, the height of the wall was 40", which interpreted into a wall height-to-length ratio of 1.0. The gap between the two cages was selected 1" and 2.5" wide (clear distance between transverse reinforcement) to

investigate the influence of the gap width on the seismic behavior of the squat wall. In the second group with the height-to-length ratio of 0.5, the height of the wall was 20". Also, this wall consisted of 6 separate cages with 2.5" gap between the cages. The concrete compressive strength for all tests approximately was in the range of 4000 to 5500 psi. The main features of the test specimen are provided in table 3.3.

Table 3-3 Description of the Test Specimen

specimen	Dimension (inch)	Aspect ratio (M/Vl_w)*	Number of separate cage	Gap width (inch)	Shear Stress (psi)	Concrete Material
SW-1	40x40x4	1 (1.22)	2	1"	$10\sqrt{f_c'}$	Regular concrete
SW-2	40x40x4	1 (1.27)	4	1"	$8\sqrt{f_c'}$	Regular concrete
SW-3	40x40x4	1 (1.27)	4	2.5"	$4.5\sqrt{f_c'}$	Regular concrete
SW-4	40x40x4	1 (1.27)	4	2.5"	$10\sqrt{f_c'}$	Regular concrete
SW-5	40x40x4	1 (1.35)	4	2.5"	$10\sqrt{f_c'}$	Regular concrete
SW-6	40x20x4	0.5 (0.77)	6	2.5"	$15\sqrt{f_c'}$	Regular concrete

* l_w is the height of the wall from the face of the footing block to the loading point

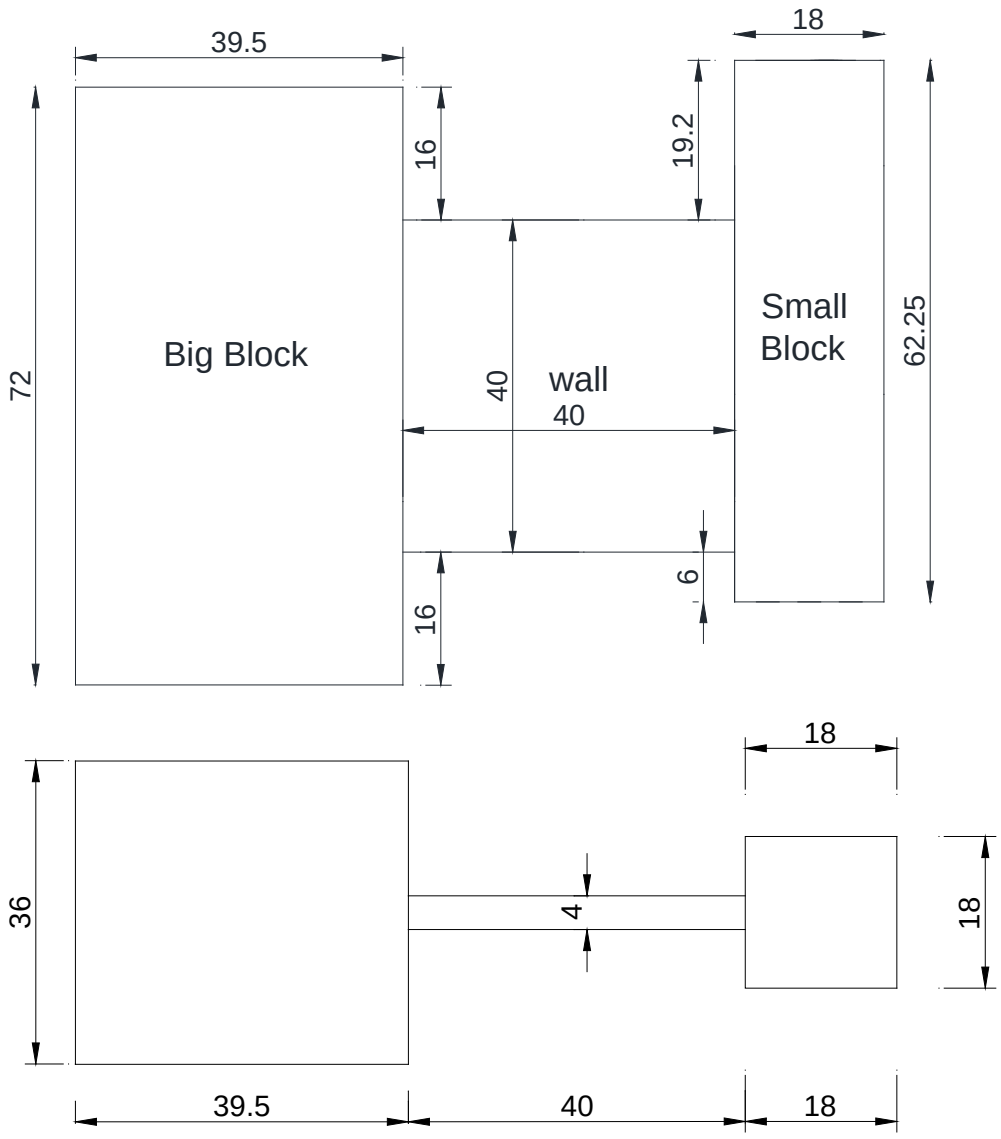

a) Specimen SW-1 (all dimensions in inches)

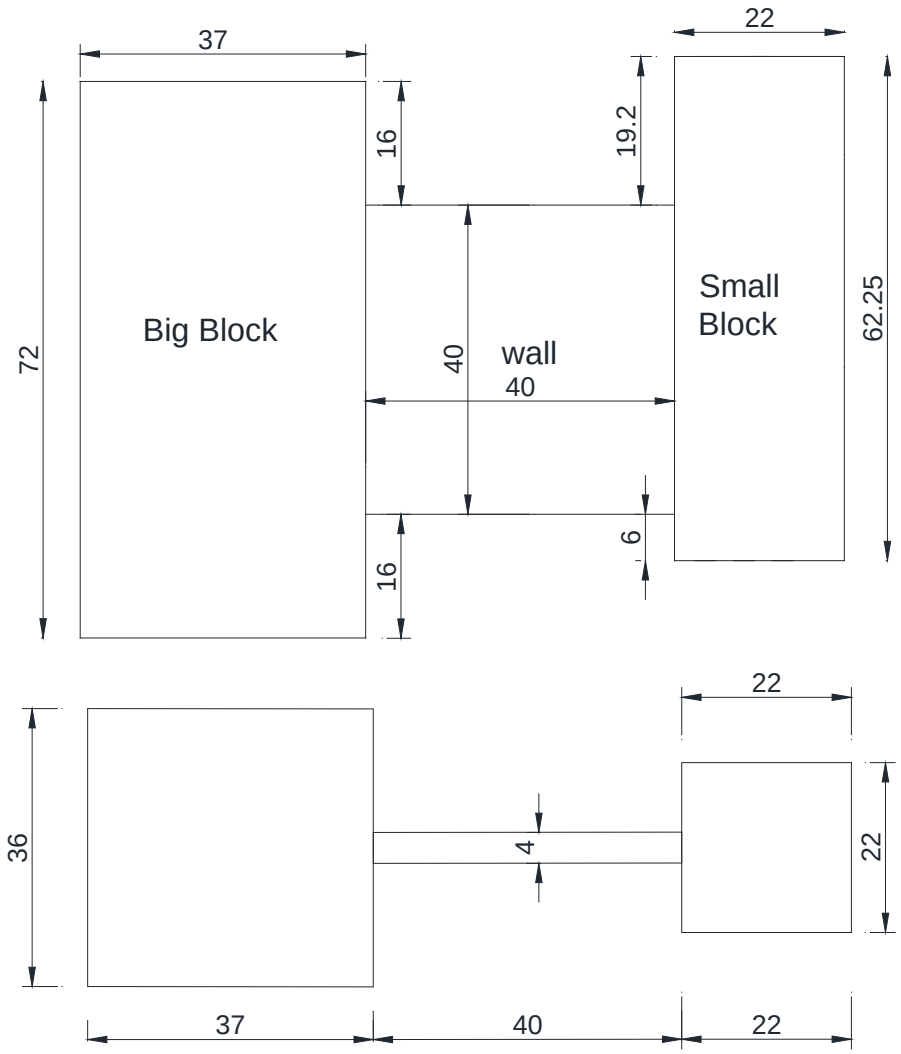

b) Specimen SW-2, SW-3, SW-4 (all dimensions in inches)

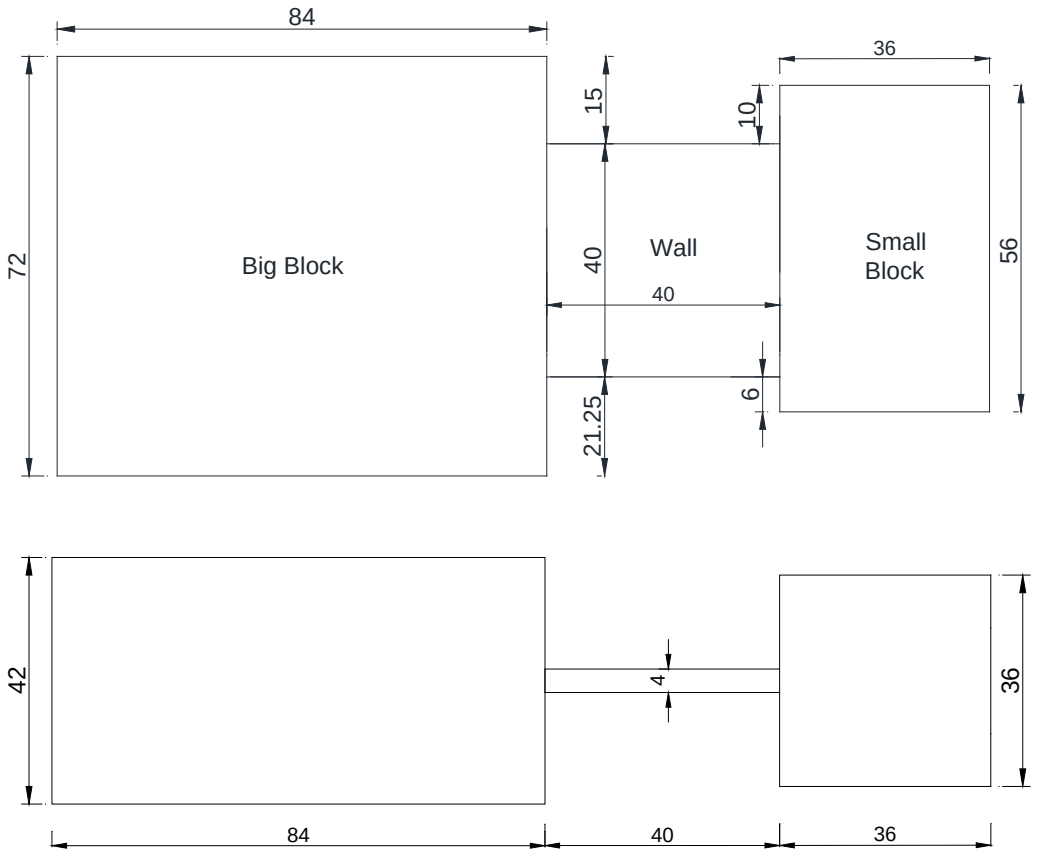

c) Specimen SW-5 (all dimensions in inches)

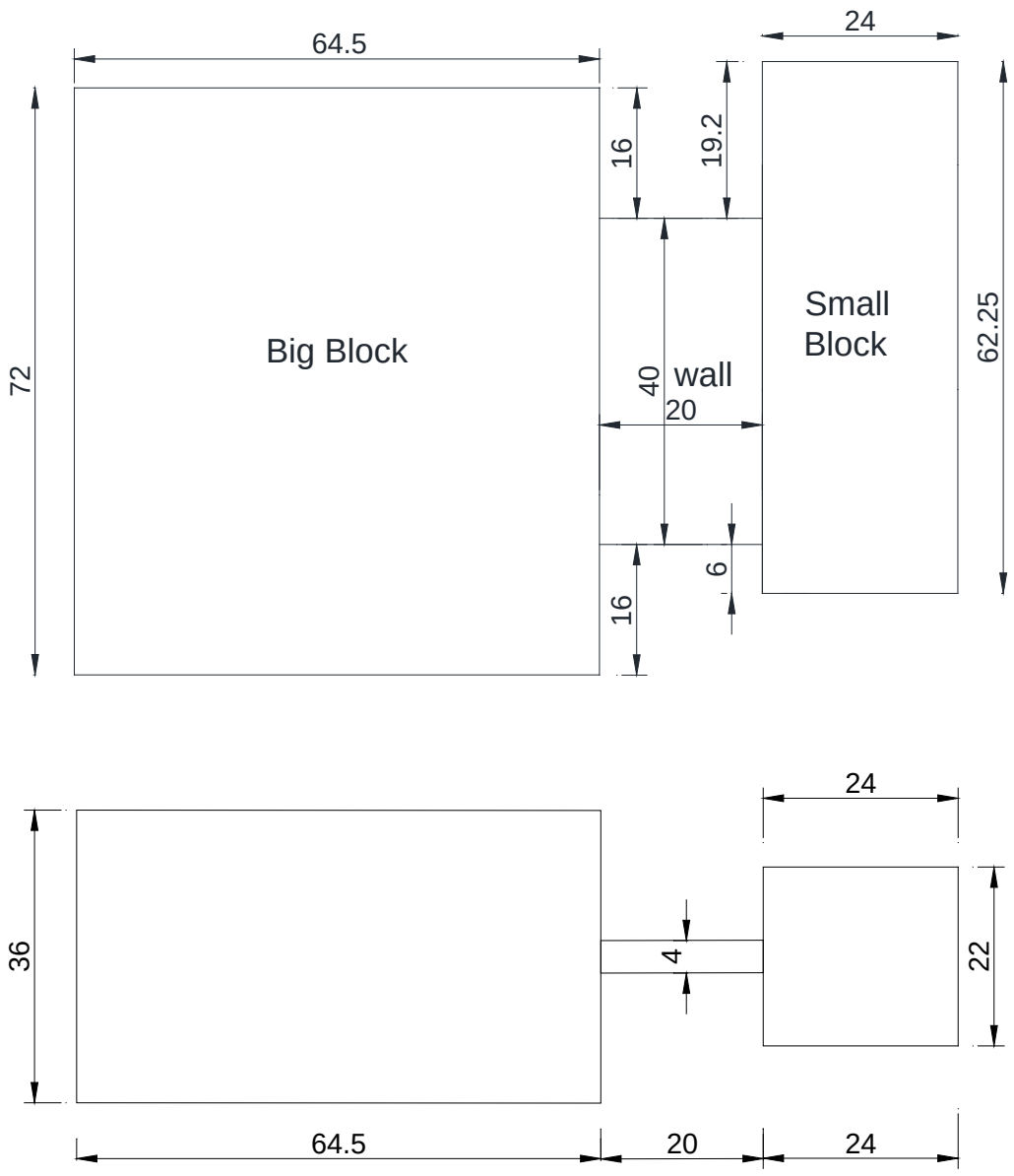

d) Specimen SW-6 (all dimensions in inches)

Figure 3-6 Dimensions of the test specimens

3.3.1 Design of the Squat Wall with New Details

Based on the conclusions drawn from the first phase, DBCB coupling beam, second phase consisted of six approximately 1/3-scale squat walls were designed. The primary intent of these tests was to study the impact of using the several separate cages with gap between the cage in the squat wall on the shear strength and ductility. These cages could make the good confinement for entire of the wall, thus leads to increase the contribution of the concrete in the peak shear strength and prevent shear failure at early drift stage in the squat wall.

The squat wall with height-to-length ratio of 0.5 and 1 was investigated in this study. The dimension of the 1/3-scale squat wall with aspect ratio of 1 was 40" length, 40" height and 4" width. For the other specimen, the height-to-length ratio was 0.5, leading to a wall height of 20". For all of the specimens, target shear stress was between to $15\sqrt{f_c'}$ (psi) which is satisfied by each cage capacity and concrete contribution.

Each cage in the squat wall was designed similar to those used for typical beams in reinforced concrete special moment frames (Section 18.6.4, ACI318-14). The longitudinal and transverse reinforcement in each cage was chosen such that the target shear stress level (V_u) could be attained without a premature shear failure. In other words, The longitudinal bars was designed based on the flexural strength demand at the base of each wall, $M_u = V_u l_w$, where l_w is the height of the squat wall from the face wall near the footing block up to the loading point.

All longitudinal bars were fully anchored in to the footing and loading block. Development length for all of specimens was considered shorter than ACI 318-14 requirement, as is shown in table 3.4, to evaluate the new assumption for the development length. For the ACI equation, compressive strength of the concrete, f_c', is

assumed 5000 psi and $\frac{C_b + K_{tr}}{d_b}$ assumed 1.5 based on the current practice construction that commentary of the ACI 318-14 mentioned.

The transverse reinforcement in these specimens was designed according to the target shear strength and confinement and requirements specified for flexural members of special moment frames in Section 18.6.4 in ACI 318-14.

Table 3.4 Development Length for Longitudinal Bars

	Development Length Equation	Bar#3	Bar#5	Bar#6	Bar#7
Development Length	-	18"	18"	18"	18"
ACI318-14	$\left(\frac{3}{40} \frac{f_y}{\lambda\sqrt{f_c'}} \frac{\Psi_t \Psi_e \Psi_s}{\left(\frac{C_b + K_{tr}}{d_b}\right)} \right) d_b$ $\left(\frac{C_b + K_{tr}}{d_b}\right) = 1.5$, $f_c' = 5000$ (psi)	17"	28"	33"	38"
ACI318-14 (18.8.5)	$\frac{1.25 \times 3.25 \times (f_y d_b)}{65\sqrt{f_c'}}$, $f_c' = 5000$ (psi)	21"	34"	41"	47"

The footing and loading block in each specimen were designed conservatively to remain elastic, and also, resist the maximum shear load which is applied to the squat wall during the test. The maximum shear loads in this study was approximately 150 and 205 kips for wall with aspect ratio 1 and 0.5 respectively. The reinforcement detailing for footing and loading blocks are demonstrating in Figure 3.7 and 3.8 respectively.

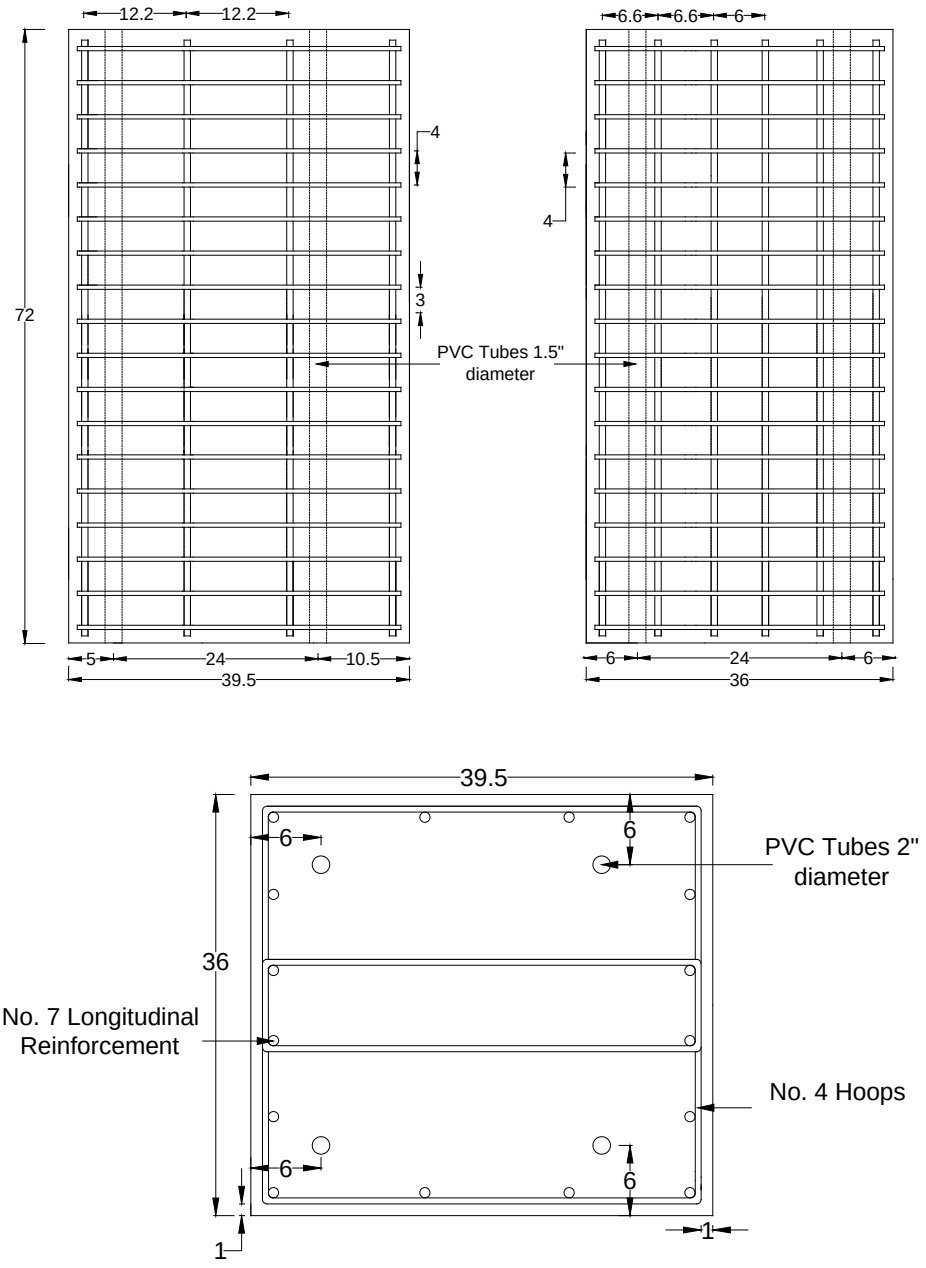

Figure 3-7 Big block reinforcement detailing for SW-1 (all dimensions in inches)

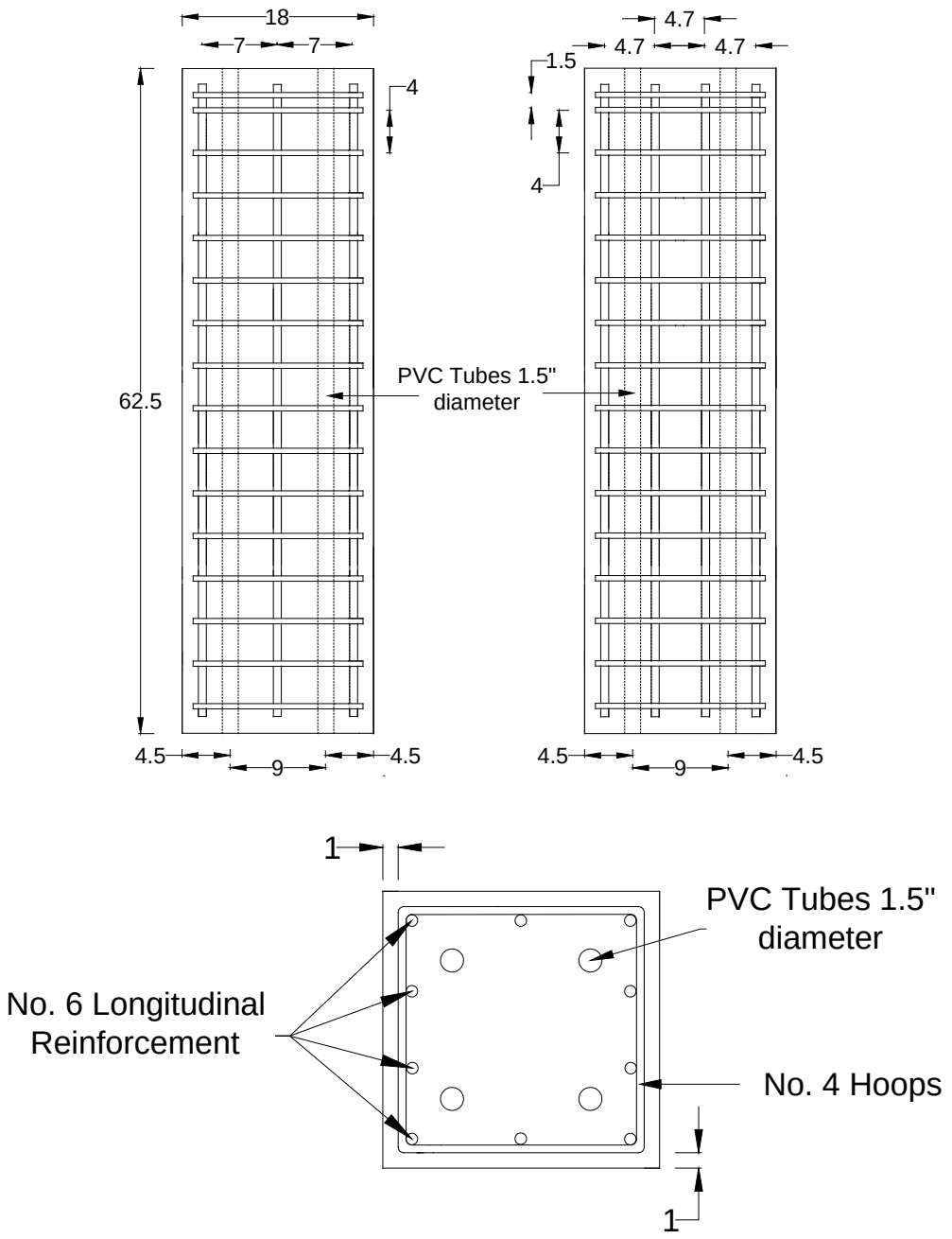

Figure 3-8 Small block reinforcement detailing for SW-1(all dimensions in inches)

Three types of reinforcement bars were used in the design of squat wall, longitudinal reinforcement, and hoops. Detailing for squat wall specimen is explained below.

3.3.1.1 Specimen SW-1 ($\ell/h = 1$)

First specimen was constructed with regular concrete with specific compressive strength of 5000 (psi) to evaluate the influence of using two separate cages with 1" gap in seismic behavior of the wall. This specimen was designed to sustain shear stress demand of approximately 10 $\sqrt{f_c'}$ (psi). The contribution of concrete to wall shear strength was assumed 3 $\sqrt{f_c'}$ (psi). Therefore, the longitudinal reinforcement for each cage was selected such that shear stress demand 7 $\sqrt{f_c'}$ (psi) would be imposed on the cage. Each cage was designed based on the half of the total moment demand which was calculated as $M_u = V_u l_w$, where l_w is equal to 49".

The main longitudinal reinforcement consisted of three layers of No.6 Grade 60 bars placed near the top, bottom, and middle of the each cage, continuous through the wall and fully anchored in the footing and loading beam.

Transverse reinforcement designed to carry the shear demand. The transverse reinforcement was provided based on the requirements of the Chapter 18 of ACI Code (ACI 318-14) for flexural member of special moment frame. No. 3 hoops were used at 4" spacing. Figure 3.8(a) shows the reinforcement details for first squat wall.

3.3.1.2 Specimen SW-2 ($\ell/h = 1$)

With test results of the first specimen in terms of shear strength, ductility, and crack pattern, the second specimen with four cages and 1" gap was designed and constructed with regular concrete to evaluate the influence of this detail on the seismic behavior of the squat wall. The specific concrete compressive strength was 4900 (psi).

This specimen was designed to carry a shear stress of approximately $8\sqrt{f_c'}$ (psi). According to the first test result, the contribution of the concert in the shear strength was higher than $3\sqrt{f_c'}$ (psi), therefore, the longitudinal reinforcement for each cage was selected based on the shear stress demand equal to $5\sqrt{f_c'}$ (psi).

The main longitudinal reinforcement consisted of two layers of No.6 Grade 60 bars placed near the top and bottom, of the each cage. All the longitudinal bars were fully developed in the footing and loading beam.

Transverse reinforcement was expected to approximately carry the shear demand target. According to the requirement of the Chapter 18 of ACI building code (ACI 318-14) for flexural member of special moment frames, close confinement was designed at the end of the wall near the footing block where first flexural yielding and spalling of the concrete shall very likely to occur. Therefore, No.3 hoops spaced at 2.25" were selected. Out of this region, No.3 hoops spaced at 4.5" were chosen. Figure 3.8(b) shows the reinforcement details for second squat wall.

3.3.1.3 Specimen SW-3 ($\ell/h = 1$)

Sliding shear played a significant role in the behavior of the specimen 2, which was constructed without adequate confinement for entire height of the wall and the longitudinal bars did not appropriate distribute over the length of the wall. Thus for the third specimen longitudinal bars were distributed along the length of the wall and for each cage close hoops were used for 2/3 of the height of the wall, as demonstrated in Figure 3.8(c). This specimen with four cages was constructed with regular concrete with specific compressive strength of 5500 (psi). On the other hand, the height of the gap was increased to 2.5" to evaluate the effect of the gap on the seismic behavior of the wall. In order to investigate the possibility of utilizing the gap; two 2.5" pipes were used in each

row of the gap. The maximum shear demand of approximately 4.5 $\sqrt{f_c'}$ (psi) was aimed for this specimen. The contribution of the concrete was assumed around 3 $\sqrt{f_c'}$ (psi). Therefore, the longitudinal bars for each cage were designed to sustain shear stress 1.5 $\sqrt{f_c'}$ (psi). Each cage was consisted of three layers. Three layers of No.3 were selected for the middle cages. The first and last cage had the same arrangement. Two No.6 bars were selected for the layer near the end of the wall for these cages to prevent the flexural cracks opening. For the other layers 2 No.3 was chosen.

According to Chapter 18 of ACI building code (ACI 318-14), the confinement reinforcement in each cage consisted of single No.3 hoops, spaced at 2.25" for 2/3 of the wall's height from the face of the footing.

3.3.1.4 Specimen SW-4 and SW-5 ($\ell/h = 1$)

Test results of the first three specimens confirmed the effectiveness of using the several cages with the gap to improve the peak shear strength of the squat wall while provided the adequate ductility. Also, Based on pervious experimental investigations, discussed in Section 2.2, maximum shear stress for rectangular squat walls is smaller than 10 $\sqrt{f_c'}$ (psi), which is upper limit of the shear strength in ACI 318-14.

Therefore, the squat wall SW-4, SW-5 with the same geometry and reinforcement detail was designed to evaluate the influence of the four cages with close confinement and large amount of longitudinal bars on the maximum shear strength and ductility of the rectangular squat wall. The difference between SW4 and 5 was in the footing block dimension. Concrete specific compressive strength for this specimen was 4000 psi. The maximum shear demand was expected more than 10 $\sqrt{f_c'}$ (psi) for these specimen. Large amount of the longitudinal reinforcement with close hoops was used to

develop the Maximum shear stress. Three layers of the No.5 bars were designed for the longitudinal reinforcement in the middle each cages based on the shear stress target 5.5 $\sqrt{f_c'}$ (psi). The large diameter of the longitudinal bars was designed for boundary cages to prevent the flexural crack opening. As a result, two No.7 bars were selected for top and bottom layer and 2 No.5 bars was used at the middle layer to reach shear stress approximately 9 $\sqrt{f_c'}$ (psi) for the first and last cage in the wall. According to Section 18.6.4 of ACI building code (ACI 318-14), No.3 hoops was selected and spaced at 2" for entire height of the wall. The reinforcement details for these specimens are shown in Figure 3.8(d).

3.3.1.5 Specimen SW-6 ($\ell/h = 0.5$)

With the successful test of the rectangular squat wall with aspect ratio 1 in term of shear stress and ductility, the possibility of using this configuration in the rectangular wall with aspect ratio 0.5 was explored. Concrete compressive strength of 4500 (psi) was specified. The range of the target shear stress for this squat wall was expected more than 15 $\sqrt{f_c'}$ based on the result for SW-5. Main flexural reinforcements for each cage were selected 2 No.7 bars at the top and bottom layer at the first and last cage. Also, for the other cage, 2 No.5 longitudinal bars were used at the top and bottom layer in each cage. The confinement reinforcement was No.3 and spaced at 2". The reinforcement configuration for this specimen is illustrated in Figure 3.8(e).

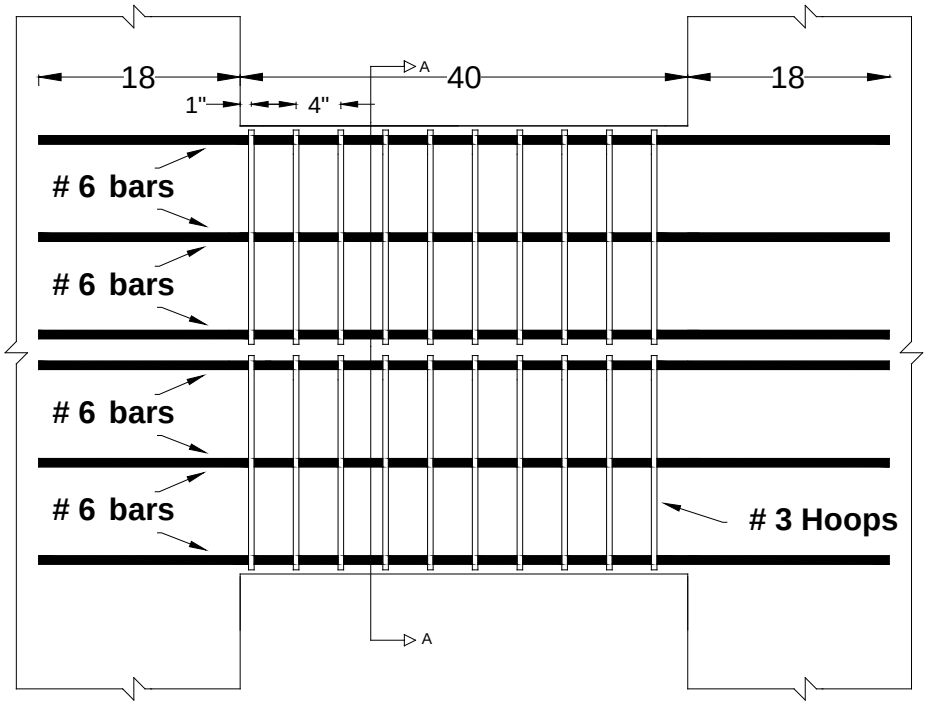

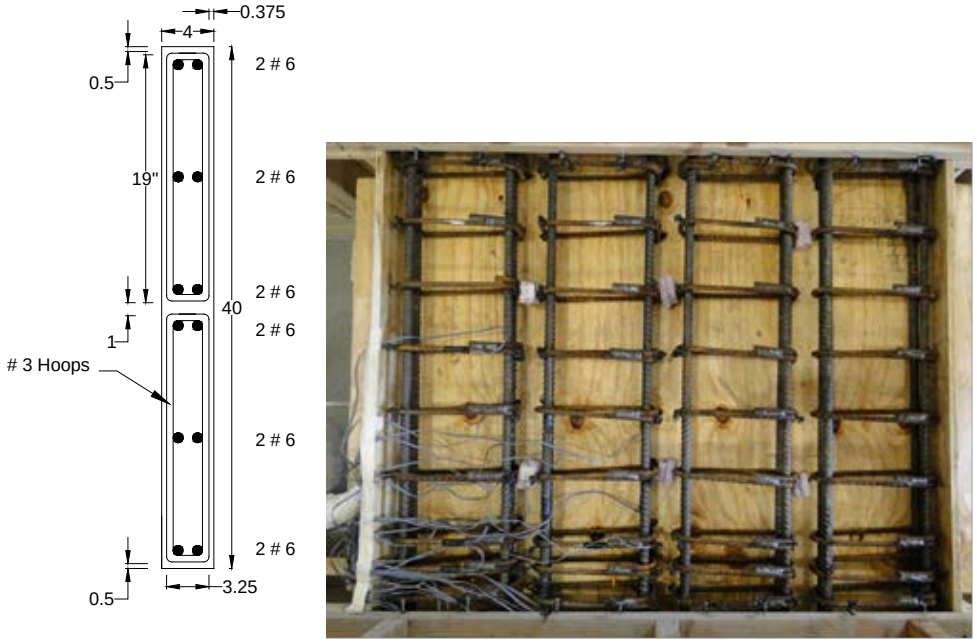

a) Specimen SW-1 (all dimensions in inches)

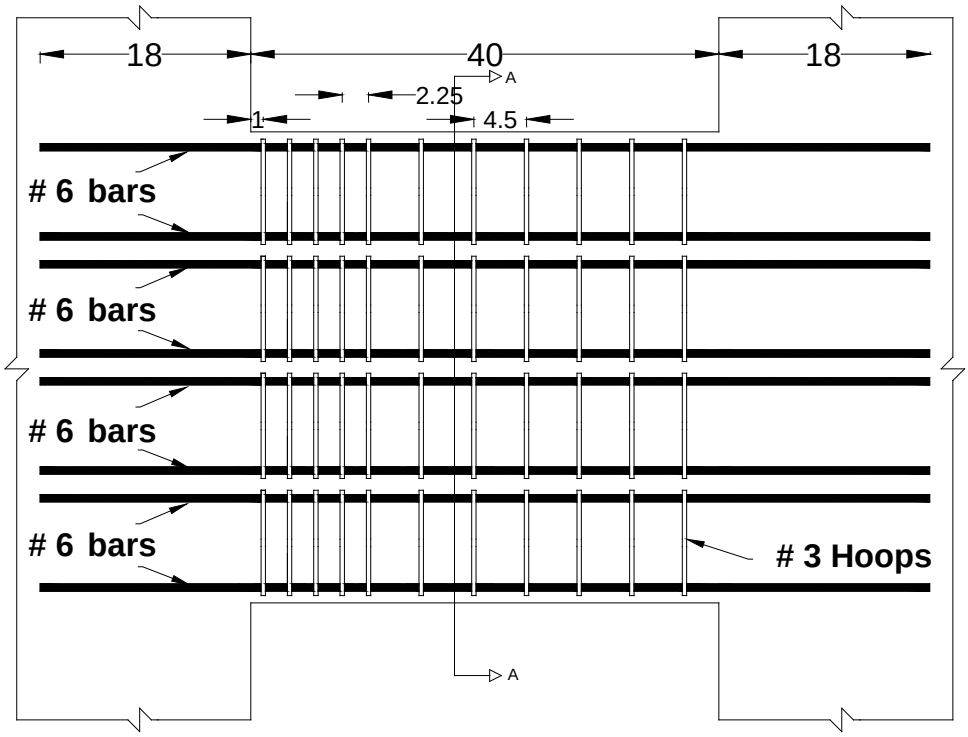

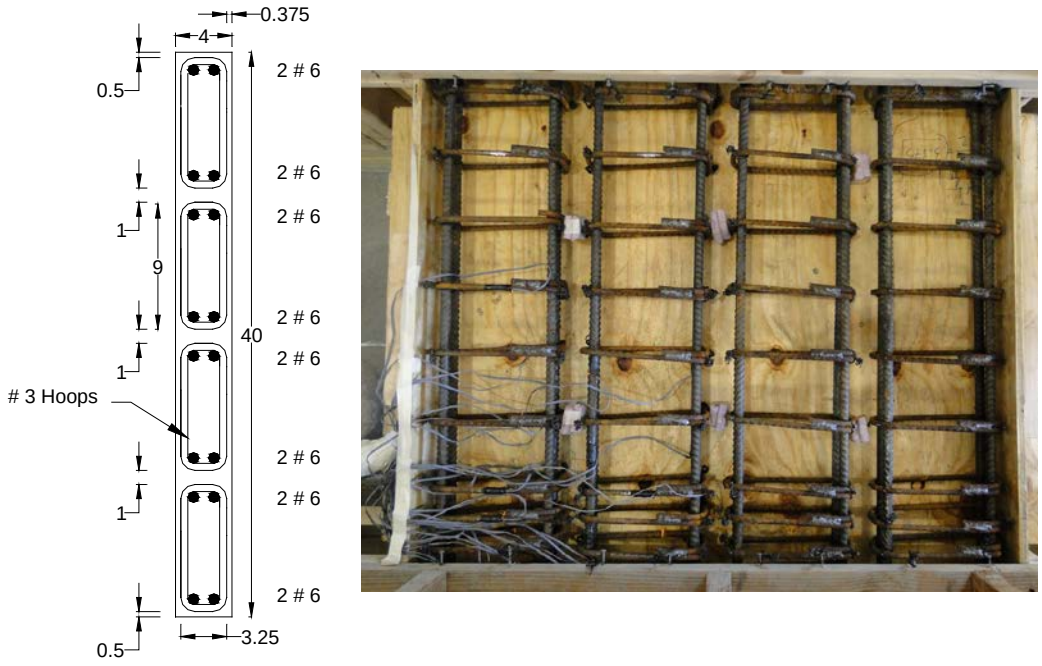

b) Specimen SW-2 (all dimensions in inches)

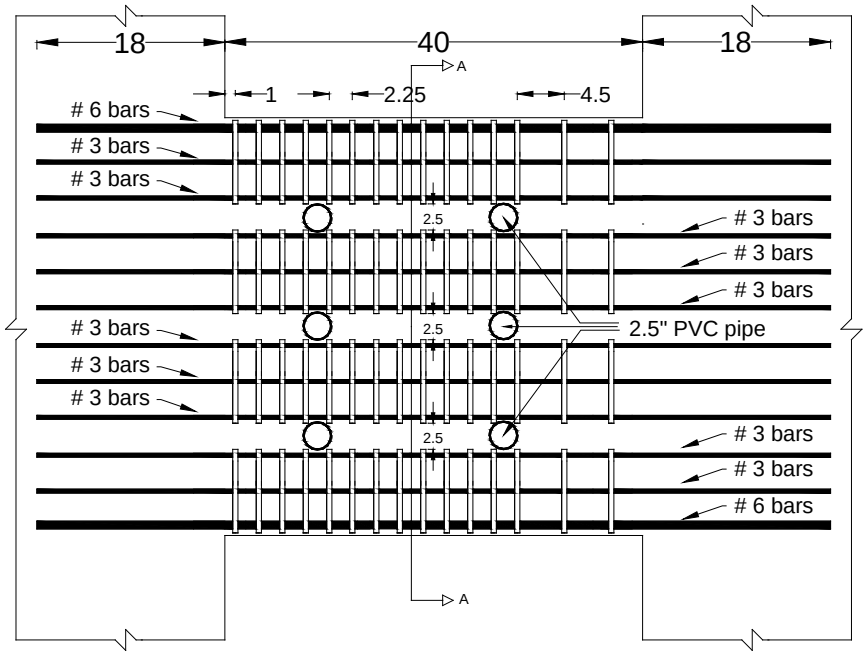

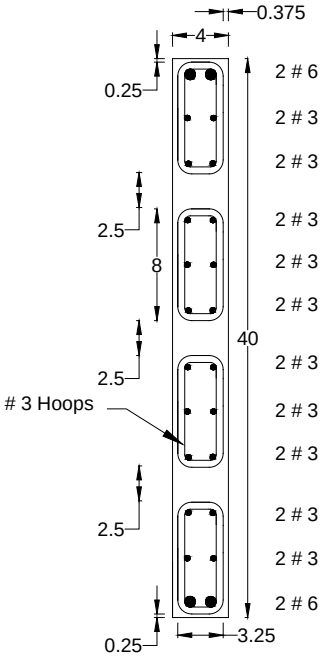

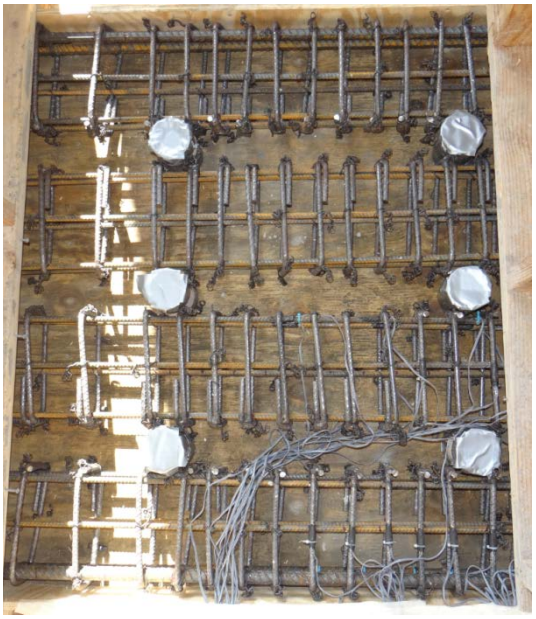

c) Specimen SW-3 (all dimensions in inches)

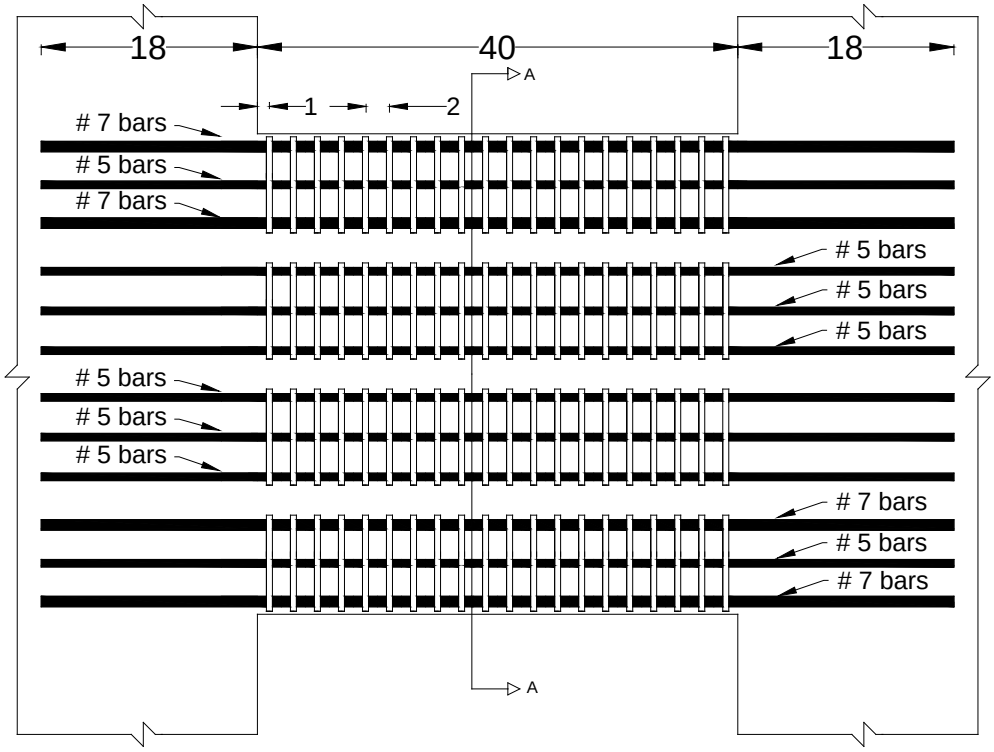
18
40
18
A
1
2
7 bars
5 bars
7 bars
5 bars
5 bars
5 bars
5 bars
5 bars
5 bars
5 bars
7 bars
5 bars
7 bars
A

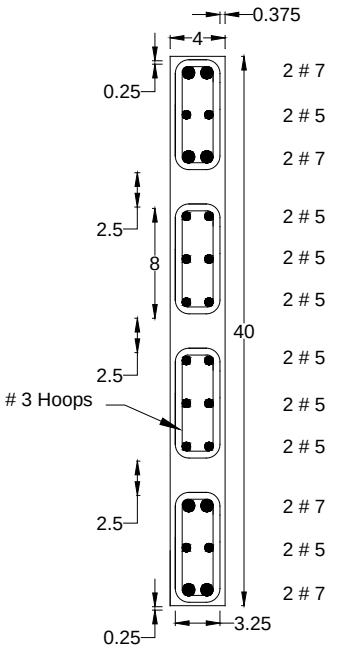
0.375
4
0.25
2.5
8
2.5
40
2.5
0.25
3.25
3 Hoops
2 # 7
2 # 5
2 # 7
2 # 5
2 # 5
2 # 5
2 # 5
2 # 5
2 # 7
2 # 5
2 # 7

SW-4

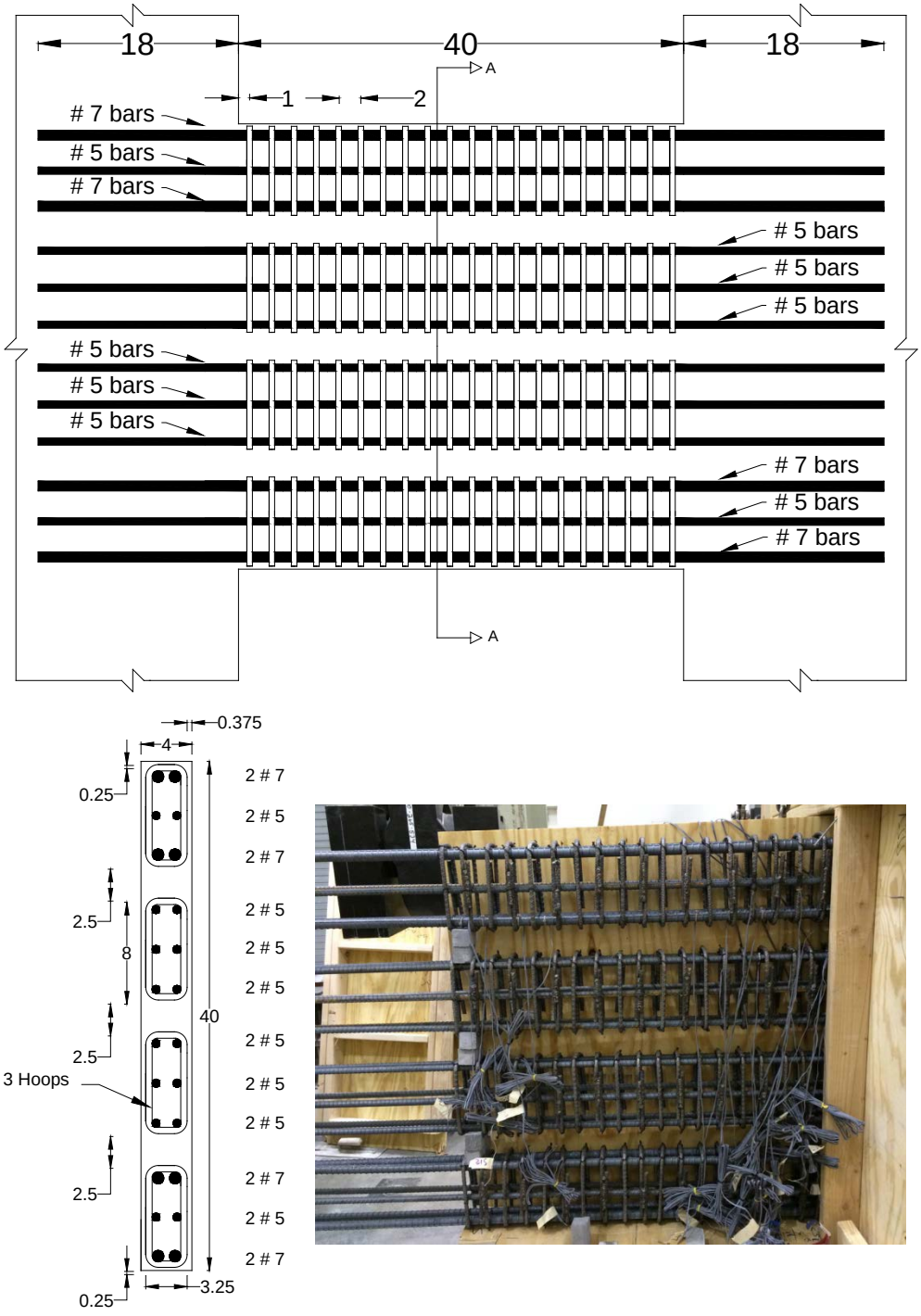

d) Specimen SW-4 and SW-5 (all dimensions in inches)

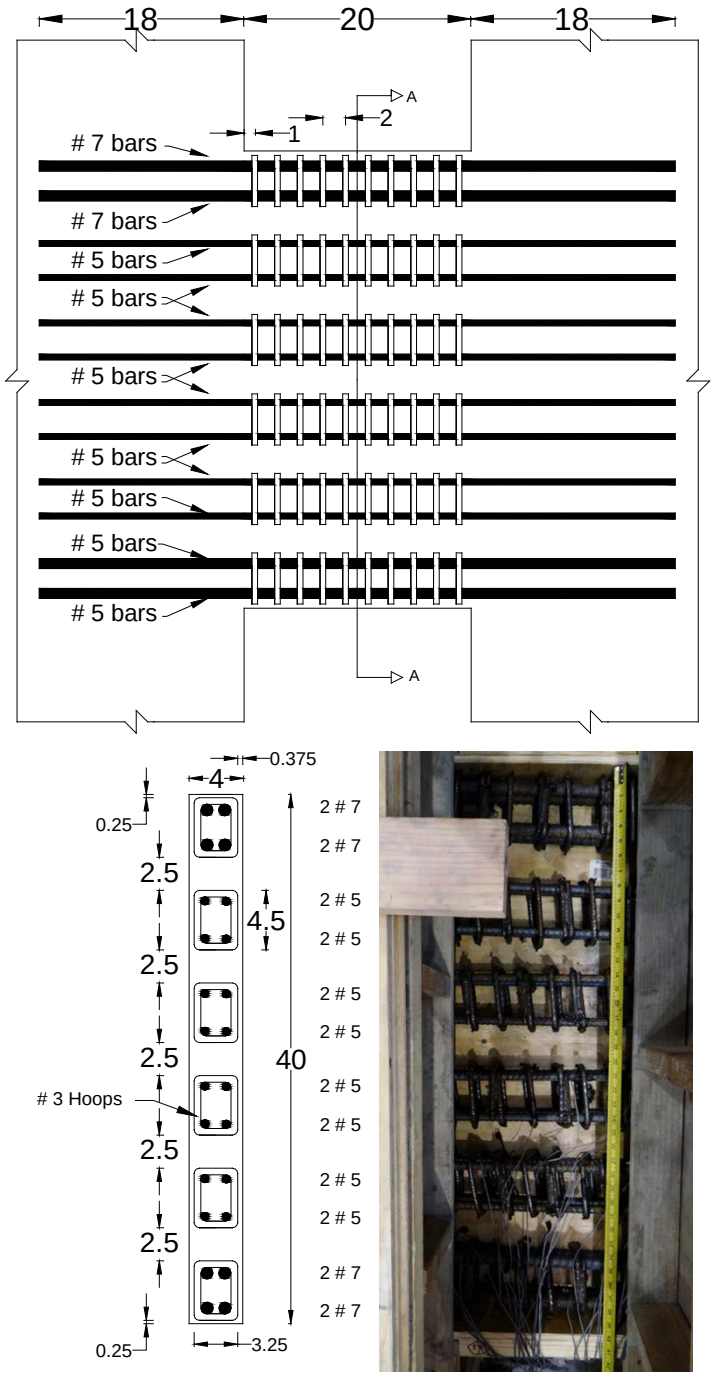

e) Specimen SW-6 (all dimensions in inches)

Figure 3-9 reinforcement layouts Squat wall

3.4 Construction of Specimens

The construction of the all specimens was completed in the University of Texas at Arlington Structure Engineering Laboratory. Reinforcing bars and hoops were obtained from a local supplier, and then cut according to the specimen details. Also, steel I-section, and several plates were ordered from local supplier. Ready-mix concrete was ordered from a local ready-mix concrete producer to cast the specimen.
Construction process for all specimens consists of several steps, as shown in 3.10 and 3.11. First, the construction of the specimens began with assembling of wooden formwork. The formwork for the big block and loading block was composed of individual pieces connecting with 3/8" bolts. Each formwork pieces consisted of the plywood that was screwed to the 2x4 wood pieces. Extra stiffeners will be laid out to resist the concrete pressure on formwork during casting. The loading block was elevated to the right height through masonry blocks. Cavities in the formwork have the right dimensions 15"x5" and 15"x6" for the coupling beam and 40"x4" for the squat wall.

Second, it is imperative to locate the PVC pipes accurately to avoid possible conflicts between strong floor and actuator holes. For embedding the PVC pipe to the formwork, wooden disk with the diameter equal to the PVC attached by screw to the formwork to hold the pipes. Third, strain gauges stuck to the several steel reinforcing bars to monitor their behavior. Third, the reinforcement cages for the small, big, and coupling beams or squat wall including the instrumented reinforcement were assembled. After the reinforcement cages were completed, the cage for the big and loading block was placed in the formwork, then the coupling beam or squat wall cage's was lifted by crane and inserted to the big block. The reinforcement cage for the loading block was then slid through the other end. Fourth, PVC pipe were placed in to the formwork for passing the high strength threaded rods that would be used to connect the concrete big blocks to

strong floor and the concrete small block to the steel wide flange section or actuator. Then, the specimen was casted with ready-mix concrete and internal vibrator was used during the casting process of all specimens.

The formwork was removed from the entire specimen after few days of casting. When the compressive strength of the concrete was more than 4 ksi, the specimen were lifted to a vertical position with a crane and a forklift, and put in the test setup.

Finally, specimens were braced laterally to prevent out-of-plane movements and twisting. The threaded bars were post tensioned with hydraulic jack and super nuts which passing through the small block and big block to fix them to the steel wide flange section or actuator and strong floor respectively.

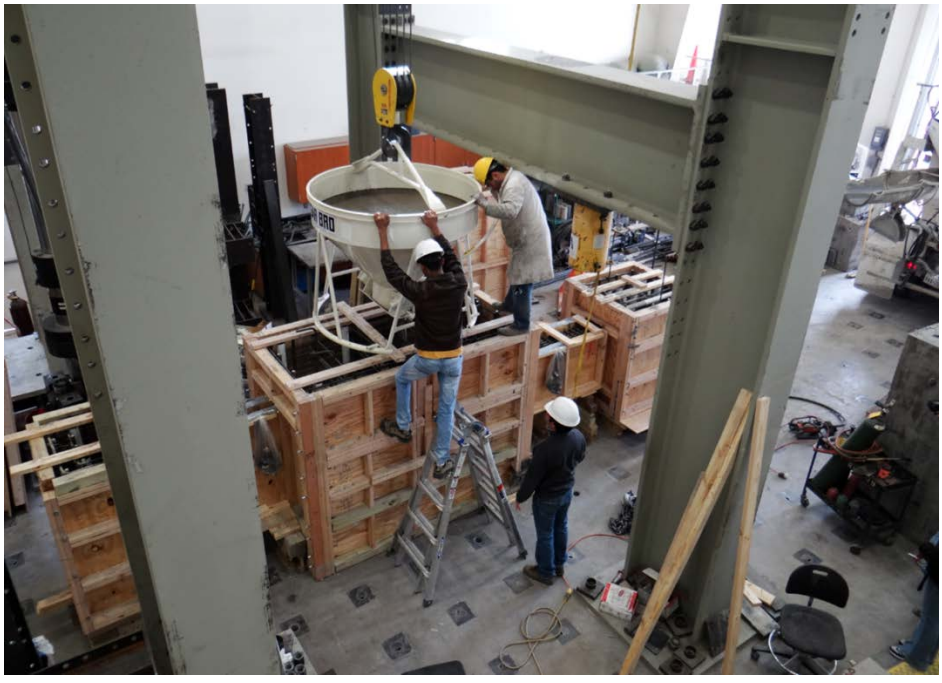

a) Construction Of full scale coupling beam

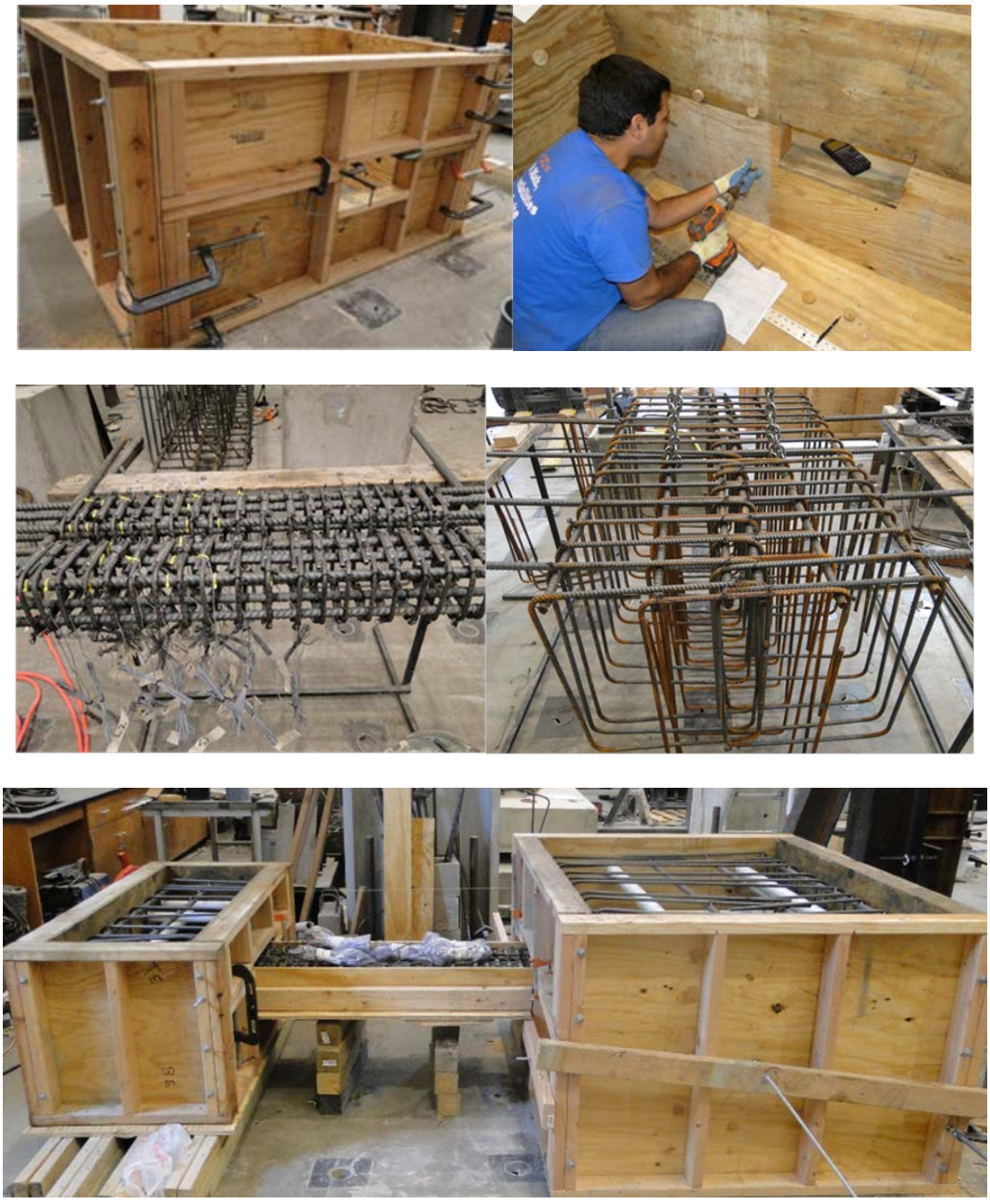

a) Construction Of half scale coupling beam

Figure 3-9 Construction of the coupling beam

Figure 3-10 Construction of the Squat wall

3.5 Test Setup

During the first phase of the coupling beam study, different test setup for coupling beam were evaluated and finalized at third specimen. The diagram of the component test setups for coupling beam and squat wall is demonstrated in figure 3.11 and 3.12. Each specimen consisted of a coupling beam or squat wall, and a pair of big and small reinforced concrete blocks representing wall boundary for coupling beam and footing and loading block for squat wall.

All of the specimens, except full scale coupling beam, were cast horizontally, then rotated and placed in the test setups with the big block fixed to the strong floor. Also, the full scale specimen was cast vertically and it was in the exact location that was tested. For test setup, the steel reaction frame that was built by UT Arlington was used. A vertical actuator was connected with four bolts to the horizontal beam for steel reaction frame. In the test set up, to provide a fixed boundary condition for coupling beam and squat wall, at least four unbonded 1.25" diameter threaded rods were used to fix the big block to the laboratory strong floor.

For the coupling beam test, the cyclic load was applied via a vertical actuator, with the line of action of the actuator forces passing through the mid-span of the test specimen to produce an antisymmetrical moment pattern in the coupling beam and zero moment at the beam mid-span. The actuator connected to the small block through a steel wide flange section. The load transferred to the small block by means of direct bearing and unbonded threaded bars passing through the small block used to attach the actuator. It is important to align the specimen according to the center of actuator so that no torsion will be induced on the coupling beam. Two steel links in the above and below the coupling beams were used to prevent rotating of the small block during the loading and to impose a state of double curvature on the coupling beam. In additional, these links were

used to provide some moderate axial restraints for the beams because, in reality, the adjacent structural walls and surrounding slab would provide non-negligible resistance to beam expansion upon cracking.

For the squat wall test, the cyclic load was applied with the vertical actuator, which placed on the top of the loading block directly to produce maximum moment near the footing block and approximately zero moment at the other end of the wall, near the loading block. All of the test specimens were also braced laterally to prevent out-of-plane movements and twisting.

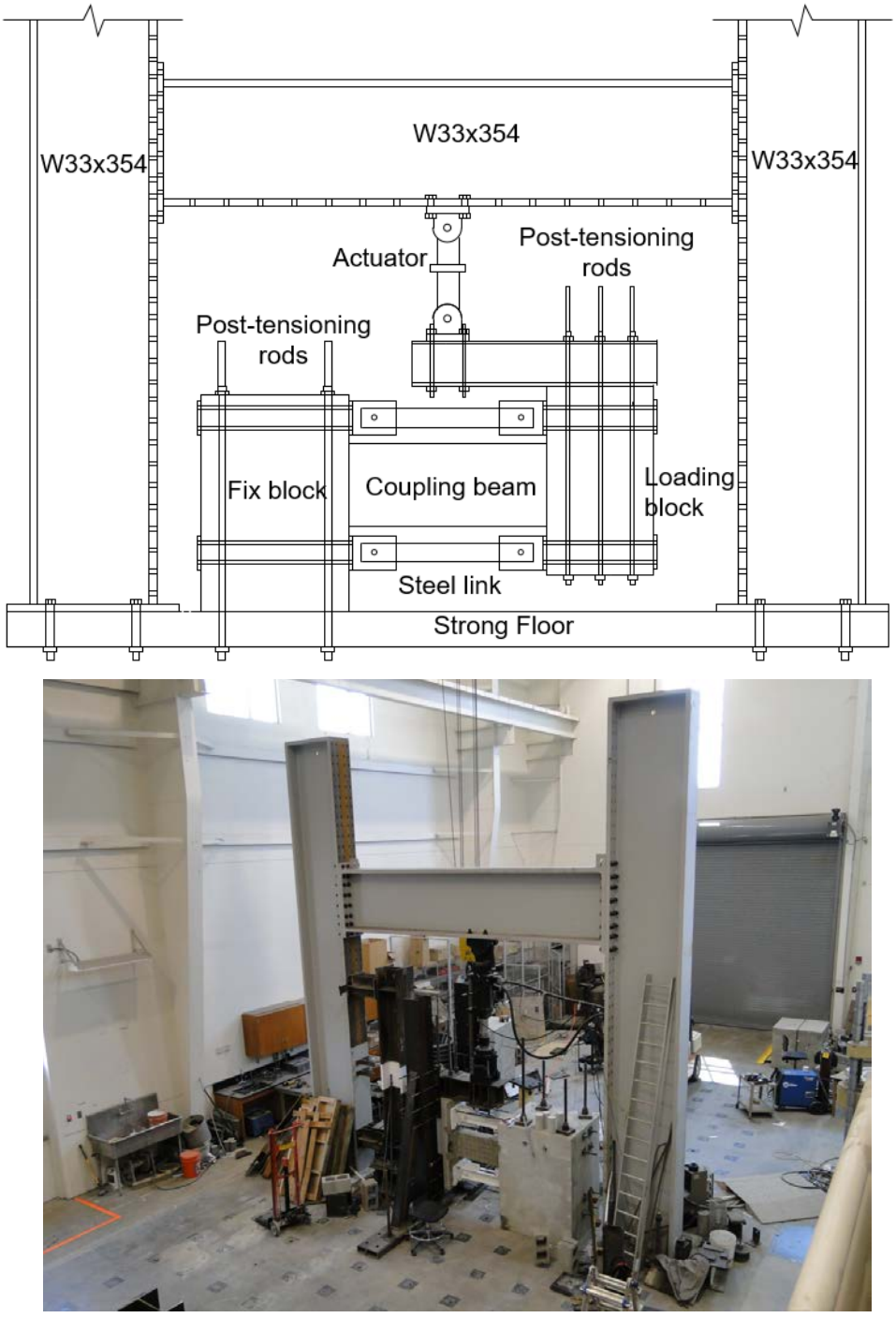

Figure 3.11 Test setup for the coupling beam experiments

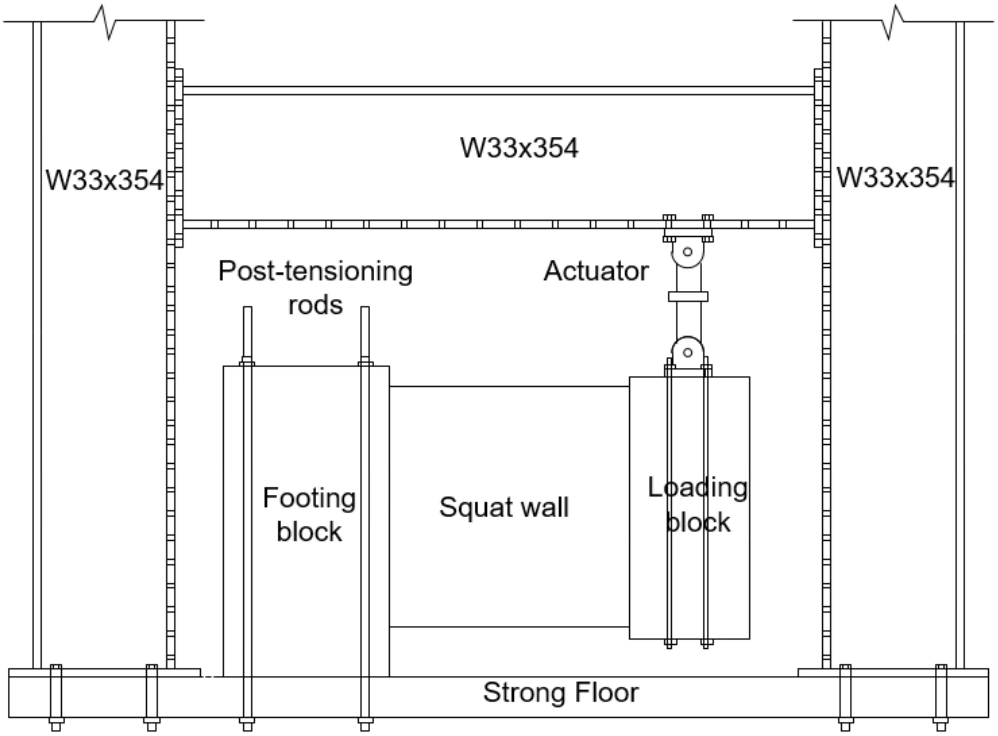

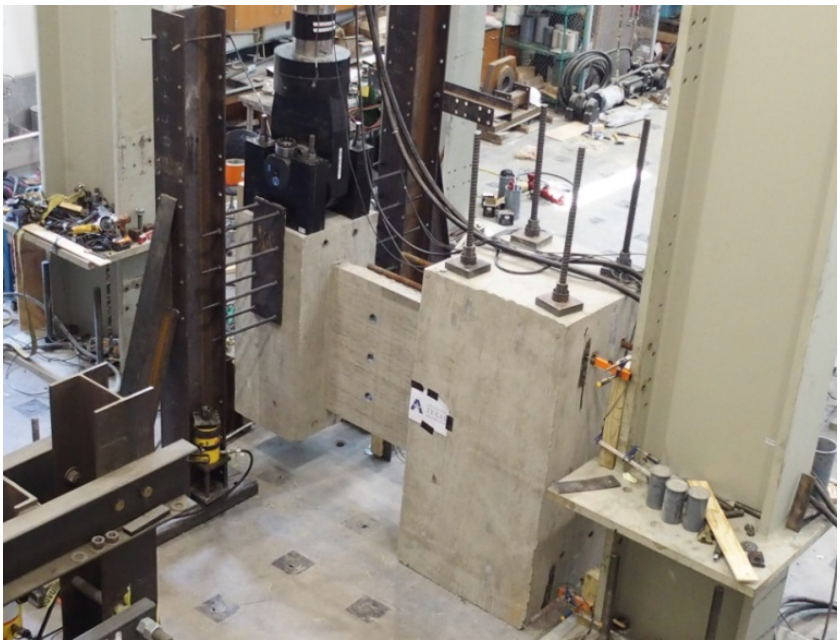

Figure 3-12 Test setup for the squat wall experiments

3.6 Instrumentation and testing procedure

Strain gauges were used to monitor the strains of the longitudinal and transverse reinforcement. The purpose of measuring the strains at the bars was to better understand the behavior of specimens. To achieve this, the locations of the strain gages were determined based on an assumed shear crack path, which was determined from literature review. The locations and labels for strain gauges placed on longitudinal, and transverses reinforcement for coupling beams and squat walls are shown in Figure 3.14. Prior to reinforcement caging, strain gauges were attached at several locations of the Longitudinal and transverse bars. For installing the strain gauges, first the locations of the strain gauges are marked accurately onto the rebars. Second, the ribs on the reinforcing bar were grinded and then sanded with 400 grit sandpaper to create a flat and smooth surface to stick the strain gauges. Third, the smooth surface on the rebars were cleaned with an acid conditioner and neutralized with a base conditioner. Each strain gauge was glued within a degreased flat area and protected by three different types of coating layers, namely polyurethance, nitrile, and rubber pad, and all were sealed by an electric liquid tape, as shown in Figure 3.13.

a) Smooth and clean the surface of the rebars

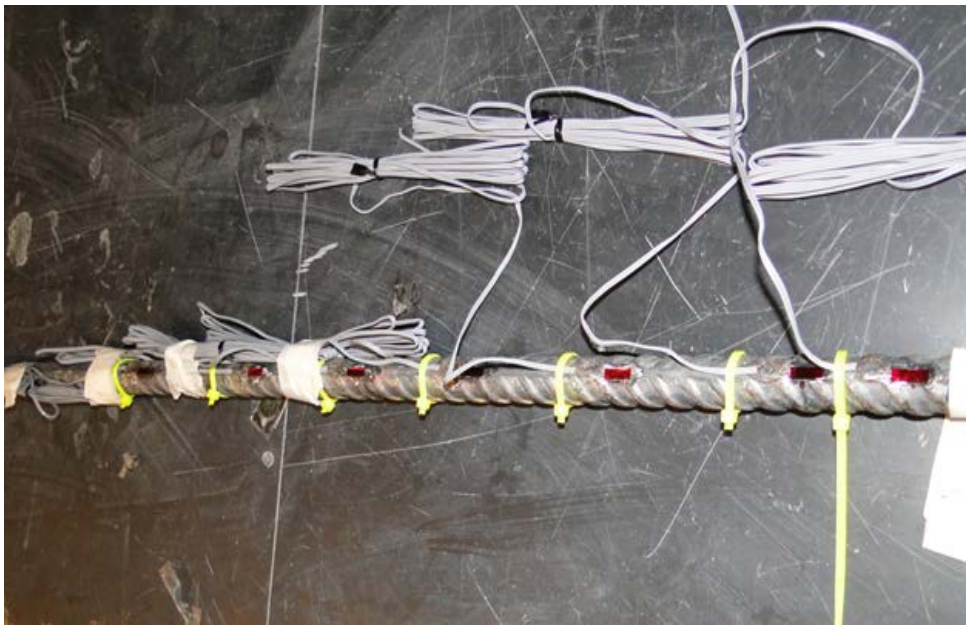

b) Stick the strain gauge and electrical tape

Figure 3-13 Strain gauges

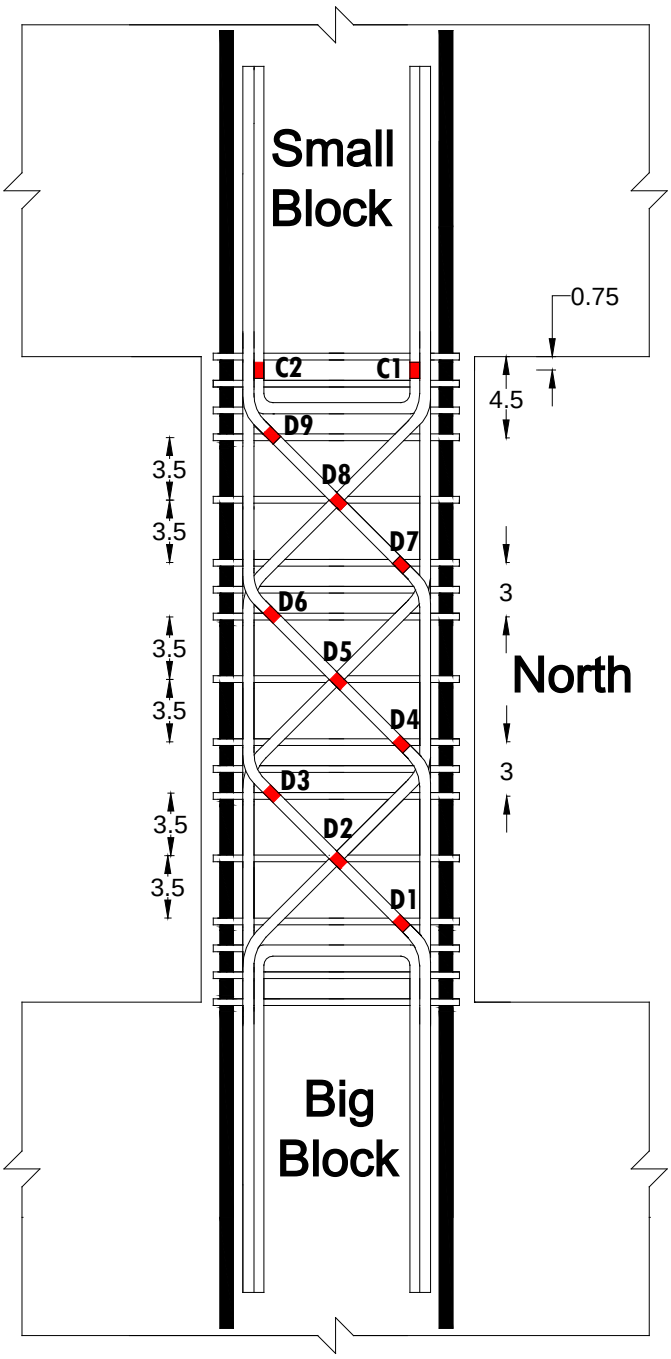

a) Specimen CB-1(North)

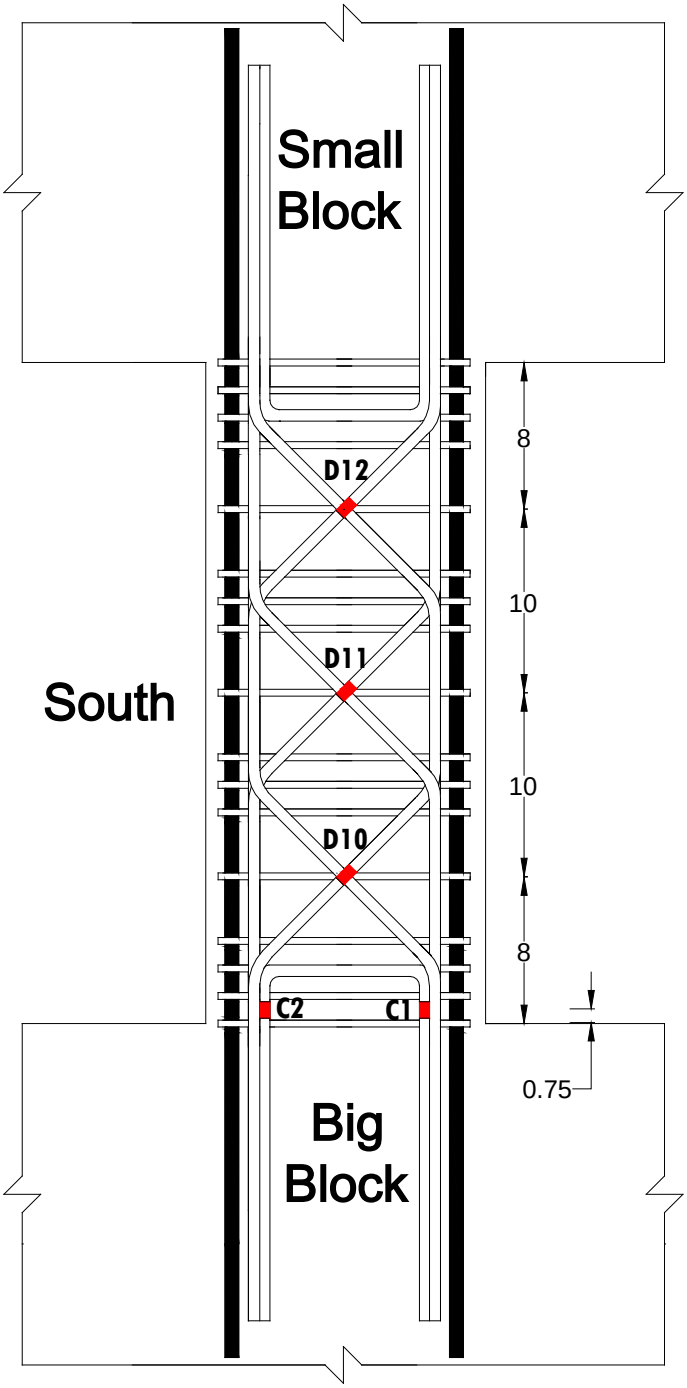

a) Specimen CB-1(South)

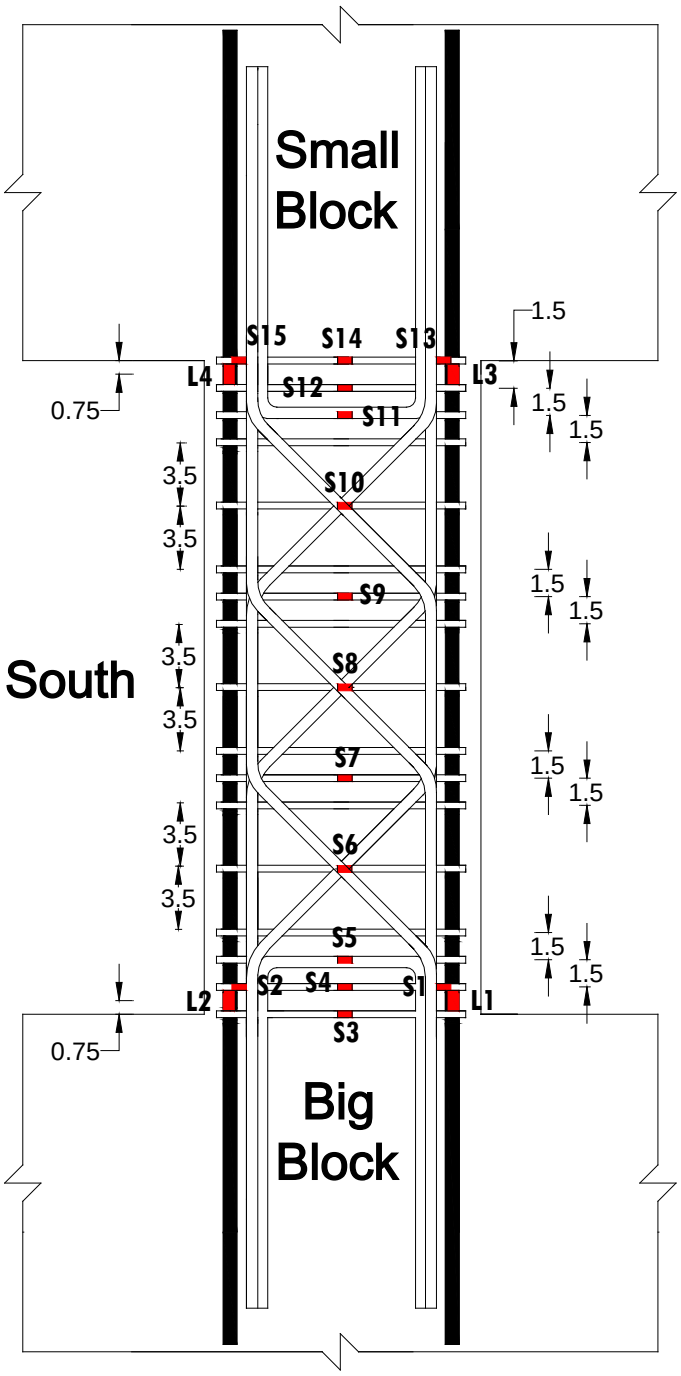

a) Specimen CB-1 (South)

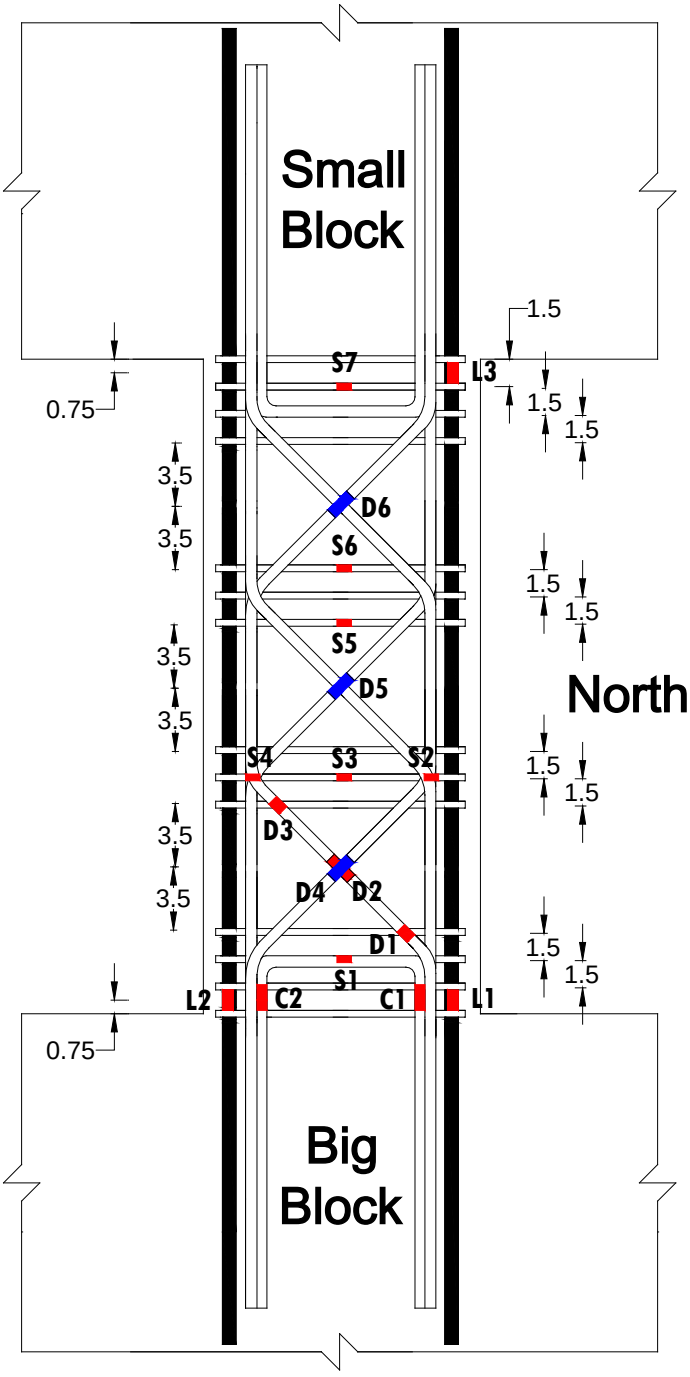

b) Specimen CB-2 (North)

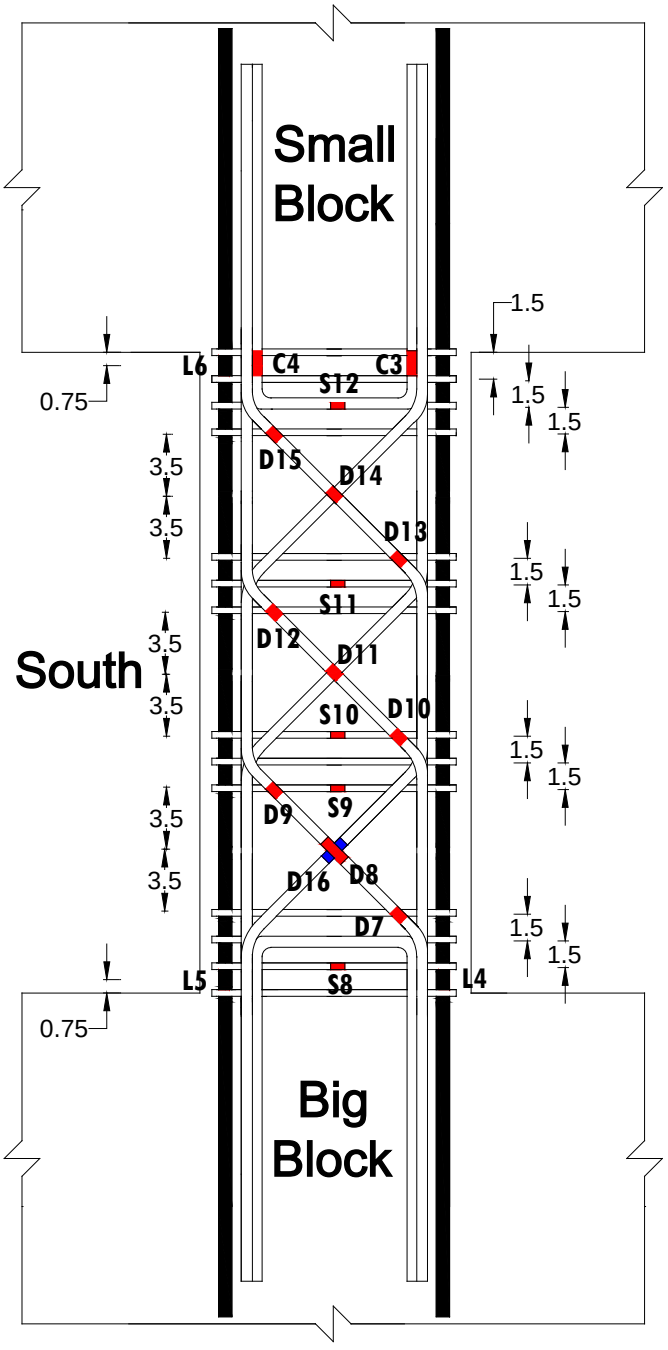

b) Specimen CB-2 (South)

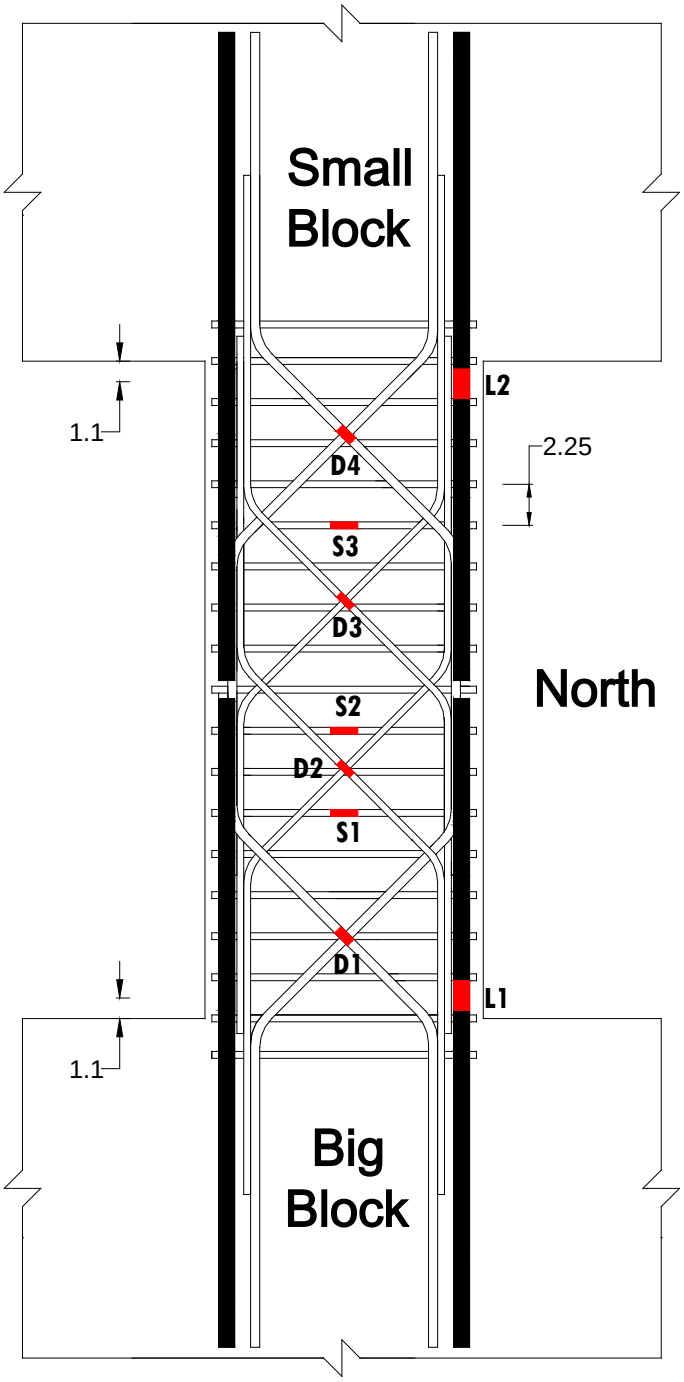

c) Specimen CB-3 (North)

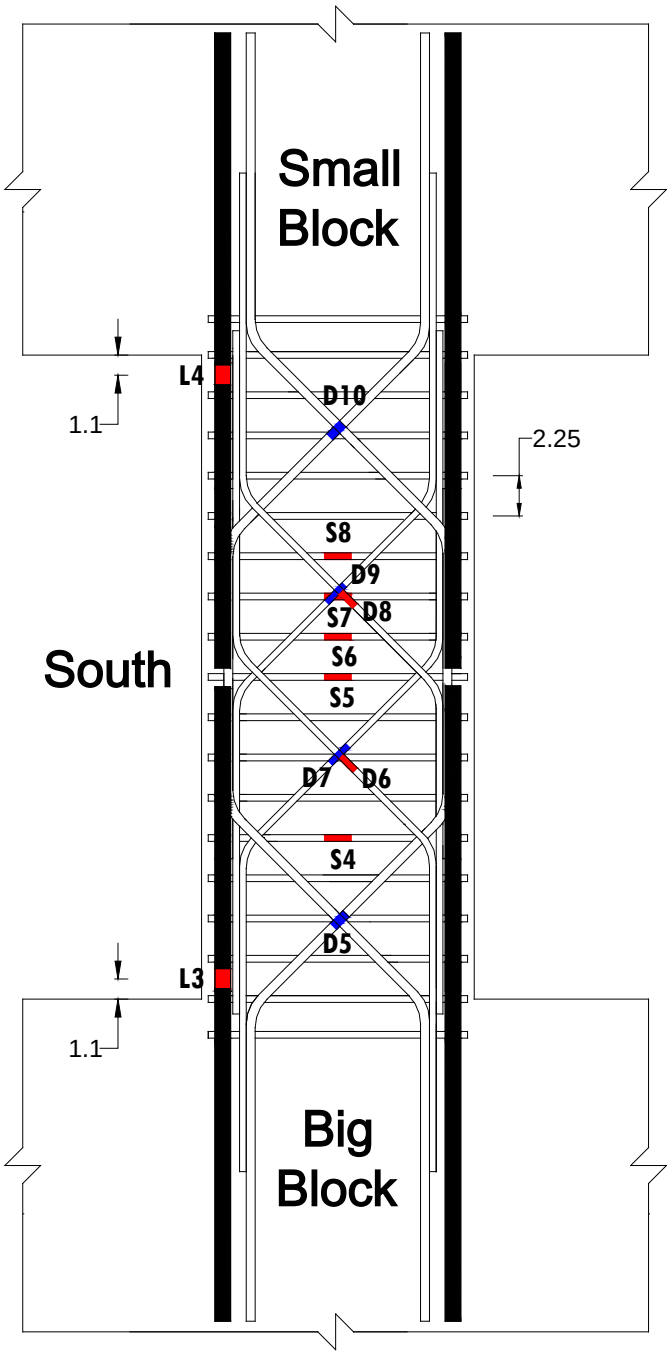

c) Specimen CB-3 (South)

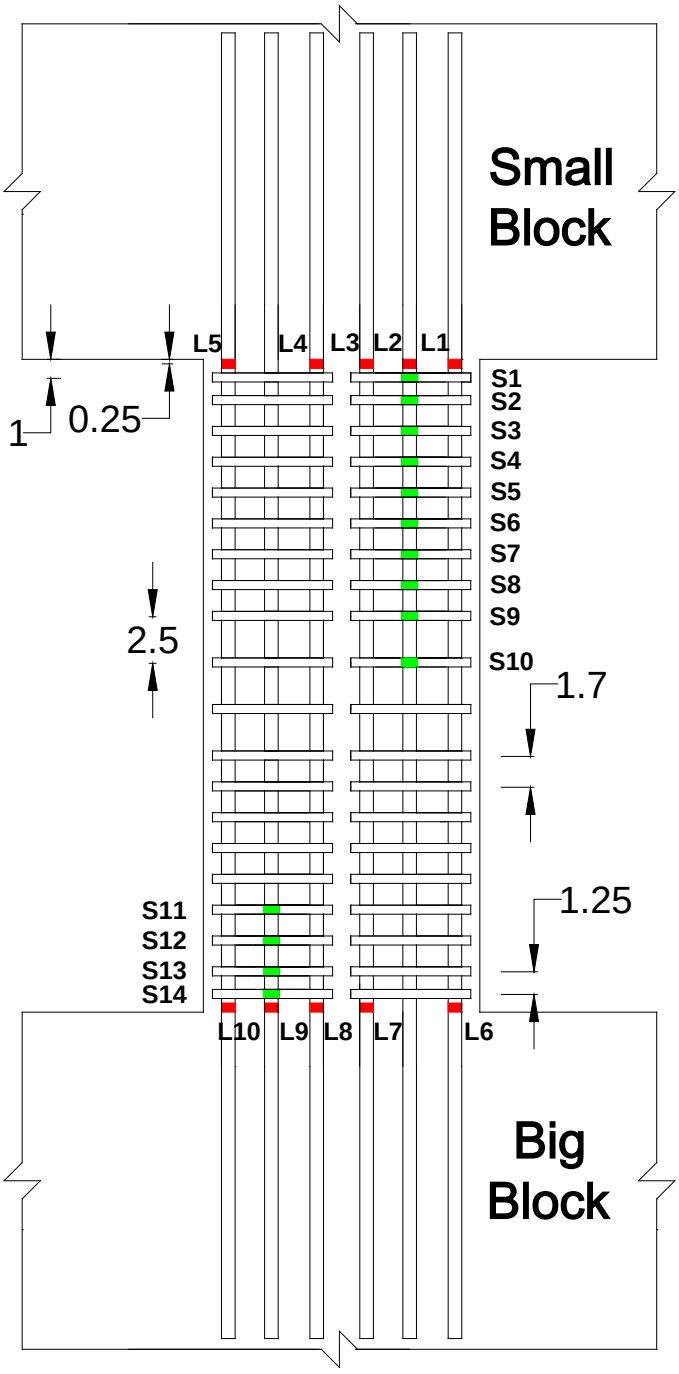

d) Specimen CB-4

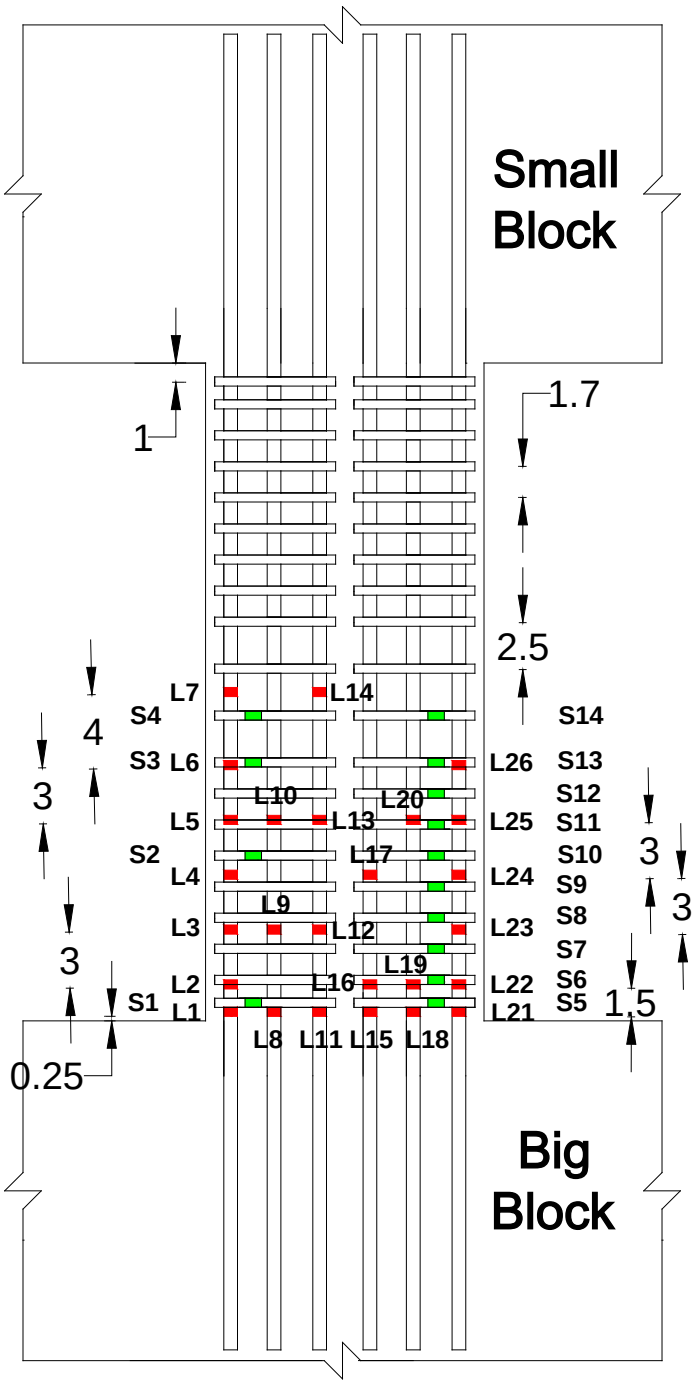

e) Specimen CB-5

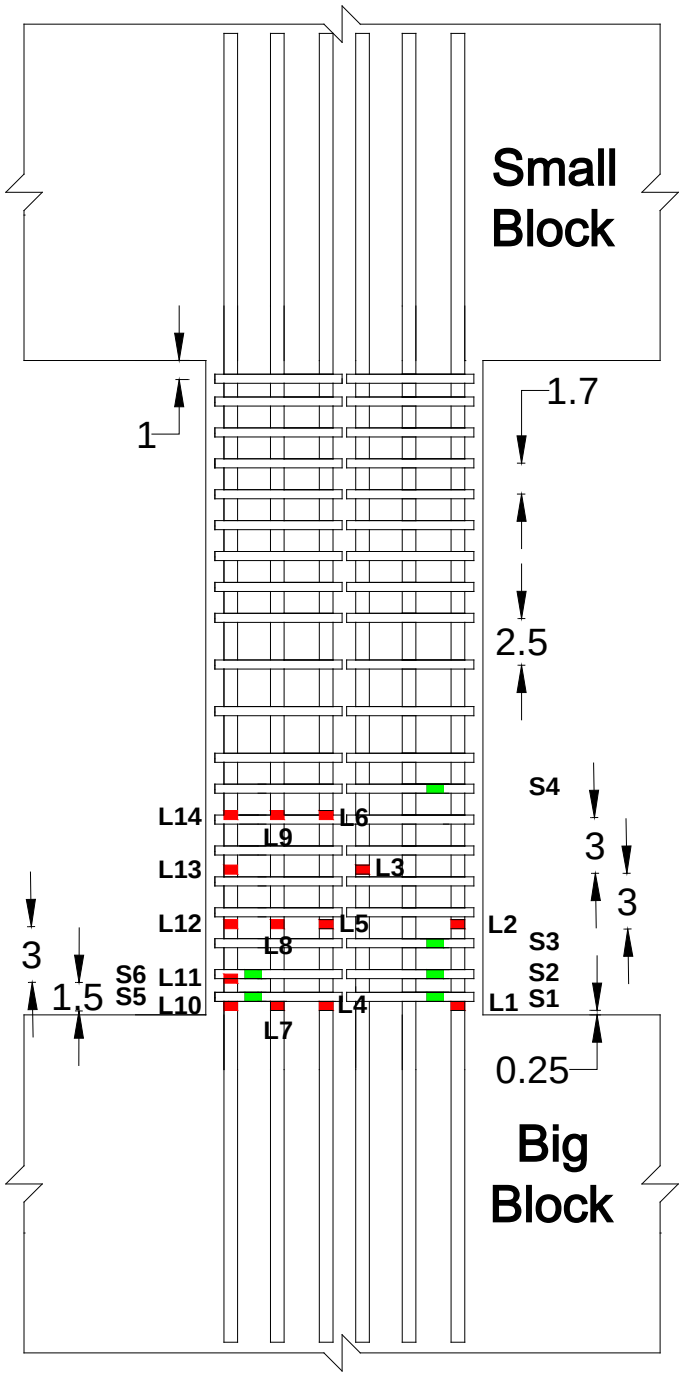

f) Specimen CB-6

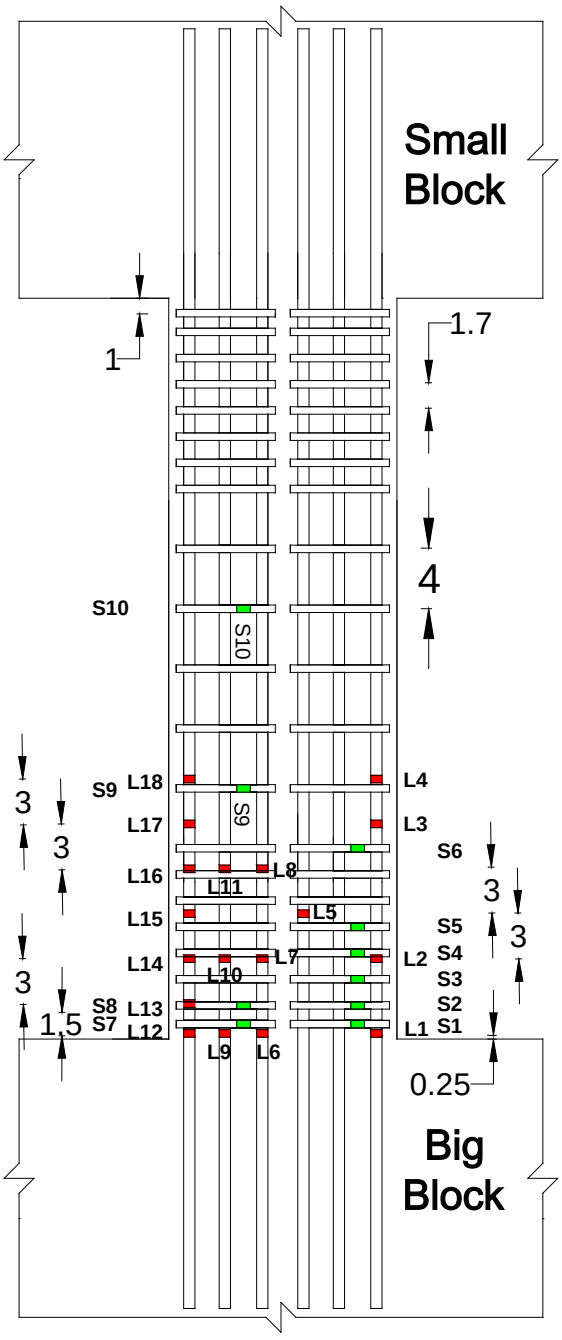

g) Specimen CB-7

Figure 3-14 Strain gauges layout

Shear force applied to the specimen was measured by the load cell attached to the hydraulic actuator. The vertical displacement reach at each drift level was monitored with Linear Variable Differential Transformers (LVDTs) because LVDT reading from the actuator were inaccurate due to deformations in the loading system. Linear Variable Differential Transformers (LVDTs) were placed on the specimen to measure key deformation quantities, as shown in Figure 3.15.

For the coupling beam, one LVDT was used vertically at the end of the coupling beams, near the loading block. Also, one LVDT was used vertically at the other end of the coupling beam near the big blocks to validate that no uplift occurred in the big block. At the top and bottom of the loading blocks parallel to the coupling beam two more LVDTs horizontally installed to measure the rotation of the blocks, as shown in Figure 3.15. As a result, measure the rotation of the coupling beam. The total rotation of the specimens was determined during testing by Equation 3-2. For the majority of specimens the rotation of the loading block was negligible. All sensors were connected to Vishay 5000 or 8000 Data Acquisition system.

$$\theta = \left[\frac{(LVDT1 - LVDT2)}{coupling\ beam\ Length} - \frac{(LVDT\ 3 - LVDT\ 4)}{Distance\ between\ LVDT3\ and\ LVDT4}\right] * 100 \qquad \text{[Equation 3-2]}$$

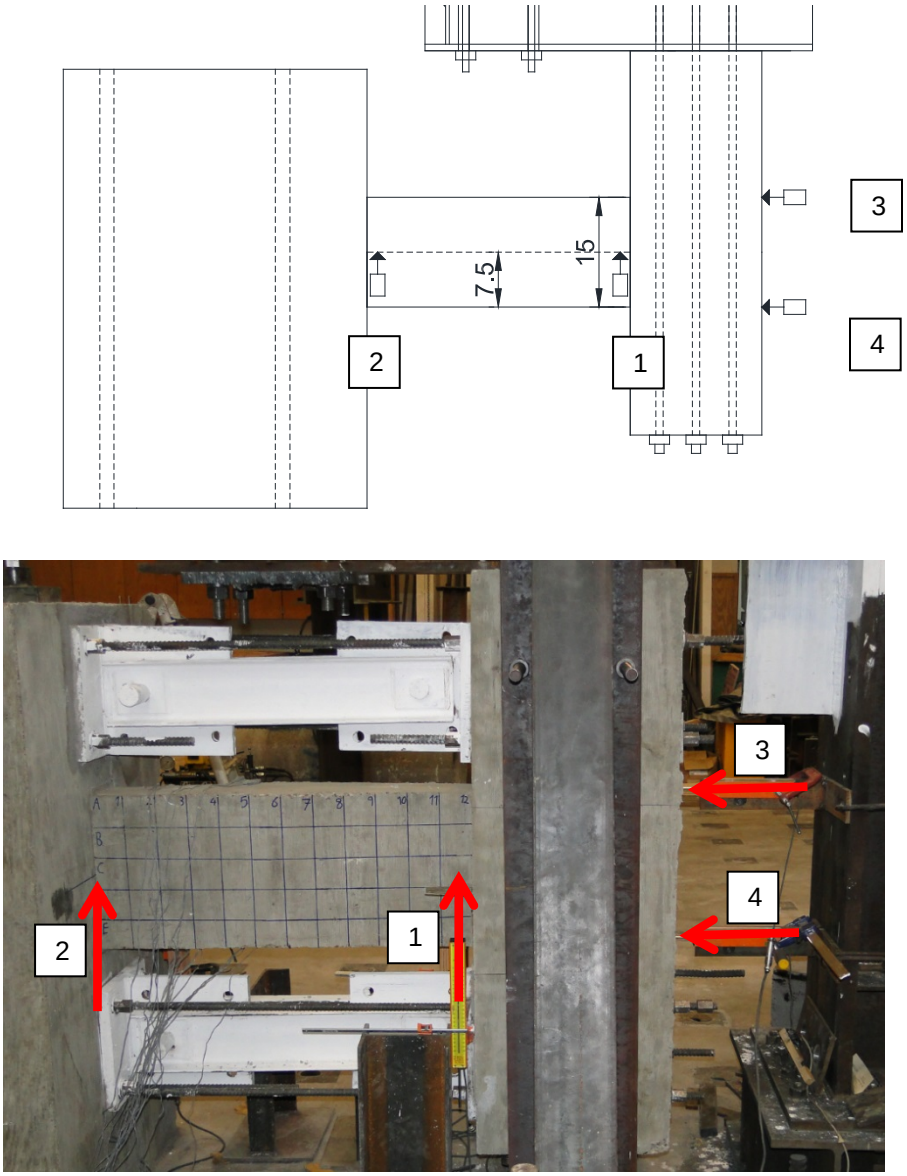

Figure 3-15 Location of the LVDT for coupling beam

For the squat wall, two LVDTs were used vertically at both side of the loading block and one LVDT was used at the end of the squat wall, near the footing block, to check that no uplift occurred in the footing block. As a result, measure the rotation of the squat wall. Two LVDTs horizontally at the top and bottom of the big block parallel to the wall were used to measure the rotation of the footing block, as shown in Figure 3.16. The total rotation of the specimens was checked during testing by Equation 3-3.

$$\theta = \left[\frac{\left(\frac{LVDT\ 1+LVDT2}{2}\right)-LVDT3}{l_w} - \frac{(LVDT\ 4-LVDT\ 5)}{Distance\ between\ LVDT4\ and\ LVDT5}\right] * 100 \qquad \text{[Equation 3-3]}$$

l_w is the height of the wall from the face of the footing block to the loading point.

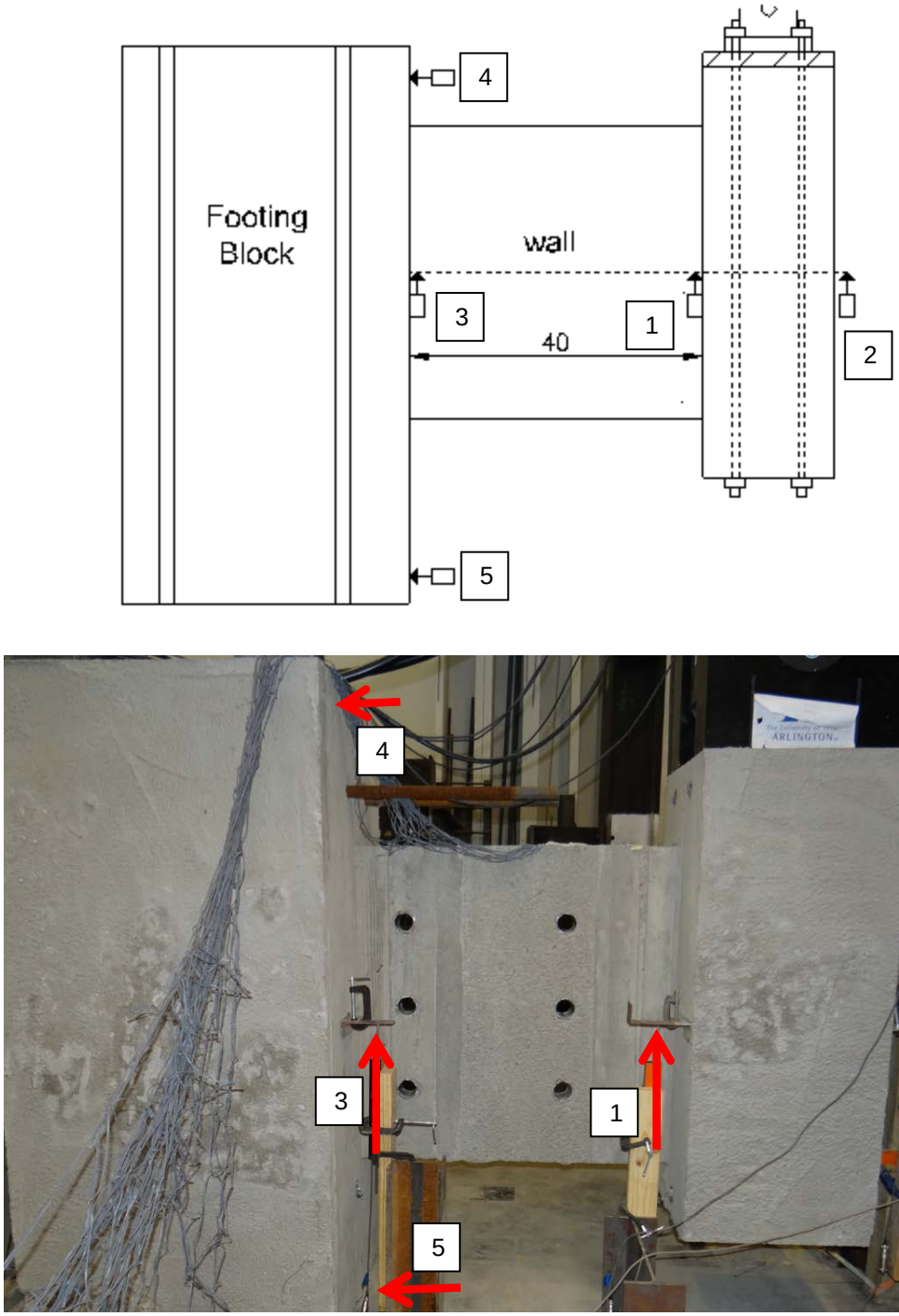

Figure 3-16 Location of the LVDT for Squat wall

In order to determine the force transfer and failure mechanisms of coupling beam and squat wall, the Digital Image Correlation (DIC) technique was used to “visualize” cracking and failure process through the observation of the full strain field. DIC system is an optical analysis system for dynamic measurement of complex materials and structures. The basic principle of the standard subset-based DIC method is to track the same physical points (a speckle pattern) located in the reference image and deformed image. The displacements are computed at each dot to obtain the full-field deformation and strain. A digital image correlation (DIC) system was used for the four half and full scale specimens tested. The setup of the DIC system is shown in Figure 3.17. Two cameras were used so the three dimensional displacement vector of each point can be determined. This was a nonabrasive process because the dots were simply formed by first spray-painting the surface of the specimen with a thin layer of white and then applying a fine mist of black spray-paint (Figure 3.18). The cameras then use the dots created by the mist of black spray-paint as the basis for determining three dimensional displacement vectors and full-field strain measurements.

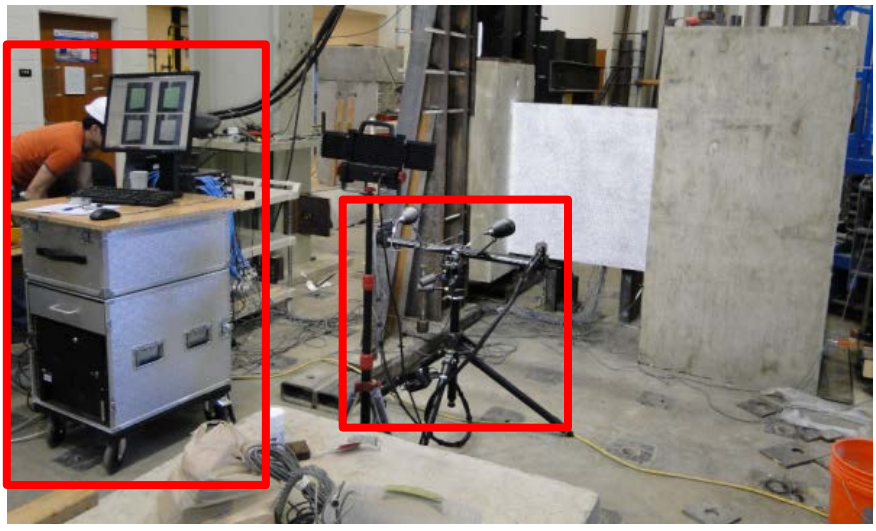

Figure 3-17 DIC System Setup

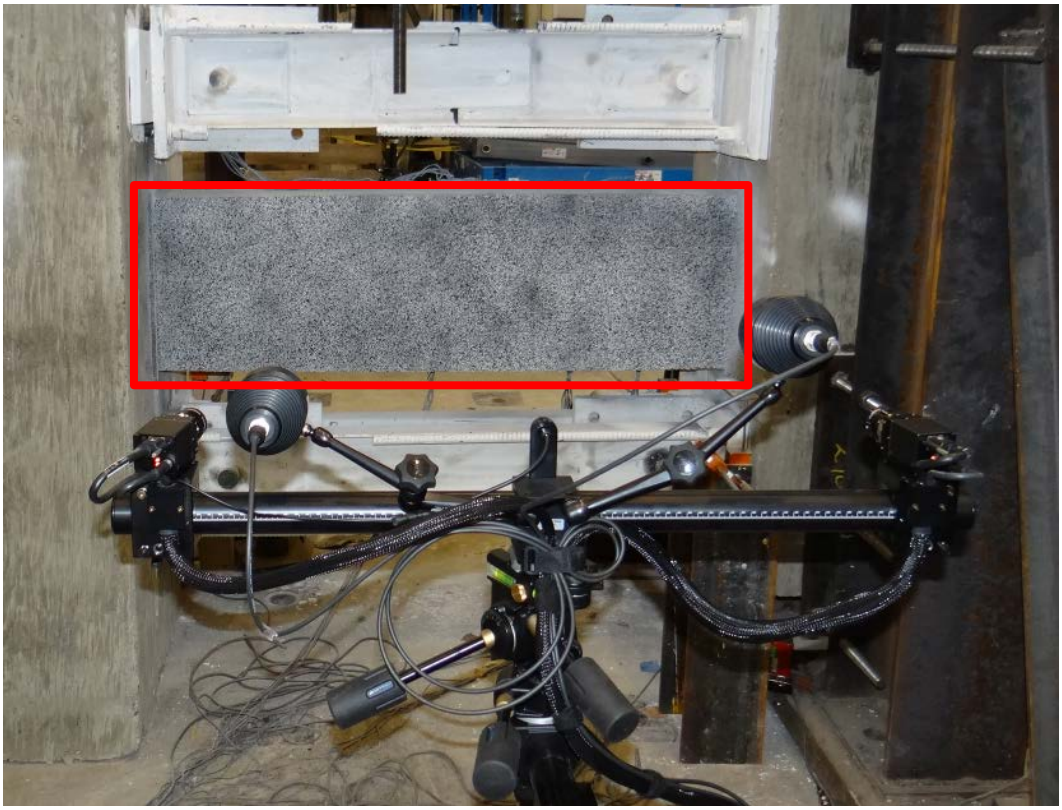

Figure 3-18 Surface Preparation for DIC System Measurements

3.7 Loading Protocol

The specimens were subjected to cyclic loading in a displacement control mode which produced predefined reversed cyclic displacement patterns. Two loading protocols were used, starting from a coupling beam chord rotation of 0.25% and reaching a maximum rotation of 12%. The first loading protocol consisted of symmetric cyclic (SC) loading utilizing 2–3 cycles per deformation level (Figure 3.19 (a)). However, this type of loading is not representative of near-collapse (NC) earthquake response, which would be unsymmetrical and would contain fewer cycles of loading; the loading protocol should contain displacements which are representative of the ratcheting effect that leads to structural collapse. Such a protocol was developed based on preliminary nonlinear

analyses (Figure 3.19 (b)). During testing, up to approximately 2 % drift, the actuator was held momentarily at peak drift for the first cycle and the last peak for the last cycle to mark cracks developed on the specimen by the students.

Also, the symmetrical loading protocol with the peak displacement at a given cycle ranging from 0.125% drift to 3.0% drift was used for squat wall as show in Figure 3.20. Every displacement cycle up to 2.0% drift was performed twice to evaluate any decrease in strength and stiffness with repeated displacement cycles.

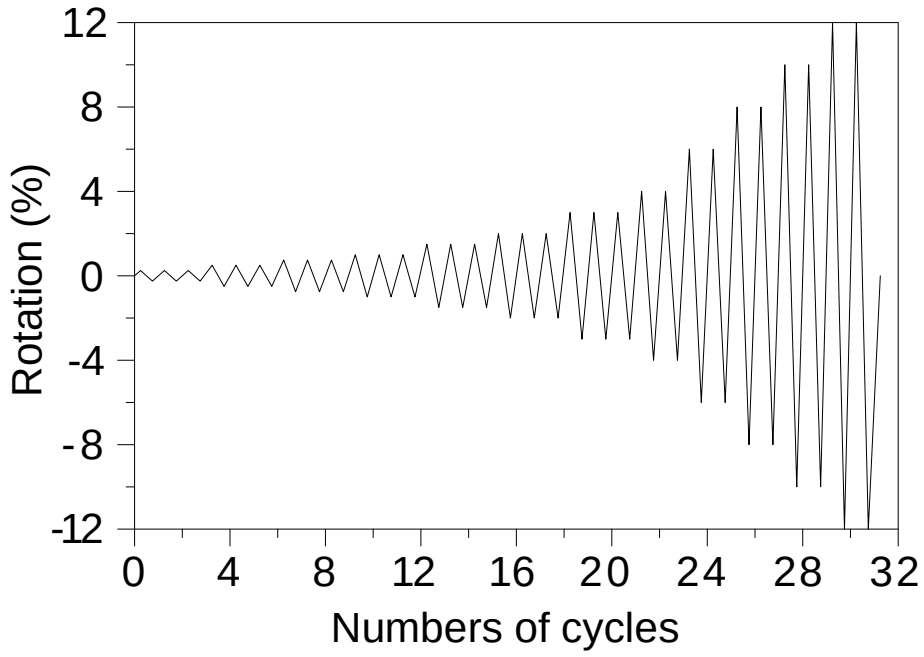

a) Symmetric cyclic loading

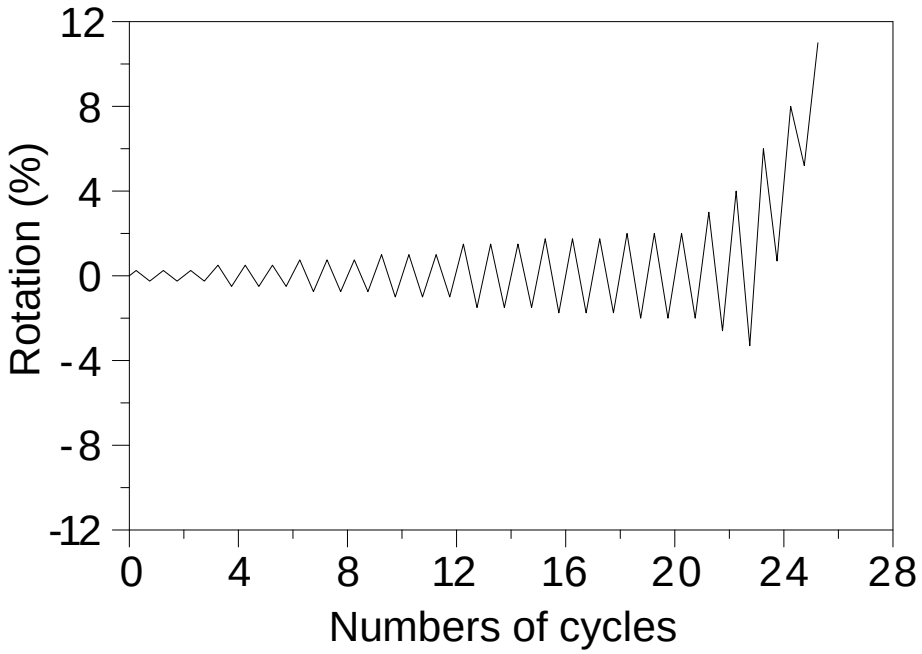

b) Symmetric then near-collapse loading.

Figure 3-19 Loading protocols for coupling beam

Table 3.5 Coupling Beam Loading Protocols

Symmetric Loading Protocol		Near Collapse Loading Protocol	
Number of Cycles	Member Drift	Number of Cycles	Member Drift*
3	0.25%	3	0.25% (0.25%)
3	0.50%	3	0.50% (0.50%)
3	0.75%	3	0.75% (0.75%)
3	1.00%	3	1.00% (1.00%)
3	1.50%	3	1.50% (1.50%)
3	2.00%	3	1.75% (1.75%)
3	3.00%	3	2.00% (2.00%)
2	4.00%	1	3.00% (3.00%)
2	6.00%	1	4.00% (3.30%)
2	8.00%	1	6.00% (0.70%)
2	10.00%	1	8.00% (5.20%)
2	12.0%	1	11.0%

* The value in parentheses () introduces the member drift for the second peak in the cycle

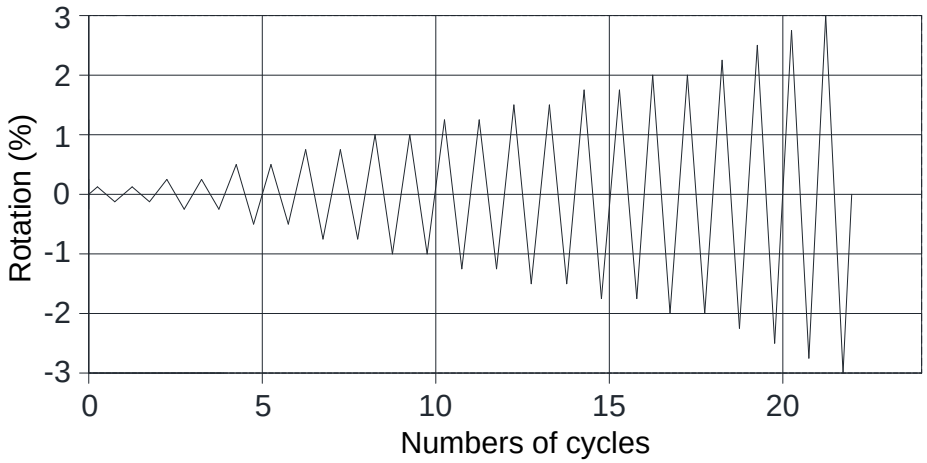

Figure 3-20 Loading protocols for squat wall

Table 3.6 Squat Wall Loading Protocols

Symmetric Loading Protocol	
Number of Cycles	Member Drift
2	0.125%
2	0.25%
2	0.5%
2	0.75%
2	1%
2	1.25%
2	1.5%
2	1.75%
2	2%
1	2.25%
1	2.5%
1	2.75%
1	3%

3.8 Material Properties

Each coupling beam and squat wall specimens explained previously was constructed with Grade 60 mild-steel reinforcement obtained from local suppliers. Also, the concrete for all of the specimens was obtained from local suppliers and deliver to University of Texas at Arlington Structure Laboratory. Material samples were tested to

estimate actual properties for both concrete compressive strength and steel tensile strengths. Concrete cylinders were tested to define f_c' for each test specimen. Six cylinders were prepared for each batch of all delivered ready-mixed concrete. All of them were tested to determine the compressive strength on the day of the testing. The results of the compressive strength are shown in Table 3.7.

Table 3-7 Compressive Strength of the Specimens

specimen	(psi) (Test day)
CB-1	5000
CB-2	5300
CB-3	7000
CB-4	6700
CB-5	5900
CB-6	6000
CB-7	6000
CB-8	4000
SW-1	5000
SW-2	4900
SW-3	5500
SW-4	4000
SW-5	4000
SW-6	4500

Rebar coupons were tested in order to determine yield and ultimate tensile strengths for steel in the coupling beam specimens. For the coupon test, No. 4 rebar with the 3o" length was used. In order to measure deformation during the test, equipment called extensometer at the mid-height of the rebar was used. The coupon test setup is shown in Figure 3.21. According to stress versus strain curve plot (figure 3.22), yield and ultimate stress of No.4 bar was approximately 70 and 98 ksi respectively. During the coupon test, extensometer should be removed from the rebar when it almost reaches to the ultimate stress in order to prevent any damage to the extensometer; that is why the curve based on the extensometer stops at approximately ultimate point.

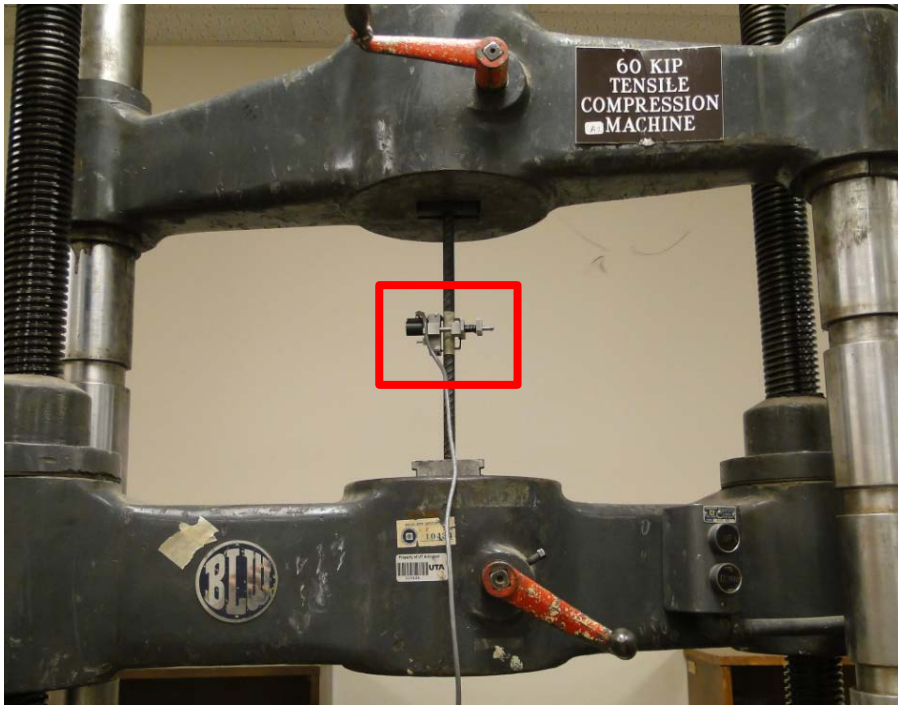

Figure 3-21 Coupon test

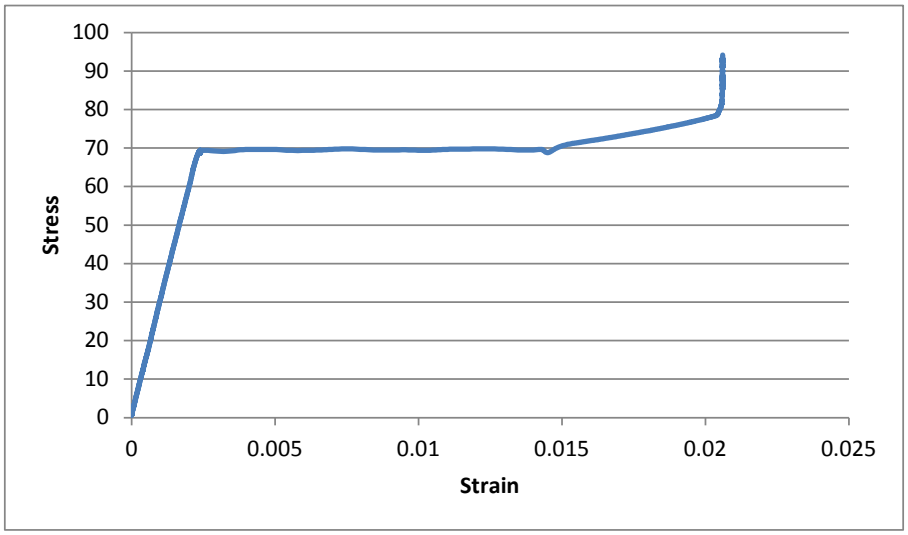

Figure 3-22 Stress versus strain for No.4 bar

Chapter 4

Experimental Result and Analysis

4.1 Evaluation of Experimental Results

In the experimental phase of the research program, eight coupling beams and six squat walls were designed and tested to evaluate the feasibility of using new configurations and the performance of these beams and walls with new details. The results were compared to the recommended arrangement for them by ACI 318-14. The test results were evaluated in terms of beam shear force versus drift response, cracking pattern and damage tolerance, shear behavior and ability to maintain stiffness under large displacement reversals.

4.2 Shear Force Versus Beam Chord Rotation Response and Damage Progression

Overall behavior of the coupling beams and squat walls was evaluated through hysteresis response of the specimen, as well as damage progress throughout the tests. The resulting hysteresis relationship for each specimen, plotted as the shear force and stress versus specimen beam chord rotation (Drift).

Average shear stress, v, was calculated by dividing the vertical load that was recorded by load cell on the actuator, by the cross-section area of the specimen. The cross section for coupling beam and squat wall is, bh, where b and h are the width and height of the beam and tl_w, where t and l_w are the thickness and length of the squat wall respectively. To compare the result for different specimen shear stress is normalized by dividing the average shear stress to root of concrete compressive strength, $\sqrt{f_c'}$.

$$v = \frac{V}{bh\sqrt{f_c'}} \text{ (Coupling beam)}$$

$$v = \frac{V}{tl_w\sqrt{f_c'}} \text{ (Squat wall)}$$

Beam chord rotation defined as the ratio of the applied vertical displacement at the end of the beam near the loading block to the length of the coupling beam. Beam chord rotation was adjusted to account for the vertical displacement of the big block and rotation of the loading block.

$$\text{Beam chord rotation} = \frac{\Delta_1 - \Delta 2}{L} - \alpha$$

Where Δ_1 is the vertical displacement at the end of the coupling beam near the loading block, Δ_2 is the vertical displacement of the big block, L is the length of the coupling beam, and α is the rotation of the small block. Two Linear Variable Transducers (LVDT) were used vertically at both end of the coupling beam to calculate the Δ_1 and Δ_2. Also, the rotation of the loading block, α, is calculated by using two horizontal LVDTs at the top and bottom of the coupling beam near the loading block. For all of specimens the rotation of the loading block , α **,** was negligible.

In squat wall drift is defined as the ratio of applied vertical displacement to the height of the squat wall from face of the footing block to loading point. Drifts were adjusted to account for the vertical displacement and rotation of the footing block.

$$\text{Drift} = \frac{\Delta_1 - \Delta 2}{\ell_w} - \beta \ell_w$$

where Δ_1 is the vertical displacement at the loading point, Δ_2 is the vertical displacement of the footing block, β is the rotation of the footing block, and ℓ_w is shear span length, defined as the distance from the base of the wall to the loading point. Also, the rotation of the footing block, β , is calculated by using two horizontal LVDTs at the top and bottom of the squat wall near the footing block. A summary of the experimental results for all test

specimens, such as maximum shear force, drift capacity, maximum shear stress, and peak normalizes shear stresses, is given in Table 4.1. Drift capacity was defined as the largest drift level before a strength loss of approximately 15%.

Table 4-1 Summery of Test Results

specimen	V_u (Kips)	ν_u (psi)	$\nu_u / \sqrt{f_c'}$ (psi)	Drift capacity (%)	
				Positive	Negative
CB-1	91	1214	17.2	0.91	0.79
CB-2	100	1111	15.2	2.42	2.1
CB-3	99	1100	13.1	1.6	1.66
CB-4	90	1000	12.3	11	3.3
CB-5	74	815	10.7	8	8
CB-6	73	815	10.5	2.3	2
CB-7	74	822	10.7	8	8
CB-8	157	531	8.3	3	2
SW-1	110	637	9.8	0.85	0.72
SW-2	92	575	8.3	1.5	1.5
SW-3	90	564	7.6	1.33	1.1
SW-4	151	943	14.9	1.1	1.07
SW-5	205	1282	19.1	0.75	0.75

4.2.1 Hysteresis response and damage progress of the Coupling Beam with Truss Arrangements

4.2.1.1 Specimen CB-1 (Truss with $\ell/h = 2.4$)

The hysteresis response of Specimen CB-1 is shown in Figure 4.1. Specimen CB-1 had the test setup and construction problem. The hysteresis loop was not symmetrical due to the test setup problem. The eccentricity of the loading due to the construction error created the out of plan torsion in the coupling beam, thus coupling beam failed by torsion, as shown in Figure 4.2. Also, based on the torsion in the coupling

beam, the accurate drift could not be achieved and crack pattern was not symmetric as demonstrated in figure 4.3, thus most of the crack was formed in one side of the beam. The maximum force applied to this specimen was approximately 91 kips. For this particular specimen, the concrete compressive strength was 5000 psi, and thus the maximum applied shear stress was equivalent to 17.1 $\sqrt{f'_c}$ (psi).

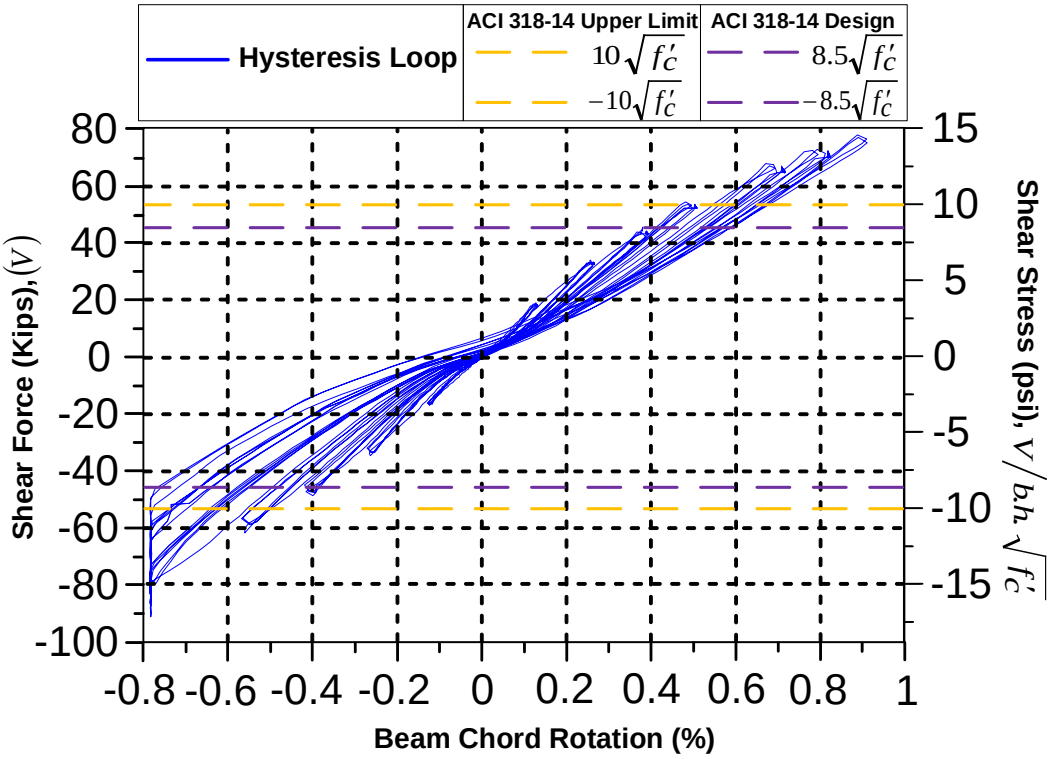

Figure 4-1 Hysteresis response of Specimen CB-1

Figure 4-2 Torsion failures for CB-1

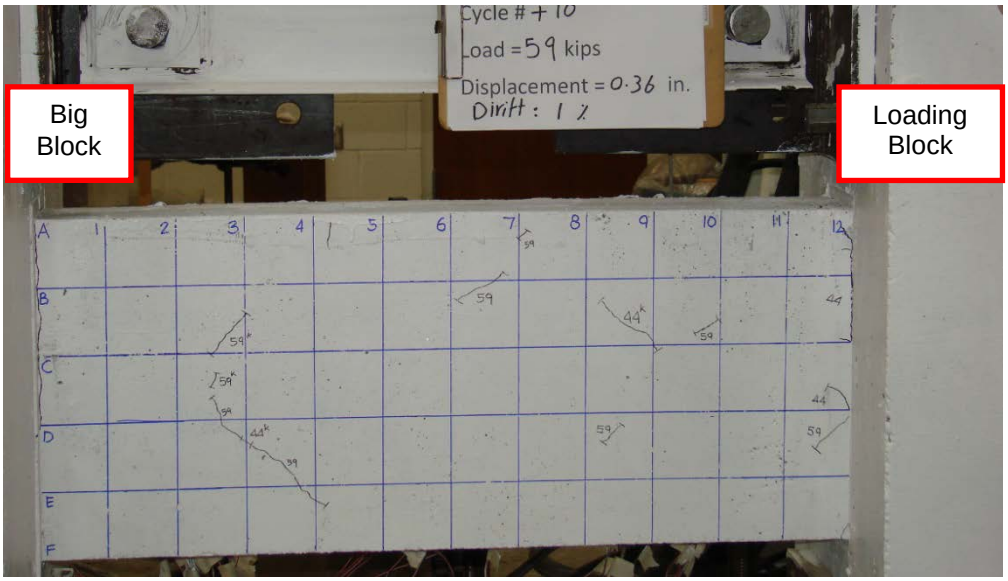

South sides at 1% drift

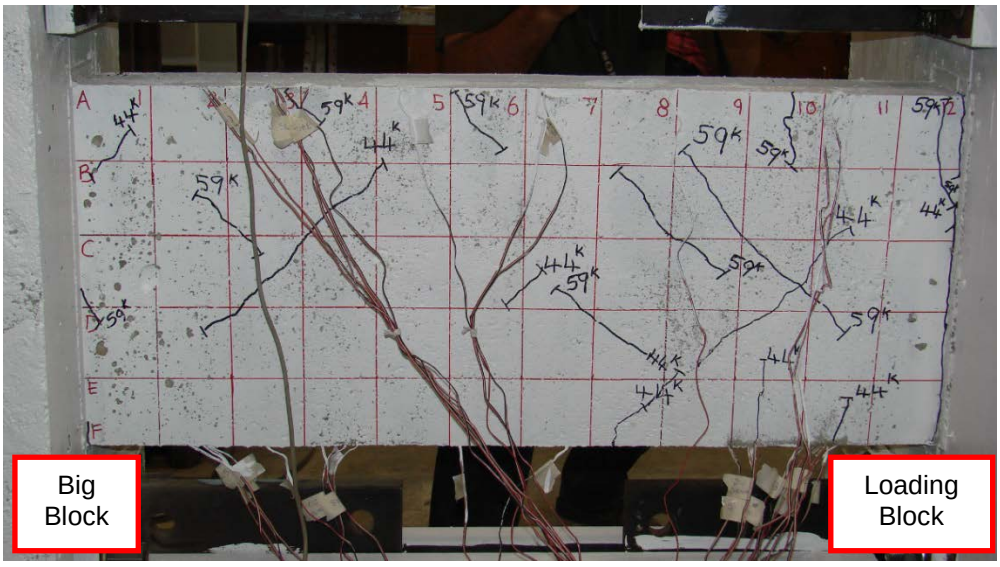

North sides at 1% drift

Figure 4-3 Crack pattern for CB-1

4.2.1.2 Specimen CB-2 (Truss with $\ell/h = 2.4$)

The shear force/stress versus drift response of Specimen CB-2, is demonstrated in Figure 4.4. For this specimen test set up was edited and the loading block was braced laterally, as shown in Figure 4.5. The actuator was connected to the loading block directly, thus could not impose the state of double curvature on the coupling beam. Therefore, the coupling beam behavior was close to the cantilever beam behavior during the test, and the crack pattern near the big block was more congested than near the loading block in each side. On the other hand the reinforcement bars in the specimen were not embedded symmetrically, meaning the cover on one side was more than the other side; therefore, this eccentricity could cause the torsion in the beam. Crack pattern was not symmetric in both sides of the coupling beam near the big block, as shown in figure 4.6. Specimen CB-2 sustained a maximum load of 100 kips at approximately 2% drift, which was equivalent to a shear stress of $15.2\sqrt{f_c'}$ (psi), based on the cylinder concrete compressive strength of 5300 psi.

The first diagonal cracks were observed at approximately 0.5% drift and 36 kips shear force. Because the surface of the specimen was painted, the first crack probably formed before but it was not visible. Multiple diagonal cracks formed in both loading direction up to approximately 1.5%. The first flexural crack was observed on the tension side at the end of the beam near the big block when the applied load and drift was 45 kips and 0.75% respectively. Because this beam behavior was similar to the cantilever beam, the flexural crack formed at the end of the beam near the big block. After a few cycles by increasing the applied displacement, the flexural crack become wider in the plastic hinge region near the big block, thus reducing shear transfer through aggregate interlock, which require most of the shear to be transferred along this crack by tension and compression of the diagonal bars, stirrups and dowel action which is provided by the

longitudinal reinforcement. Ultimately, concrete at the end of the beam was destroyed by spalling and sliding developed along a plane parallel to the transverse reinforcement due to the wide flexural crack, thus leading to loss of beam stiffness and strength, as demonstrated in Figure 4.7.

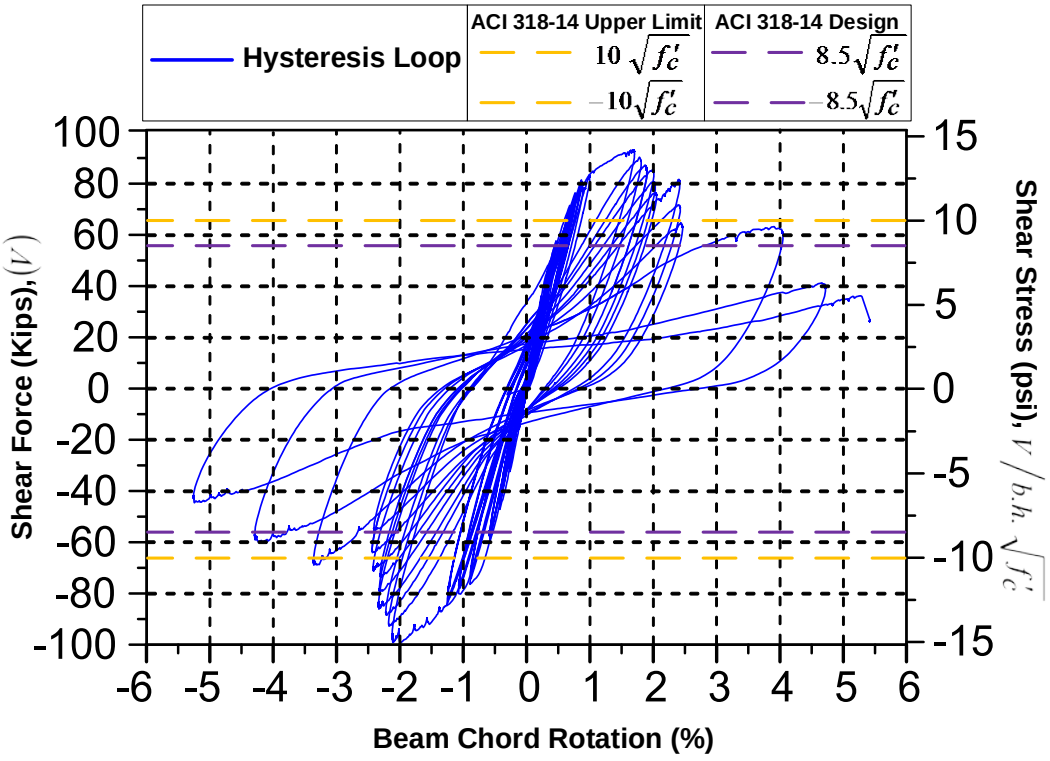

Figure 4-4 Hysteresis response of Specimen CB-2

Figure 4-5 Test setup for CB-2

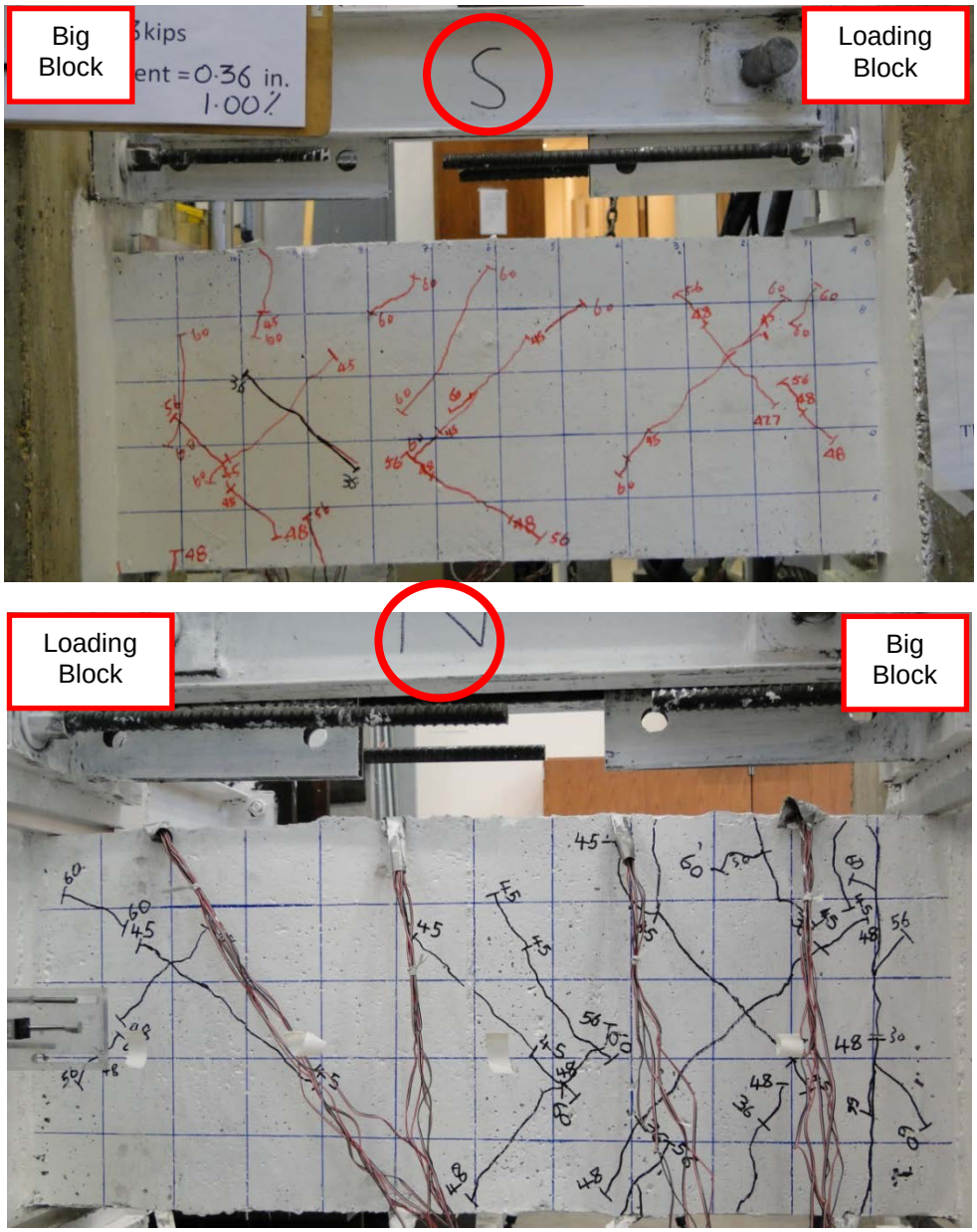

Figure 4-6 Unsymmetrical crack pattern for CB-2 (1% Drift)

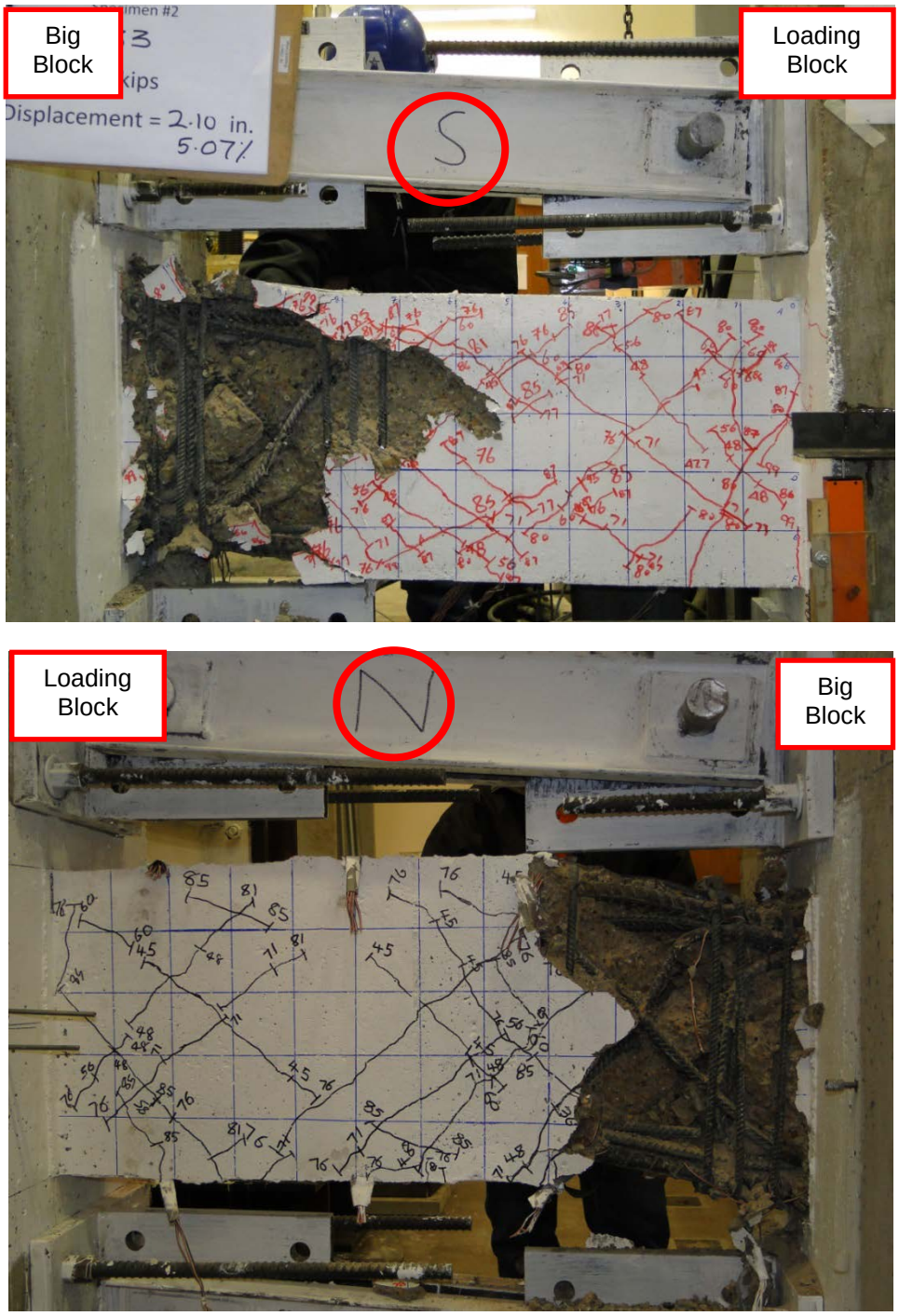

Figure 4-7 Sliding shear failures for CB-2

4.2.1.3 Specimen CB-3 (Truss with $\ell/h = 2.4$)

The shear force/stress versus drift response of Specimen CB-3, is demonstrated in Figure 4.8. Links on the top and bottom of the coupling beam did not use during the test for this specimen. Therefore, could not impose the state of double curvature on the coupling beam completely based on the rotation of the loading block and also, could not prevent the elongation of the beam due to the cracks. LVDT's used to calculate the vertical displacement of the big block did not install, thus, the accurate drift could not be achieved. The maximum load imposed on this specimen was approximately 99 kips at 1.66% drift, which was equivalent to an average shear stress of $13.2\sqrt{f_c'}$ (psi). The first observed cracks were flexural cracks near the big block that developed at 0.25% drift and approximately 29 kip. As specimen was pushed to 0.75% drift, first diagonal cracks were observed. The critical flexural crack was formed at the mid-length of the beam where the beam did not have the longitudinal bars. Therefore, after few cycles the diagonal crack and flexural crack opened wider and also, the diagonal bars were yielded, thus leading to a less effective aggregate interlocking resistance along the open cracks. On the other hand, the dowel action resistance was equal to zero at the mid-length of the beam due to no longitudinal bars at that location, thus sliding developed along a plane parallel to the transverse reinforcement due to the wide cracks and no reinforcement resistance which leads to loss of beam stiffness and strength, as shown in Figure 4.9.

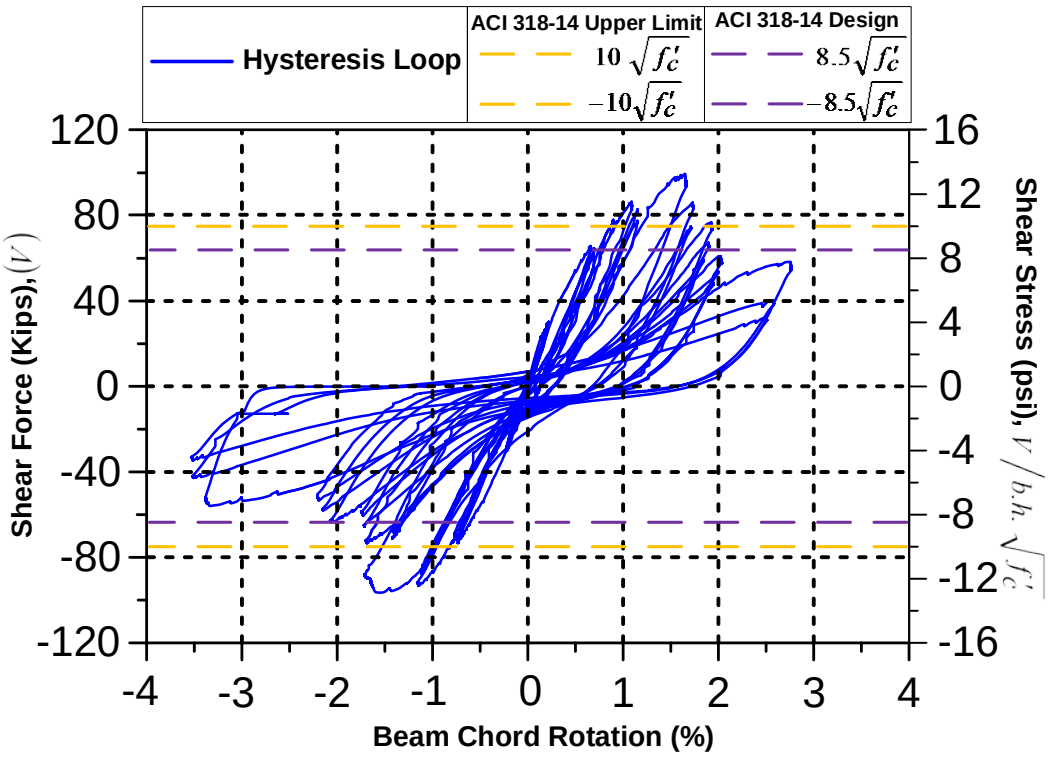

Figure 4-8 Hysteresis response of Specimen CB-3

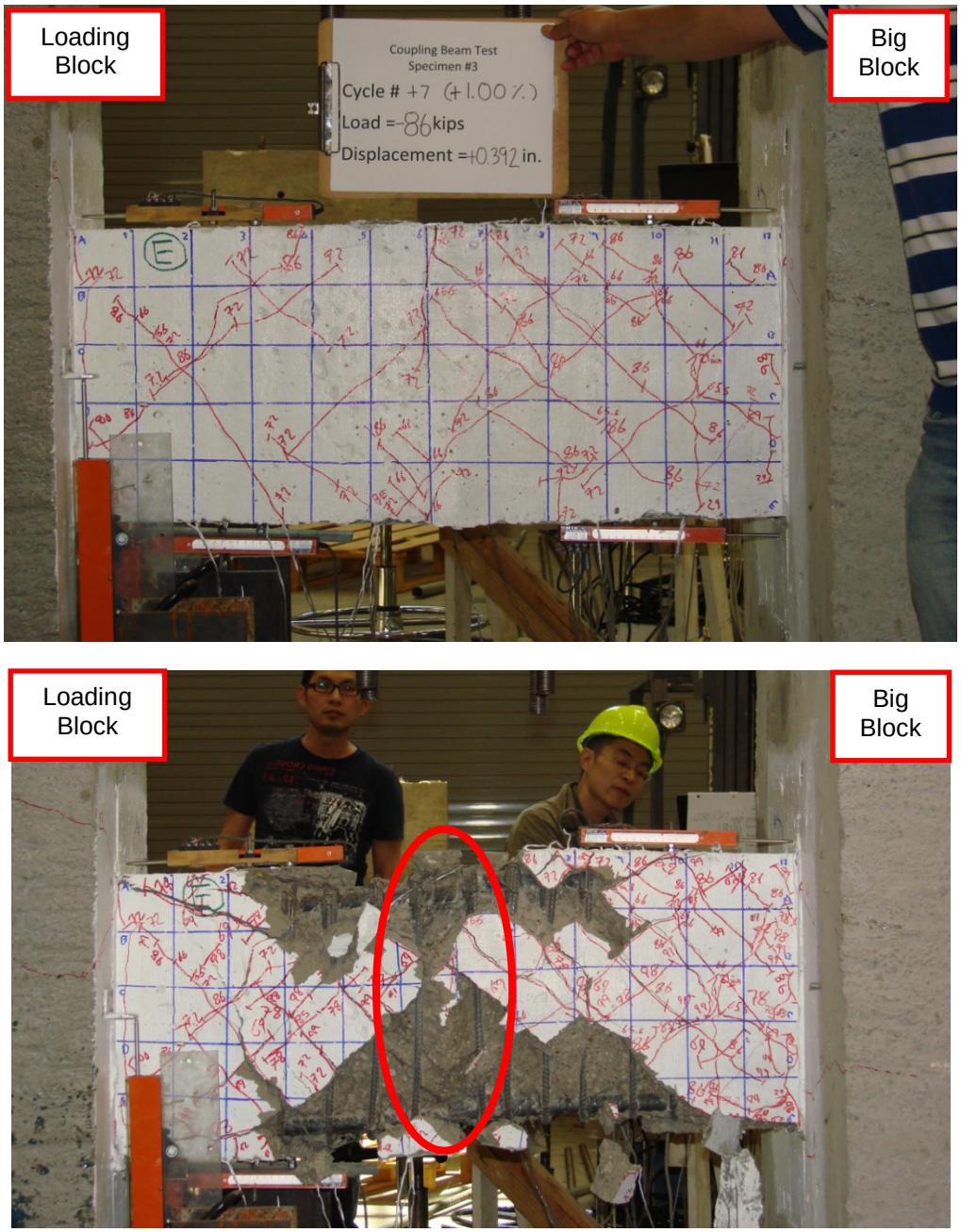

Figure 4-9 Sliding shear failures for CB-3

4.2.2 Double Beam Coupling Beam

Use of truss arrangements in the coupling beam did not result in the anticipated improvement in performance. Therefore, five Double-beam coupling beams (DBCB) designed to resist high shear stress ($10\sqrt{f_c'}$ (psi)) and tested to evaluate the performance of this arrangement with different gap width on the seismic behavior of the coupling beam. Overall behavior of the Double-beam coupling beam was evaluated through the shear force/stress versus beam chord rotation, as well as damage progress throughout the tests and stiffness.

4.2.2.1 Hysteresis response of the Double Beam Coupling Beam with 1" gap width

4.2.2.1.1 Specimen CB-4 (DBCB with $\ell/h = 2.4$)

Using the Double-Beam coupling beam (DBCB) resulted in significantly more stable hysteresis behavior than that observed in coupling beam with truss arrangement. Figure 4.10 shows the shear force/stress versus beam chord rotation response of the specimen CB-4. The response of specimen CB-4 was stable up to large drift levels. Also, Specimen CB-4 showed no strength degradation up to 11% rotation when subjected to the near-collapse loading protocol. This specimen sustained a maximum load of 90 kips at approximately 11 % drift in positive direction, which was equivalent to shear stress ($12.3\sqrt{f_c'}$ (psi)). The test was stopped at 11% beam chord rotation due to reach the stroke limit of the LVDTs near the loading blocks.

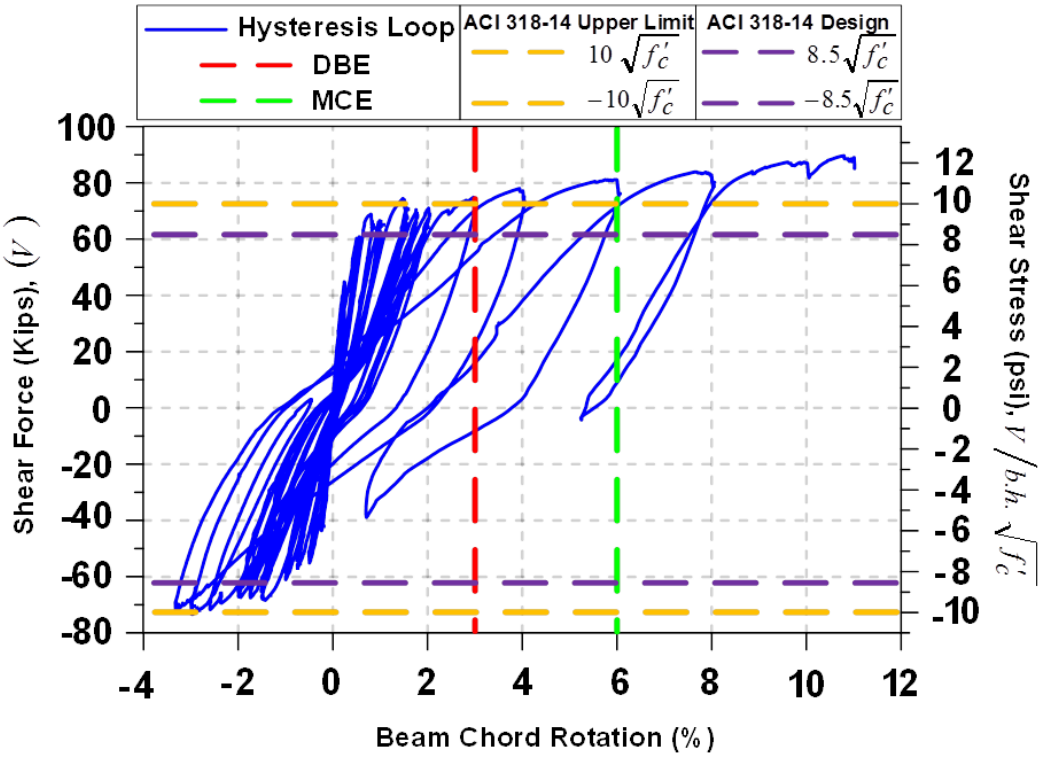

Figure 4-10 Shear force/stress vs. rotation response for Specimen CB-4

4.2.2.1.2 Specimen CB-5 (DBCB with $\ell/h = 2.4$)

The shear force and stress versus beam chord rotation response of the specimen CB-5 is shown in Figure 4.11. This specimen was able to maintain very high shear stress under symmetric loading protocol without degradation ($10\sqrt{f'_c}$ (psi)) up to a rotation of 6%. Also, it could still resist 85% of the peak stress at 8% rotation. The maximum load imposed on this specimen was approximately 74 kips at 3% drift, which was equivalent to an average shear stress of $10.7\sqrt{f'_c}$ (psi).

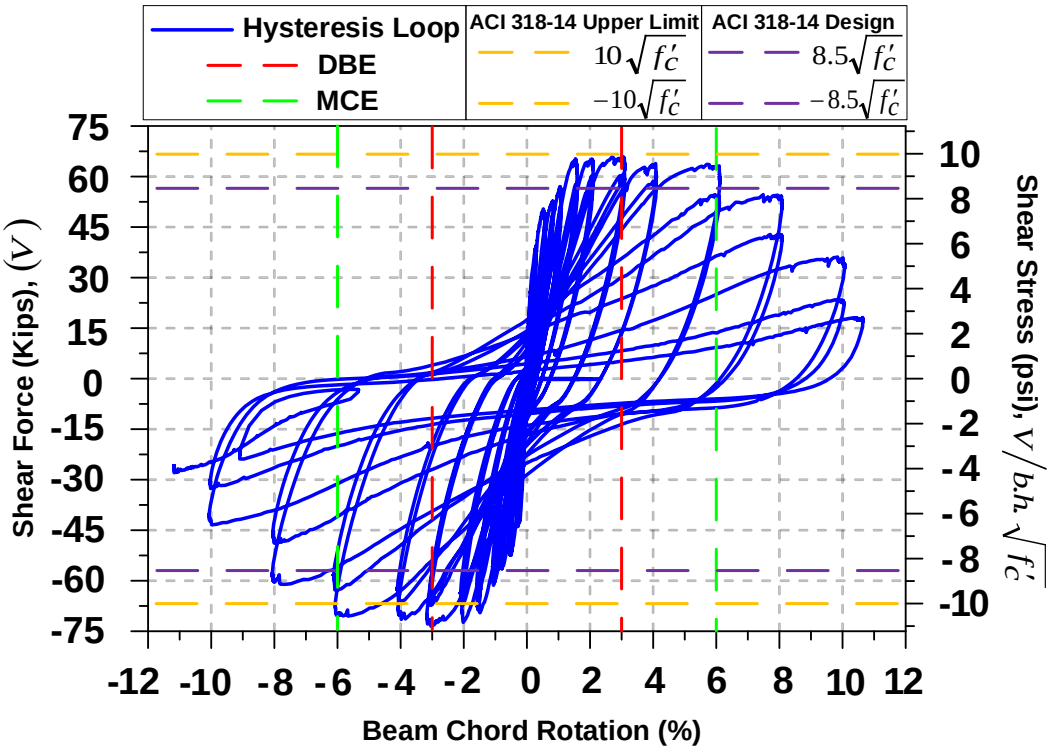

Figure 4-11 Shear force/stress vs. rotation response for Specimen CB-5

4.2.2.1.3 Specimen CB-7 (DBCB with $\ell/h = 3.3$)

The shear stress and strength versus drift response of specimen CB-7, shown in figure 4.12, indicates excellent rotational capacity and good energy dissipation under symmetric loading protocol. Specimen CB-7 sustained a maximum load of 74 kips, which is equivalent to shear stress $10.7\sqrt{f'_c}$ (psi). A stable hysteresis response was observed up to 8% drift in both directions.

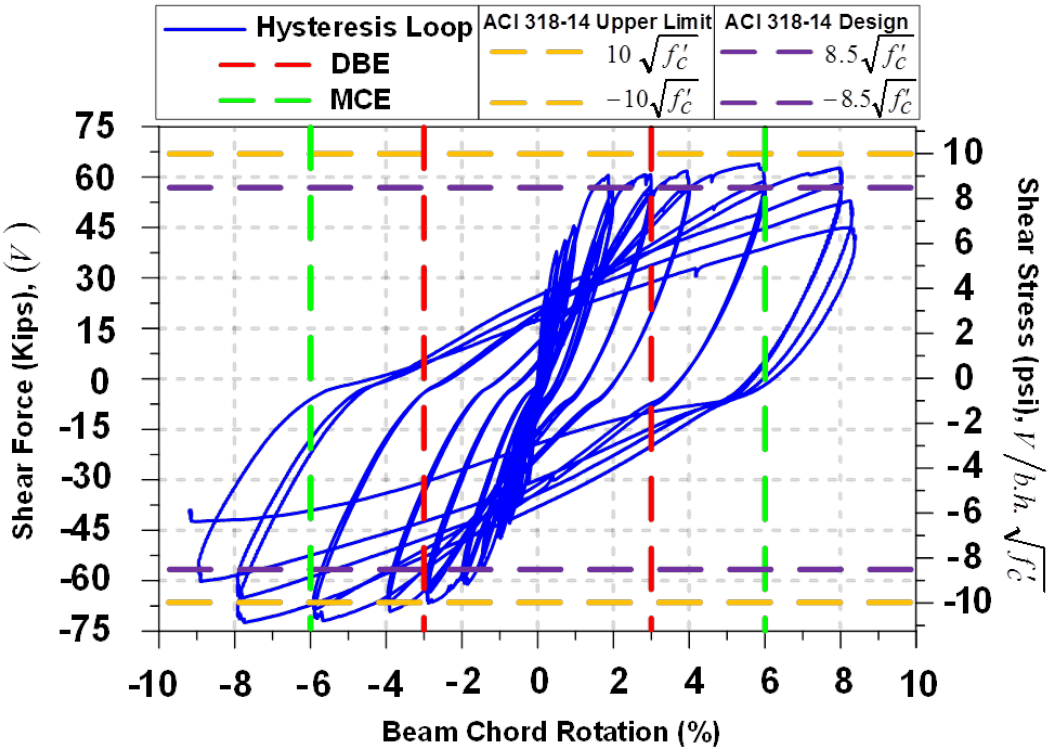

Figure 4-12 Shear force/stress vs. rotation response for Specimen CB-7

Consequently, the hysteresis response of the specimen CB-4, CB-5, and CB-6 showed high ductility and were able to maintain high strength beyond 6% rotation that is required to sustain MCE level ground motions (Harries and McNeice, 2006).

4.2.2.2 Cracking Pattern and Damage Progress for DBCB with 1" gap

The crack development and damage pattern for the DBCB specimen CB-1, CB-2, CB-3 is shown in Figure 4.13. At 0.25% rotation, the initial cracking developed at the narrow gap was located. It was a shear-type cracking near the mid-span and mid-height of the beam. Upon large displacements, the cracks gradually propagated along the intended location and towards the beam's ends. The cracks eventually separated the DBCB into two slender beams where each has nearly twice the aspect ratio of the original coupling beam. On the other hand, the other reason for the separation is the sliding of the top cage on the bottom cage (strong composite material) after several cracks at the gap reign (soft material) due to the horizontal shear force with different direction in these cages. This behavior clearly is demonstrated at large drift in Figure 4.13 (b) by check the vertical line on the specimen.

This separation in the coupling beam, essentially transforms the shear-dominated behavior into a flexure-dominated behavior, thereby duplicating the behavior of conventional slender beams. Because the damage initiated from the center of the beam; then spread towards the ends, the beam's ends maintained their integrity even under very large displacements, effectively eliminating the sliding shear failure at the beam-to-wall interface, which is commonly seen in conventional coupling beams. At 1.5% drift, diagonal cracks widened up to 4 mm. It is noted that Canbolat et al. (2005) reported that the first crack for all their coupling beam specimens occurred at 0.25% rotation. Also, the diagonal cracks were first observed during the cycles at 0.25% drift for the specimen with diagonal reinforcement. At 1.5% drift, diagonal cracks widened up to 3 mm (0.12 in.). This indicates that the occurrence of initial cracks in DBCBs and their widths are similar to that of conventional DCBs.

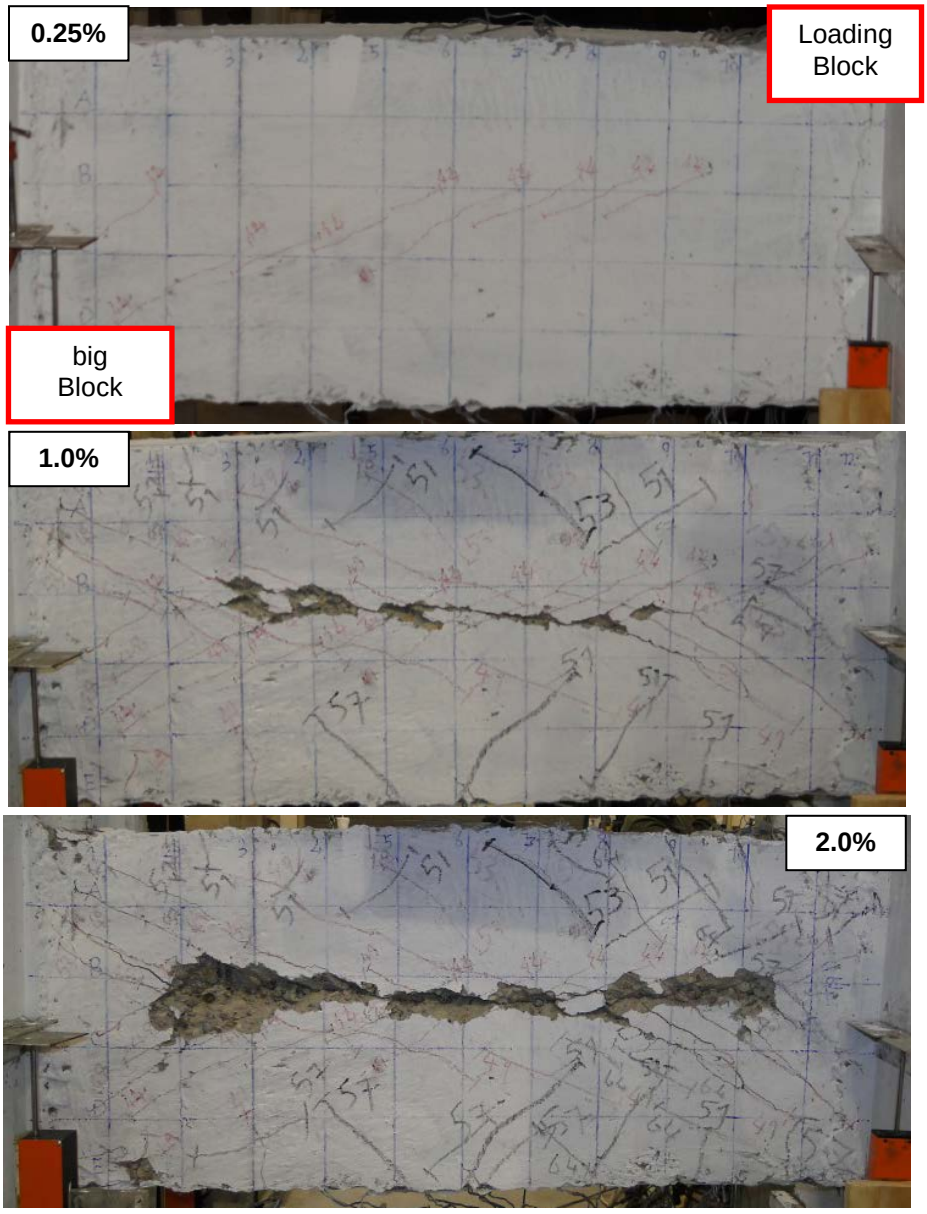

Specimen CB-5

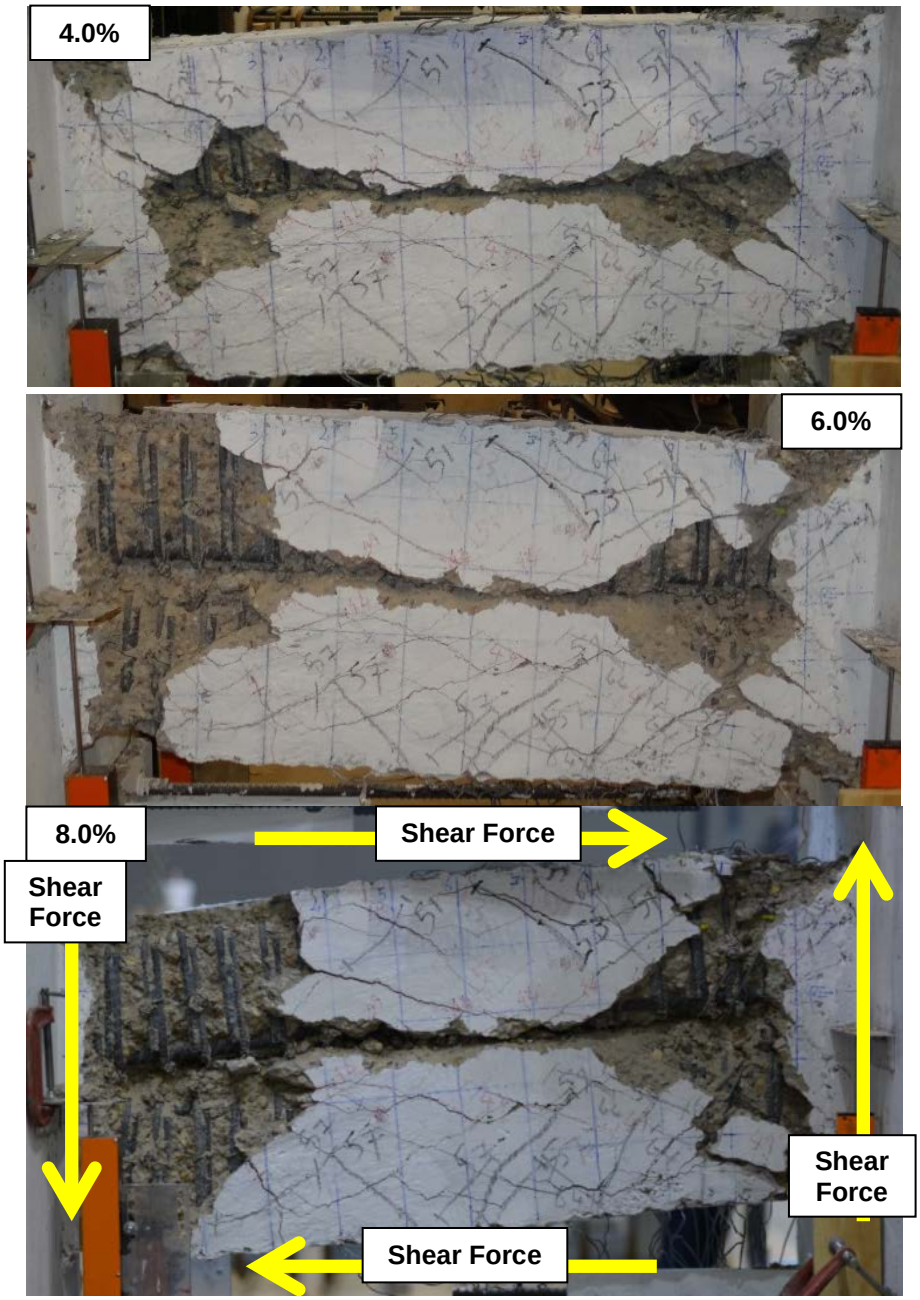

a) Specimen CB-5

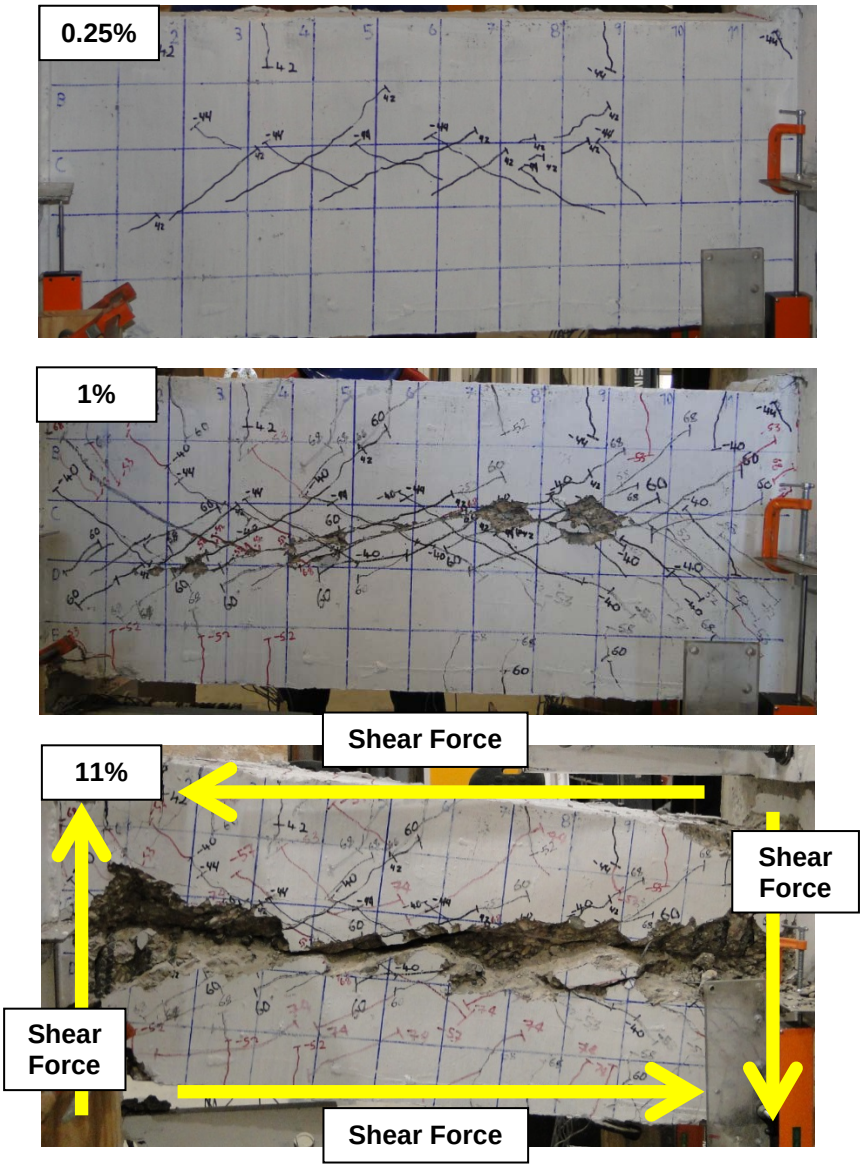

b) Specimen CB-4

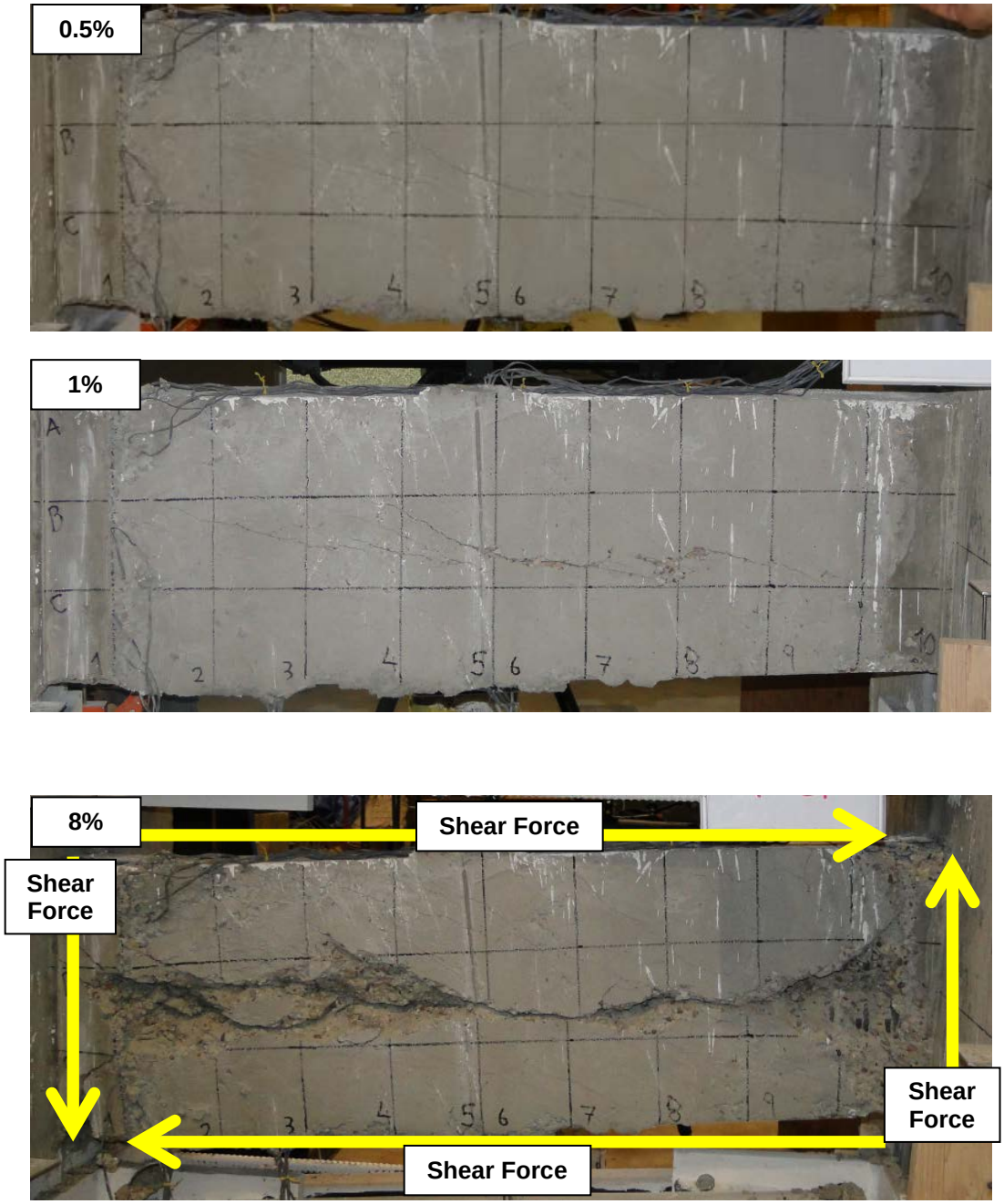

c) Specimen CB-7

Figure 4-13 Crack pattern and damage progress of DBCBs with 1" gap width

4.2.2.3 Digital Image Correlation (DIC) results for DBCB with 1" gap

In order to determine the force transfer and failure mechanisms of DBCBs, the Digital Image Correlation (DIC) technique was used to “visualize” cracking and failure process through the observation of the full strain field. Figure 4.14 shows some selected images at various rotations. The red color indicates the maximum tensile strains. As can be seen, the maximum strains were first developed in the vicinity of the mid-span and mid-height of the DBCB, and then gradually extended towards the beam ends upon lager rotations. The specimen gradually became two slender beams at 1.5% rotation. It is interesting to note that the highest strains in these two slender beams were initially in the mid-span as shown in the 1.5% rotation image. Flexural strains at the slender beams’ end became more significant at 3.0% rotation, and the entire slender beams were subjected to large strains when the DBCB totally separated into two halves (4% and 6% rotations, also see Figure 4.13 (c)). The DIC images clearly show that the entire DBCB was utilized to dissipate the seismic energy, and the damage initiated from the mid-span and mid-height then gradually propagated toward the ends. This is different from conventional coupling beams where the damage is typically localized at the beam ends only. It was also observed from the recorded videos that the “rubbing action” between the upper and lower slender beams resulting from relative horizontal movement could have provided an additional energy dissipation mechanism.

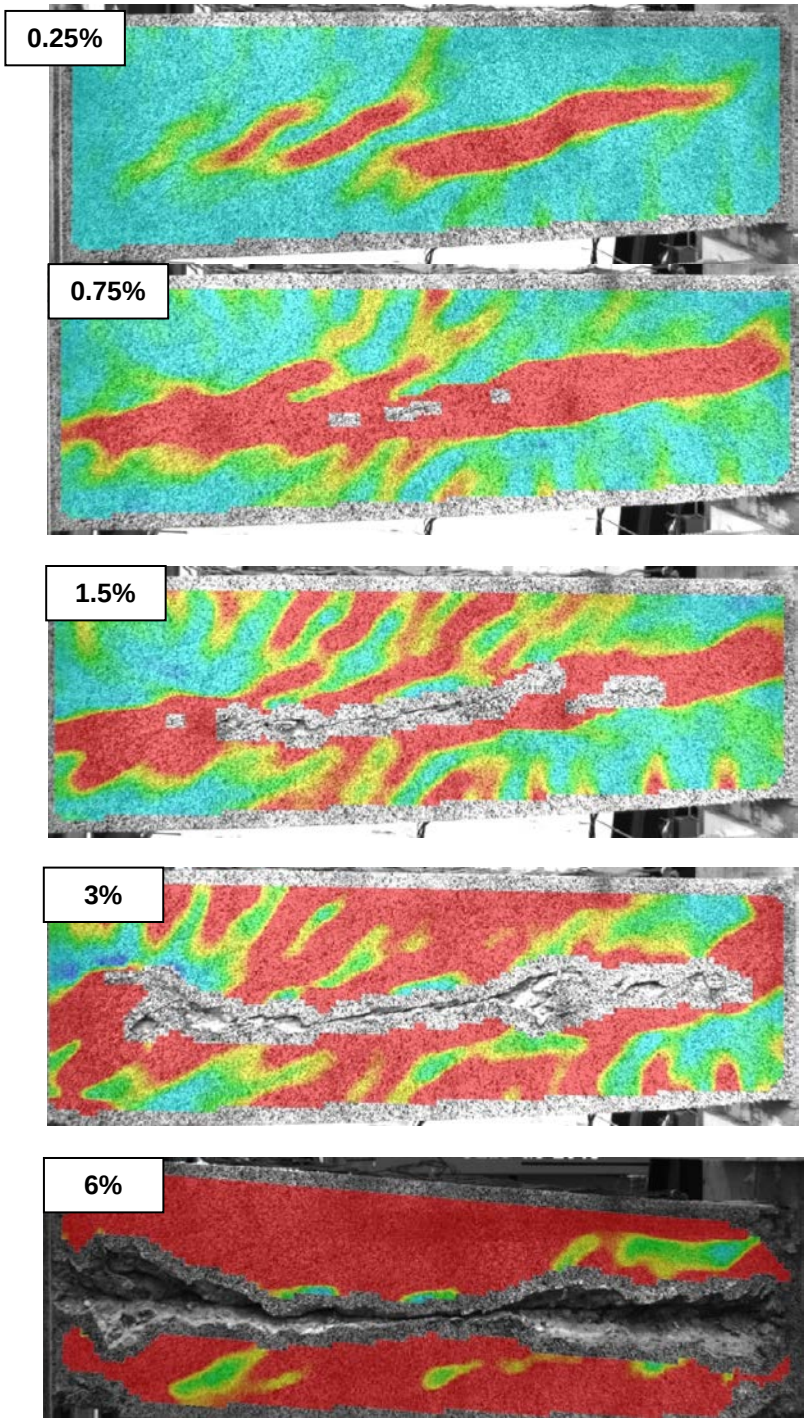

Figure 4.14 DIC results for Specimen CB-7

4.2.2.4 Stiffness retention

The normalized shear stress versus beam chord rotation of the DBCBs (CB-5 and CB-7) and diagonal coupling beam (confinement of individual diagonals) tested by Naish et al. (2009) is shown in Figure 4.15. Note that both specimens had similar loading protocols (symmetrical cycling loading). Normalized shear stress measured from peak-to-peak shear stress point in each direction, divided to the maximum shear stress. The results show that DBCB has high stiffness and acts like a conventional coupling beam under small displacements (elastic part).

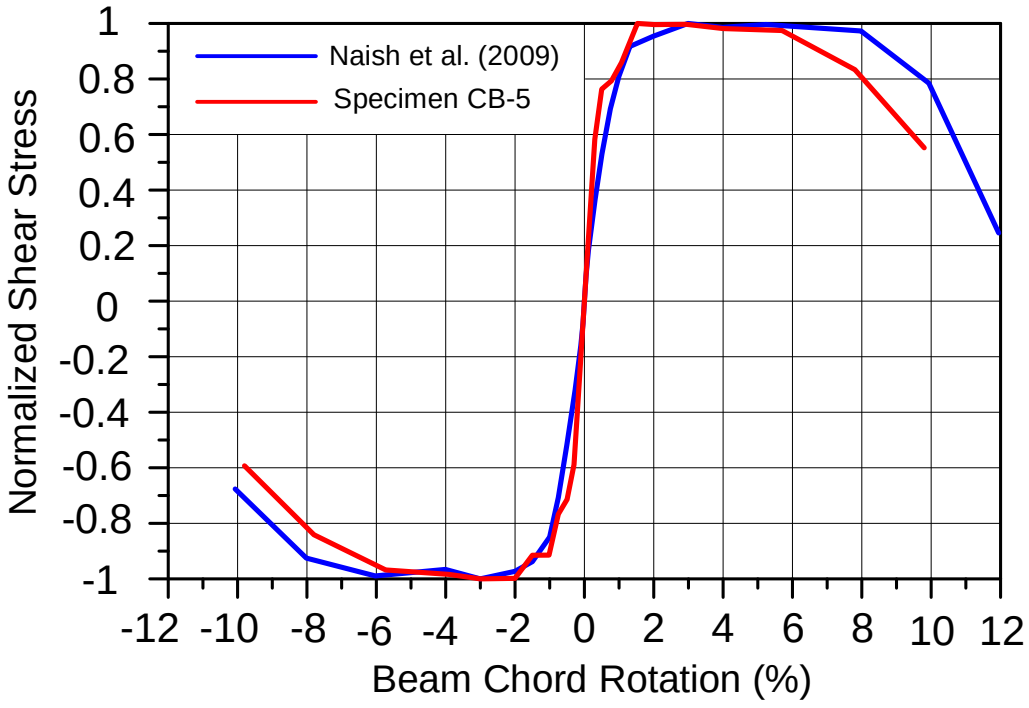

a) CB-5

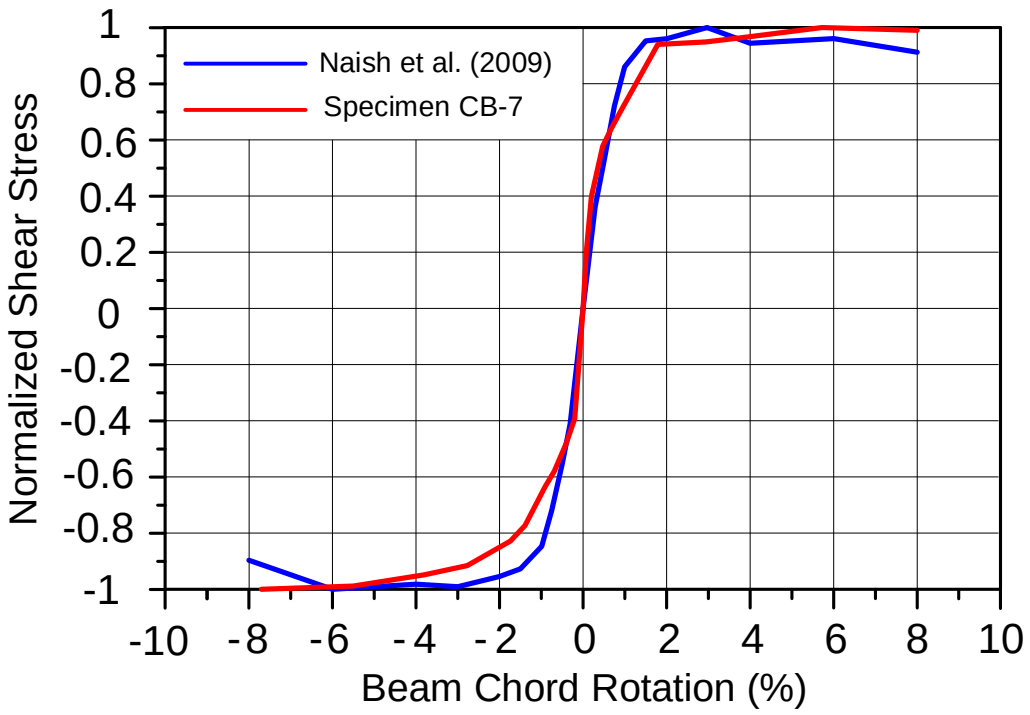

b) CB-7

Figure 4.15 Normalized shear stress versus beam chord rotation

4.2.2.5 Hysteresis Response and Damage Progress of the Double Beam Coupling Beam with 0.25" and 1.5" gap width

4.2.2.4.1 Specimen CB-6 (DBCB with $\ell/h = 2.4$)

Specimen CB-6 with a 0.25" wide gap was tested under symmetrical cyclic loading, to investigate the influence of gap width. The shear force/stress versus beam chord rotation for specimen CB-6 is shown in figure 4.16. The maximum load impose on this specimen was 73 kips, which was equivalent to an average shear stress of $10.7\sqrt{f_c'}$ (psi). The strength deteriorated rapidly beyond 2% rotation due to the formation of major shear cracks.

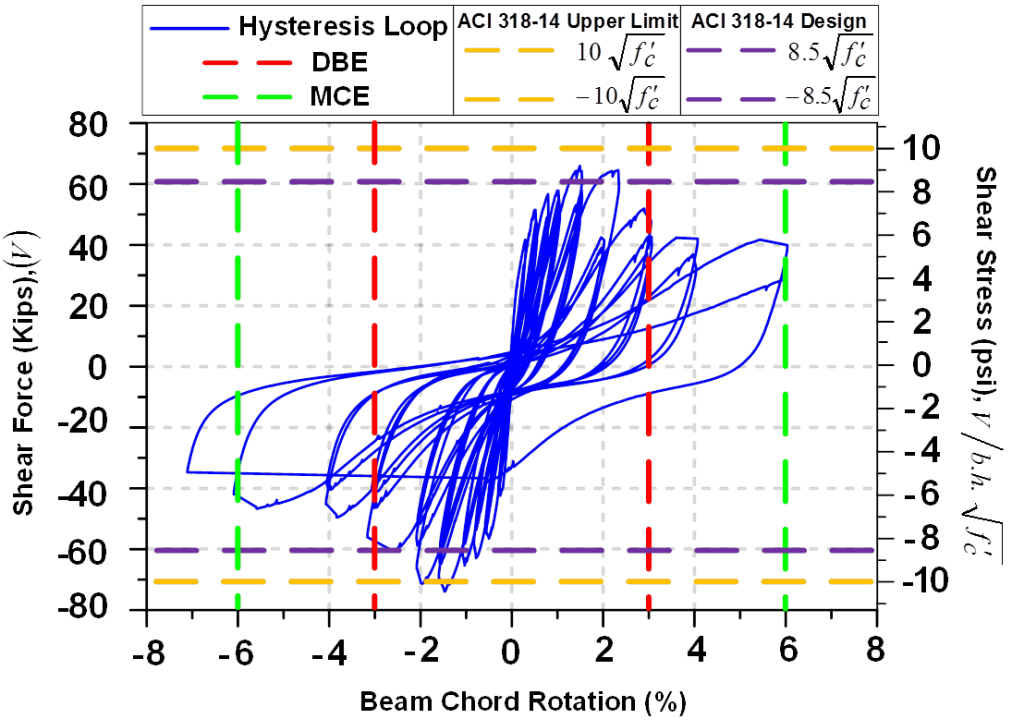

Figure 4.16 Shear force/stress vs. rotation response for Specimen CB-6

In Specimen CB-6, diagonal cracks were first observed during the cycles to 0.25% drift, as shown in Figure 4.17. At 1% drift diagonal cracks widened up to 4mm, and spread in the entire beam. Gap could not get open up to end of the test thus at drift levels larger than 2%, damage become severe with diagonal cracks 6 mm wide, concrete spalling and yielding of the longitudinal bars and hoops. Therefore, Specimen CB-6 failed by shear-dominant mechanism.

Test results clearly showed that a smaller gap could not effectively separate the two beams; thus, the entire specimen acted as a conventional coupling beam reinforced with horizontal and vertical rebars.

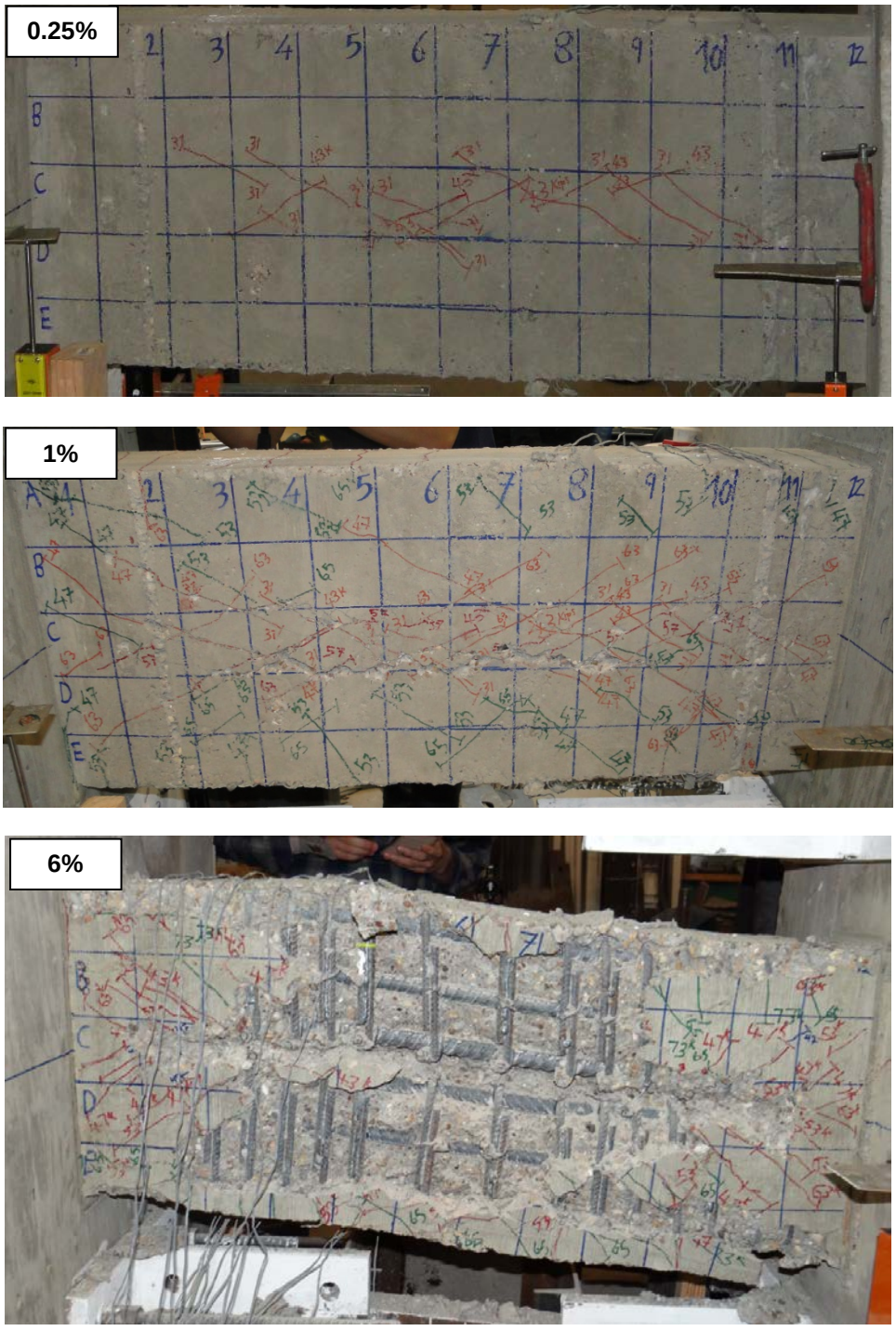

Figure 4.17 Crack pattern and damage progress of DBCBs with 1" gap width

4.2.2.4.2 Specimen CB-8 (DBCB with $\ell/h = 2.2$)

The recent construction needs several utility pipes embedded in the coupling beam due to the electrical and mechanical requirement, therefore full scale double-beam coupling beam with 1.5" width gap which was utilized with two pipes with 2.5" diameter was constructed and tested. The hysteresis response of Specimen CB-1 is shown in Figure 4.18. The maximum force applied to this specimen was approximately 157 kips at approximately 1% drift. The strength deteriorated rapidly beyond 2% rotation due to the formation of major shear cracks same as Specimen CB-8.

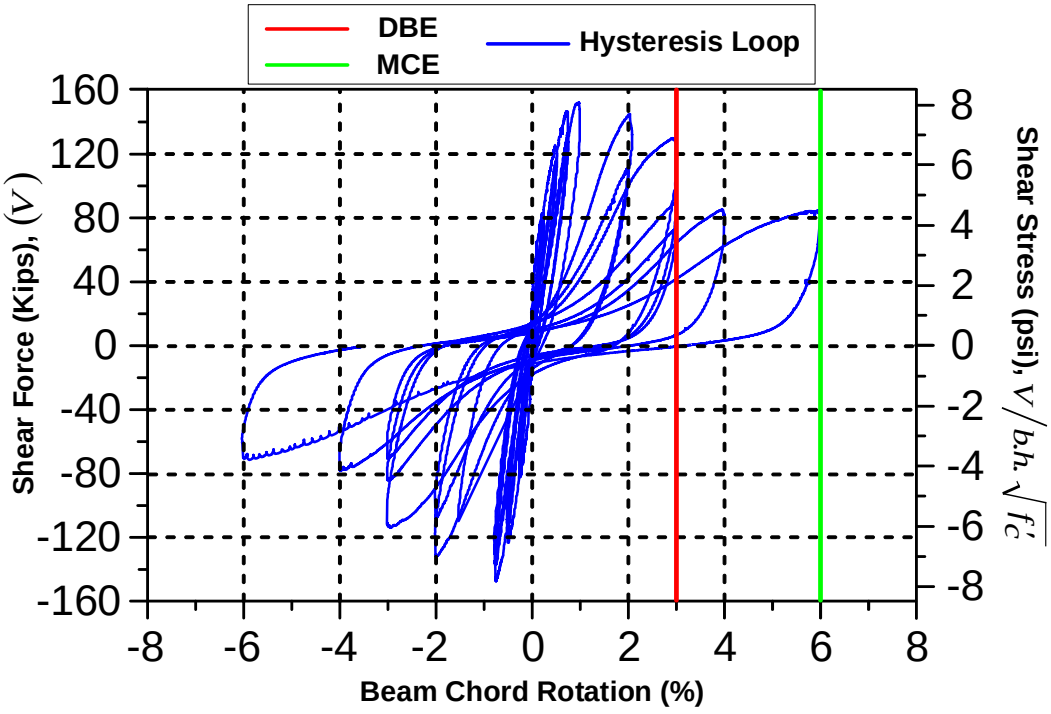

Figure 4.18 Shear force/stress vs. rotation response for Specimen CB-8

Crack pattern for Specimen CB-8 shows that this specimen did not completely separate to two slender beams and, thus, failed by shear based on several reasons. The first reason is the aspect ratio of this beam and the gap width. In contrast to the DBCBs with an aspect ratio of 2.4 at the small drift (0.125%), the crack pattern for these specimens is not even close to the DBCBs with an aspect ratio 2.2 (Figure 4.19). It is really important for DBCB's specimen that the gap opens and the coupling beam separates at a small drift before shear cracks destroy the specimen.

Due to the small aspect ratio at 0.125% drift, several flexural and shear cracks occurred in the beam but in the previous successful DBCB's tests these cracks were not noticed. Additionally, opposed to Specimen Cb-4, 5, and 6 at 0.25% drift, the flexural cracks developed over the length of the beam and joined the diagonal cracks which means the cracks spread over the entire beam instead of its mid-height. This result in small drifts are due to insufficient gap width and small aspect ratio of this coupling beam.

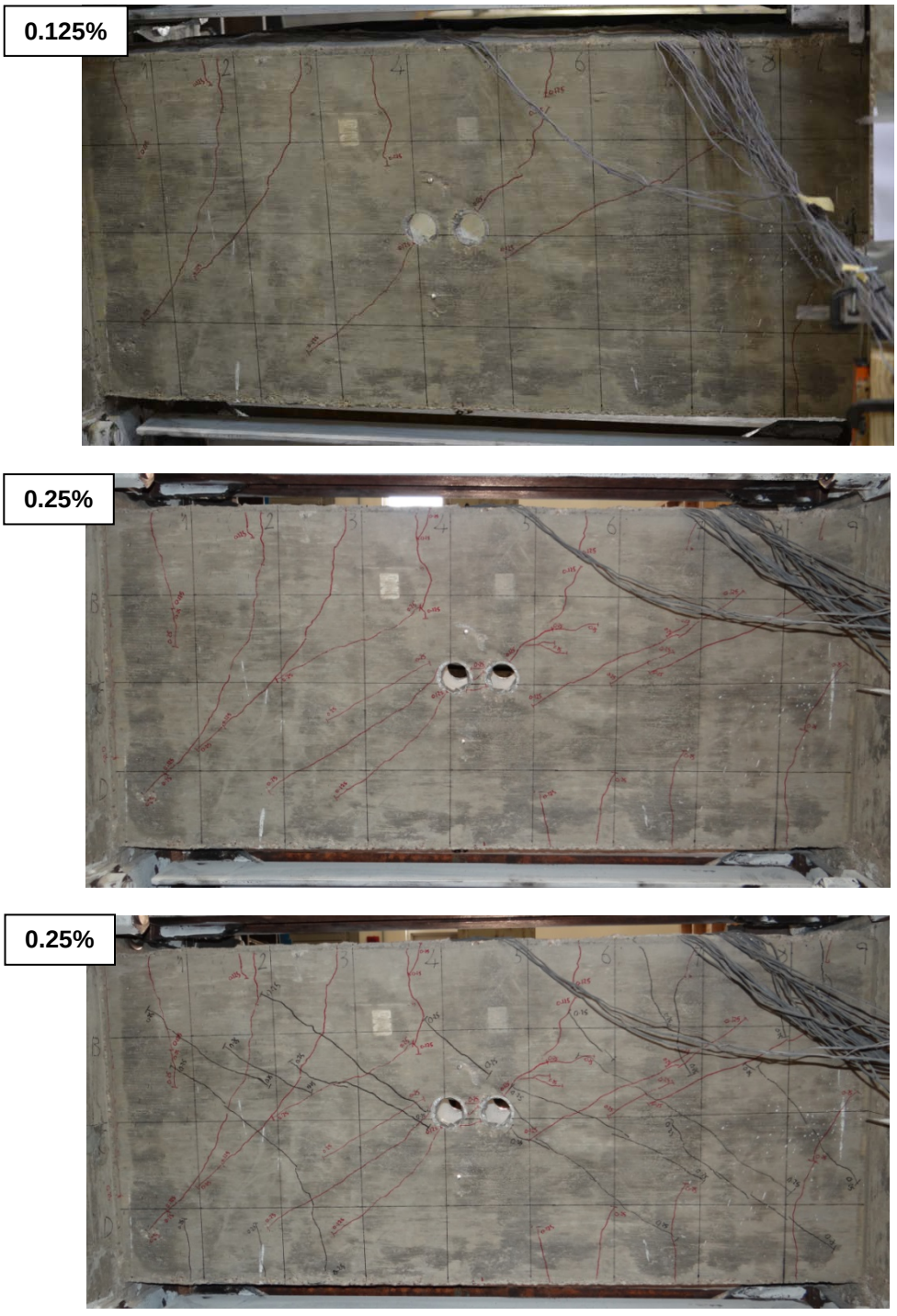

Figure 4.19 Crack pattern and damage progress of full scale DBCBs with 1.5" gap

The second reason is the stress concentration around the PVC pipes which has created several wide shear cracks (Figure 4.20) in that region at small drift (0.25%, 0.5%). These wide diagonal cracks propagate from middle of the gap near the pipes to the extreme fiber of the coupling beam. Therefore, in contrast to the Specimen CB-4, 5, and 6, at small drift, the wide diagonal crack already existed in the Specimen CB-8 and the cracks did not concentrate around the gap region which damages the two slender beams in the coupling beam before separation.

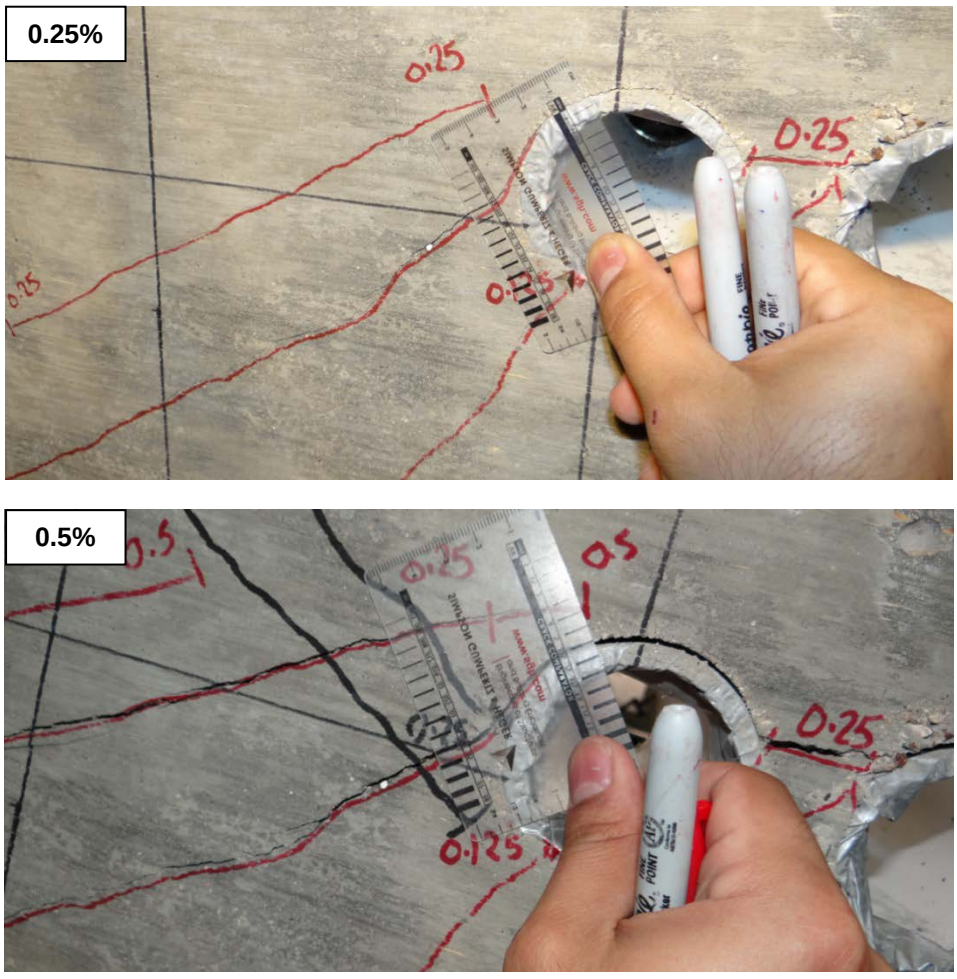

Figure 4.20 Crack widths for full scale DBCBs with 1.5" gap width

The third reason is the PVC pipes and hoops around the pipes. As shown in Figure 4.21, PVC pipes were tightly embedded between two hoops. By increasing the displacement, the large horizontal shear apply to the top and bottom of the coupling beam which is the reason of the sliding the top cage on the bottom cage. Due to the hoops around the PVC pipes, the bearing forces partially resisted the horizontal shear, thus, did not allow the top and bottom cage to slide on each other freely. As a result, this delayed the separation of the coupling beam into two slender beams which caused severe diagonal cracks in the coupling beam.

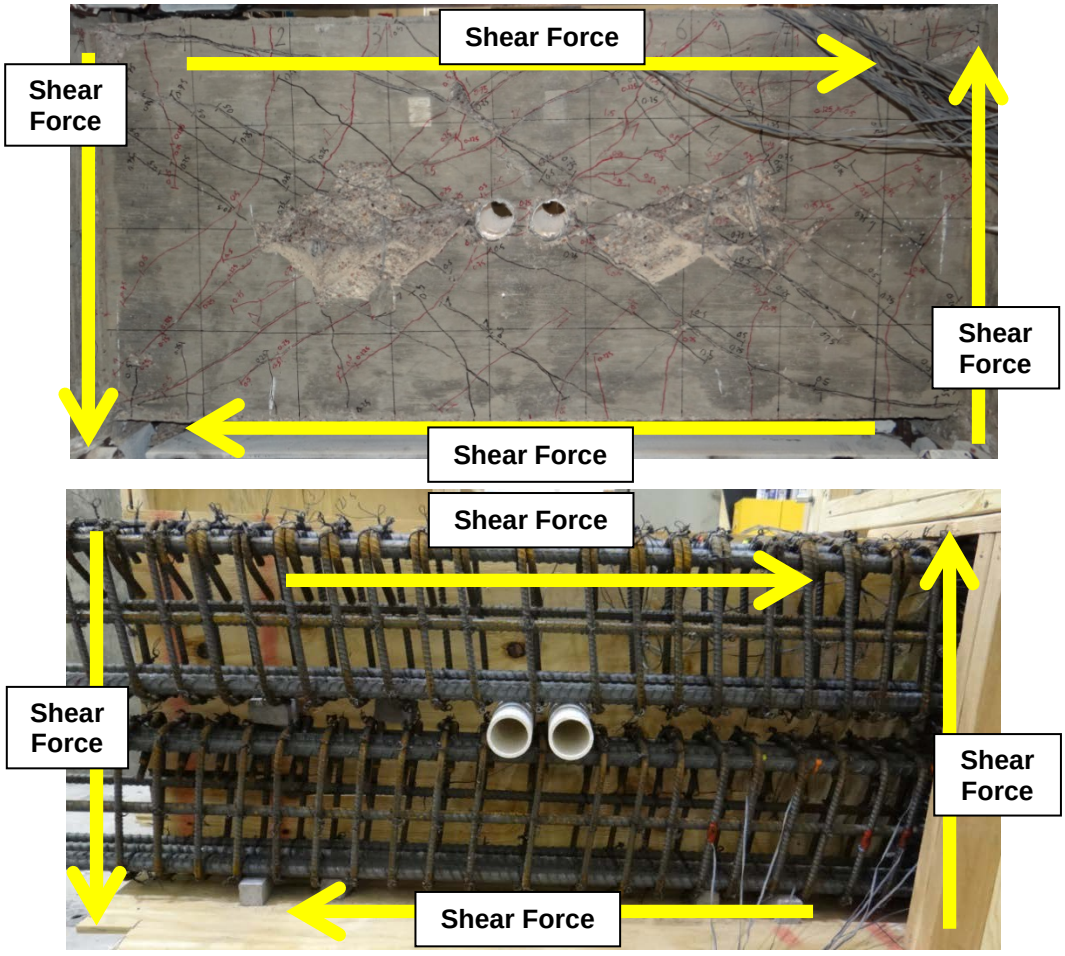

a) Full scale details

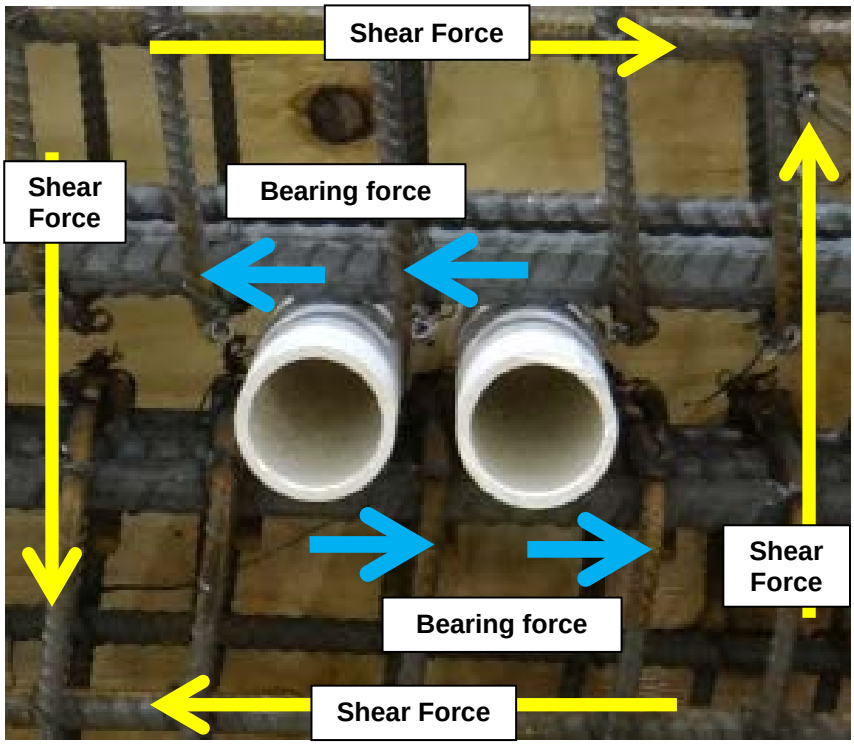

Figure 4.21 PVC pipes and hoops location

Consequently, based on the results and crack patterns for previous experimental tests, the best location for the PVC pipes is at the ends of the gap near the boundary blocks which is approximately 4" length form the boundary blocks toward the middle of the beam.

4.2.3 Rectangular Squat Wall

Using new concept in the coupling beam design resulted in the anticipated improvement in seismic performance. Therefore, six squat walls designed with the same concept of using the several cages which is used in the coupling beam to evaluate the performance of the squat walls with the new design approach. Overall behavior of the

squat wall was evaluated through the shear force/stress versus drift, as well as damage progress throughout the tests.

4.2.3.1 Hysteresis response and damage progress of the Squat wall

4.2.3.1.1 Specimen SW-1 ($h/\ell = 1$)

The hysteresis response of Specimen SW-1 is shown in Figure 4.22. Due to the limited actuator stroke's, test was not finished. The maximum load imposed on this specimen was approximately 111 kips. The specimen exhibited a stable hysteretic response up to the 0.85% drift while the shear stress was approximately 9.8 $\sqrt{f'_c}$ (psi) which indicate that rectangular squat wall with two separate cages can perform adequately under high shear demand.

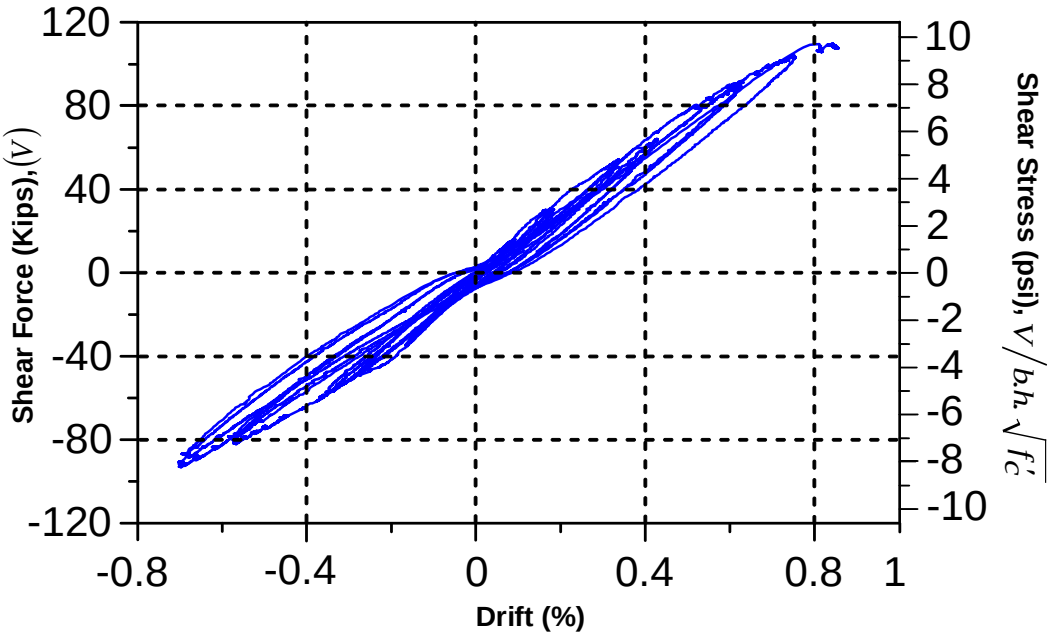

Figure 4.22 Shear force/stress versus drift for SW-1

The crack pattern for this specimen is shown in figure 4.23. At 0.25% drift, the shear cracks developed at mid-span where the narrow gap was located and spread from

footing to 2/3 of the wall heights. Additionally, the flexural cracks were observed at 0.25% drift at the tension side of the wall. The sliding shear was not observed up to end of the test (0.85% drift) and most of the shear cracks developed in the mid height of the wall.

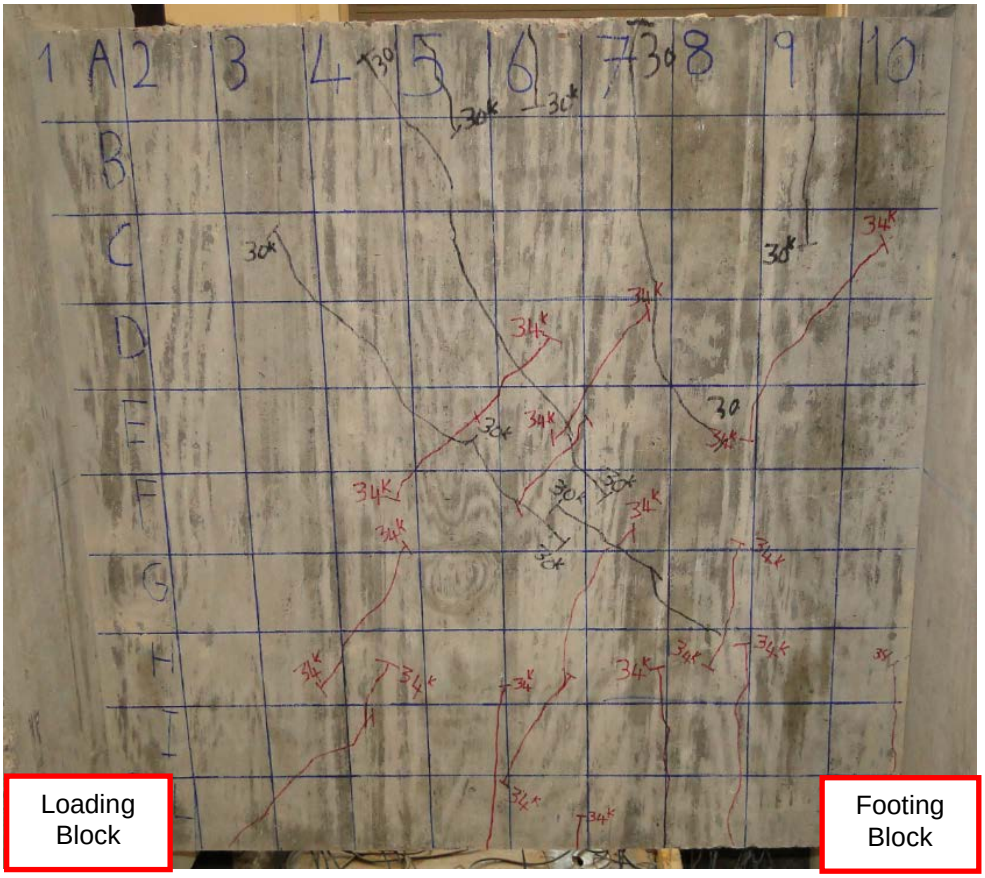

a) 0.25% drift

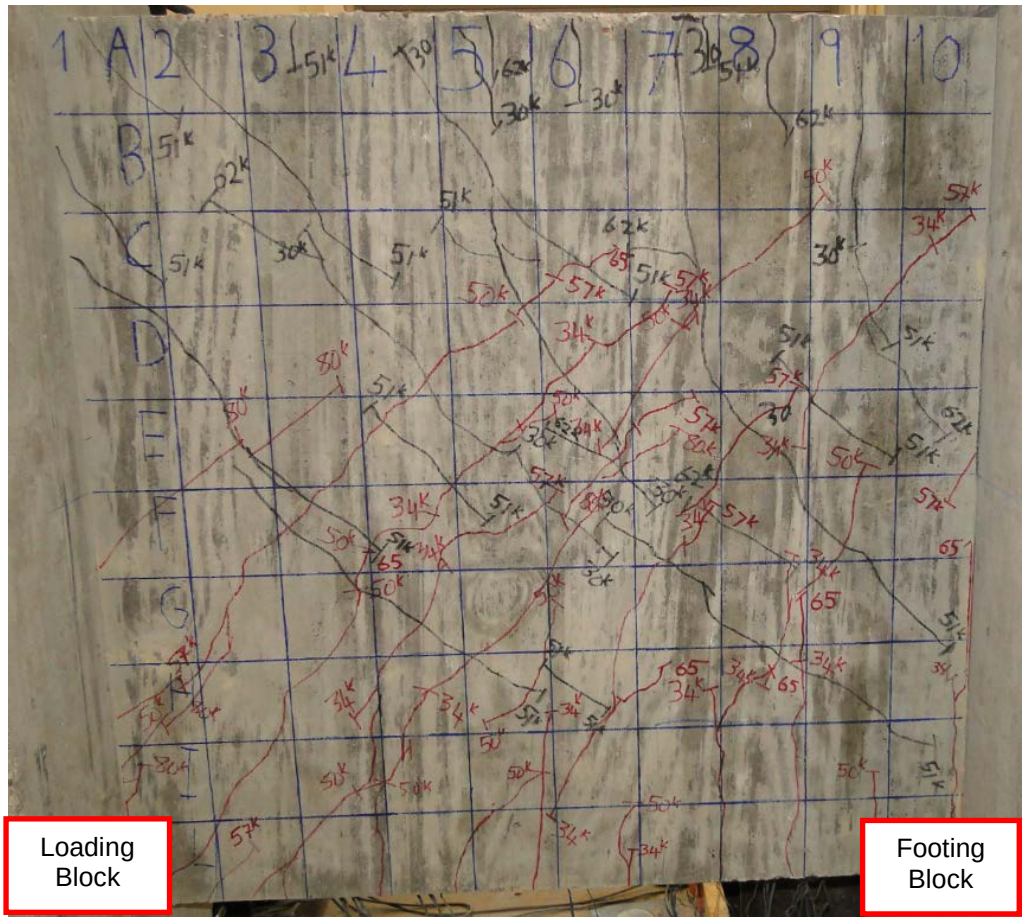

b) 0.85% drift

Figure 4.23 Crack pattern

Use two cages in the rectangular squat wall cause construction difficulty due to the size of the cage. Full scale squat wall needs two huge cages with a lot of hoops and details to satisfy the ACI 318-14 requirement. Width of each cage is approximately equal to half of the wall length. Embedding these two cages in the foundation and floor cause the construction difficulty. Therefore the new concept using four cages with different gap width was resulting in a smaller cage width was evaluated for the other specimen.

4.2.3.1.2 Specimen SW-3 ($h/\ell = 1$)

Due to the architectural requirement sometimes needs to pass the pipes through the squat wall. Specimen SW-3 with 2.5" gap width was utilized with two pipes with 2.5" diameter in each gap was constructed and tested. Figure 4.24 shows the shear force/stress versus drift response of the specimen SW-3.

Test results indicated that using four cages with pipes in appropriate location between them can transfer shear-dominated behavior to a flexure-dominated one after reach high shear stress and drift same as conventional wall. The transition point was at approximately 1.2% drift ratio, which is the same drift ratio when the fast strength degradation started in the conventional wall specimen. The four beams started separating as noted by the crack pattern (Figure 4.25). Note that the separation cracks did not initiate from the openings. Hysteresis loop shows that after 1.2% drift ratio, the strength dropped from $7.6\sqrt{f'c}$ to $5\sqrt{f'c}$, and the stress was maintained up to 2.5% drift ratio without rapid strength degradation as conventional squat walls. The specimen eventually separated into four slender beams as intended (Figure 4.25). The sliding shear failure was completely eliminated in our specimen.

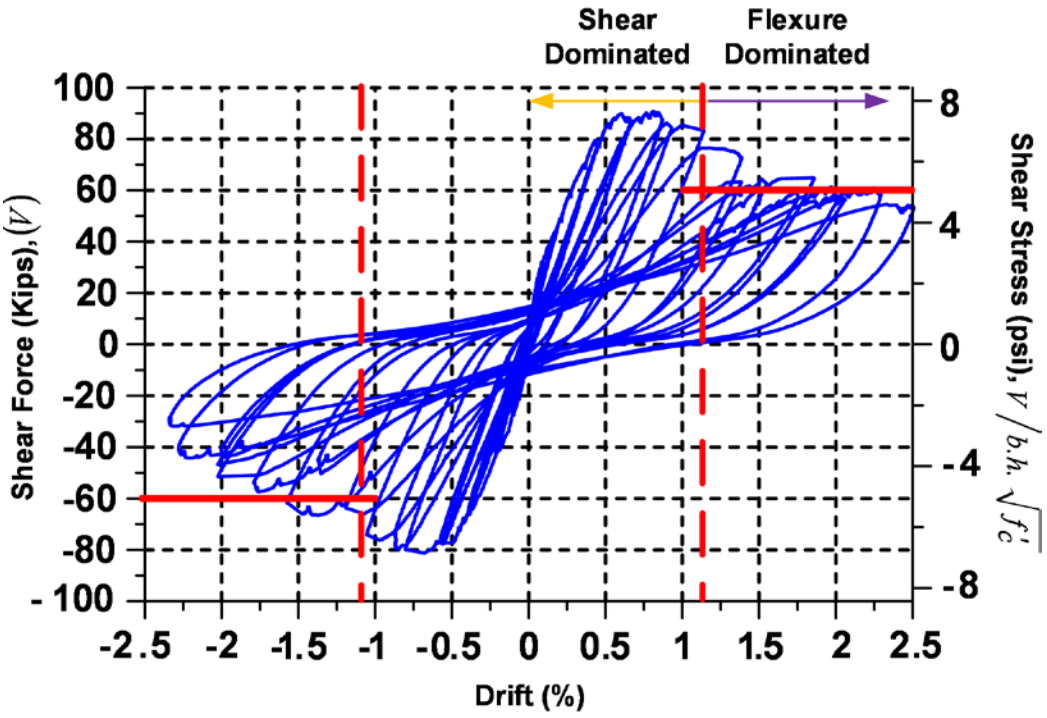

Figure 4.24 Shear force/stress versus drift for SW-3

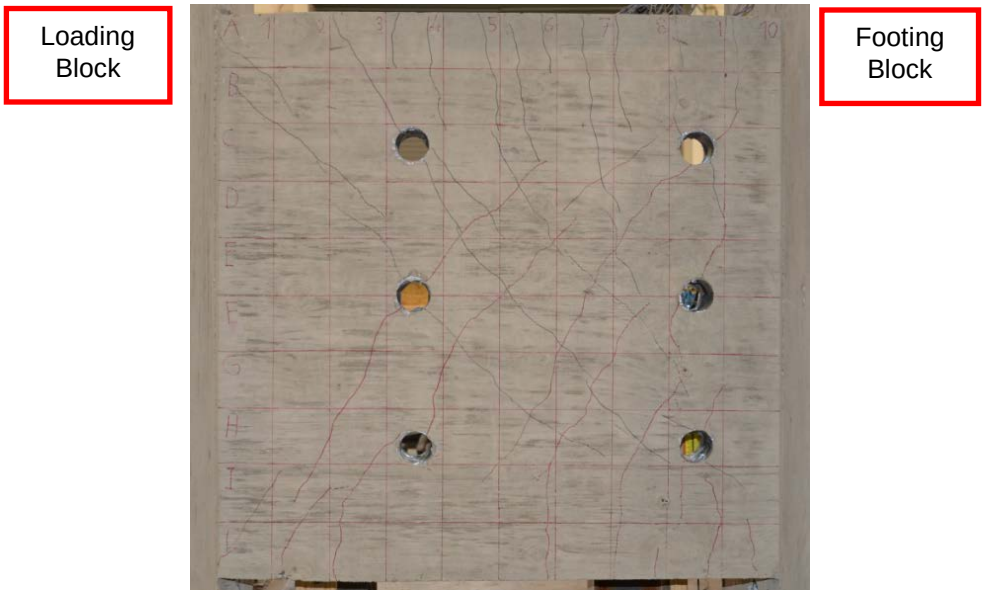

a) 0.25% drift

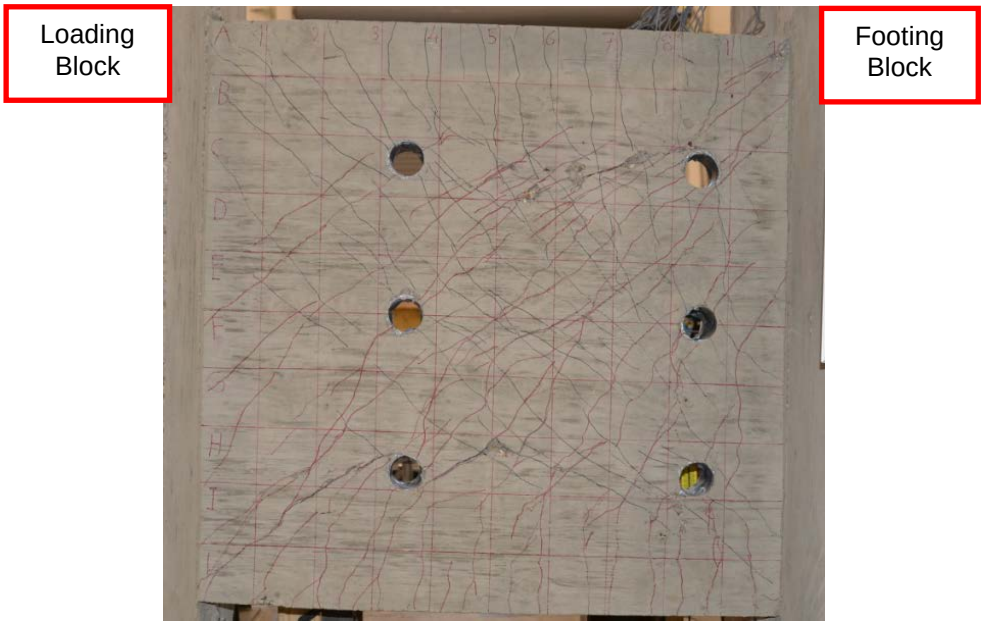

b) 1.2% drift

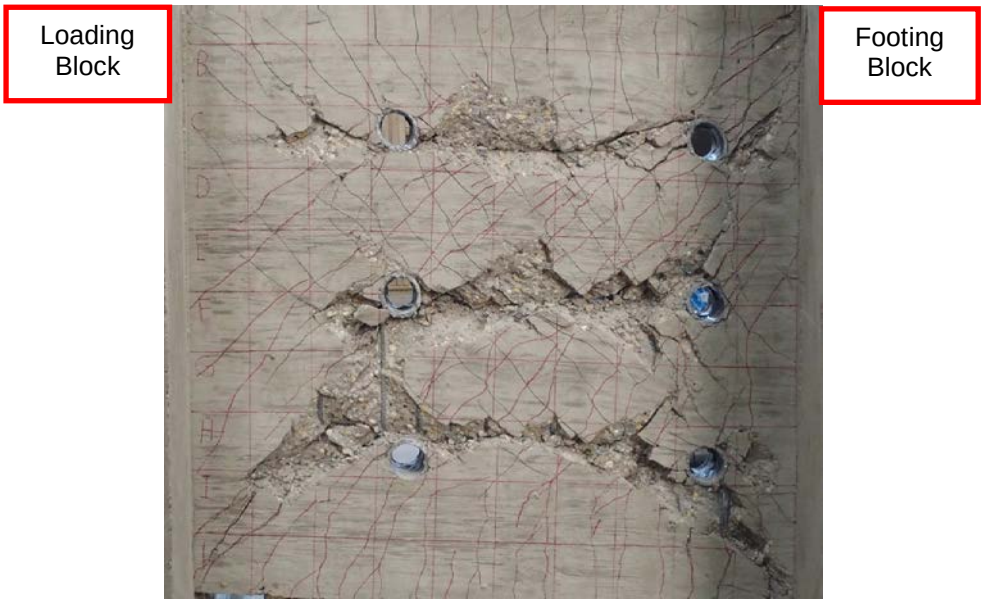

b) 2.5% drift

Figure 4.25 Crack pattern for SW-3

4.2.3.1.3 Specimen SW-2 ($h/\ell = 1$)

The shear stress/strength versus drift response of specimen SW-2, shown in figure 4.26, indicates excellent rotational capacity and good energy dissipation. Specimen SW-2 sustained a maximum load of 92 kips, which is equivalent to shear stress $8.3\sqrt{f'_c}$ (psi). A stable hysteresis response was observed up to 1.25% drift in both directions. Additionally, it could still resist approximately 85% of the peak stress at 1.5% rotation.

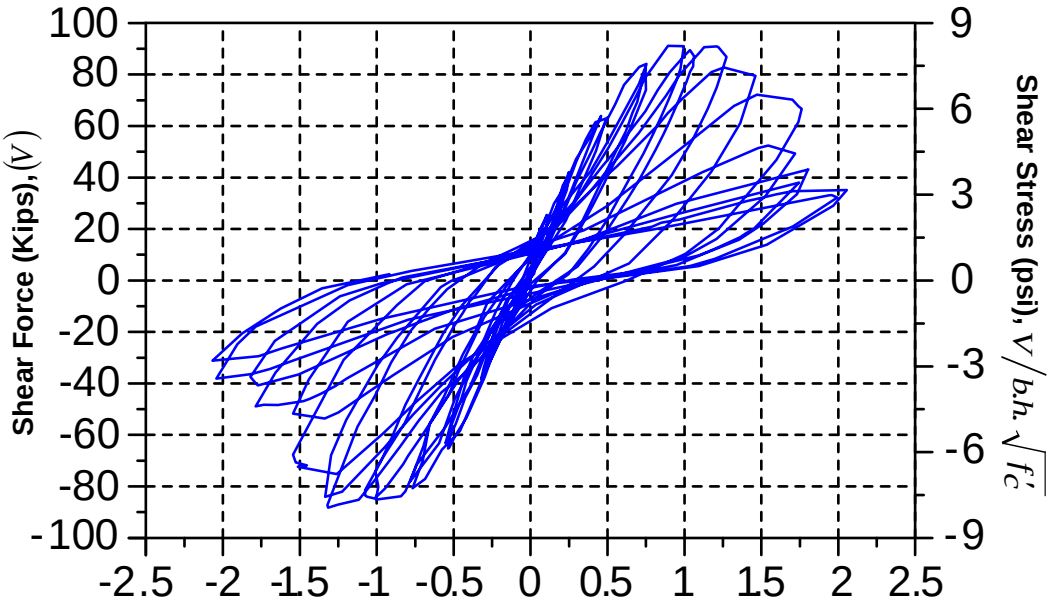

Figure 4.26 Shear force/stress versus drift for SW-2

4.2.3.1.4 Specimen SW-5 ($h/\ell = 1$)

Using the four cages with close hoops in the squat wall resulted in significantly more stable hysteresis behavior than that observed in conventional squat wall. Figure 4.27 shows the shear force/stress versus drift response of the specimen SW-5. This specimen was able to maintain very high shear stress under symmetric loading protocol without degradation ($14.9\sqrt{f'_c}$ (psi)) up to a rotation of 0.75% which is approximately 50%

more than the shear stress in conventional wall with same aspect ratio. Also, it could still resist 90% of the peak stress at 1% rotation.

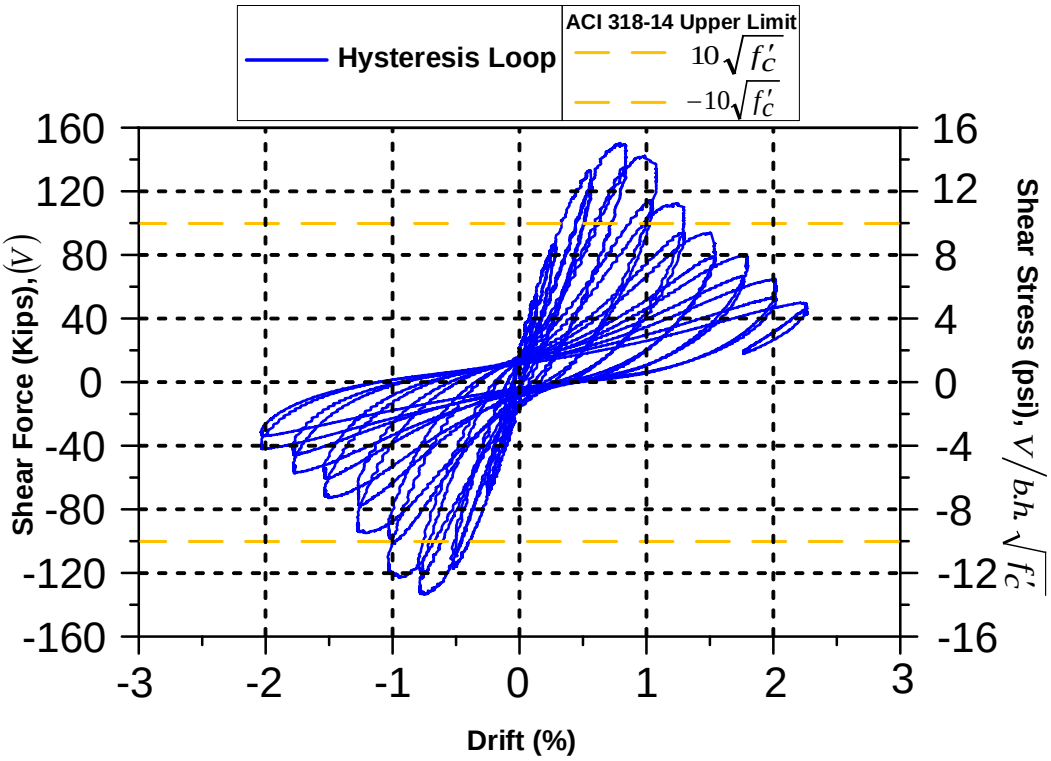

Figure 4.27 Shear force/stress versus drift for SW-5

4.2.3.1.5 Specimen SW-6 ($h/\ell = 0.5$)

The shear stress/strength versus drift response of specimen SW-2, shown in Figure 4.28, indicates excellent rotational capacity and good energy dissipation for squat wall with aspect ratio 0.5. Specimen SW-2 sustained a maximum load of 205 kips, which is equivalent to shear stress $19.1\sqrt{f'_c}$ (psi). A stable hysteresis response was observed up to 0.75% drift in both directions.

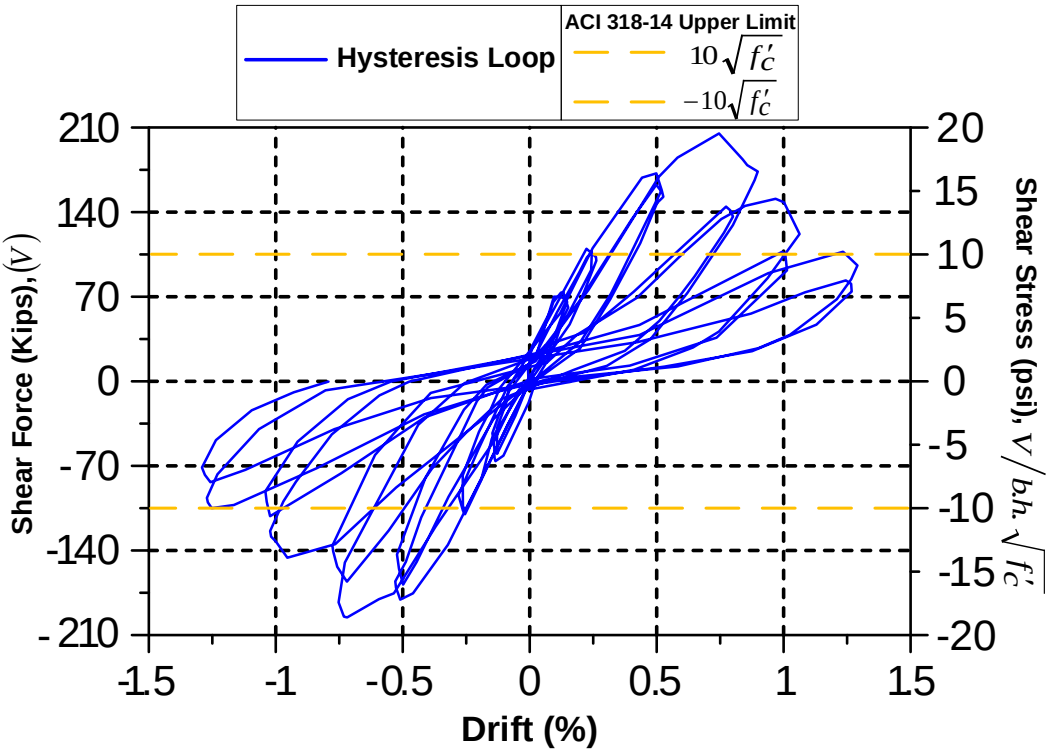

Figure 4.28 Shear force/stress versus drift for SW-6

4.2.3.1.6 Cracking Pattern for Specimen SW-2, SW-5, SW-6

Minor flexural cracks and shear cracks were visible at 0.25% drift in all of these specimens. The shear cracks developed around the gaps and spread from footing to 2/3 of the wall heights. Also, the flexural cracks were observed at the tension side of the wall.

At 1.25% drift more shear and flexural cracks had formed on Specimen SW-2 and also, concrete crushing in the compression edge. In the cycles leading to a drift of 1.5%, the wall exhibited significant concrete cover spalling and concrete crushing in the web region and significant loose strength. The crack pattern for this specimen is shown in Figure 4.29.

The main diagonal cracks formation in Specimen SW-5 had already occurred by the end of the 0.75% drift cycle (Figure 4.30). As the test progressed, the exciting

diagonal cracks widened at 1% drift and also, concrete cover spalling and concrete crushing in the compression edge was observed, as a result, loose strength. At drift larger than 1 % the damage in the wall concentrated near the footing block by spalling the concrete cover and gaps, and concert destroyed in each cage, consequently significant loose strength.

At 0.75% drift dense diagonal cracks had formed in specimen SW-6 (Figure 4.31). At drift larger than 0.75 %, the wall exhibited significant concrete cover spalling and concrete crushing in the web region at mid-height of the wall thus, leading to significant loose strength.

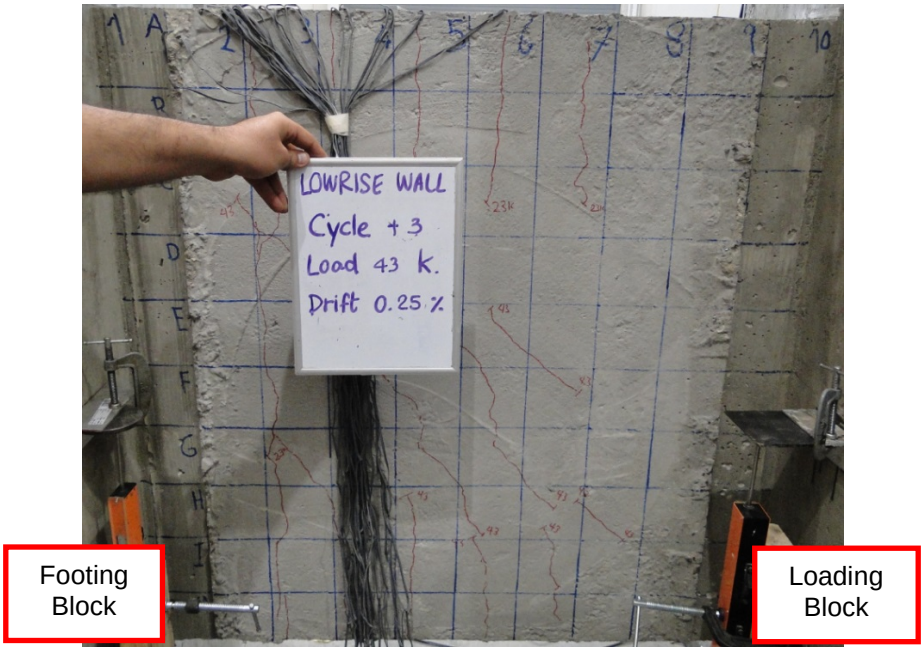

b) 0.25% drift

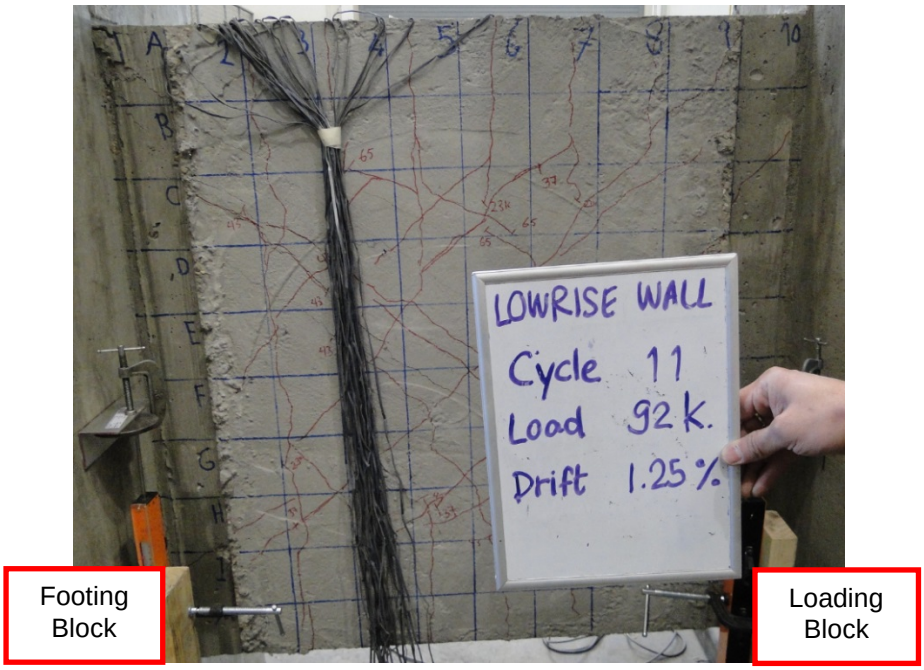

b) 1.25% drift

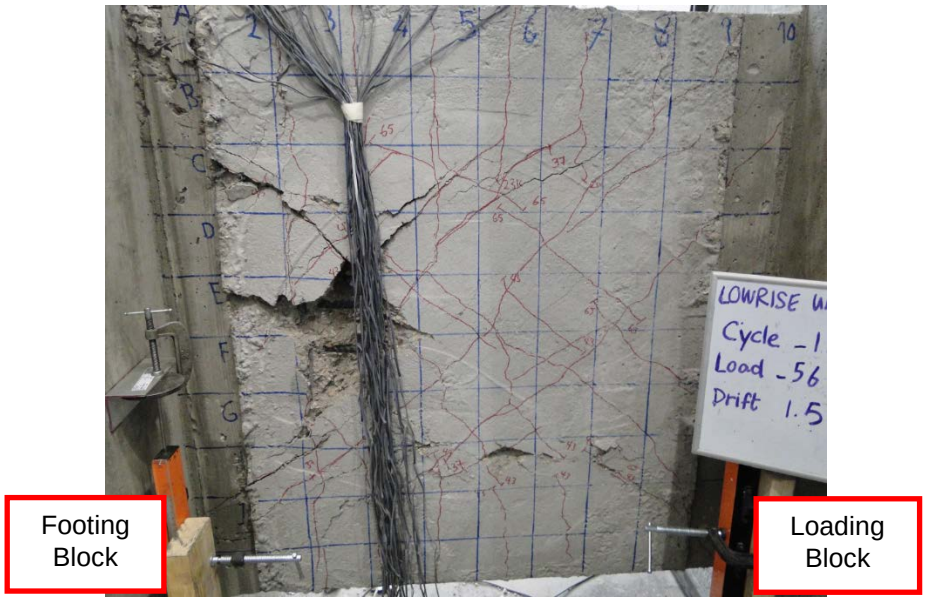

b) 1.5% drift

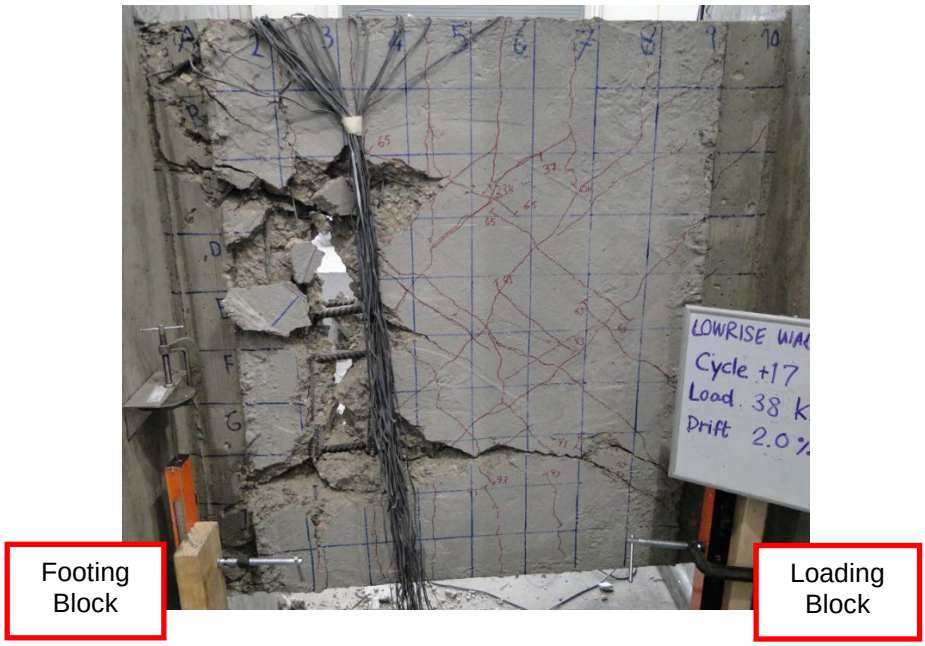

c) 2% drift

Figure 4.29 Crack pattern for SW-2

b) 0.25% drift

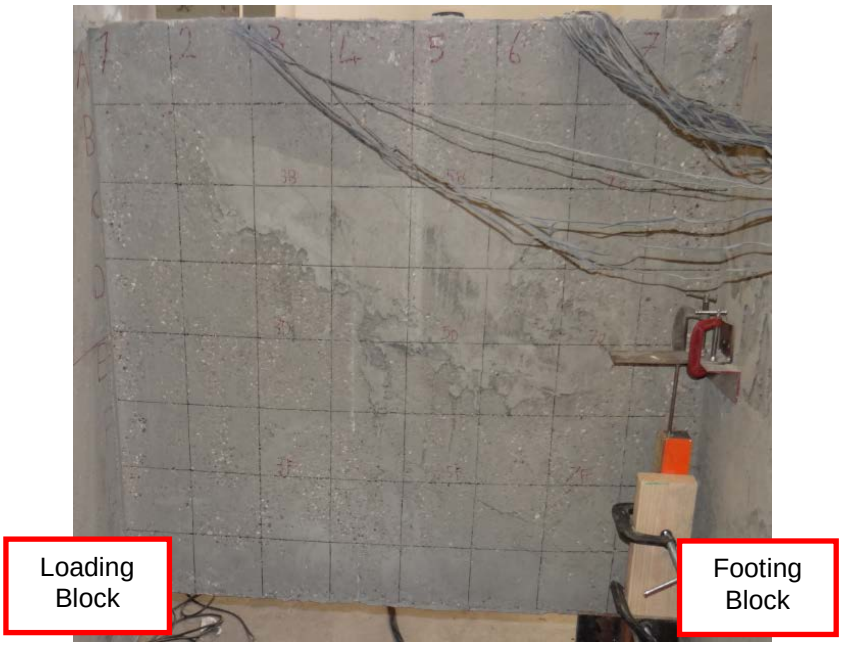

b) 0.75% drift

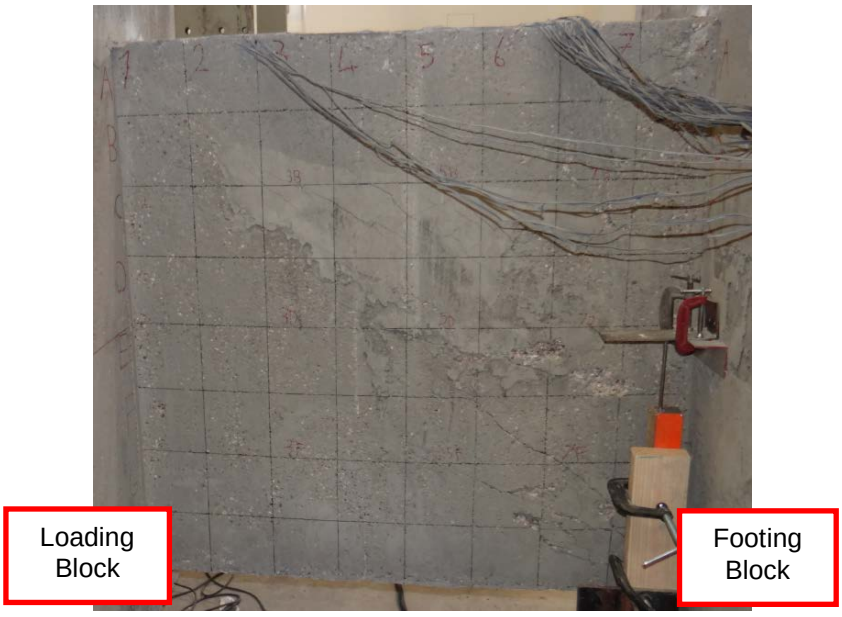

b) 1 % drift

b) 2% drift

Figure 4.30 Crack pattern for SW-5

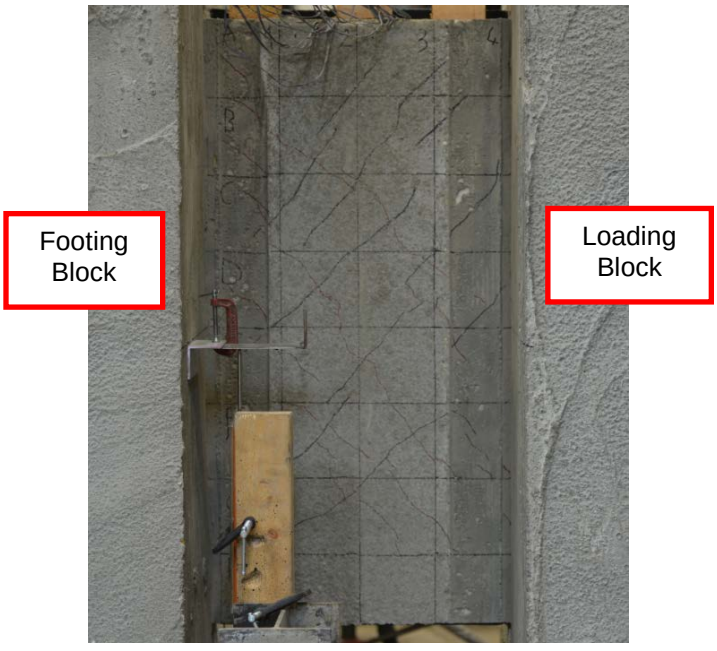

a) 0.25% drift

b) 0.75% drift

c) 1% drift

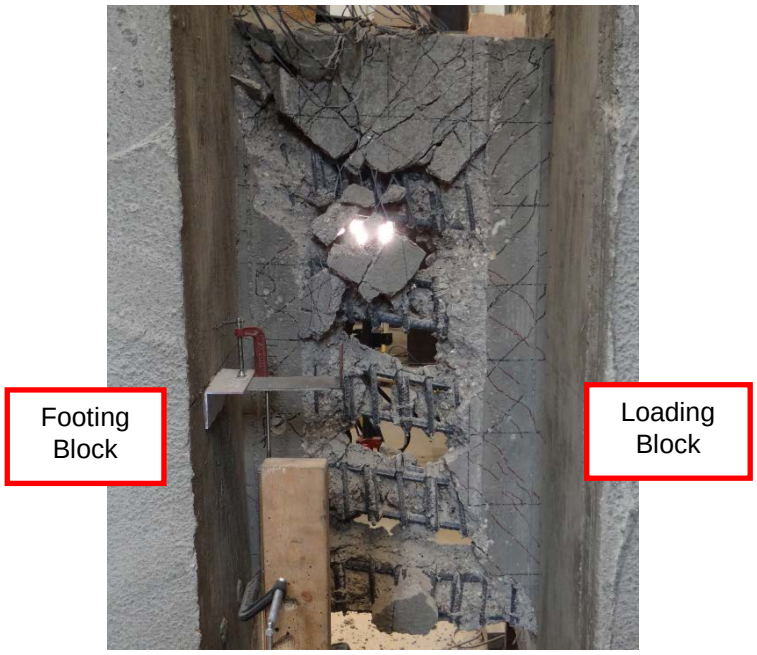

b) 2% drift

Figure 4.31 Crack pattern for SW-6

Test results of the SW-2, SW-5, and SW-6 using the new design concept are shown (red dots) in Figure 4.32, and 4.33 and compared with prior test results with ACI compliant SWs (blue dots) which is tested cyclically. Figure 4.30 present the variation of the experimentally measured peak shear strength (V_{peak}) which is normalized by the A_w and $\sqrt{f_c'}$, with moment-to-shear ratio (M/Vl_w) for the rectangular low-rise walls (Gulec et al. (2010)). A_w is the web area calculated as the length of the wall (l_w) times web thickness (t_w) and f_c' is the concrete compressive strength. Figure 4.31 present the drift capacity of the rectangular squat wall which had the shear stress higher than $8\sqrt{f_c'}$ (psi) with moment-to-shear ratio (M/Vl_w). Important observations are summarized as follows:

1. As shown in prior studies [Gulec et al., 2008] and Figure 4.32, none of the ACI compliant rectangular squat walls had a strength of more than $10\sqrt{f_c'}$ psi. On the other hand as revealed in Figure 4.30, the SWs using the proposed new design concept were able to reach a peak shear stress close to $15\sqrt{f_c'}$ to $20\sqrt{f_c'}$ psi. The volumetric ratio of confining hoops had a great influence on the peak shear strength of SWs.

2. Peak drift capacities of the test SWs were between 0.75% to 1.3%, which are in general greater than those of ACI compliant SWs. The peak drift capacities are also greater than the maximum allowed drift limits for squat walls specified in ASCE/SEI 43 (2005); that is, 0.75% for collapse prevention and 0.4% for essentially elastic behavior.

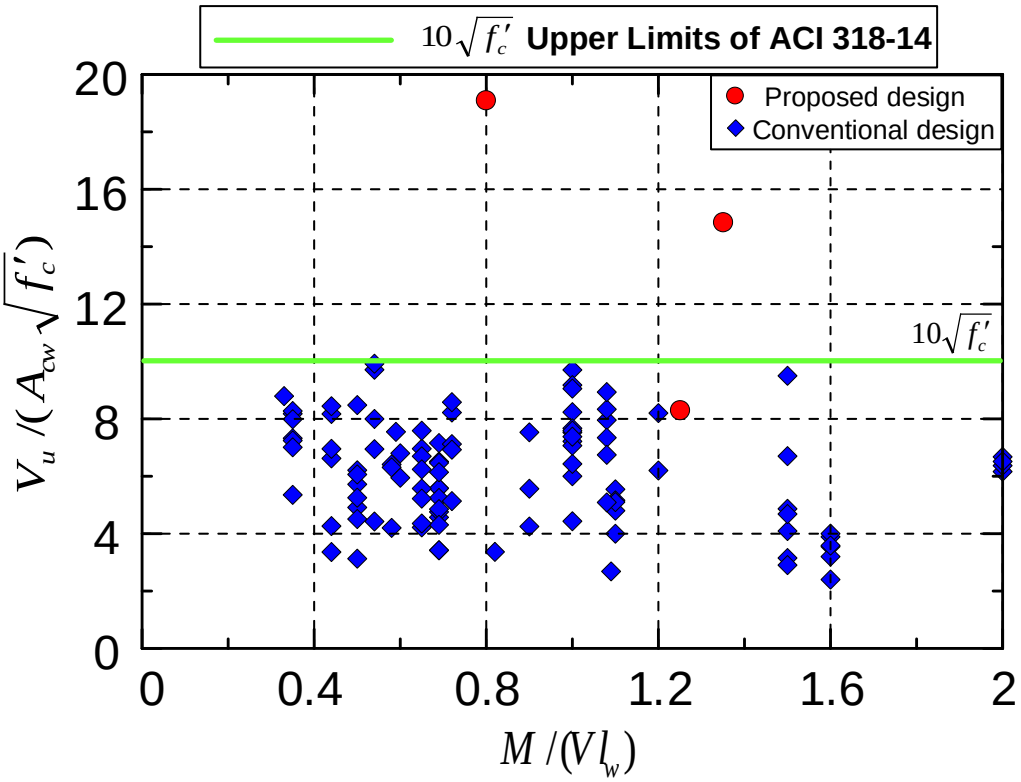

Figure 4.32 Peak shear strength versus moment-to-shear ratio

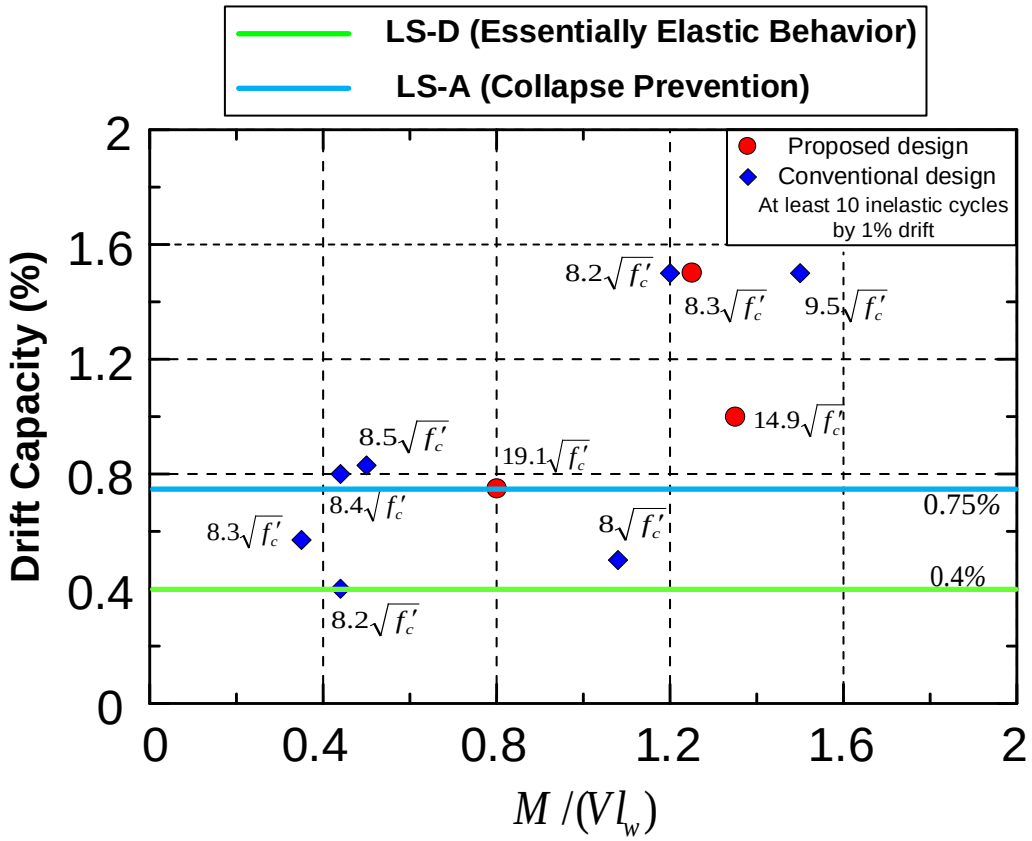

Figure 4.33 Drift versus moment-to-shear ratio

4.3 Nonlinear Finite Element Analysis

Before start the second phase of the coupling beams construction and test, It was important that is identified the clear span between the two cages in DBCB. After a lot of trials analysis with VecTor2, the final width chosen for this region was one inch, based on two reasons. First, make sure the height of clear span is enough, because after a few cyclic loads more crack should happen in this region consequence the coupling beam is separated to two slender beams. Second, the coupling beam shows adequate stiffness and strength capacity.

The FE model was created to evaluate the gap width, shown in figure 4.33. The dimension of the coupling beams in all of the models was defined 6"x15"x36" similar to the first six coupling beam's. All the nodes for the block which is represented the big block were constrained in X and Y direction. Also, all the nodes for the small block restrained in X direction, thus the steel link is omitted in this model. The coupling beam models were subjected to monotonic displacement at the block which is represented the small block. The assumptions used in this model are shown in Table 4.2.

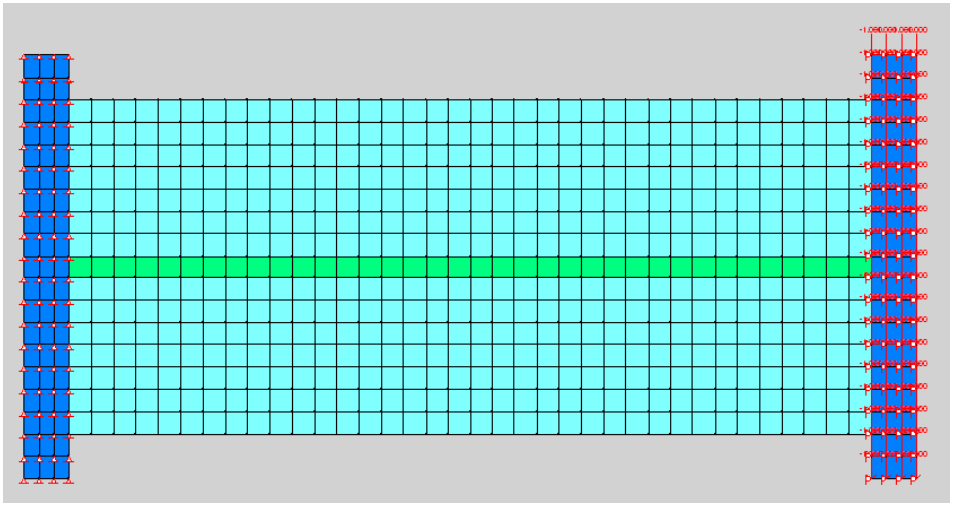

VecTor2 model

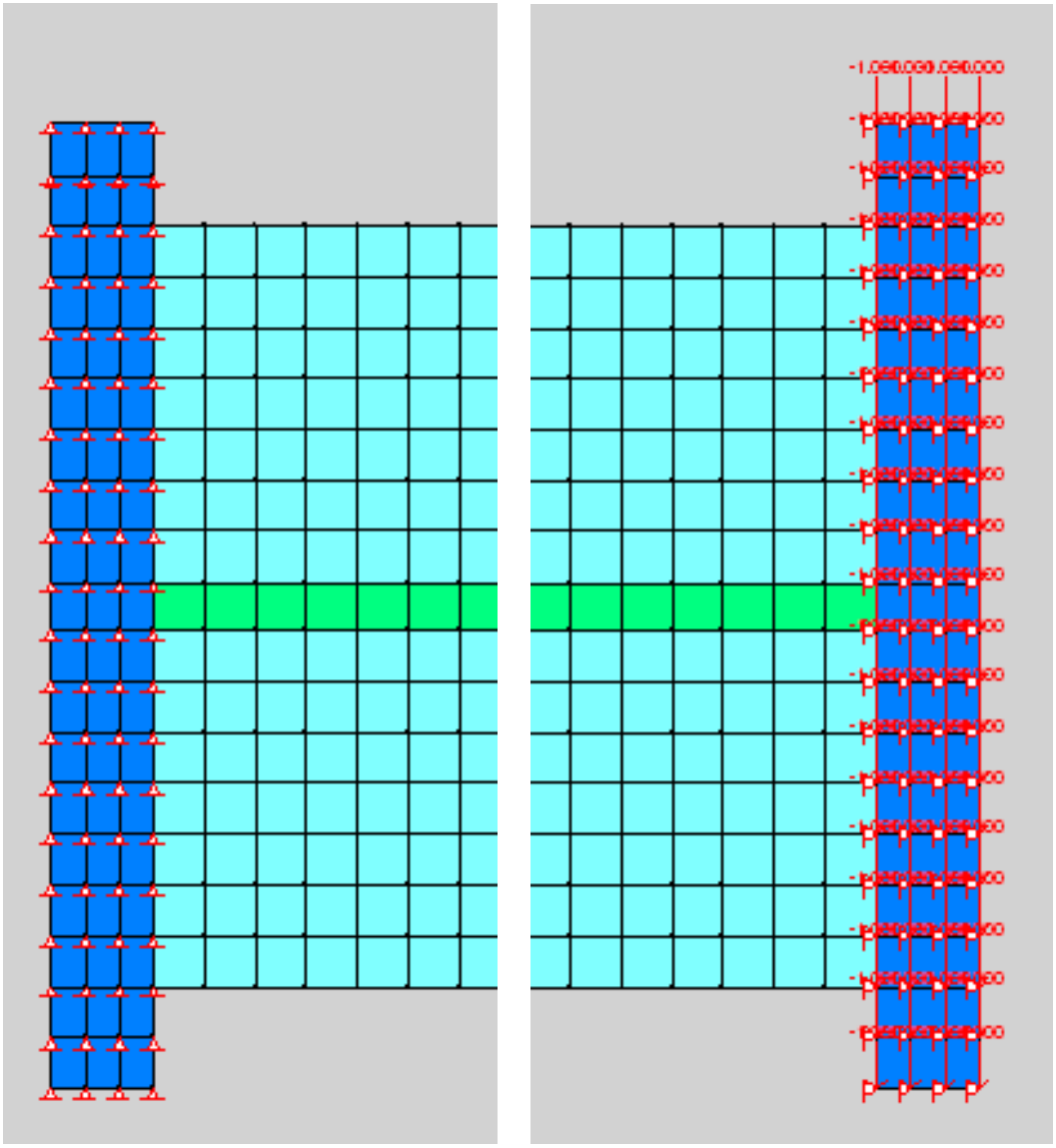

Figure 4.34 VecTor2 model

Table 4-2 Material and Analysis Models Used for Modeling the Test Coupling Beams

Concrete Models	
Compression Pre-Peak	Hogmestad (Parabpla)
Compression Post-Peak	Modified Park-Kent
Compression Softening	Vecchio 1992-A
Tension Stiffening	Modified Bentz 2003
Tension Softening	Linear
FRC Tension	Not Considered
Confined Strength	Kupfer / Richart
Dilation	Variable – Kupfer
Cracking Criteria	Mohr – Coulomb (Stress)
Crack Stress Calculation	Basic (DSFM/MCFT)
Crack Width Check	Agg/5 Max Crack Width
Crack Slip Calculation	Walraven (Monotonic)
Creep and Relaxation	No Available
Hysteretic Response	Nonlinear w/ Plastic Offsets)
Concrete Bond	Eligehausen
Reinforcement Models	
Hysteretic Response	Bauschinger Effect (Seckin)
Dowel Action	Tassios (Crack Slip)
Buckling	Refined Dhakal-Maekawa

Rectangular mesh was used in the model with a mesh size of 25.4 mm. Each finite element model consisted of three types of concretes. Concrete type 1 represented regular concrete with specific compressive strength of 5000 (psi) in the mid-height of the coupling beam (green region), where the gap is located. Both top and bottom regions of the coupling beam, were modeled concrete type 2 which is included the regular concrete with specific compressive strength of 5000 (psi) and smeared reinforcement. Reinforcements were automatically placed based on the given area of reinforcement when using the smeared reinforcement. These regions were reinforced with 6.3% longitudinal reinforcement ratio and 4% transverse reinforcement ratios, according to the design of the coupling beams. The two concrete blocks simulating the wall boundary regions were modeled using concrete type 3 and assumed to be rigid elements. Concrete type 3 represented regular concrete with specific compressive strength of 5000 (psi) and

15% longitudinal reinforcement ratio and 10% transverse reinforcement ratios. Also, the detail of the reinforcement is demonstrated in Figure 4.35.

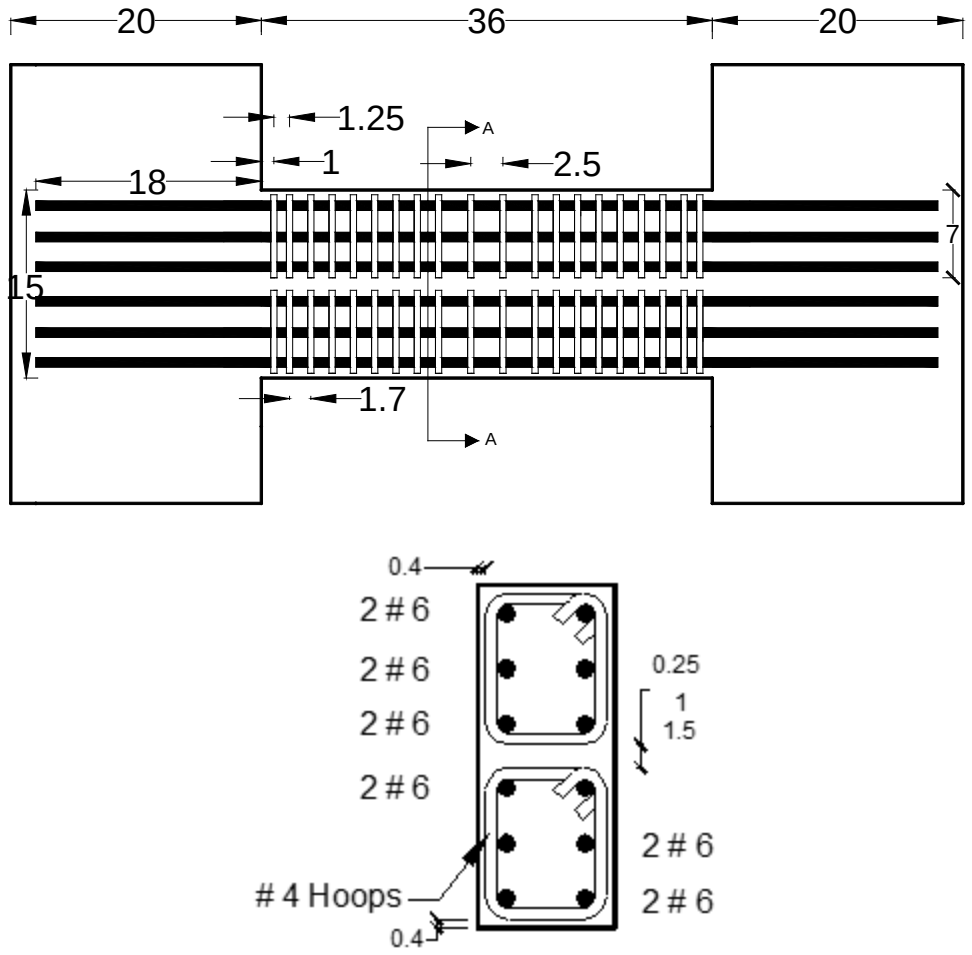

Figure 4.35 Cross sections of the models

The load vs. rotation plot for four different gap widths is shown in figure 4.23. The model with a 0.25" wide gap failed earlier than the others, and exhibited the highest strength but poor ductility. On the other hand, the model with a 1.5" wide gap exhibited the highest ductility, but lowest strength due to the reduced height of each cage in the coupling beam. As a result, the strength of the models increased as the width of the gap

decreased (Figure 4.36). Consequently, one inch gap was selected for the DBCB specimens.

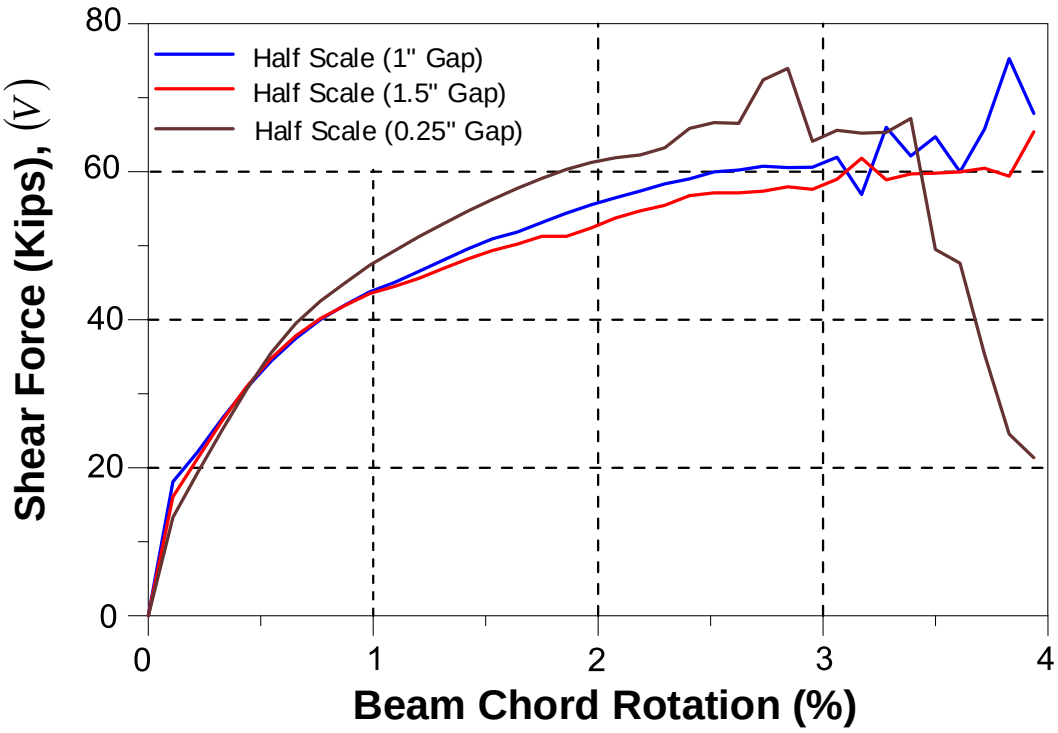

Figure 4.36 Stiffness retention of each model

Chapter 5

Summary and Conclusions

This research investigated two innovative design concepts that could considerably improve the constructability, seismic performance, or reparability, and meet architectural requirements for access of utilities for reinforced concrete (RC) coupling beams and squat walls.

In the first phase of this study an innovative and simplistic reinforcing layout for RC coupling beams that significantly reduces design and construction difficulties when using diagonally reinforced coupling beams was extensively studied by large scale experimental testing. The new double-beam coupling beam (DBCB) consists of two separate cages similar to those used for typical beams in reinforced concrete special moment frames. The two cages are separated by a small spacing from one to two inches. Only vertical and horizontal rebars are needed. Upon large displacements, cracks begin developing at the DBCB's mid-span and mid-height, and then gradually propagate towards the beam's ends. The cracks eventually separate the coupling beam into two slender beams where each has nearly twice the aspect ratio of the original coupling beam. This split essentially transforms the shear-dominated single deep beam behavior into a flexure-dominated slender beam behavior. Because damage initiates from the center of the beam, and then spreads towards the ends, the beam ends are able to maintain their integrity even under very large displacements, thereby eliminating the sliding shear failure at the beam-to-wall interface. The following conclusions are drawn from the study:

1. Preliminary testing results on half-scale coupling beam specimens with a span-to-depth ratio of 2.4 and 3.3 showed that coupling beams with the proposed reinforcement scheme were able to sustain high shear stresses $8\sqrt{f_c'}$ (10~12

$\sqrt{f'_c}$) and large rotations (8~11%) before significant strength degradation occurred.

2. Experimental results showed that the ductility of a DBCB with 3.3 aspect ratio is greater than that of an ACI compliant diagonally reinforced coupling beam (DCB).
3. The beam-wall boundary in DBCBs experienced much less damage when compared to that of DCBs; therefore, a smaller development length is required for the longitudinal rebars (approximately 60% of that required by ACI 318-14 Section 18.8.5.3(b)).
4. Experimental and nonlinear FEA shows that the gap width does not affect the elastic stiffness of the DBCBs. However a smaller gap width (0.25 in.) could not separate the two beams before the major diagonal cracks developed, thereby reducing the ductility of the DBCBs. On the other hand, a large gap width will decrease the moment arm of each beam, leading to a smaller capacity. Nevertheless, this can be easily compensated by using slightly large rebars.
5. Another potential advantage of DBCBs is that the utility pipes can be passed through the beam at the gap location without compromising the performance. Experimental and nonlinear FEA indicated that the location of these pipes, if placed, can be critical. It is shown that the utility pipes should not be placed at mid-span of DBCBs. A suitable location is at both ends of the beam.
6. Because the cracks always initiate at the mid-span and mid-height of the DBCBs, the damage location can be easily predicted, this makes repair work easier after moderate earthquakes.

In the second phase of this study a new arrangement was proposed for the squat wall (SW). The new arrangement consists of several separate cages similar to those used for the DBCBs. However, the purpose is completed different. In DBCBs, the cages

are separated by a gap to increase the aspect ratio of the cage in an attempt to transfer the shear behavior to flexural behavior. For squat wall, on the other hand, the multiple cages are used to increase the confinement of the web of the wall, thus enhancing the strength and ductility. Using the close hoops for each cage increases the shear strength due to improved strength and ductility of the concrete, thereby preventing the premature shear failure that occurs in conventionally reinforced squat walls. From the experimental and analysis conducted in this research, the following conclusions can be drawn:

1. While none of the ACI compliant rectangular squat walls found in our literature review had a strength of more than $10\sqrt{f_C'}$ psi (Figure 4.30), rectangular squat wall with aspect ratio 1 and 0.5 having the proposed reinforcing scheme exhibited a stable hysteresis behavior with shear stress of approximately 14.9~19.1$\sqrt{f_C'}$ which is more than the expected limit in ACI 318-14 and close to the expected upper limit in ASCE 43-05.
2. Peak drift ratio capacities of the test SWs were in the range of 0.75% to 1.5% (i.e., the drift ratios before the strength degradation starts), which are in general greater than those of ACI compliant SWs. The peak drift capacities are also greater than the maximum allowed drift limits for squat walls specified in ASCE43-05; that is, 0.75% for “collapse prevention” and 0.4% for “essentially elastic behavior”.
3. Another potential advantage of using multiple cages with gaps between them is that the utility pipes can be passed through the wall at the gap location without compromising the performance. Our experimental testing indicated that the location of these pipes, if placed, can be critical. A suitable location is at 1/3 of the height from both ends of the wall.

Appendix A

Strain Gauge Information

Strains in the reinforcing steel were measured by strain gauges which were fixed to the longitudinal, diagonal and transverse steel reinforcements. The locations and labels for strain gauges placed on longitudinal, and transverses reinforcement is shown in Figure 3.14. Those strain gauges in coupling beam which were yielded will show in this appendix.

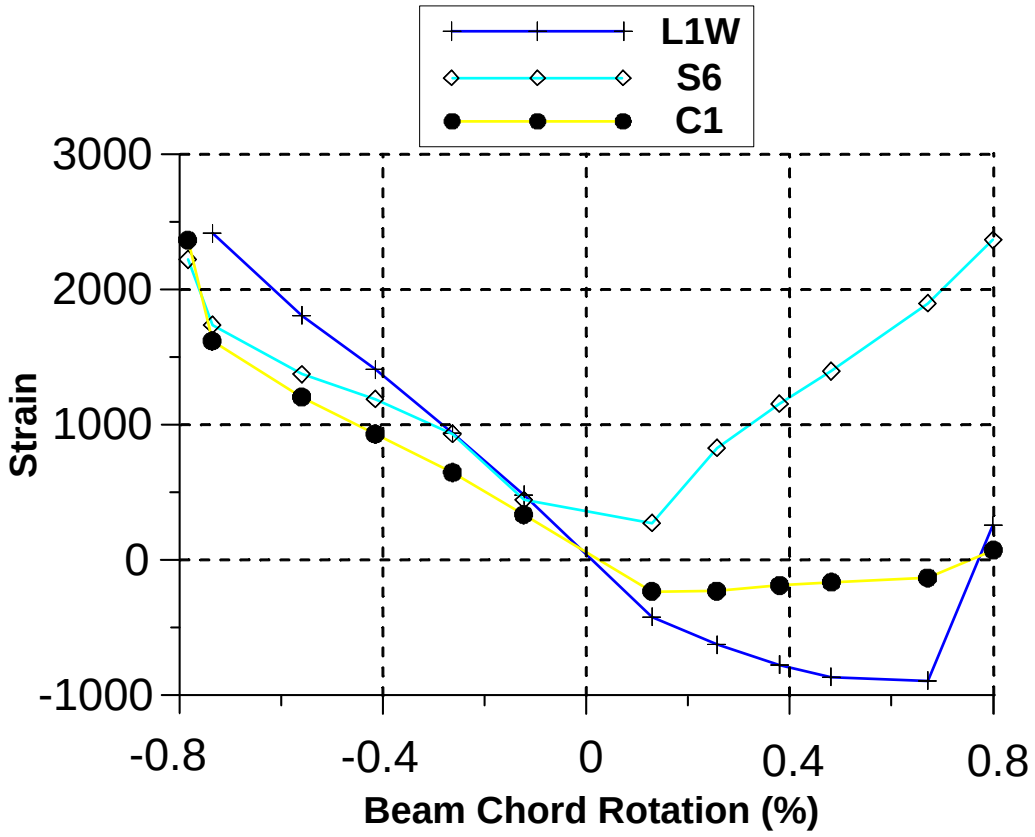

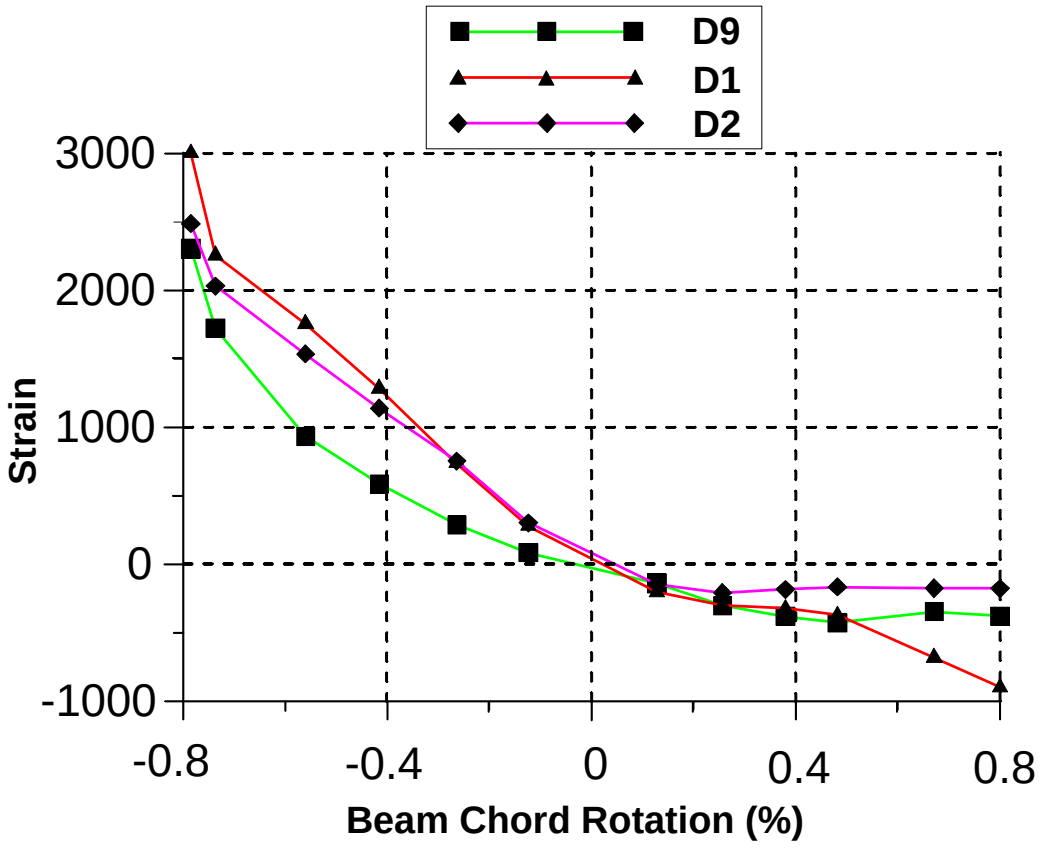

Strain gauge results for CB-1

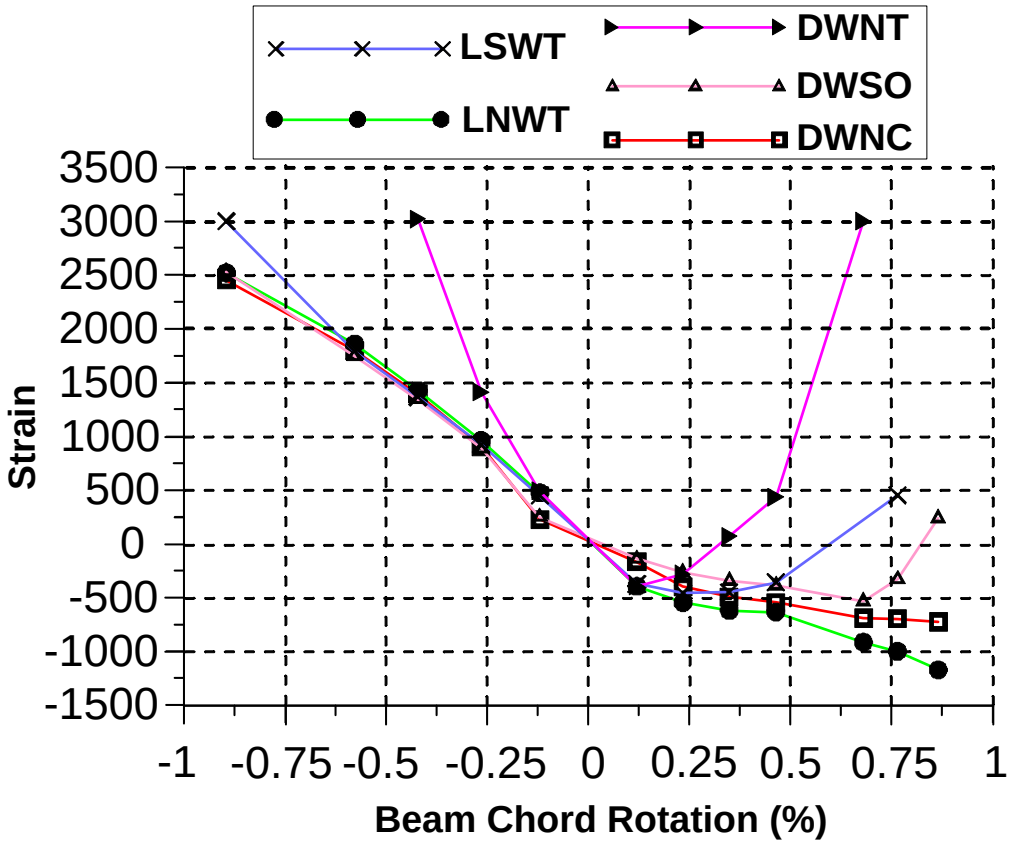
LSWT
LNWT
DWNT
DWSO
DWNC
Strain
3500
3000
2500
2000
1500
1000
500
0
-500
-1000
-1500
-1
-0.75
-0.5
-0.25
0
0.25
0.5
0.75
1
Beam Chord Rotation (%)

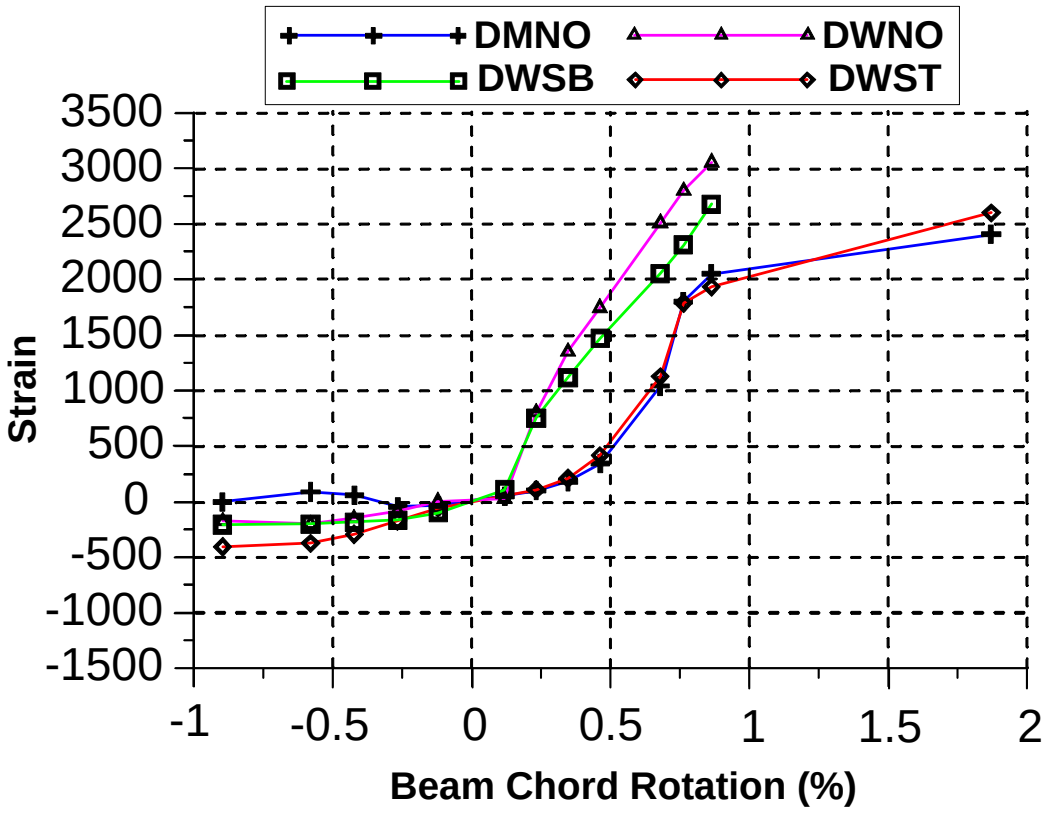

Strain gauge results for CB-2

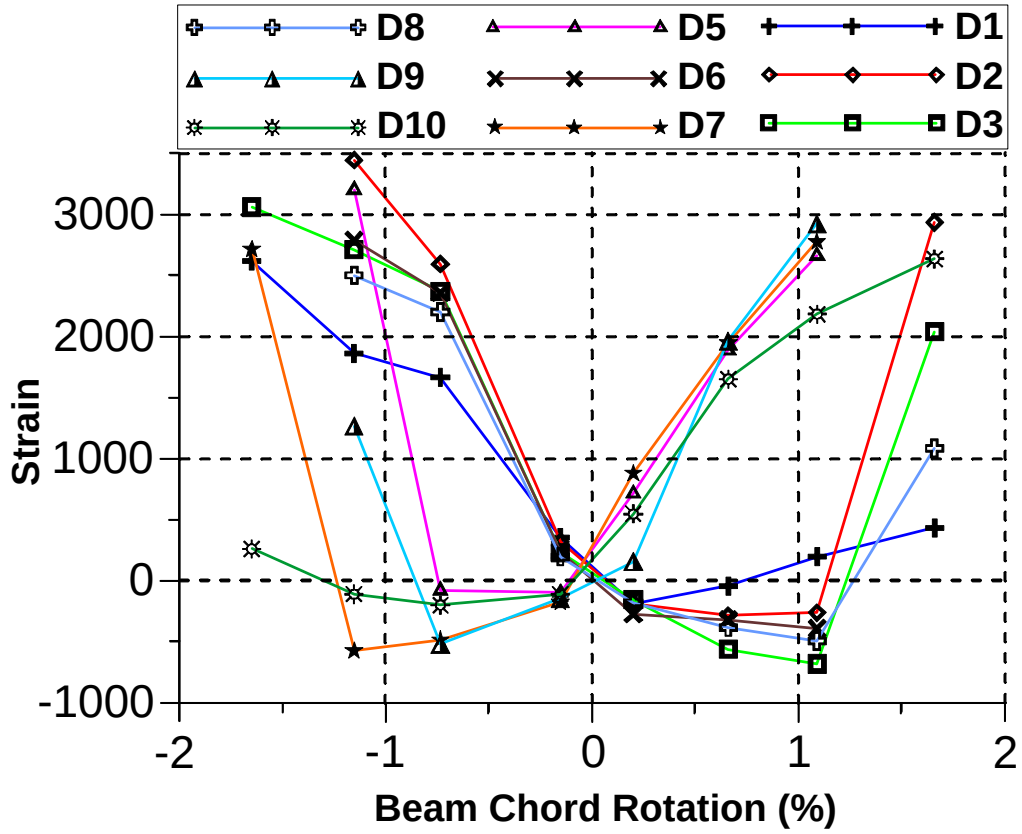

Strain gauge results for CB-3

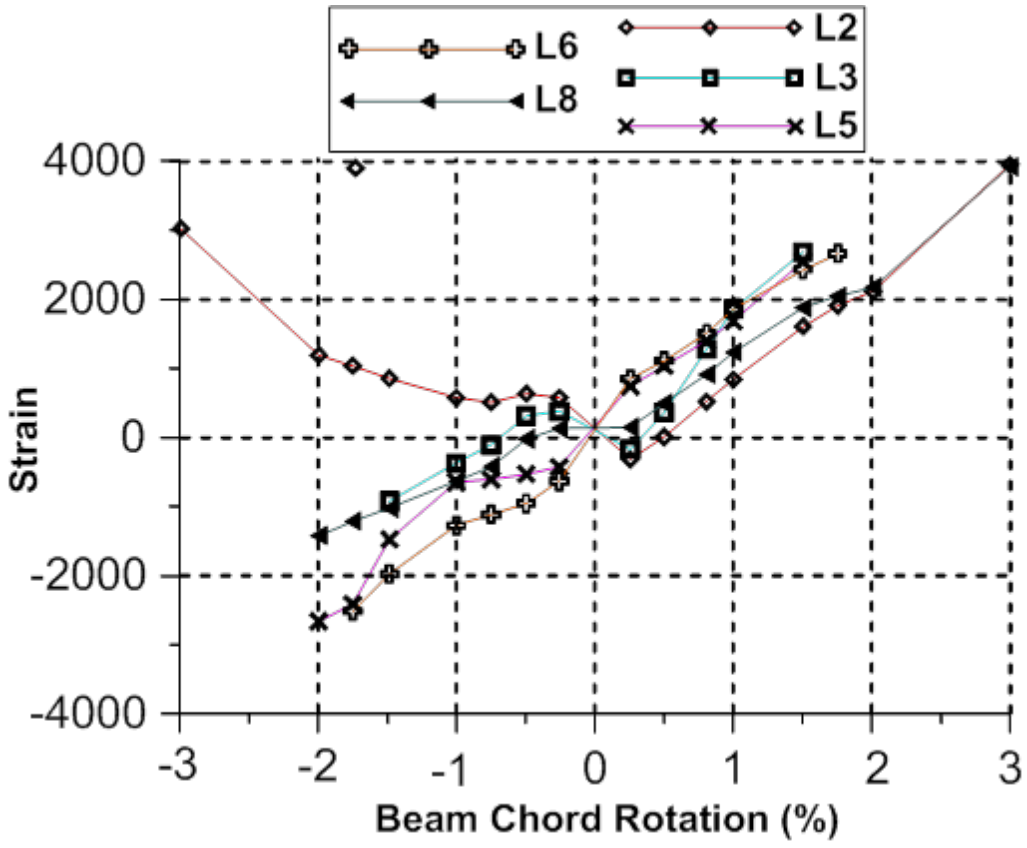
L6
L2
L8
L3
L5
4000
2000
0
-2000
-4000
Strain
-3
-2
-1
0
1
2
3
Beam Chord Rotation (%)

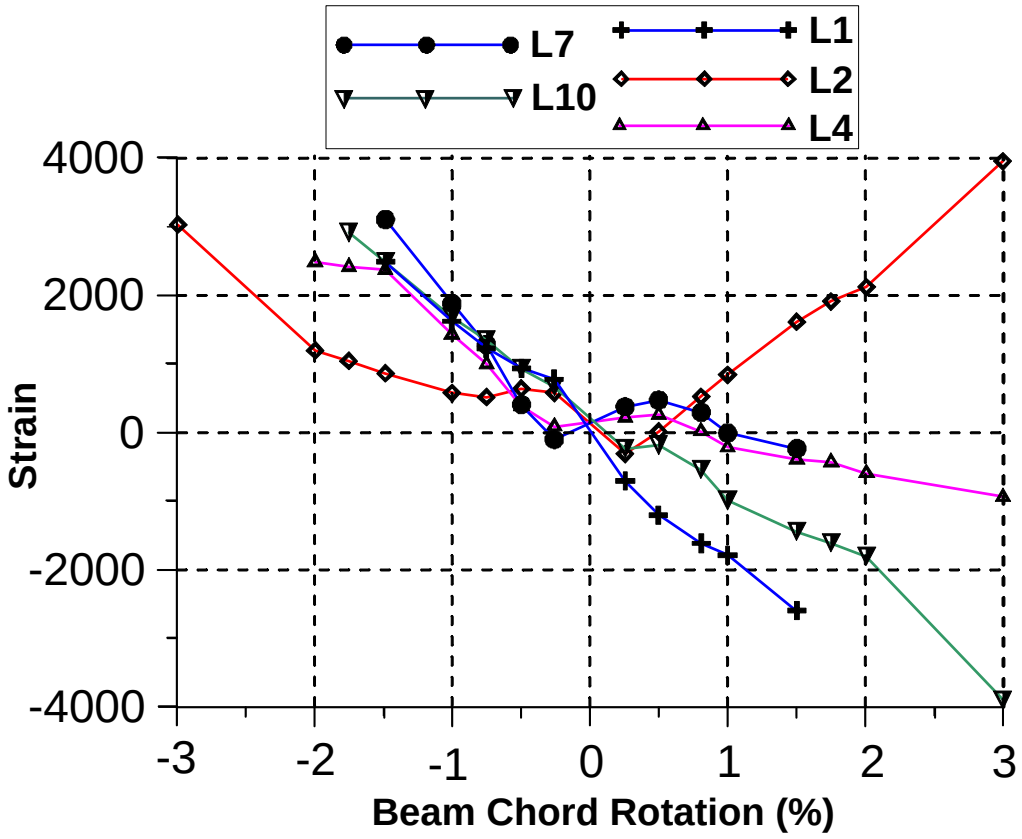

Strain gauge results for CB-4

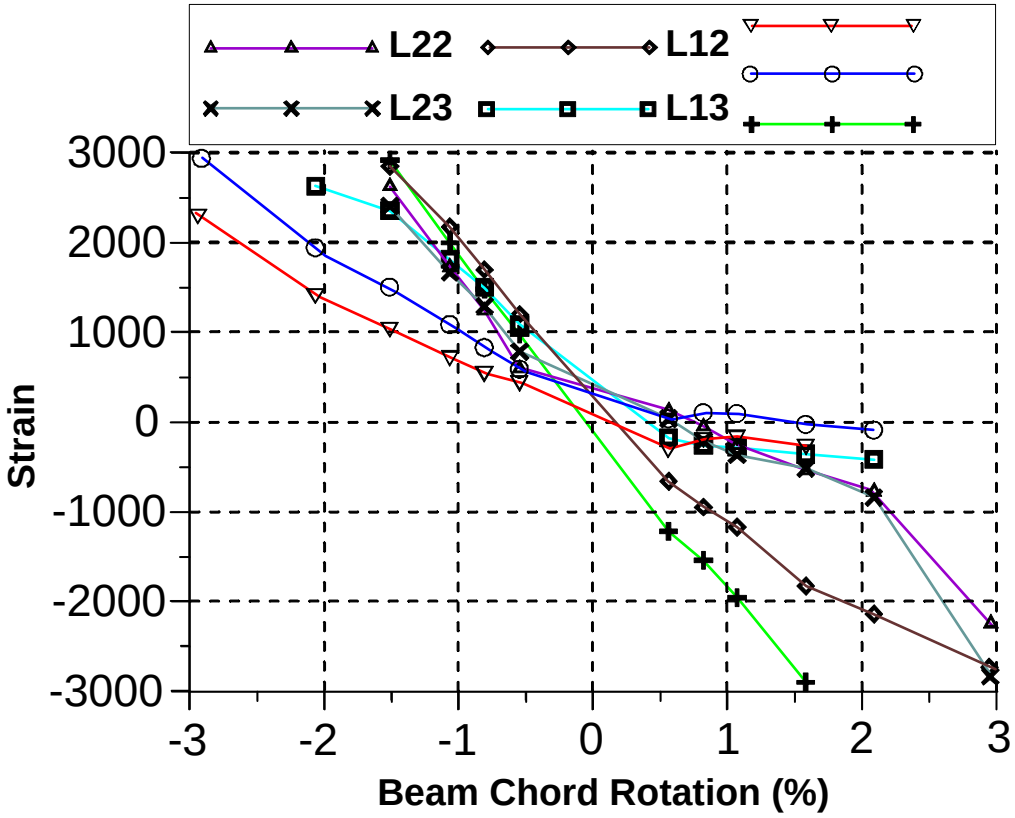
L22
L12
L23
L13
3000
2000
1000
0
-1000
-2000
-3000
Strain
-3
-2
-1
0
1
2
3
Beam Chord Rotation (%)

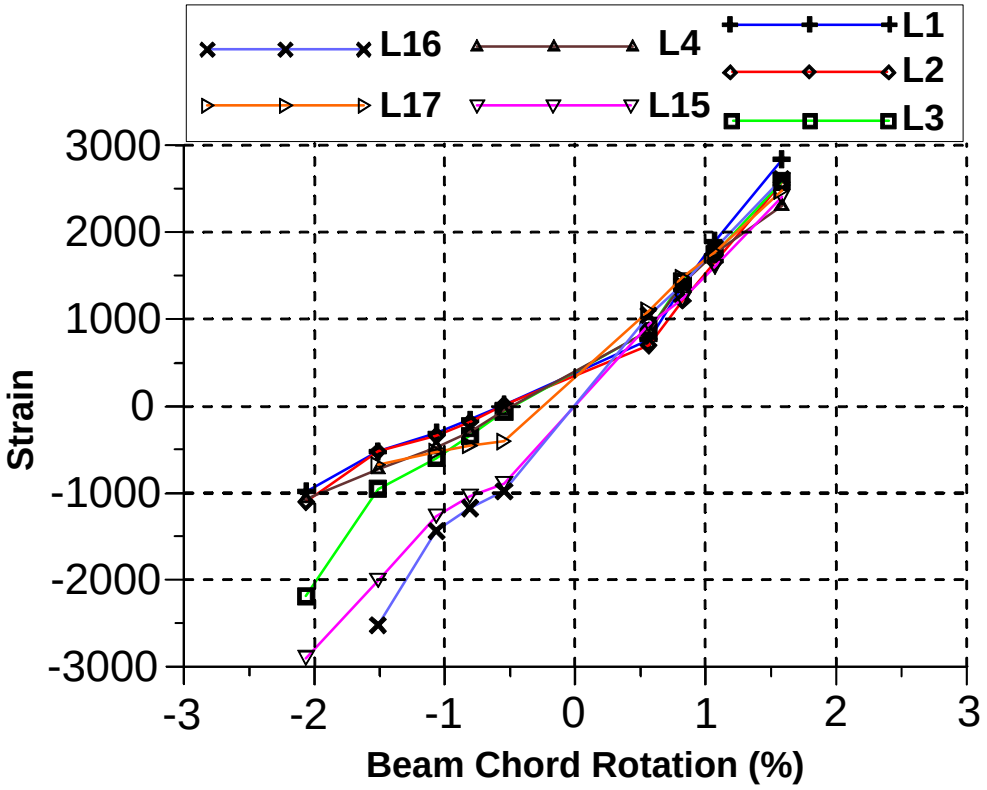

Strain gauge results for CB-5

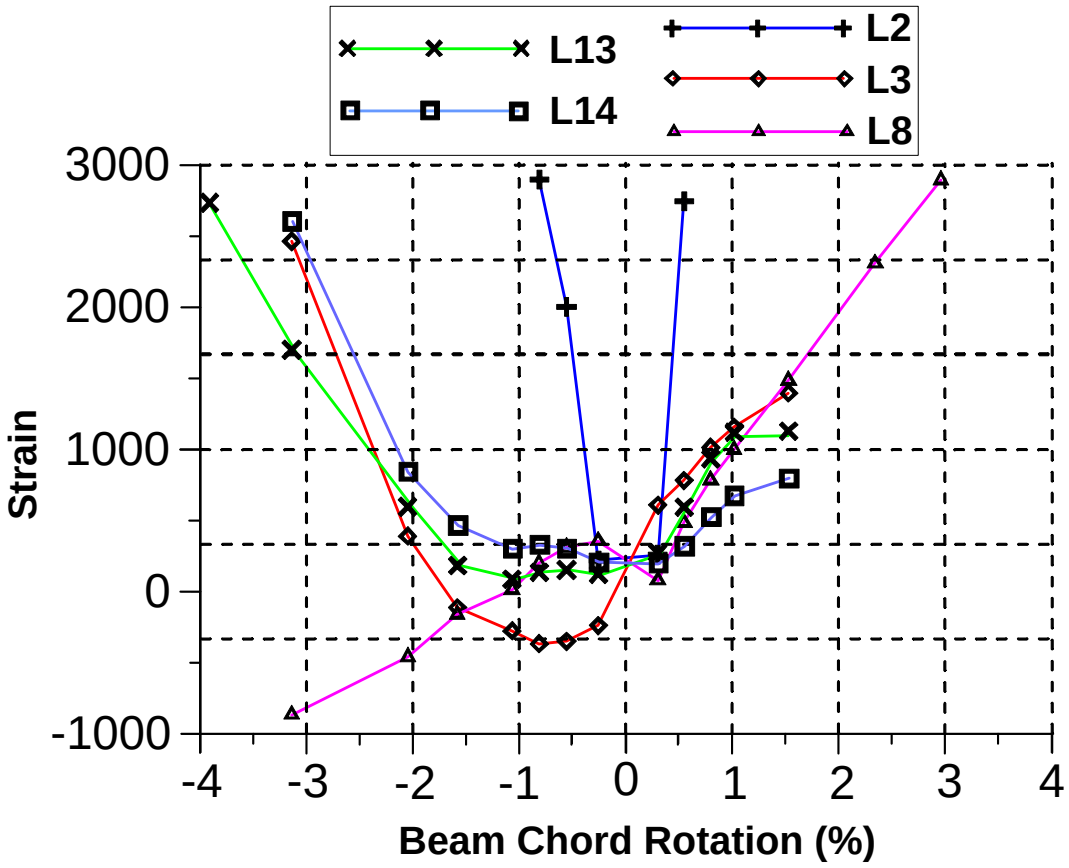

Strain gauge results for CB-6

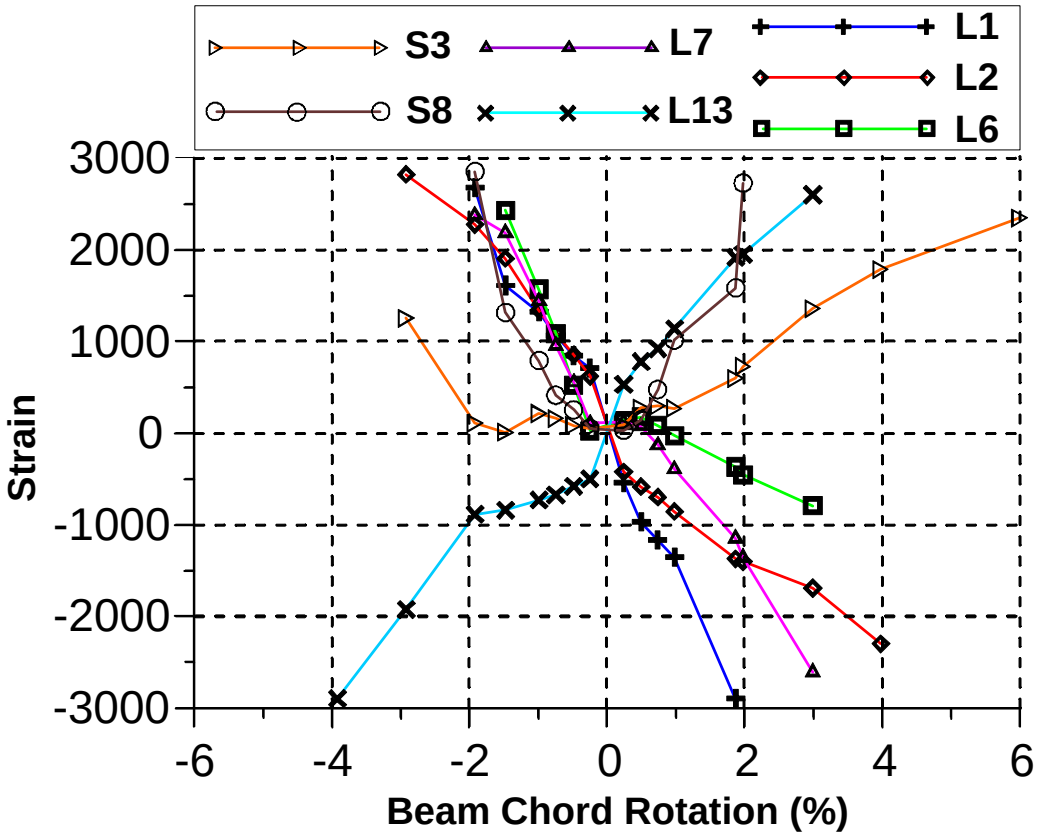

Strain gauge results for CB-7

References

1. American Concrete Institute. *Building Code Requirements for Structural Concrete (ACI 318-11) and Commentary (ACI318R-11),* Farmington Hills, Michigan, 2011.
2. Aktan, A. E., and Bertero, V. V., 1981, "The Seismic Resistant Design of R/C Coupled Structural Walls," Report No. UCB/EERC-81/07, *Earthquake Engineering Research Center*, University of California, Berkeley.
3. Adamantia, A., Parra-Montesinos, G. J., 2013," Experimental Study on the Seismic Behavior of High-Performance Fiber-Reinforced Concrete Low-Rise Walls*," ACI Structural Journal*, V. 110, No. 5, pp. 767-777.
4. Aristizabal-Ochoa, J. D., 1987, "Seismic Behavior of Slender Coupled Wall Systems," *Journal of the Structural Division*, V. 113, No. ST10, pp. 2221-2234.
5. Barda F., Hanson J. M., and Corley W. G., 1977 "Shear Strength of Low-Rise Walls with Boundary Elements", *ACI Special Publications*, Reinforced Concrete in Seismic Zones, SP-53-8, pp.149-202. (Also, Research and Development Bulletin, No. RD043.01D, Portland Cement Association.)
6. Bismarck N. L., Jonathan P. R., Andrew S. W. 2015," Seismic Behavior of Low-Aspect-Ratio Reinforced Concrete Shear Walls," *ACI Structural Journal*, V. 112, No. 5, pp 593-603.
7. Canbolat, B. A., Parra-Montesinos, G. J., and Wight, J. K. (2005), "Experimental Study on Seismic Behavior of High-Performance Fiber-Reinforced Cement Composite Coupling Beams," *ACI Structural Journal*, 102 (1), 159-166.
8. Cardenas A. E., Hanson J. M., Corley W. G., and Hognestad E., 1973, "Design Provisions for Shear Walls," *ACI Journal*, Vol. 70, No. 23, Code Background Paper, Background Material used in preparing ACI 318-71, pp. 221-230.

9. Galano, L., and Vignoli, A., 2000, “Seismic Behavior of Short Coupling Beams with Different Reinforcement Layouts,” *ACI Structural Journal*, V. 97, No. 6, Nov.-Dec., pp. 876-885. 3.

10. Greifenhagen, C. and Lestuzzi, P., 2005 “Static Cyclic Tests on Lightly Reinforced Concrete Shear Walls,” *Engineering Structures*, Vol. 27, pp. 1705-1721.

11. Gulec, C.K., Whittaker, A.S., and Stojadinovic, B., 2008 “Shear Strength of Squat Rectangular Reinforced Concrete Walls,” *ACI Structural Journal*, Vol. 105, No. 4, , pp. 488-497.

12. Gulec, C.K., Whittaker, A.S., and Stojadinovic, B., 2009”Peak Shear Strength of Squat Reinforced Concrete Walls with Boundary Barbells or Flanges*,” ACI Structural Journals*, Vol. 106, No. 3, pp. 368-377.

13. Gong, B. and Shahrooz, B. M. (2001a), “Concrete-Steel Composite Coupling Beams. II: Subassembly Testing and Design Verification,” *Journal of Structural Engineering*, ASCE, 127 (6), 632-638.

14. Gong, B. and Shahrooz, B. M. (2001b), “Steel-Concrete Composite Coupling Beams – Behavior and Design,” *Engineering Structures*, 23, 1480-1490.

15. Hidalgo P. A., Ledezma C. A., and Jordan R. M., 2002 “Seismic Behavior of Squat Reinforced Concrete Shear Walls,” *Earthquake Spectra*, Vol. 18, No. 2, pp. 287-308.

16. Harries, K. A., Mitchell, D., Redwood, R. G. and Cook, W. D. (1998), “Nonlinear Seismic Response Predictions of Walls Coupled with Steel and Concrete Beams,” *Canadian Journal of Civil Engineering*, 25 (5), 803-818.

17. Harries, K. A., Fortney, P. J., Shahrooz, B.M., and Brienen, P. J. (2005), “Practical Design of Diagonally Reinforced Concrete Coupling Beams” – Critical Review of

ACI 318 Requirements, *ACI Structural Journal*, 102 (6), 876-882.

18. Harries, K. A., McNeice, D. S. (2006), “Performance-Based Design of high-Rise Coupling Wall Systems” *The Structural Design of Tall and Special Buildings.* 15, 289-306.
19. Lam, W.-Y., Su, R. K.-L. and Pam, H.-J. (2005), “Experimental Study on Embedded Steel Plate Composite Coupling Beams,” *Journal of Structural Engineering*, ASCE, 131 (8), 1294-1302.
20. Lefas, I.D., Kotsovos, M.D. and Ambraseys, N.N., “Behavior of Reinforced Concrete Structural Walls: Strength, Deformation Characteristics and Failure Mechanism,” *ACI Structural Journal*, Vol. 87, No. 1, January-February 1990, pp. 23-31.
21. Lequesne, R. D. (2011). Behavior and Design of High-Performance Fiber-Reinforced Concrete Coupling Beams and Coupled-Wall Systems. *Doctoral dissertation*, Department of Civil and Environmental Engineering, the University of Michigan, Ann Arbor, 277 pp.
22. Lopes, M.S. (a), “Experimental Shear-Dominated Response of RC Walls. Part I: Objectives, Methodology and Results,” *Engineering Structures*, Vol. 23, 2001, pp.229- 239.
23. Lopes, M.S. (b), “Experimental Shear-Dominated Response of RC Walls. Part II: Discussion of Results and Design Implications,” *Engineering Structures*, Vol. 23, 2001, pp. 564-574.
24. Maier, J., and Thürlimann, B., 1985, "Bruchversuche an Stahlbetonscheiben," Institut für Baustatik und Konstruktion, Eidgenössische Technische Hochschule (ETH) Zürich, Zürich, Switzerland, 130 pp. (in German)
25. Mohammadi-Doostdar, H., 1994, "Behavior and Design of Earthquake Resistant

Low-Rise Shear Walls," Department of Civil Engineering, University of Ottawa, Ottawa, ON, Canada, 234 pp.

26. Naish, D., Wallace, J., Fry, J. A., and Klemencic, R. (2009), “Reinforced Concrete Link Beams: Alternative Details for Improved Constructability,” *Report to Charles Pankow Foundation*. UCLA-SGEL, 103 pp.
27. Paparoni, M., 1972, “Model Studies of Coupling Beams”, *Proceedings of the International Conference on Tall Concrete and Masonry Buildings*, pp. 671-681.
28. Paulay, T. (1969), The Coupling of Shear Walls, PhD Dissertation, University of Canterbury, Christchurch, New Zealand, 435 pp.
29. Paulay, T. (1971), “Coupling Beams of Reinforced Concrete Shear Walls,” *Journal of the Structural Division*, ASCE, 97 (ST3), 843-861.
30. Paulay, T., and Binney, J. R., 1974, “Diagonally Reinforced Coupling Beams of Shear Walls,” *Shear in Reinforced Concrete*, SP-42, V. 2, American Concrete Institute, Farmington Hills, Mich., pp. 579-598. 4.
31. Pauley T. M. (a), 1986 “The Design of Ductile Reinforced Concrete Structural Walls for Earthquake Resistance,” Earthquake Spectra, Vol. 2, No. 4, pp.783-823.
32. Pauley T., Priestley M. J. N., Synge A. J., 1982 “Ductility in Earthquake Resisting Squat Shear walls,” *ACI Journal*, Vol. 79, No. 26, pp. 257-269.
33. Paulay, T. and Santhakumar, A. R. (1976), “Ductile Behavior of Coupled Shear Walls,” *Journal of the Structural Division*, ASCE, 102 (ST1), 93-108.
34. Paulay, T. and Spurr, D. D. (1977), “Frame-Shear Wall Assemblies Subjected to Simulated Seismic Loading,” Proceedings of the Sixth World Conference on Earthquake Engineering, New Delhi, India, 1195-1200.
35. Pilette, F. C., 1987, "Behavior of Earthquake Resistant Squat Shear Walls," MS

Thesis, Department of Civil Engineering, University of Ottawa, Ottawa, ON, Canada, 177 pp.

36. Salonikios, N. T., Kappos, J. A., Tegos, A. I., Penelis, G. G., 1999 “Cyclic Load Behavior of Low-Slenderness Reinforced Concrete Walls: Design Basis and Test Results,” *ACI Structural Journal*, Vol. 96, No. 4, pp. 649-660.
37. Salonikios, N. T., Kappos, J. A., Tegos, A. I., Penelis, G. G., 2000“Cyclic Load Behavior of Low-Slenderness Reinforced Concrete Walls: Failure Modes, Strength and Deformation Analysis, and Design Implications,” *ACI Structural Journal*, Vol. 97, No. 1, pp. 132-142.
38. Shahrooz, B. M. and Gong, B. (1998), “Steel-Concrete Coupling Beams: A Critical Overview of Design Guidelines,” *Structural Engineers World Wide* 1998. 275.
39. Shahrooz, B. M., Remmetter, M. A. and Qin, F. (1993), “Seismic Design and Performance of Composite Coupled Walls, *Journal of the Structural Division*, ASCE, 119 (11), 3291-3309.
40. Shiu, N. K., Barney, G. B., Fiorato, A. E., and Corley W. G. (1978), “Reversing. Load Tests of Reinforced Concrete Coupling Beams,” *Proceedings of the Central American Conference on Earthquake Engineering*, El Salvador, pp. 239-249.
41. Subedi, N. K. (1991), “RC-Coupled Shear Wall Structures. I: Analysis of Coupling Beams,” *Journal of Structural Engineering*, ASCE, 117 (3), 667-680.
42. Synge, A.J., 1980 “Ductility of Squat Shear Walls,” Research Report 80-8, Department of Civil Engineering, University of Canterbury, Christchurch, New Zealand.
43. Tassios, T. P.; Moretti, M.; and Bezas A., 1996, “On the Behavior and Ductility of Reinforced Concrete Coupling Beams of Shear Walls,” *ACI Structural Journal*, V.

93, No. 6, Nov.-Dec., pp. 711-720.

44. Tegos, I. A. and Penelis, G. G. (1988), “Seismic Resistance of Short Columns and Coupling Beams reinforced with Inclined Bars,” ACI Structural Journal, 85 (1), 82 88.

45. Teshigawara, M., Kato, M., Sugaya, K. and Matsushima, Y. (1998), “Energy Absorption Mechanism and the Fluctuation of shear Force in the Coupled shear Walls,” *Structural Engineering World Wide 1998 – Proceedings*, Paper Number T-186-5, Elsevier Science Ltd., 8 pp.

46. Wong, P. S. and Vecchio, F. J.,” VecTor2 & Formworks User’s Manual”, August 2002.

Biographical Information

Poorya Hajyalikhani was born in Tehran, Iran. He obtained a Bachelor of Science in Civil Engineering from the Azad University of Semnan (2005). He completed his Master degree in Marine Structure in Tehran University (2009). In 2010 he started his PhD in Structures at the University of Texas at Arlington. His research interests are seismic concrete research, structural dynamics, structural stability, performance based plastic design, structural adhesives, and other areas.